

University of Montana

ScholarWorks at University of Montana

Graduate Student Theses, Dissertations, &
Professional Papers

Graduate School

2023

INTERACTIONS AMONG CLIMATE, FIRE, AND ECOSYSTEM PROCESSES ACROSS MULTIPLE SPATIAL AND TEMPORAL SCALES IN ROCKY MOUNTAIN FORESTS

Kyra Diane Clark-Wolf

Follow this and additional works at: <https://scholarworks.umt.edu/etd>

Let us know how access to this document benefits you.

Recommended Citation

Clark-Wolf, Kyra Diane, "INTERACTIONS AMONG CLIMATE, FIRE, AND ECOSYSTEM PROCESSES ACROSS MULTIPLE SPATIAL AND TEMPORAL SCALES IN ROCKY MOUNTAIN FORESTS" (2023). *Graduate Student Theses, Dissertations, & Professional Papers*. 12047.

<https://scholarworks.umt.edu/etd/12047>

This Dissertation is brought to you for free and open access by the Graduate School at ScholarWorks at University of Montana. It has been accepted for inclusion in Graduate Student Theses, Dissertations, & Professional Papers by an authorized administrator of ScholarWorks at University of Montana. For more information, please contact scholarworks@mso.umt.edu.

INTERACTIONS AMONG CLIMATE, FIRE, AND ECOSYSTEM PROCESSES ACROSS
MULTIPLE SPATIAL AND TEMPORAL SCALES IN ROCKY MOUNTAIN FORESTS

By

KYRA DIANE CLARK-WOLF

B.A., Colorado College, Colorado Springs, CO, 2016

Dissertation
presented in partial fulfillment of the requirements
for the degree of
Doctor of Philosophy in Systems Ecology
The University of Montana
Missoula, MT
January 2023

Approved by:

Dr. Alan Townsend
W.A. Franke College of Forestry and Conservation Dean

Dr. Philip Higuera, Committee Chair
Department of Ecosystem and Conservation Sciences
University of Montana

Dr. Ashley Ballantyne
Department of Ecosystem and Conservation Sciences
University of Montana

Dr. Cory Cleveland
Department of Ecosystem and Conservation Sciences
University of Montana

Dr. Kendra McLauchlan
Division of Environmental Biology
National Science Foundation

Dr. Carl Seielstad
Department of Forest Management
University of Montana

© COPYRIGHT

by

Kyra Diane Clark-Wolf

2023

All Rights Reserved

Interactions among climate, fire, and ecosystem processes across multiple spatial and temporal scales in Rocky Mountain subalpine forests

Chairperson: Dr. Philip Higuera

ABSTRACT

Warmer and drier climate conditions over recent decades are contributing to widespread increases in fire activity across western North America. The combined impacts of changing climate and fire activity threaten to undermine the longstanding resilience of forest ecosystems to wildfires, potentially leading to ecological transformations. This context creates a pressing need to understand the direct effects of climate and wildfire on ecosystem processes, and how longer-term changes in climate, fire activity, and ecosystem processes interact to determine ecological trajectories.

This dissertation advances our understanding of the causes and ecosystem consequences of wildfire and changing fire regimes in northern Rocky Mountain forests over years to millennia. In Chapter 1, I utilized extensive field sampling in two recent wildfires in western Montana to document how fires alter microclimatic conditions in biologically meaningful ways for regenerating and surviving vegetation. Through a subsequent study that tracked conifer seedling demography over the first three years following these wildfires, Chapter 2 highlights how spatial heterogeneity in fire effects can facilitate tree regeneration following wildfires, provided suitable post-fire climate. Overall, forests are exhibiting early signs of resilience to these two fire events.

Chapters 3 and 4 utilized paleoecological methods to address questions of long-term ecosystem change, and relationships among climate, fire activity, and ecosystem processes. In Chapter 3 I used a high-resolution, multiproxy lake-sediment record from the northern Rockies to reconstruct fire activity and ecosystem change over the past 4800 years. Changes in vegetation and fire activity coincident with increased effective moisture c. 2000 years ago highlight the overarching impact of climate on shaping ecosystem processes. Past wildfires had diverse, detectable impacts on biogeochemical processes, and evidence of ecosystem resilience to wildfires was consistent across variations in climate, vegetation, and fire activity over the late Holocene. Chapter 4 addressed variability in fire activity across a broader landscape, much of it burned during the historic 1910 fire season. I developed a network of 12 lake-sediment records to reconstruct a landscape-scale fire history over the past 2500 years and quantify the historical range of variability. This perspective reveals that contemporary burning, including the 1910 fires, remains within the historical range of fire activity in subalpine forests in this region.

My findings imply that northern Rocky Mountain subalpine forests are currently experiencing fire activity and ecological dynamics broadly consistent with historical variability. However, each chapter also highlights the sensitivity of multiple forest ecosystem processes to climate conditions and climate variability. Given the rapid rate of ongoing climatic change, subalpine forests will become increasingly vulnerable to widespread shifts in composition and structure. Future research could focus on identifying thresholds to change and early warning signals.

ACKNOWLEDGEMENTS

I am very grateful for the funding provided by the National Science Foundation and the Joint Fire Science Program's Graduate Research Innovation (GRIN) award. I would like to thank and acknowledge all of those involved with the "Big Burns Project", and specifically Kendra McLauchlan, Bryan Shuman, Tara Hudiburg, Meredith Parish, Kristina Bartowitz, Barrie Chileen, David Pompeani, Jennifer Roozeboom, Amelia Hagen-Dillon, and Dylan Darter. This has been an exciting project, and I look forward to continuing this work through Big Burns 2.0.

I deeply thank my advisor, Philip Higuera, for his unfailing kindness, encouragement, and enthusiasm, not to mention the work that went into endless rounds of revision. I am a better scientist and a much better writer for my time working with him. My gratitude also extends to my lab mates. Foremost among them is Kim Davis, who welcomed me when I jumped into studying post-fire tree regeneration, and helped me develop what are now the first two chapters of this dissertation. I also thank Tyler Hoecker, Spencer Viera, Jamie Peeler, Jesse Smyth, and Lacey Hankin for productive lab meetings and constructive feedback.

This dissertation would not have been possible without the many research assistants who supported the lab and field components of this work, including, but not limited to, Allison Hendryx, Madison Miller, Isabella Evavold, Yulia Misevich-Crofutt, Andie Sonnen, Abigail Matheny, Rosa Kirk-Davidoff, and Lauren Converse. The effort that went into sieving and counting the many hundreds of charcoal samples that are a part of this work was no small feat, and certainly not one I could complete alone.

I would like to recognize my committee members for their support and guidance, including Cory Cleveland, Ash Ballantyne, Carl Seielstad, and Kendra McLauchlan. It is not every committee that makes the process of completing a Ph.D. not only productive and interesting, but also enjoyable. I also acknowledge Solomon Dobrowski for his contribution to this work, and those at the U.S. Forest Service who provided additional input and logistical support, including Vince Archer.

Finally, my gratitude extends to my parents, Steve and Cathy, and my husband, TJ. My parents taught me a love of lifelong learning, and they supported me to pursue a liberal arts education, which, despite its impracticality, started me on this path. My husband has been with me throughout this process, and has given me the love and encouragement I needed, even when I was frustrated. Last but not least, I cannot forget to acknowledge my most enthusiastic field helper: my dog, Nighthawk.

This dissertation is dedicated to my grandfather, John L. Sprague, who was a scientist at heart.

TABLE OF CONTENTS

ABSTRACT.....	iii
ACKNOWLEDGEMENTS.....	iv
TABLE OF CONTENTS.....	v
LIST OF TABLES.....	vii
LIST OF FIGURES.....	viii
DISSERTATION INTRODUCTION AND OVERVIEW.....	1
Literature Cited.....	10
CHAPTER 1: Wildfire impacts on forest microclimate vary with biophysical context.....	26
Abstract.....	26
Introduction.....	27
Methods.....	29
Results.....	36
Discussion.....	38
Literature Cited.....	45
Tables.....	54
Figures.....	56
Supplementary Materials.....	61
Appendix A: Supplementary Methods.....	61
Appendix B: Supplementary Results.....	69
CHAPTER 2: Conifer seedling demography reveals mechanisms of initial forest resilience to wildfires in the northern Rocky Mountains.....	72
Abstract.....	72
Introduction.....	73
Methods.....	77
Results.....	84
Discussion.....	87
Literature Cited.....	95
Tables.....	108
Figures.....	111
Supplementary Materials.....	118
Appendix A: Supplementary Methods.....	118
Appendix B: Supplementary Results.....	129
CHAPTER 3: Climate change, pyrodiversity, and ecosystem resilience to wildfire over the past 4800 years in a Rocky Mountain forest.....	140
Abstract.....	140
Study area and site description.....	145

Methods.....	146
Results.....	153
Discussion	159
Literature Cited	170
Tables	189
Figures.....	190
Supplementary Materials	202
Appendix A: Supplementary Methods.....	202
Appendix B: Supplementary Results	209
CHAPTER 4: Widespread burning across northern Rocky Mountain subalpine forests over the past 2500 yr: precedence and implications for contemporary fire-regime change	219
Abstract.....	219
Introduction.....	220
Methods.....	223
Results.....	228
Discussion	231
Literature Cited	237
Figures.....	248
Supplementary Materials	254
Appendix A: Supplementary Methods.....	254
Appendix B: Supplementary Results	263

LIST OF TABLES

CHAPTER 1

Table 1. Description of the response and predictor variables used in the statistical models

Table 2. Comparison among candidate models

CHAPTER 2

Table 1. Description of the four sets of models used to understand controls of post-fire demographic processes

Table 2. Predictors of seedling regeneration considered in statistical models

CHAPTER 3

Table 1. Zones used to test changes in fire frequency, giving estimated mean fire return intervals

\

LIST OF FIGURES

CHAPTER 1

Figure 1. Map of sampling locations in the 2017 Sunrise (n = 12) and Lolo Peak (n = 21) fires

Figure 2. Diurnal variability in VPD (kPa) and temperature (°C)

Figure 3. Bivariate relationship between the difference in canopy cover above the sensor in paired burned and unburned plots (Δ Canopy, x-axis) and Δ Tmax (top panel), and Δ Vmax (bottom panel)

Figure 4. Model predictions of Δ Tmax after controlling for differences in canopy cover between paired burned and unburned sites

Figure 5. Model predictions of Δ Vmax after controlling for differences in canopy cover between paired burned and unburned sites

CHAPTER 2

Figure 1. Demographic filter framework predicting key factors governing post-fire tree regeneration in the context of climate change

Figure 2. Map of study area and sample sites in the Lolo Peak (n = 35 sites) and Sunrise fires (n = 34)

Figure 3. Estimates of total regeneration, annual recruitment, seedling survivorship, and height measurements over the first three years after fire

Figure 4. Best-fit models of seedling density in year three after fire in burned sites

Figure 5. Partial effects plots for best-fit model of annual seedling recruitment in burned sites

Figure 6. Partial effects plots for best-fit model of seedling survivorship

CHAPTER 3

Figure 1. Site map showing the location of Silver Lake and its bathymetry

Figure 2. Local paleoclimate and regional vegetation history, which provide a foundation for the study design

Figure 3. Age-depth relationship over the past 5,000 years for the Silver Lake record

Figure 4. Fire history from Silver Lake over the past 4800 yr

Figure 5. Pollen diagram, showing percent abundance of major pollen taxa

Figure 6. Timeseries of isotope values

Figure 7. Principal components analysis summarizing variation in biogeochemical proxies

Figure 8. Post-fire responses of select geochemical proxies

Figure 9. Boxplots comparing pollen abundance of major taxa among samples with differing time since fire

Figure 10. Fire, geochemical, vegetation, and paleoclimate history over the past 4800 yr at Silver Lake

CHAPTER 4

Figure 1. Map of northern and southern Rocky Mountain study regions and lake sites

Figure 2. Modern fire history in the northern Rocky Mountain ecoregion (M333D) over 1900-2021

Figure 3. Fire history in the Northern Rockies study landscape over the past 2500 yr

Figure 4. Paleoclimate and fire history in the Northern Rockies region

Figure 5. Fire history in the Northern and Southern Rockies study areas

Figure 6. Paleo, modern, and future scenarios of fire rotation period in subalpine forests in the Northern Rockies study area

DISSERTATION INTRODUCTION AND OVERVIEW

The Anthropocene is marked by rapid rates of climatic change beyond those experienced during recent millennia, which will transform ecological systems across much of the globe (Nolan et al. 2018, Williams et al. 2021). One key mechanism of ecological change is through altered disturbance processes, including fire. Fire has been an important process on Earth for hundreds of millions of years (Bowman et al. 2009). At broad spatiotemporal scales, fire acts as an evolutionary pressure on plant traits (Keeley and Pausas 2022), drives global patterns of biodiversity (Kelly et al. 2020), and shapes global biogeochemical cycles and the distribution of biomes (Bond et al. 2005). Within flammable ecosystems, the characteristics of fire regimes – describing the typical frequency, seasonality, and effects of fires over time – strongly influence ecological structure and function. Fire regimes, in turn, are shaped by top-down climatic controls, bottom-up controls of topography and vegetation (Whitlock et al. 2010), and human activities (Bowman et al. 2011). Direct and indirect anthropogenic impacts are altering the conditions that control fire regimes through changes in climate, ignitions, and fuels (Pausas and Keeley 2021).

At continental and global scales, anthropogenic impacts of land use intensification, fire suppression, and the cessation of Indigenous burning in the Americas have reduced fire activity within the past one to two centuries (Marlon et al. 2012, Andela et al. 2017, Arora and Melton 2018, Lake and Christianson 2019). In recent decades, however, the effects of anthropogenic, directional climate change are contributing to higher fire danger – defined based on daily surface weather variables related to ignitability and fire spread – in many areas of the globe (Jolly et al. 2015, Abatzoglou et al. 2019). Future climate conditions will support higher fire activity, particularly at mid to high latitudes (Pechony and Shindell 2010, Moritz et al. 2012). Trends of

Introduction

increasing fire activity in recent decades are especially evident across western North America, driven in large part by warmer, drier summer climate conditions that enhance fuel aridity and enable widespread fire in flammability-limited forest ecosystems (Westerling 2016, Abatzoglou and Williams 2016, McKenzie and Littell 2017). As climate conditions become increasingly fire-conducive, fire activity is projected to increase substantially in western U.S. forests over the remainder of the 21st century (Westerling et al. 2011, Gao et al. 2021, Abatzoglou et al. 2021).

Forest ecosystems of the West have persisted across variation in climate and disturbance regimes for millennia (e.g., Minckley et al. 2012), but the pace and magnitude of ongoing changes threaten to undermine this longstanding resilience (Anderson-Teixeira et al. 2013), defined as the capacity for ecosystem structure and function to recover to pre-disturbance conditions (Gunderson 2000). Shifting patterns of disturbance act in concert with climate change to alter the biotic and abiotic conditions in which post-fire recovery and reorganization take place (Johnstone et al. 2016), and this combination can catalyze rapid changes in plant communities (Johnstone et al. 2016, Crausbay et al. 2017, Coop et al. 2020). For example, declines in post-fire tree regeneration in the western U.S. highlight the vulnerability of seed-obligate conifers to changing conditions (e.g., Stevens-Rumann et al. 2018). Mechanisms of ecosystem change in forests dominated by seed-obligate conifers include disruptions to demographic processes from shortening fire intervals (Enright et al. 2015), more stressful post-fire climate conditions that inhibit tree regeneration (Davis et al. 2018, 2019), and interactions among drought, wildfires, and other disturbances (Paine et al. 1998, van Mantgem et al. 2013, Buma et al. 2014). In turn, shifts in vegetation composition or structure have the potential to alter future fire risk through self-limiting or self-reinforcing feedbacks (Tepley et al. 2018), and carbon and nutrient budgets are also sensitive to increased fire activity and associated ecological changes (e.g., Kelly et al. 2015).

Introduction

Individual wildfires influence a range of biogeochemical processes, the effects of which scale up across multiple fire intervals to influence ecosystem trajectories over decades, centuries, and even millennia (McLauchlan et al. 2014). Fires alter element stocks and fluxes directly through combustion and volatilization, and indirectly through subsequent changes in vegetation, substrate availability, and soil microclimate, biota, and physiochemical properties (Certini 2005, Smithwick et al. 2005, Hart et al. 2005, Dooley and Treseder 2012, Ferrenberg et al. 2013), as well as enhanced hydrologic and erosional losses (Bormann et al. 2008, Gustine et al. 2022). These effects are often short-lived, with a recovery to pre-fire ecosystem conditions occurring over years or decades (Turner et al. 2007, Smithwick et al. 2009, Kashian et al. 2013). Thus, when disturbance intervals typically exceed recovery times, ecosystems tend to be resilient to wildfires, and C and nutrient pools remain stable over the long term (Dunnette et al. 2014, Hudiburg et al. 2017). However, elevated fire frequency can lead to net losses of C and N (Pellegrini et al. 2018, 2020, Tierney et al. 2019, Walker et al. 2019), such that shifting fire regimes may reduce the carbon carrying capacity of terrestrial ecosystems (Bartowitz et al. 2019). Given that nutrient availability often constrains forest productivity (LeBauer and Treseder 2008), fire-induced shifts in element cycling can also interact with changes in forest structure and function over successional and longer (e.g., multi-century) timescales (Smithwick 2011).

While contemporary studies of fire-affected ecosystems offer valuable insights into how wildfires influence ecological processes, a key challenge to investigating the causes and consequences of fire activity is the scarcity of data spanning multiple intervals of disturbance and recovery, particularly in ecosystems characterized by infrequent stand-replacing fires. Paleocological methods offer a unique opportunity to “observe” patterns in fire activity and ecosystem properties over centuries to millennia, during periods of past changes in climate and

Introduction

vegetation. Lake sediments have been particularly valuable archives that have allowed development of proxy records of fire and vegetation change over millennia (e.g., Jackson and Overpeck 2000, Whitlock and Larsen 2001, Brunelle et al. 2005, Power et al. 2008). Charcoal particles preserved in lake sediments have been used to reconstruct fire activity in many ecosystems on Earth (Marlon et al. 2013). These records reveal substantial temporal and spatial variability in fire regimes owing to climatic change and variability, local controls (e.g., vegetation), and stochasticity (Gavin et al. 2007). Additionally, methods to reconstruct biogeochemical properties of forested catchments using lake-sediment records, in conjunction with other proxies, have helped infer the patterns and drivers of biogeochemical change over decadal to millennial time scales (McLauchlan et al. 2007, 2013, Dunnette et al. 2014, Leys et al. 2016b, 2016a, Chipman and Hu 2019, Pompeani et al. 2020). Taken together, the paleoecological approach allows a valuable long-term perspective on the complex relationships among fire activity, climate and vegetation change, and ecosystem processes.

Given uncertainties about forest resilience to changing climate and fire activity, there is a pressing need to understand not only the direct effects of fire and post-fire climate on ecosystem processes, but also how climate, fire regimes, and ecosystem processes interact to determine ecological trajectories over longer timescales. In particular, understanding the historical precedence of contemporary ecological and fire-regime changes will aid in anticipating the likelihood, and potential consequences, of ecological transformations under climate change.

This dissertation seeks to advance our understanding of the mechanisms and controls of forest ecosystem resilience to wildfires and fire-regime variability. I approached these issues at multiple spatial and temporal scales, from microsites to landscapes and years to millennia, using a combination of field sampling and paleoecological reconstructions of past fire activity and

Introduction

ecosystem change. Focal ecosystems were mixed-conifer and subalpine forests of the northern Rocky Mountains of western Montana and northern Idaho, USA, between approximately 46.5-47.5 °N, and 114-116 °W. This region is significant for two reasons: (1) because it has strongly contributed to trends in area burned in the western U.S. in recent decades (Westerling 2016), and (2) because extensive and impactful wildfires in 1910, known as “The Big Burn,” strongly shaped 20th century fire policy in the U.S. (Egan 2009). I sought to characterize the biophysical and demographic effects of recent large wildfires, test the ecosystem impacts of past climatic changes, and evaluate the long-term precedence for extensive burning like that in 1910.

A key uncertainty in anticipating future ecological changes is how broad-scale climatic change interacts with the biophysical impacts of wildfires to alter the environmental conditions that influence processes of post-fire tree regeneration. For example, a growing body of work details how forest microclimatic buffering can shape vegetation responses to warming by reducing exposure to climatic extremes (De Frenne et al. 2013, 2021, Zellweger et al. 2020, De Lombaerde et al. 2021). In **Chapter 1** I evaluated the impacts of wildfire on microclimate conditions using paired field sampling in unburned and recently burned forest in two large fires in western Montana, the 2017 Lolo Peak and Sunrise fires. I found that, by removing live canopy cover, wildfires created biologically meaningful increases in warm-dry microclimatic extremes near the ground surface, which varied across gradients in fire severity and topography.

To elucidate the effects of microclimate and other microsite factors on forest demographic processes, in **Chapter 2** I quantified conifer seedling establishment, survival, and growth by monitoring >1000 individual seedlings in 69 field plots over the first three years following the same fires. This work highlighted mechanisms supporting forest resilience that operate initially following fire. My results demonstrated how heterogeneity in fire severity at

Introduction

multiple spatial scales can facilitate tree regeneration by providing seed sources and creating diverse microsite environments for seedling recruitment and survival, provided that post-fire climate is suitable for regeneration.

Scaling up to further explore dynamics of post-fire forest recovery and ecosystem change on decadal through millennial timescales, in **Chapter 3** I explicitly tested the effects of a late-Holocene increase in effective moisture on subalpine forest vegetation, fire regimes, and biogeochemical states and processes using a lake-sediment record. I developed a 4800-year, high-resolution record from Silver Lake, Montana, with pollen, charcoal, and a suite of biogeochemical proxies. I found evidence of diverse ecosystem responses to individual wildfires on decadal timescales, indicative of variation in fire severity and fire effects throughout the late Holocene. Moreover, forest vegetation and catchment biogeochemical processes exhibited resilience to wildfires, returning to pre-fire conditions within decades, despite variability in fire severity and directional changes in fire frequency, climate, and vegetation over recent millennia.

To assess late-Holocene fire-regime variability at a broader spatial scale, in **Chapter 4** I developed a landscape-scale fire-history reconstruction using a densely sampled network of 12 lake-sediment charcoal records from a landscape that burned extensively in 1910. These records revealed widespread burning throughout the past 2500 years, which, on average, exceeded that of the early 20th and 21st century in subalpine forests. Thus, fire regimes in the northern Rocky Mountains remain, so far, within the historical range of variability of recent millennia.

Altogether, my findings paint a picture of northern Rocky Mountain forests at mid to high elevations that are currently operating within the “safe operating space” defined by the alignment between fire activity and information legacies, in the form of species traits (e.g., cone serotiny) that enable forest recovery under the current fire regime (Johnstone et al. 2016).

Introduction

Although wildfires affect a range of environmental conditions in burned landscapes, as shown in **Chapters 1-2**, my findings reveal that patch and microsite heterogeneity in fire effects help maintain information and material legacies that support forest resilience to wildfires. This spatial variability in fire effects within even large contemporary wildfires is mirrored by temporal diversity in disturbance processes and ecosystem impacts reconstructed over millennia (**Chapter 3**). Together, these findings provide evidence of ecological and biogeochemical resilience to a range of fire effects across space and time. Given contemporary fire activity that is within the historical range of variability of recent millennia (**Chapter 4**), and the climate suitability of post-fire conditions for tree regeneration in the region (Davis et al In Revision), we can expect that northern Rocky Mountain subalpine forests will likely continue to be resilient to future wildfires in the near term of the next several decades. The region studied in this dissertation – the northern Rocky Mountains – contrasts with other regions of the western U.S. during the early 21st century, where ongoing climate changes (e.g., increased aridity) are leading to shifting fire regimes (Higuera et al. 2021), and declines in regeneration of subalpine tree species (Andrus et al. 2018).

Longer-term outcomes of climate change in the northern Rocky Mountains, through mid-late century or beyond, will depend on the continued alignment among fire regimes, climate conditions, and species traits (e.g., reproductive strategies and climatic tolerances). Warming and drying climate is expected to result in large increases in area burned in the region (Gao et al. 2021), with snow-dominated forests particularly vulnerable to increased burning (Alizadeh et al. 2021, Kampf et al. 2022). Thus, the frequency component of fire regimes is changing, and may eventually surpass the bounds of historical variation. Warmer, drier conditions in recent decades also contribute to increased fire severity (Harvey et al. 2016, Parks and Abatzoglou 2020), which my findings highlight as a key control of the ecosystem impacts of fires (**Chapters 1-3**). As

Introduction

these dimensions of fire regimes change, subalpine species will decline in abundance if demographic processes cannot keep pace with higher fire frequency (Enright et al. 2015), or if environmental conditions inhibit regeneration in burned areas (Turner et al. 2019, Hoecker et al. 2020), leading to eventual shifts in forest composition, structure, and function.

Large uncertainties remain as to the pace and timing of fire-regime and ecosystem changes, and how feedbacks among vegetation, wildfire, and biogeochemical processes may operate under future conditions. For example, long-term shifts in vegetation and fuels under future climate may eventually lead to reductions in fire severity (Parks et al. 2016, Turner et al. 2022), and could offset some expected reductions in C uptake (e.g., Mack et al. 2021). Further, wildfire-catalyzed shifts in composition favoring relatively drought-tolerant or fire-resistant species would help to ensure continued alignment among climate, fire regimes, and plant traits as subalpine forests undergo compositional and/or structural shifts (e.g., Hoecker and Turner 2022). Resulting ecological changes would more closely track rates of climatic change, alleviating lags between climate forcing and ecological responses that are common in tree-dominated systems (Williams et al. 2021). Future research is needed to identify climatic thresholds governing ecological processes, assess the range of plausible ecosystem trajectories (Crausbay et al. 2022), and evaluate how climate-change impacts in subalpine forests may vary regionally.

From a management perspective, the implications of climatic and fire-regime changes in the northern Rocky Mountains will depend on short- and long-term management objectives. The large majority of my study area is in National Forest land, managed by the United States Forest Service for multiple benefits, including timber yield, recreation, wildlife habitat, and water resources. Additionally, a key goal of the National Cohesive Wildland Fire Management Strategy is to create resilient landscapes (Wildland Fire Executive Council 2014), which will

Introduction

require consideration of future conditions. Given my findings that fire activity and ecological dynamics in the first part of the 21st century are broadly consistent with historical variability, goals to maintain forest composition or cover in a similar state, for example, may require relatively little intervention in northern Rocky Mountain subalpine forests at present. However, a number of processes studied in this dissertation exhibit non-linear responses to climate change, including fire activity (Young et al. 2017, Juang et al. 2022) and tree regeneration (Davis et al. 2019). The forest resilience to fire and climate change exhibited in the past may be undermined if or when future climate crosses thresholds governing these processes, leading to a “ratchet of events” driving declines in forest density, forest cover, and carbon stocks (Jackson et al. 2009, Turner et al. 2022). Monitoring to identify declines in tree density – wildfire-related or otherwise – could serve as early warning signs of ultimate reductions in forest extent (Turner et al. 2022).

In future decades, a strategy of accepting or facilitating changes in forest composition may become the most salient management approach (Schuurman et al. 2022). Management focused on promoting landscape heterogeneity through, for example, managed wildfire use, could serve to support forest resilience to wildfires (Halofsky et al. 2018), but would not prevent extensive burning under extreme seasonal climate conditions (Hansen et al. 2020). Where very large high-severity patches or short-interval fires inhibit natural regeneration through seed limitation, targeted planting would prevent lags in forest recovery and could be used to accelerate upslope range shifts of species with fire-resistant traits. Ultimately, natural or directed ecological changes that maintain forest cover will help support essential ecosystem services such as snowpack retention.

Critically, my finding that the 1910 fires were not unprecedented over the long term implies that future years with extreme fire-season climate will likewise see extensive burning in

Introduction

the northern Rocky Mountains (**Chapter 4**). While reduced fire activity in subsequent decades after 1910 kept 20th-century fire activity within the range of past variation and helped support forest recovery, events like that of 1910 will increase in likelihood with directional climate change (Coop et al. 2022). As such, what are now record-setting fire events will become more common under future climate conditions. The increasing frequency of extreme fire events and fire seasons require enormous resources for firefighting, and pose risks to society via structure loss, smoke exposure, and impacts on water resources (Iglesias et al. 2022, Williams et al. 2022, Wilmot et al. 2022). Land managers and communities need risk management planning that accounts for the likelihood of events that exceed those experienced in the recent past, and which embrace adaptation strategies to reduce the impacts on vulnerable populations (Iglesias et al. 2022). Understanding the historical range of variability and processes driving past fire activity and ecosystem change through paleoecological approaches can help plan for this future.

Literature Cited

Abatzoglou, J. T., D. S. Battisti, A. P. Williams, W. D. Hansen, B. J. Harvey, and C. A. Kolden. 2021. Projected increases in western US forest fire despite growing fuel constraints. *Communications Earth & Environment* 2:1–8.

Abatzoglou, J. T., and A. P. Williams. 2016. Impact of anthropogenic climate change on wildfire across western US forests. *Proceedings of the National Academy of Sciences* 113:11770–11775.

Abatzoglou, J. T., A. P. Williams, and R. Barbero. 2019. Global Emergence of Anthropogenic Climate Change in Fire Weather Indices. *Geophysical Research Letters* 46:326–336.

Introduction

- Alizadeh, M. R., J. T. Abatzoglou, C. H. Luce, J. F. Adamowski, A. Farid, and M. Sadegh. 2021. Warming enabled upslope advance in western US forest fires. *Proceedings of the National Academy of Sciences* 118:e2009717118.
- Andela, N., D. C. Morton, L. Giglio, Y. Chen, G. R. van der Werf, P. S. Kasibhatla, R. S. DeFries, G. J. Collatz, S. Hantson, S. Kloster, D. Bachelet, M. Forrest, G. Lasslop, F. Li, S. Mangeon, J. R. Melton, C. Yue, and J. T. Randerson. 2017. A human-driven decline in global burned area. *Science (New York, N.Y.)* 356:1356–1362.
- Anderson-Teixeira, K. J., A. D. Miller, J. E. Mohan, T. W. Hudiburg, B. D. Duval, and E. H. DeLucia. 2013. Altered dynamics of forest recovery under a changing climate. *Global Change Biology* 19:2001–2021.
- Andrus, R. A., B. J. Harvey, K. C. Rodman, S. J. Hart, and T. T. Veblen. 2018. Moisture availability limits subalpine tree establishment. *Ecology* 99:567–575.
- Arora, V. K., and J. R. Melton. 2018. Reduction in global area burned and wildfire emissions since 1930s enhances carbon uptake by land. *Nature Communications* 9:1326.
- Bartowitz, K. J., P. E. Higuera, B. N. Shuman, K. K. McLauchlan, and T. W. Hudiburg. 2019. Post-Fire Carbon Dynamics in Subalpine Forests of the Rocky Mountains. *Fire* 2:58.
- Bond, W. J., F. I. Woodward, and G. F. Midgley. 2005. The global distribution of ecosystems in a world without fire. *New Phytologist* 165:525–538.
- Bormann, B. T., P. S. Homann, R. L. Darbyshire, and B. A. Morrisette. 2008. Intense forest wildfire sharply reduces mineral soil C and N: the first direct evidence. *Canadian Journal of Forest Research* 38:2771–2783.
- Bowman, D. M. J. S., J. Balch, P. Artaxo, W. J. Bond, M. A. Cochrane, C. M. D’Antonio, R. DeFries, F. H. Johnston, J. E. Keeley, M. A. Krawchuk, C. A. Kull, M. Mack, M. A.

Introduction

- Moritz, S. Pyne, C. I. Roos, A. C. Scott, N. S. Sodhi, and T. W. Swetnam. 2011. The human dimension of fire regimes on Earth. *Journal of Biogeography* 38:2223–2236.
- Bowman, D. M. J. S., J. K. Balch, P. Artaxo, W. J. Bond, J. M. Carlson, M. A. Cochrane, C. M. D'Antonio, R. S. DeFries, J. C. Doyle, S. P. Harrison, F. H. Johnston, J. E. Keeley, M. A. Krawchuk, C. A. Kull, J. B. Marston, M. A. Moritz, I. C. Prentice, C. I. Roos, A. C. Scott, T. W. Swetnam, G. R. van der Werf, and S. J. Pyne. 2009. Fire in the Earth System. *Science* 324:481–484.
- Brunelle, A., C. Whitlock, P. Bartlein, and K. Kipfmüller. 2005. Holocene fire and vegetation along environmental gradients in the Northern Rocky Mountains. *Quaternary Science Reviews* 24:2281–2300.
- Buma, B., R. E. Poore, and C. A. Wessman. 2014. Disturbances, Their Interactions, and Cumulative Effects on Carbon and Charcoal Stocks in a Forested Ecosystem. *Ecosystems* 17:947–959.
- Certini, G. 2005. Effects of fire on properties of forest soils: a review. *Oecologia* 143:1–10.
- Chipman, M. L., and F. S. Hu. 2019. Resilience of lake biogeochemistry to boreal-forest wildfires during the late Holocene. *Biology Letters* 15:20190390.
- Coop, J. D., S. A. Parks, C. S. Stevens-Rumann, S. D. Causbay, P. E. Higuera, M. D. Hurteau, A. Tepley, E. Whitman, T. Assal, B. M. Collins, K. T. Davis, S. Dobrowski, D. A. Falk, P. J. Fornwalt, P. Z. Fulé, B. J. Harvey, V. R. Kane, C. E. Littlefield, E. Q. Margolis, M. North, M. A. Parisien, S. Prichard, and K. C. Rodman. 2020. Wildfire-Driven Forest Conversion in Western North American Landscapes. *BioScience* 70:659–673.

Introduction

Coop, J. D., S. A. Parks, C. S. Stevens-Rumann, S. M. Ritter, and C. M. Hoffman. 2022.

Extreme fire spread events and area burned under recent and future climate in the western USA. *Global Ecology and Biogeography* 31:1949–1959.

Crausbay, S. D., P. E. Higuera, D. G. Sprugel, and L. B. Brubaker. 2017. Fire catalyzed rapid ecological change in lowland coniferous forests of the Pacific Northwest over the past 14,000 years. *Ecology* 98:2356–2369.

Crausbay, S. D., H. R. Sofaer, A. E. Cravens, B. C. Chaffin, K. R. Clifford, J. E. Gross, C. N. Knapp, D. J. Lawrence, D. R. Magness, A. J. Miller-Rushing, G. W. Schuurman, and C. S. Stevens-Rumann. 2022. A Science Agenda to Inform Natural Resource Management Decisions in an Era of Ecological Transformation. *BioScience* 72:71–90.

Davis, K. T., S. Z. Dobrowski, P. E. Higuera, Z. A. Holden, T. T. Veblen, M. T. Rother, S. A. Parks, A. Sala, and M. P. Maneta. 2019. Wildfires and climate change push low-elevation forests across a critical climate threshold for tree regeneration. *Proceedings of the National Academy of Sciences* 116:6193–6198.

Davis, K. T., et al. In Revision. Reduced fire severity offers near-term buffer to climate-driven declines in conifer resilience across the western United States. *Proceedings of the National Academy of Sciences*.

Davis, K. T., P. E. Higuera, and A. Sala. 2018. Anticipating fire-mediated impacts of climate change using a demographic framework. *Functional Ecology* 32:1729–1745.

De Frenne, P., J. Lenoir, M. Luoto, B. R. Scheffers, F. Zellweger, J. Aalto, M. B. Ashcroft, D. M. Christiansen, G. Decocq, K. De Pauw, S. Govaert, C. Greiser, E. Gril, A. Hampe, T. Jucker, D. H. Klimes, I. A. Koelemeijer, J. J. Lembrechts, R. Marrec, C. Meeussen, J. Ogée, V. Tyystjärvi, P. Vangansbeke, and K. Hylander. 2021. Forest microclimates and

Introduction

climate change: Importance, drivers and future research agenda. *Global Change Biology* 27:2279–2297.

De Frenne, P., F. Rodríguez-Sánchez, D. A. Coomes, L. Baeten, G. Verstraeten, M. Vellen, M. Bernhardt-Römermann, C. D. Brown, J. Brunet, J. Cornelis, G. M. Decocq, H. Dierschke, O. Eriksson, F. S. Gilliam, R. Hédli, T. Heinken, M. Hermy, P. Hommel, M. A. Jenkins, D. L. Kelly, K. J. Kirby, F. J. G. Mitchell, T. Naaf, M. Newman, G. Peterken, P. Petřík, J. Schultz, G. Sonnier, H. Van Calster, D. M. Waller, G. R. Walther, P. S. White, K. D. Woods, M. Wulf, B. J. Graae, and K. Verheyen. 2013. Microclimate moderates plant responses to macroclimate warming. *Proceedings of the National Academy of Sciences of the United States of America* 110:18561–18565.

De Lombaerde, E., P. Vangansbeke, J. Lenoir, K. Van Meerbeek, J. Lembrechts, F. Rodríguez-Sánchez, M. Luoto, B. Scheffers, S. Haesen, J. Aalto, D. M. Christiansen, K. De Pauw, L. Depauw, S. Govaert, C. Greiser, A. Hampe, K. Hylander, D. Klinges, I. Koelemeijer, C. Meeussen, J. Ogée, P. Sanczuk, T. Vanneste, F. Zellweger, L. Baeten, and P. De Frenne. 2021. Maintaining forest cover to enhance temperature buffering under future climate change. *Science of The Total Environment*:151338.

Dooley, S. R., and K. K. Treseder. 2012. The effect of fire on microbial biomass: a meta-analysis of field studies. *Biogeochemistry* 109:49–61.

Dunnette, P. V., P. E. Higuera, K. K. McLauchlan, K. M. Derr, C. E. Briles, and M. H. Keefe. 2014. Biogeochemical impacts of wildfires over four millennia in a Rocky Mountain subalpine watershed. *New Phytologist* 203:900–912.

Egan, T. 2009. *The Big Burn: Teddy Roosevelt and the Fire That Saved America*. Mariner Books, Boston.

Introduction

Enright, N. J., J. B. Fontaine, D. M. J. S. Bowman, R. A. Bradstock, and R. J. Williams. 2015.

Interval squeeze: Altered fire regimes and demographic responses interact to threaten woody species persistence as climate changes. *Frontiers in Ecology and the Environment* 13.

Ferrenberg, S., S. P. O’neill, J. E. Knelman, B. Todd, S. Duggan, D. Bradley, T. Robinson, S. K.

Schmidt, A. R. Townsend, M. W. Williams, C. C. Cleveland, B. A. Melbourne, L. Jiang, and D. R. Nemergut. 2013. Changes in assembly processes in soil bacterial communities following a wildfire disturbance. *ISME Journal* 7:1102–1111.

Gao, P., A. J. Terando, J. A. Kupfer, J. Morgan Varner, M. C. Stambaugh, T. L. Lei, and J.

Kevin Hiers. 2021. Robust projections of future fire probability for the conterminous United States. *Science of The Total Environment* 789:147872.

Gavin, D. G., D. J. Hallett, F. S. Hu, K. P. Lertzman, S. J. Prichard, K. J. Brown, J. A. Lynch, P.

Bartlein, and D. L. Peterson. 2007. Forest fire and climate change in western North America: insights from sediment charcoal records. *Frontiers in Ecology and the Environment* 5:499–506.

Gunderson, L. H. 2000. Ecological Resilience—In Theory and Application. *Annual Review of Ecology and Systematics* 31:425–439.

Gustine, R. N., E. J. Hanan, P. R. Robichaud, and W. J. Elliot. 2022. From burned slopes to streams: how wildfire affects nitrogen cycling and retention in forests and fire-prone watersheds. *Biogeochemistry* 157:51–68.

Halofsky, J. S., D. C. Donato, J. F. Franklin, J. E. Halofsky, D. L. Peterson, and B. J. Harvey.

2018. The nature of the beast: examining climate adaptation options in forests with stand-replacing fire regimes. *Ecosphere* 9:e02140.

Introduction

- Hansen, W. D., D. Abendroth, W. Rammer, R. Seidl, and M. G. Turner. 2020. Can wildland fire management alter 21st-century subalpine fire and forests in Grand Teton National Park, Wyoming, USA? *Ecological Applications* 30:e02030.
- Hart, S. C., T. H. DeLuca, G. S. Newman, M. D. MacKenzie, and S. I. Boyle. 2005. Post-fire vegetative dynamics as drivers of microbial community structure and function in forest soils. *Forest Ecology and Management* 220:166–184.
- Harvey, B. J., D. C. Donato, and M. G. Turner. 2016. Drivers and trends in landscape patterns of stand-replacing fire in forests of the US Northern Rocky Mountains (1984–2010). *Landscape Ecology*.
- Higuera, P. E., B. N. Shuman, and K. D. Wolf. 2021. Rocky Mountain subalpine forests now burning more than any time in recent millennia. *Proceedings of the National Academy of Sciences* 118:e2103135118.
- Hoecker, T. J., W. D. Hansen, and M. G. Turner. 2020. Topographic position amplifies consequences of short-interval stand-replacing fires on postfire tree establishment in subalpine conifer forests. *Forest Ecology and Management* 478:118523.
- Hoecker, T. J., and M. G. Turner. 2022. A short-interval reburn catalyzes departures from historical structure and composition in a mesic mixed-conifer forest. *Forest Ecology and Management* 504:119814.
- Hudiburg, T. W., P. E. Higuera, and J. A. Hicke. 2017. Fire-regime variability impacts forest carbon dynamics for centuries to millennia. *Biogeosciences* 14:3873–3882.
- Iglesias, V., N. Stavros, J. K. Balch, K. Barrett, J. Cobian-Iñiguez, C. Hester, C. A. Kolden, S. Leyk, R. C. Nagy, C. E. Reid, C. Wiedinmyer, E. Woolner, and W. R. Travis. 2022. Fires

Introduction

that matter: reconceptualizing fire risk to include interactions between humans and the natural environment. *Environmental Research Letters* 17:045014.

Jackson, S. T., J. L. Betancourt, R. K. Booth, and S. T. Gray. 2009. Ecology and the ratchet of events: climate variability, niche dimensions, and species distributions. *Proceedings of the National Academy of Sciences of the United States of America* 106 Suppl 2:19685–92.

Jackson, S. T., and J. T. Overpeck. 2000. Responses of plant populations and communities to environmental changes of the late Quaternary. *Paleobiology* 26:194–220.

Johnstone, J. F., C. D. Allen, J. F. Franklin, L. E. Frelich, B. J. Harvey, P. E. Higuera, M. C. Mack, R. K. Meentemeyer, M. R. Metz, G. L. W. Perry, T. Schoennagel, and M. G. Turner. 2016. Changing disturbance regimes, ecological memory, and forest resilience. *Frontiers in Ecology and the Environment* 14:369–378.

Jolly, W. M., M. A. Cochrane, P. H. Freeborn, Z. A. Holden, T. J. Brown, G. J. Williamson, and D. M. J. S. Bowman. 2015. Climate-induced variations in global wildfire danger from 1979 to 2013. *Nature Communications* 6:7537.

Juang, C. S., A. P. Williams, J. T. Abatzoglou, J. K. Balch, M. D. Hurteau, and M. A. Moritz. 2022. Rapid Growth of Large Forest Fires Drives the Exponential Response of Annual Forest-Fire Area to Aridity in the Western United States. *Geophysical Research Letters* 49:e2021GL097131.

Kampf, S. K., D. McGrath, M. G. Sears, S. R. Fassnacht, L. Kiewiet, and J. C. Hammond. 2022. Increasing wildfire impacts on snowpack in the western U.S. *Proceedings of the National Academy of Sciences* 119:e2200333119.

Introduction

- Kashian, D. M., W. H. Romme, D. B. Tinker, M. G. Turner, and M. G. Ryan. 2013. Postfire changes in forest carbon storage over a 300-year chronosequence of *Pinus contorta* - dominated forests. *Ecological Monographs* 83:49–66.
- Keeley, J. E., and J. G. Pausas. 2022. Evolutionary Ecology of Fire. *Annual Review of Ecology, Evolution, and Systematics* 53:203–225.
- Kelly, L. T., K. M. Giljohann, A. Duane, N. Aquilué, S. Archibald, E. Batllori, A. F. Bennett, S. T. Buckland, Q. Canelles, M. F. Clarke, M. J. Fortin, V. Hermoso, S. Herrando, R. E. Keane, F. K. Lake, M. A. McCarthy, A. Morán-Ordóñez, C. L. Parr, J. G. Pausas, T. D. Penman, A. Regos, L. Rumpff, J. L. Santos, A. L. Smith, A. D. Syphard, M. W. Tingley, and L. Brotons. 2020. Fire and biodiversity in the Anthropocene. *Science* (New York, N.Y.) 370.
- Kelly, R., H. Genet, A. D. McGuire, and F. S. Hu. 2015. Palaeodata-informed modelling of large carbon losses from recent burning of boreal forests. *Nature Climate Change* 6:79.
- Lake, F. K., and A. C. Christianson. 2019. Indigenous Fire Stewardship. Pages 1–9 in S. L. Manzello, editor. *Encyclopedia of Wildfires and Wildland-Urban Interface (WUI) Fires*. Springer International Publishing, Cham.
- LeBauer, D. S., and K. K. Treseder. 2008. Nitrogen limitation of net primary productivity in terrestrial ecosystems is globally distributed. *Ecology* 89:371–379.
- Leys, B. A., P. E. Higuera, K. K. McLauchlan, and P. V. Dunnette. 2016a. Wildfires and geochemical change in a subalpine forest over the past six millennia. *Environmental Research Letters* 11:125003.

Introduction

Leys, B. A., G. E. Likens, C. E. Johnson, J. M. Craine, B. Lacroix, and K. K. McLauchlan.

2016b. Natural and anthropogenic drivers of calcium depletion in a northern forest during the last millennium. *Proceedings of the National Academy of Sciences* 113:6934–6938.

Mack, M. C., X. J. Walker, J. F. Johnstone, H. D. Alexander, A. M. Melvin, M. Jean, and S. N. Miller. 2021. Carbon loss from boreal forest wildfires offset by increased dominance of deciduous trees. *Science* 372:280–283.

van Mantgem, P. J., J. C. B. Nesmith, M. Keifer, E. E. Knapp, A. Flint, and L. Flint. 2013.

Climatic stress increases forest fire severity across the western United States. *Ecology Letters* 16:1151–1156.

Marlon, J. R., P. J. Bartlein, A.-L. Daniau, S. P. Harrison, S. Y. Maezumi, M. J. Power, W.

Tinner, and B. Vanni re. 2013. Global biomass burning: a synthesis and review of Holocene paleofire records and their controls. *Quaternary Science Reviews* 65:5–25.

Marlon, J. R., P. J. Bartlein, D. G. Gavin, C. J. Long, R. S. Anderson, C. E. Briles, K. J. Brown, D. Colombaroli, D. J. Hallett, M. J. Power, E. A. Scharf, and M. K. Walsh. 2012. Long-term perspective on wildfires in the western USA. *Proceedings of the National Academy of Sciences* 109:E535–E543.

McKenzie, D., and J. S. Littell. 2017. Climate change and the eco-hydrology of fire: Will area burned increase in a warming western USA. *Ecological Applications* 27:26–36.

McLauchlan, K. K., J. M. Craine, W. W. Oswald, P. R. Leavitt, and G. E. Likens. 2007. Changes in nitrogen cycling during the past century in a northern hardwood forest. *Proceedings of the National Academy of Sciences* 104:7466–7470.

McLauchlan, K. K., P. E. Higuera, D. G. Gavin, S. S. Perakis, M. C. Mack, H. Alexander, J.

Battles, F. Biondi, B. Buma, D. Colombaroli, S. K. Enders, D. R. Engstrom, F. S. Hu, J.

Introduction

- R. Marlon, J. Marshall, M. McGlone, J. L. Morris, L. E. Nave, B. Shuman, E. A. H. Smithwick, D. H. Urrego, D. A. Wardle, C. J. Williams, and J. J. Williams. 2014. Reconstructing Disturbances and Their Biogeochemical Consequences over Multiple Timescales. *BioScience* 64:105–116.
- McLauchlan, K. K., J. J. Williams, J. M. Craine, and E. S. Jeffers. 2013. Changes in global nitrogen cycling during the Holocene epoch. *Nature* 495:352.
- Minckley, T. A., R. K. Shriver, and B. Shuman. 2012. Resilience and regime change in a southern Rocky Mountain ecosystem during the past 17 000 years. *Ecological Monographs* 82:49–68.
- Moritz, M. A., M.-A. Parisien, E. Batllori, M. A. Krawchuk, J. Van Dorn, D. J. Ganz, and K. Hayhoe. 2012. Climate change and disruptions to global fire activity. *Ecosphere* 3:1–22.
- Nolan, C., J. T. Overpeck, J. R. M. Allen, P. M. Anderson, J. L. Betancourt, H. A. Binney, S. Brewer, M. B. Bush, B. M. Chase, R. Cheddadi, M. Djamali, J. Dodson, M. E. Edwards, W. D. Gosling, S. Haberle, S. C. Hotchkiss, B. Huntley, S. J. Ivory, A. P. Kershaw, S. H. Kim, C. Latorre, M. Leydet, A. M. Lézine, K. B. Liu, Y. Liu, A. V. Lozhkin, M. S. McGlone, R. A. Marchant, A. Momohara, P. I. Moreno, S. Müller, B. L. Otto-Bliesner, C. Shen, J. Stevenson, H. Takahara, P. E. Tarasov, J. Tipton, A. Vincens, C. Weng, Q. Xu, Z. Zheng, and S. T. Jackson. 2018. Past and future global transformation of terrestrial ecosystems under climate change. *Science* 361:920–923.
- Paine, R. T., M. J. Tegner, and E. A. Johnson. 1998. Compounded Perturbations Yield Ecological Surprises. *Ecosystems* 1:535–545.

Introduction

Parks, S. A., and J. T. Abatzoglou. 2020. Warmer and Drier Fire Seasons Contribute to Increases in Area Burned at High Severity in Western US Forests From 1985 to 2017. *Geophysical Research Letters* 47:e2020GL089858.

Parks, S. A., C. L. Miller, J. Abatzoglou, L. M. Holsinger, M. A. Parisien, and S. Dobrowski. 2016. How will climate change affect wildland fire severity in the western US? *Environmental Research Letters* 11:35002.

Pausas, J. G., and J. E. Keeley. 2021. Wildfires and global change. *Frontiers in Ecology and the Environment*.

Pechony, O., and D. T. Shindell. 2010. Driving forces of global wildfires over the past millennium and the forthcoming century. *Proceedings of the National Academy of Sciences* 107:19167–19170.

Pellegrini, A. F. A., A. Ahlström, S. E. Hobbie, P. B. Reich, L. P. Nieradzik, A. C. Staver, B. C. Scharenbroch, A. Jumpponen, W. R. L. Anderegg, J. T. Randerson, and R. B. Jackson. 2018. Fire frequency drives decadal changes in soil carbon and nitrogen and ecosystem productivity.

Pellegrini, A. F. A., K. K. McLauchlan, S. E. Hobbie, M. C. Mack, A. L. Marcotte, D. M. Nelson, S. S. Perakis, P. B. Reich, and K. Whittinghill. 2020. Frequent burning causes large losses of carbon from deep soil layers in a temperate savanna. *Journal of Ecology* 108:1426–1441.

Pompeani, D. P., K. K. McLauchlan, B. V. Chileen, W. J. Calder, B. N. Shuman, and P. E. Higuera. 2020. The biogeochemical consequences of late Holocene wildfires in three subalpine lakes from northern Colorado. *Quaternary Science Reviews* 236:106293.

Introduction

- Power, M. J., J. Marlon, N. Ortiz, P. J. Bartlein, S. P. Harrison, F. E. Mayle, A. Ballouche, R. H. W. Bradshaw, C. Carcaillet, C. Cordova, S. Mooney, P. I. Moreno, I. C. Prentice, K. Thonicke, W. Tinner, C. Whitlock, Y. Zhang, Y. Zhao, A. A. Ali, R. S. Anderson, R. Beer, H. Behling, C. Briles, K. J. Brown, A. Brunelle, M. Bush, P. Camill, G. Q. Chu, J. Clark, D. Colombaroli, S. Connor, A.-L. Daniau, M. Daniels, J. Dodson, E. Doughty, M. E. Edwards, W. Finsinger, D. Foster, J. Frechette, M.-J. Gaillard, D. G. Gavin, E. Gobet, S. Haberle, D. J. Hallett, P. Higuera, G. Hope, S. Horn, J. Inoue, P. Kaltenrieder, L. Kennedy, Z. C. Kong, C. Larsen, C. J. Long, J. Lynch, E. A. Lynch, M. McGlone, S. Meeks, S. Mensing, G. Meyer, T. Minckley, J. Mohr, D. M. Nelson, J. New, R. Newnham, R. Noti, W. Oswald, J. Pierce, P. J. H. Richard, C. Rowe, M. F. Sanchez Goñi, B. N. Shuman, H. Takahara, J. Toney, C. Turney, D. H. Urrego-Sanchez, C. Umbanhowar, M. Vandergoes, B. Vanniere, E. Vescovi, M. Walsh, X. Wang, N. Williams, J. Wilmshurst, and J. H. Zhang. 2008. Changes in fire regimes since the Last Glacial Maximum: an assessment based on a global synthesis and analysis of charcoal data. *Climate Dynamics* 30:887–907.
- Schuurman, G. W., D. N. Cole, A. E. Cravens, S. Covington, S. D. Crausbay, C. H. Hoffman, D. J. Lawrence, D. R. Magness, J. M. Morton, E. A. Nelson, and R. O'Malley. 2022. Navigating Ecological Transformation: Resist–Accept–Direct as a Path to a New Resource Management Paradigm. *BioScience* 72:16–29.
- Smithwick, E. A. H. 2011. Pyrogeography and Biogeochemical Resilience. Pages 143–163 *in* D. McKenzie, C. Miller, and D. A. Falk, editors. *The Landscape Ecology of Fire*. Springer Netherlands, Dordrecht.

Introduction

- Smithwick, E. A. H., D. M. Kashian, M. G. Ryan, and M. G. Turner. 2009. Long-Term Nitrogen Storage and Soil Nitrogen Availability in Post-Fire Lodgepole Pine Ecosystems. *Ecosystems* 12:792–806.
- Smithwick, E. A. H., M. G. Turner, M. C. Mack, and F. S. Chapin. 2005. Postfire Soil N Cycling in Northern Conifer Forests Affected by Severe, Stand-Replacing Wildfires. *Ecosystems* 8:163–181.
- Stevens-Rumann, C. S., K. B. Kemp, P. E. Higuera, B. J. Harvey, M. T. Rother, D. C. Donato, P. Morgan, and T. T. Veblen. 2018. Evidence for declining forest resilience to wildfires under climate change. *Ecology Letters* 21:243–252.
- Tepley, A. J., E. Thomann, T. T. Veblen, G. L. W. Perry, A. Holz, J. Paritsis, T. Kitzberger, and K. J. Anderson-Teixeira. 2018. Influences of fire-vegetation feedbacks and post-fire recovery rates on forest landscape vulnerability to altered fire regimes. *Journal of Ecology* 106:1925–1940.
- Tierney, J. A., L. O. Hedin, and N. Wurzburger. 2019. Nitrogen fixation does not balance fire-induced nitrogen losses in longleaf pine savannas. *Ecology* 100.
- Turner, M. G., K. H. Braziunas, W. D. Hansen, and B. J. Harvey. 2019. Short-interval severe fire erodes the resilience of subalpine lodgepole pine forests. *Proceedings of the National Academy of Sciences of the United States of America* 166:11319–11328.
- Turner, M. G., K. H. Braziunas, W. D. Hansen, T. J. Hoecker, W. Rammer, Z. Ratajczak, A. L. Westerling, and R. Seidl. 2022. The magnitude, direction, and tempo of forest change in Greater Yellowstone in a warmer world with more fire. *Ecological Monographs* 92:e01485.

Introduction

Turner, M. G., E. A. H. Smithwick, K. L. Metzger, D. B. Tinker, and W. H. Romme. 2007.

Inorganic nitrogen availability after severe stand-replacing fire in the Greater Yellowstone ecosystem. *Proceedings of the National Academy of Sciences* 104:4782–4789.

Walker, X. J., J. L. Baltzer, S. G. Cumming, N. J. Day, C. Ebert, S. Goetz, J. F. Johnstone, S.

Potter, B. M. Rogers, E. A. G. Schuur, M. R. Turetsky, and M. C. Mack. 2019. Increasing wildfires threaten historic carbon sink of boreal forest soils. *Nature* 572:520–523.

Westerling, A. L. 2016. Increasing western US forest wildfire activity: sensitivity to changes in the timing of spring. *Philosophical transactions of the Royal Society of London. Series B, Biological sciences* 371:20150178.

Westerling, A. L., M. G. Turner, E. A. H. Smithwick, W. H. Romme, and M. G. Ryan. 2011.

Continued warming could transform Greater Yellowstone fire regimes by mid-21st century. *Proceedings of the National Academy of Sciences of the United States of America* 108:13165–70.

Whitlock, C., P. E. Higuera, D. B. McWethy, and C. E. Briles. 2010. Paleoeological

Perspectives on Fire Ecology: Revisiting the Fire-Regime Concept. *The Open Ecology Journal* 3:6–23.

Whitlock, C., and C. Larsen. 2001. Charcoal as a fire proxy. Pages 75–97 in J. P. Smol Birks, HJB and Last, WM., editor. *Tracking environmental change using lake sediments.*

Volume 3: terrestrial, algal, and siliceous indicators. Kluwer Academic Publishers.

Wildland Fire Executive Council. 2014. *The national strategy: the final phase in the development of the National Cohesive Wildland Fire Management Strategy.* Washington, D.C.

Introduction

- Williams, A. P., B. Livneh, K. A. McKinnon, W. D. Hansen, J. S. Mankin, B. I. Cook, J. E. Smerdon, A. M. Varuolo-Clarke, N. R. Bjarke, C. S. Juang, and D. P. Lettenmaier. 2022. Growing impact of wildfire on western US water supply. *Proceedings of the National Academy of Sciences* 119:e2114069119.
- Williams, J. W., A. Ordonez, and J.-C. Svenning. 2021. A unifying framework for studying and managing climate-driven rates of ecological change. *Nature Ecology & Evolution* 5:17–26.
- Wilmot, T. Y., D. V. Mallia, A. G. Hallar, and J. C. Lin. 2022. Wildfire activity is driving summertime air quality degradation across the western US: a model-based attribution to smoke source regions. *Environmental Research Letters* 17:114014.
- Young, A. M., P. E. Higuera, P. A. Duffy, and F. S. Hu. 2017. Climatic thresholds shape northern high-latitude fire regimes and imply vulnerability to future climate change. *Ecography* 40:606–617.
- Zellweger, F., P. D. Frenne, J. Lenoir, P. Vangansbeke, K. Verheyen, M. Bernhardt-Römermann, L. Baeten, R. Hédl, I. Berki, J. Brunet, H. V. Calster, M. Chudomelová, G. Decocq, T. Dirnböck, T. Durak, T. Heinken, B. Jaroszewicz, M. Kopecký, F. Máliš, M. Macek, M. Malicki, T. Naaf, T. A. Nagel, A. Ortmann-Ajkai, P. Petřík, R. Pielech, K. Reczyńska, W. Schmidt, T. Standovár, K. Świerkosz, B. Teleki, O. Vild, M. Wulf, and D. Coomes. 2020. Forest microclimate dynamics drive plant responses to warming. *Science* 368:772–775.

CHAPTER 1: Wildfire impacts on forest microclimate vary with biophysical context

*This chapter is published with the following co-authors and citation:

Wolf, K. D., P. E. Higuera, K. T. Davis, and S. Z. Dobrowski. 2021. Wildfire impacts on forest microclimate vary with biophysical context. *Ecosphere* 12:e03467. doi: 10.1002/ecs2.3467.

Abstract

Increasing wildfire activity in western North America has the potential to remove forest canopy cover over large areas, increasing the vulnerability of understory plants and juvenile trees to microclimatic extremes. To understand the impacts of wildfire on forest microclimatic buffering, we monitored daily temperature and vapor pressure deficit (VPD) in 33 plots over the first two growing seasons following two wildfires from 2017. The Lolo Peak and Sunrise fires occurred during a regionally extensive fire season, burning mixed-conifer and subalpine forests across complex mountainous topography in western Montana. Sensors were deployed from June to September in 2018 and 2019 in sites stratified by aspect, elevation, and fire severity (unburned, moderate, high) to capture a range of forest types, biophysical contexts, and fire effects. Loss of canopy and understory vegetation had marked effects on microclimate: on average, sites burned at high severity had 3.7 °C higher daily maximum temperatures and 0.81 kPa higher daily maximum VPD relative to paired unburned sites. Differences between burned and unburned sites were most pronounced when ambient temperatures were high, across diurnal and seasonal time scales. Differences were also more pronounced at sites with less canopy cover, more bare ground post-fire, and greater long-term water availability (i.e., low climatic water deficit). Our results reveal fire-caused changes in microclimate extremes that are biologically meaningful for the post-fire establishment of tree seedlings and understory vegetation. These effects depend strongly on biophysical context, with cool-wet forest more vulnerable to fire-caused changes in microclimate compared to warm-dry setting. Our results further highlight the

Chapter 1

functional importance of standing dead trees for moderating surface temperature in post-fire environments. Anticipating forest ecosystem responses to increased warming and wildfire activity, and the potential for fire to catalyze vegetation changes, thus requires considering the substantial impacts of fire on microclimate.

Introduction

Wildfire is a longstanding natural disturbance in forest ecosystems of western North America, where increased aridity in recent decades is well linked to increased area burned and fire severity (Gillett et al. 2004, Westerling 2016, Abatzoglou and Williams 2016, Holden et al. 2018, Parks and Abatzoglou 2020). Such trends are expected to continue in upcoming decades under warmer and drier conditions (Flannigan et al. 2005, Westerling et al. 2011, McKenzie and Littell 2017, Young et al. 2017) and, combined with increasingly stressful conditions for tree regeneration, are expected to lead to widespread vegetation change (Anderson-Teixeira et al. 2013, Serra-Diaz et al. 2018, Coop et al. 2020). While wildfire plays an important role in stimulating tree regeneration and understory growth by increasing the availability of light, nutrients, and mineral seedbeds (e.g., Hesketh et al. 2009, Ma et al. 2010, Crotteau et al. 2013, Brown et al. 2015), fire-caused tree mortality also alters microclimate conditions. Given that tree seedlings are sensitive to climatic stressors (Johnson et al. 2011, Andrus et al. 2018, Davis et al. 2018, 2019a, Kemp et al. 2019), fire-induced changes in microclimate are a likely mechanism through which warming and increased wildfire activity will impact forest ecosystems.

Wildfires can alter understory microclimates through several mechanisms, perhaps most importantly by reducing canopy cover. Relative to areas with no tree canopy, environments under forest canopies experience smaller variations between maximum and minimum

Chapter 1

temperatures due to reduced direct insolation and longwave emission, with more pronounced differences as canopy cover increases (Montes-Helu et al. 2009, Suggitt et al. 2011, von Arx et al. 2013, Frey et al. 2016, Davis et al. 2019b, De Frenne et al. 2019). Microclimatic buffering also varies spatially and temporally with macroclimate. Buffering is more pronounced in forests with greater local water availability to support evaporative cooling (Davis et al. 2019b), and buffering is often more pronounced when ambient conditions are warmer and drier (i.e., warmer and drier, von Arx et al. 2013). Thus, based on canopy loss alone, recently burned areas are expected to experience greater temperature extremes relative to unburned forests, with larger changes in areas of greater canopy loss (Ma et al. 2010) and in forests with greater pre-fire evaporative cooling.

Wildfires do more than simply reduce canopy cover, however, and the potential impacts of these changes on microclimatic buffering have received relatively little attention (Ma et al. 2010, Brown et al. 2014, Refsland and Fraterrigo 2018). Recently burned areas comprise a mosaic of varying fire effects, including tree mortality and impacts on understory cover, which in turn affect the degree to which shading, surface roughness, evapotranspiration, and albedo are altered relative to unburned forest (Liu 2005, Chambers 2005, Liu et al. 2019). For example, structural features such as standing dead trees may lessen the impacts of canopy loss on microclimate in burned areas (Hoecker et al. 2020), and changes in surface cover after fire affect land surface temperatures (Liu et al. 2019). Anticipating the vulnerability of forest vegetation to the combined effects of changing climate and fire regimes thus requires understanding the impacts of wildfires on microclimatic buffering, and the degree to which these impacts vary across fire severity and biophysical gradients.

Chapter 1

To understand how fire severity and biophysical context interact to influence microclimate conditions relevant to plant regeneration, we monitored near-ground air temperature and vapor pressure deficit (VPD) over the first two growing seasons after two wildfires in the U.S. northern Rocky Mountains. We sampled 33 sites, 11 of which were unburned, spanning gradients in fire severity, local water balance, and forest type. We focused on areas that burned at moderate or high severity, where post-fire tree regeneration is most critical for forest resilience to wildfire, and where microclimate is most likely to be influenced by fire-induced changes in forest canopy and understory cover. We expected that recently burned forests would experience greater microclimate extremes relative to unburned forests, with effects scaling directly with fire severity due to greater canopy loss, reduction in evapotranspiration, and initial decreases in surface albedo. We further expected that the relative effect of wildfire on microclimate would vary across time and space, with greater effects during times when ambient temperatures were high (e.g., hours within a day, and days within a season), and in more mesic sites where high evapotranspiration leads to greater microclimatic buffering capacity (von Arx et al. 2013, Davis et al. 2019b).

Methods

Study area and site selection

The study was conducted in the Lolo National Forest, in the northern Bitterroot Mountains of Montana (Fig. 1). The region is characterized by complex mountainous topography, with vegetation composition varying with elevation, slope, and aspect. At low to mid elevations (i.e., <1500 m) and xeric aspects, ponderosa pine (*Pinus ponderosa*), Douglas-fir (*Pseudotsuga menziesii*), and western larch (*Larix occidentalis*) typically dominate. Subalpine forest extends from c. 1500-2200 m in elevation, with dominant species including lodgepole pine

Chapter 1

(*Pinus contorta* var. *latifolia*), subalpine fir (*Abies lasiocarpa*), and Engelmann spruce (*Picea engelmannii*). In the northern end of the study area, mountain hemlock (*Tsuga mertensiana*) is also present at high elevations. Common understory species include green alder (*Alnus viridis*) and common huckleberry (*Vaccinium globulare*), with fireweed (*Epilobium angustifolium*) typically present in recently burned areas. Averaged across sites for the period 1981-2010, mean annual temperature is 5.2 °C and annual precipitation is 987 mm, with 20% falling during the snow-free season from June - September (PRISM Climate Group (Oregon State University) 2015).

We sampled 33 plots within two large fires that burned from July to September, 2017, a regionally extensive fire year associated with above-average warmth and aridity (Balch et al. 2018; Fig. 1). The Lolo Peak Fire affected c. 22,000 ha, with 20% of the fire area classified as high severity, 20% as moderate severity, 37% as low severity, and 23% unburned (MTBS Project (USDA Forest Service/U.S. Geological Survey) 2019). The Sunrise Fire affected c. 11,000 ha, with 15% high severity, 28% moderate severity, 53% low severity, and 4% unburned (MTBS). Potential study areas within each fire were identified using USFS Burned Area Reflectance Classification soil burn severity maps (30-m resolution), which are based on satellite imagery with field verification by emergency response teams, and are available prior to publication of MTBS burn severity products (fsapps.nwcg.gov). To achieve the goal of sampling across biophysical gradients, sites were stratified by elevation (low [1000-1500 m] and high [1500-2000 m]) and aspect (northern [315-45°] and southern [135-225°]). Within each stratum, we sampled an unburned plot, a plot that burned at high severity, and a plot that burned at moderate severity; each unburned plot was used as a reference for the two burned plots in the same stratum. This yielded 11 plots each in the unburned, moderate-, and high-severity

Chapter 1

categories. The median distance between paired burned and unburned sites was 0.48 km (Table A.1). Exact sampling locations were randomly identified in a geographic information system to satisfy these criteria and avoid planned salvage logging (K. Wetzstein, personal communication), while also being within 2 km of a road to ensure accessibility. Precise plot locations were shifted in the field where necessary to sample in the targeted severity class, based on a visual assessment of tree mortality and, for unburned plots, the absence of charred surface fuels and trees. Of the 33 plots, seven were moved up to 100 m from their original locations, and one unburned plot was moved 2 km.

Field measurements and data aggregation

Plot characteristics were measured using a 60-m long belt transect parallel to the fall line, which in most cases extended upslope from a microclimate sensor post (described below). Within each transect, overstory tree density, species composition, and percent mortality were quantified, and live and dead basal area were measured at meter 0, 30, and 60 on the transect. At six to 10 evenly spaced points along each transect, live and dead canopy cover were measured using a spherical densiometer, the distance to the nearest live tree was measured using a laser range finder, and bole scorch height of the nearest tree was measured as a coarse metric of fire behavior. At each of these points, ground cover measurements were taken using a 1-m² quadrat to quantify percent cover of bare ground or rock, litter, and vegetation. Plot averages of each metric were calculated. In addition, canopy cover at the location of the sensor post was measured and recorded separately as the sensor-specific canopy cover.

At each plot, a sensor measuring temperature and relative humidity was attached to a metal conduit pole 10 cm above the ground surface, within a radiation shield that performs similarly to commercially available shields (Holden et al. 2013). In 2018, data were collected

Chapter 1

from a total of 15 plots (five in each severity class) in the Lolo Peak Fire to capture the first post-fire growing season. In 2019, microclimate was monitored again at six of these original plots in the Lolo Peak Fire. In addition, 18 new plots were sampled in 2019: six in the Lolo Peak Fire and 12 in the Sunrise Fire. This yielded a sample size of 33 plots across both fires and years (Table A.1).

Sensors recorded temperature (T , °C) and relative humidity (RH, %) on half-hourly time steps over the snow-free season (June-September). Appendix A describes sensor calibration, used to account for the use of two different sensor models over the study, as well as quality control procedures. Vapor pressure deficit (VPD, kPa) was calculated based on temperature and relative humidity, using the following equation (cf. Monteith and Unsworth 2013):

$$\text{VPD} = \left[0.6112 \times e^{\frac{17.62 \times T}{T+243.12}} \right] \times \text{RH}/100$$

Data for each plot were aggregated to daily maximum temperature and daily maximum VPD by selecting the highest value over each 24-hour calendar day, regardless of the time at which it occurred (Appendix A). The difference in daily maximum temperature and VPD between each burned site and its paired unburned site was then calculated (ΔT_{max} , ΔV_{max}) and used as a response variable in further analyses. We focused on daily maxima because these represent stressful conditions for plants, and we used ΔT_{max} and ΔV_{max} as a metric of fire-caused change in warm-dry microclimatic extremes.

Site-level metrics of fire severity

We used both categorical (satellite-derived) and continuous (field-based) metrics of fire severity in our analyses. First, we used the plot-averaged dNBR metric from the Monitoring Trends in Burn Severity program (released after site selection, in 2018) to classify plots into discrete fire severity classes. We report non-parametric statistical comparisons of microclimate

Chapter 1

conditions among these discrete classes using Wilcoxon rank-sum tests. Second, we characterized fire severity at each plot using a suite of field measurements reflecting fire effects more precisely than satellite-derived metrics alone. We summarized these measurements using a PCA, described in detail in Appendix A. We used the first two principal components as predictor variables in our statistical models, allowing us to quantify distinct aspects of fire severity that do not covary. PCA Axis 1 (hereafter Axis1) reflects plot-averaged live canopy cover and basal area (positive values), and dead canopy cover and basal area, tree mortality, scorch height, and distance to seed source (negative values). PCA Axis 2 (hereafter Axis2) primarily reflects ground cover, with positive values associated with greater bare ground cover and negative values associated with greater vegetation cover; in burned plots, these values represent understory regrowth after fire. We thus interpret Axis1 as a metric of overstory fire effects and Axis2 as a metric of understory fire effects, and refer to these metrics as “field-based fire severity.”

Macroclimate gradients

To characterize the biophysical context of each plot, we calculated the long-term climatic water deficit (DEF, mm) by averaging annual values from 1981-2015 from a 250-m resolution downscaled climate product described by Holden et al. (2016, 2018). DEF thus represents a time-integrated measure of local water balance. We also calculated the heat load index (HLI) at 1/3 arc-second (c. 10-m) resolution following the McCune & Keon (2002) method using the *spatialEco* package in R. HLI is a unitless index that integrates the effects of aspect, slope, and latitude on potential solar heating. HLI and DEF were not significantly correlated ($r = 0.28$; $p = 0.21$, $t = 1.3$, $df = 20$).

To characterize temporal variability in ambient climate conditions at each plot, we used daily maximum temperature over the 2018 and 2019 sampling periods from the 4-km resolution

Chapter 1

gridMet product (Abatzoglou 2013). Study plots spanned seven distinct grid cells, with all but three sets of paired plots falling within a single grid cell. We used the gridMet-based temperature as a proxy for daily ambient (free-air) conditions at each plot ($T_{\max A}$, °C). This is well-justified, given that gridMet-derived daily temperatures were significantly correlated with sensor-measured daily temperature maxima at each plot, with an average correlation coefficient of 0.95 across all plots ($p < 0.0001$, $t = 34$, $df = 100$).

Statistical analyses

We used linear mixed-effects models to quantify the relative influence of field-based fire severity, biophysical site characteristics, and ambient weather conditions on daily differences in maximum temperature and VPD between burned and unburned sites (ΔT_{\max} and ΔV_{\max}). To minimize the effects of temporal autocorrelation, we subsampled each timeseries to retain one day out of every eight consecutive days, for a total of 29 days of observations (i.e., 13 days in 2018 and 16 days in 2019). This subsetting procedure was selected because a preliminary analysis of temporal autocorrelation at each site indicated significant autocorrelation for up to seven to eight days. Random intercept terms for the effects of site and sampling year, nested within site, were included to account for repeated measurements from the same sites within and between years. Predictor variables included site characteristics describing fire severity (Axis1 and Axis2) and biophysical context (DEF and HLI), as well as daily ambient weather conditions ($T_{\max A}$; Table 1). We also considered three additional predictor variables to account for biophysical differences between paired burned and unburned plots (Table 1). These were the difference in HLI and DEF between each paired burned and unburned plot, ΔHLI and ΔDEF , and the difference in canopy cover above the sensor post, $\Delta Canopy$. While values of ΔHLI and ΔDEF were generally small due to our stratified sampling design, $\Delta Canopy$ varied among sites

Chapter 1

and was retained in the reduced models. Alternate modeling approaches yielded similar results (e.g., directly modeling maximum temperature or VPD of the burned plots as a function of measured conditions in the unburned plots).

To evaluate the relative influence of canopy cover, topography, and fire severity on microclimate, we conducted model selection with different subsets of predictor variables and compared among the resulting “subset” models. A simple “null” model assumed that ΔT_{\max} and ΔV_{\max} were a function of ambient temperature ($T_{\max}A$) and the difference in canopy cover between the burned and unburned plot (ΔCanopy). The “topo” subset model added variables describing the biophysical context (DEF and HLI) to the null model, based on the hypothesis that topography mediates the effect of canopy loss on microclimate. The “fire” subset model added variables describing fire severity (Axis1 and Axis2) to the null model, based on the hypothesis that canopy loss and other fire effects (e.g., tree mortality, understory change) influence microclimate conditions. The full “topo + fire” model considered all predictors noted above. All models considered a quadratic term for $T_{\max}A$ as well as interaction terms (up to two-way) among predictors (e.g., $T_{\max}A$, HLI, DEF, Axis1, and Axis2).

We conducted model selection for each subset model described above and used cross-validated root mean squared error (RMSE) to evaluate model skill, ultimately selecting a single final model each for temperature and VPD (Table 2). Models were selected initially through backward elimination to retain all significant terms based on F-tests ($p < 0.05$) using the lmerTest package in R (Kuznetsova et al. 2017). To avoid overfitting the data, we considered dropping additional terms based on cross-validated RMSE. We used a leave-one-out cross-validation procedure by holding out the data from one plot and training the model on the data from the remaining 21 plots, and then predicting on the holdout data and calculating the RMSE;

this was repeated for all plots to obtain an average cross-validated RMSE. In selecting the final models for ΔT_{\max} and ΔV_{\max} , we balanced predictive skill (RMSE) with parsimony.

Results

Daily differences in maximum temperature (ΔT_{\max}) and VPD (ΔV_{\max}) between paired burned and unburned plots varied throughout the season, with the largest differences occurring when daily temperatures were highest (Fig. B.1). Averaged across the season, daily maximum temperatures were 3.7 ± 2.4 °C (standard deviation) higher in sites classified as high severity relative to unburned sites ($p = 0.015$, $W = 82$, $n = 11$). Across both severity classes, maximum temperatures were 2.6 ± 2.7 °C higher on average in burned sites than in unburned sites ($p = 0.048$, $W = 338$, $n = 22$; Fig. 2). Maximum daily VPD was 0.81 ± 0.40 kPa (58%) higher on average in sites burned at high severity than in unburned sites ($p = 0.003$, $W = 107$, $n = 11$), and 0.52 ± 0.54 kPa (30%) higher in burned than unburned sites across both fire severity classes ($p = 0.024$, $W = 180$, $n = 22$). Average daily minimum temperature and VPD were not significantly different in burned compared to unburned sites (p -values > 0.10 ; Fig. 2).

When predicting ΔT_{\max} , the model including topography and fire severity (“topo + fire” model) provided the best predictive skill, with an average cross-validated RMSE of 2.50 °C \pm 0.90 (standard deviation) (Table 2). Differences in daily maximum temperatures (ΔT_{\max}) were explained by canopy cover (ΔCanopy), ambient weather conditions ($T_{\max A}$), long-term climatic water deficit (DEF), ground cover (Axis2), potential solar heating (HLI), and interaction terms among these variables (Table B.1). Burned and unburned sites with greater differences in canopy cover above the sensor tended to have larger differences in daily maximum temperatures (Fig. 3). Values of ΔCanopy were not significantly correlated with Axis1 values ($r = 0.27$; $p = 0.23$, $t =$

1.2, $df = 20$) or dNBR ($r = -0.11$; $p = 0.63$, $t = -0.48$, $df = 20$), suggesting that this effect of canopy cover is not reflected in field-based fire severity metrics at the plot scale.

After accounting for differences in canopy cover, ΔT_{\max} generally increased with $T_{\max A}$, but the effect was contingent on DEF. Differences in daily maximum temperatures (ΔT_{\max}) tended to be low in sites with high DEF (i.e., warm-dry sites), and varied little with ambient temperatures ($T_{\max A}$) (Fig. 4); in contrast, ΔT_{\max} increased with $T_{\max A}$ in sites with low DEF (i.e., cool-moist sites). For example, on days when ambient temperatures were high (i.e., exceeding the 75th percentile of 26.7 °C), ΔT_{\max} averaged 6.1 ± 2.1 °C among sites with low DEF (i.e., below the 25th percentile) and -0.02 ± 3.1 °C among sites with high DEF (i.e., above the 75th percentile). In addition, ΔT_{\max} was lower in sites with above-average HLI (i.e., above the 50th percentile), averaging 1.6 ± 2.1 °C; this contrasts with an average ΔT_{\max} of 2.6 °C across all sites. This effect was contingent on both DEF and Axis2. Differences in maximum temperatures (ΔT_{\max}) tended to be low in warm, dry sites with high HLI and DEF, but varied little with HLI among sites with low DEF or high vegetation cover (i.e., negative Axis2 values; Fig. 4). Further, ΔT_{\max} tended to be greater in sites with more exposed ground (i.e. above the 75th percentile of Axis2 values), averaging 4.4 ± 2.2 °C, with smaller ΔT_{\max} among sites with high HLI (Fig. 4). Overall, ΔT_{\max} depended on canopy cover, ambient weather conditions, biophysical context, and fire severity.

When predicting ΔV_{\max} , the model including topography only (“topo” model) had the best combination of predictive skill and parsimony, with an average cross-validated RMSE of $0.62 \text{ kPa} \pm 0.25$ (standard deviation; Table 2). Differences in daily maximum VPD (ΔV_{\max}) were explained ΔCanopy , $T_{\max A}$, DEF, a quadratic term of $T_{\max A}$, and an interaction term between $T_{\max A}$ and DEF (Table B.1). Average ΔV_{\max} was greater in sites with larger differences in canopy

Chapter 1

cover (Fig. 3). After accounting for this effect, ΔV_{\max} tended to increase at higher ambient temperatures ($T_{\max A}$), but the effect was contingent on DEF, exhibiting a pattern similar to the model for ΔT_{\max} described above. Cooler, moister sites (i.e., low DEF) had a strong positive relationship between ΔV_{\max} and $T_{\max A}$, whereas warmer, drier sites (i.e., high DEF) had less variation in ΔV_{\max} (Fig. 5). For example, on days when ambient temperatures were high (i.e., exceeding the 75th percentile), ΔV_{\max} averaged 1.55 ± 0.56 kPa at sites with low DEF (i.e., below the 25th percentile), and -0.22 ± 0.90 kPa at sites with relatively high DEF (i.e., above the 75th percentile). The topographic variable representing potential solar exposure (HLI) was not retained in the final model, perhaps because the effect of topography on local climate is, to some degree, reflected in the calculation of climatic water deficit, although at a different spatial resolution. Overall, ΔV_{\max} depended on canopy cover, ambient weather conditions, and local water balance.

Discussion

Our study documents substantial impacts wildfire on microclimatic extremes in forest ecosystems, quantifying changes that are biologically meaningful for the post-fire reestablishment of tree seedlings and understory vegetation. We also highlight that these impacts vary significantly based not only on ambient conditions and fire severity, but also on the biophysical context of a site, including long-term climatic water deficit. Our findings thus have important implications for anticipating forest ecosystem responses to increasing moisture deficits and fire activity expected in the future, and they provide quantitative information useful in modeling such scenarios.

Fire-related changes in microclimate are biologically meaningful

Our results indicate that warm, dry microclimatic extremes near the ground surface are amplified in the post-fire environment relative to unburned forest stands, with the strongest effects occurring when ambient temperatures are highest (Fig. 2; Fig. B.1). These effects are likely due to increased surface radiation intensity, reduced evaporative cooling, and increased sensible heating in the post-fire environment. The buffering effects of canopies are largely a function of light interception and evaporative cooling through transpiration (von Arx et al. 2013, Davis et al. 2019b). Initially after a fire, reduced light interception and reduced albedo due to charring and loss of plant cover increases surface radiation intensity during the snow-free season, which contributes to higher surface temperatures and greater potential for heating of soil and air (Ripley and Archibold 1999, Chambers 2005, Tsuyuzaki et al. 2009, Ma et al. 2010, Liu et al. 2019). Further, reduced evapotranspiration decreases latent heat flux and increases sensible heating in recently burned forests (Liu 2005, Chambers 2005, Liu et al. 2019). While we cannot directly infer the mechanisms through which wildfires alter microclimates because we did not fully characterize the surface energy budget, our results are consistent with studies documenting increased air temperature or VPD after fires (Ripley and Archibold 1999, Ma et al. 2010, Bello-Rodríguez et al. 2019), and studies that examined the influence of canopy cover on microclimate independent of fire (e.g., Davis et al. 2019b).

The differences in daily maximum temperature and VPD observed in this study are large enough to be biologically meaningful for understory plants and tree regeneration. Survival of tree seedlings in early life stages depends on environmental conditions near the ground surface (Johnson et al. 2011). High temperatures can directly girdle stems, and high evaporative potential (i.e., VPD) in the absence of ample soil water causes moisture stress and ultimately mortality (Kolb and Robberecht 1996, Johnson et al. 2011, Reinhardt et al. 2015). For example, an

Chapter 1

increase in mean midday air temperatures during the growing season of 3.2-4.4 °C reduced seedling survival of *P. ponderosa* and *P. menziesii* by c. 30-60% in an experimental study in Colorado (Rother et al. 2015). In the current study, we found that daily differences in maximum temperature and VPD between burned and unburned plots averaged 4.8 ± 4.5 °C and 1.2 ± 1.3 kPa during the hottest 10 consecutive days of the study period, with maxima of 12.8 °C and 4.7 kPa. Since our study was not designed to quantify the precise conditions experienced by seedlings, we can only make limited inferences into the biotic impacts of the observed changes. Nevertheless, fire-induced changes in microclimate of the magnitude documented clearly have the potential to impact the establishment and survival of tree seedlings and likely other understory vegetation (Stevens et al. 2015, Rother et al. 2015, Davis et al. 2019a, Hansen and Turner 2019).

Fire-related changes in microclimate vary with fire severity

While it is evident that wildfire affects post-fire microclimate conditions, we found that these effects were not uniform across environmental and fire-severity gradients. Consistent with our hypotheses, warm-dry microclimate extremes were greatest among sites that experienced high-severity fire (Fig. B.2). This effect of fire severity on microclimate was due in part to canopy loss, as evidenced by our statistical models predicting differences in daily maximum temperature and VPD between paired burned and unburned plots. Fire-caused differences in microclimate were greater at sites that had larger differences in canopy cover (Fig. 3), consistent with studies that demonstrate the strong influence of canopy cover on microclimatic buffering capacity (e.g., Rambo and North 2009, Suggitt et al. 2011, von Arx et al. 2013, Davis et al. 2019b). After accounting for variability in total canopy cover, our final statistical models revealed no additional effect of variability in live versus dead canopy cover among plots

Chapter 1

(represented by the Axis1 metric); this suggests that moderate- and high-severity fire most strongly affected microclimate directly through the loss of canopy shading. Residual dead trees, including the fine branches that are retained for several years after fire, can thus contribute significantly to regulating near-ground microclimates after fire (Fontaine et al. 2010, Hoecker et al. 2020), potentially increasing the likelihood of successful post-fire tree regeneration where seed availability is not limiting.

In addition to the importance of canopy cover, our statistical models suggest that fire severity also affects microclimate through its impact on understory cover, which interacts with topography (i.e., solar exposure) to influence temperature extremes. Maximum temperatures tended to be higher at sites with more bare ground and less understory vegetation (Fig. 4). Several mechanisms likely account for this pattern. Understory plant transpiration may contribute to evaporative cooling, which was likely most important in severely burned areas where overstory transpiration was low. This effect was least pronounced in sites with high solar exposure, where midday temperatures are more likely to be driven by direct solar radiation, particularly if plants reduce stomatal conductance in response to moisture stress (Marshall and Waring 1984). Further, albedo tends to increase with total vegetation cover after fire (Tsuyuzaki et al. 2009), suggesting that greater reflectance in sites with more understory vegetation regulated temperature extremes. These results imply that microclimate extremes will attenuate over time as vegetation reestablishes, although the microclimatic buffering capacity of structurally complex stands may take decades to develop (Frey et al. 2016, Kovács et al. 2017, Bello-Rodríguez et al. 2019).

Fire-related changes in microclimate vary with biophysical context

Chapter 1

The effect of wildfire on microclimate also depends strongly on biophysical context. We found that sites with high long-term climatic water availability experienced larger fire-caused changes in microclimate. The effect of water availability on microclimate is both direct, through evaporative cooling (i.e., latent heat flux), and indirect, through its influence on vegetation. Drier sites, with lower water availability to support evapotranspiration, have less potential to buffer microclimatic extremes independent of differences in canopy cover (Davis et al. 2019b). Sites with low long-term water availability also support less vegetation, consistent with a modest negative correlation between total basal area and climatic water deficit ($r = -0.47$; $p = 0.005$, $t = -3.0$, $df = 31$). Under canopies with low leaf area, the capacity for microclimatic buffering is low and declines as ambient conditions become warmer and drier (von Arx et al. 2013), perhaps due to greater direct solar radiation and turbulent air mixing. In contrast, in cool-mesic sites, conditions in burned areas became increasingly warm and dry relative to unburned forest as ambient temperatures increased, revealing greater relative impacts of fire on microclimate compared with warm-dry sites (Fig 4, 5). Although we did not distinguish between the direct and indirect effects of local water balance on microclimate, our results indicate that moisture availability, and to a lesser extent solar exposure, govern the degree to which wildfires impact microclimate.

The remaining unexplained variability in temperature and VPD in our models likely reflects the lack of information on daily and seasonal changes in insolation or soil moisture, and fire effects on soil hydrology. Differences in canopy structure interact with soil water to influence understory microclimates (von Arx et al. 2013), and fire can result in either increased or decreased soil moisture (Certini 2005, Ma et al. 2010, Cardenas and Kanarek 2014). Further, soil moisture affects both microclimate conditions and the vulnerability of vegetation to changes

in air temperature and VPD. Despite this caveat, our results suggest that the impacts of wildfires on microclimatic extremes increase with fire severity, decrease with vegetation regrowth, and are greatest in climatically cool-wet sites.

Implications for forest response to climate warming and increased wildfire activity

Altered microclimate in post-fire environments is a key mechanism through which fire can catalyze vegetation changes that otherwise unfold more slowly with ongoing climate change. Microclimatic buffering mitigates the effects of climate change on understory organisms by reducing their exposure to climatic extremes (Jentsch and Beierkuhnlein 2008, De Boeck et al. 2011, Reyer et al. 2013). Empirical evidence highlights that plant-water relations are particularly sensitive to extremes in aridity (Reyer et al. 2013), implying that fire-induced losses of forest buffering capacity increase the vulnerability of understory plants to climatic stressors. Further, given strong linkages between VPD and fire activity in western North America (Sedano and Randerson 2014, Parks and Abatzoglou 2020, Higuera and Abatzoglou 2021), elevated VPD may increase the vulnerability of recently burned areas to subsequent fire if fuel is not limiting, which can ultimately erode forest resilience (Turner et al. 2019). While our results suggest that retention of standing dead trees and post-fire vegetation recovery would attenuate the impacts of fire on microclimate, fire-induced changes in microclimate are nevertheless significant enough to impact patterns of plant regeneration. These impacts may be direct, by favoring species that are more drought-tolerant or species that are able to regenerate through resprouting (Davis et al. 2018), or indirect, by altering future patterns of burning.

Our results also suggest that we may be underestimating the potential impacts of fire-caused changes in microclimate in cool-moist settings. While fire-catalyzed vegetation shifts are considered most likely near the warm-dry edges of species ranges (e.g., Donato et al. 2016,

Chapter 1

Davis et al. 2019a), we found that cool-moist forests experienced greater relative impacts of fire on microclimate due to differences in canopy cover and local water balance (Davis et al. 2019b). This suggests that fire-caused changes in microclimate could amplify regional warming, further pushing conditions closer to climatic limits for tree regeneration (Andrus et al. 2018, Davis et al. 2019a). Anticipating vegetation responses to the combined impacts of climate warming and increasing fire activity in cool-moist forests should thus take into account the substantial effects of fire on microclimate conditions.

Finally, our study informs management goals focused on maintaining forests for a host of ecosystem services. Our findings suggest that management actions aimed at reducing fire severity in low-elevation forests would help ameliorate post-fire microclimate extremes, particularly in cooler and moister settings. This is consistent with the recognized importance of potential “fire refugia” that promote forest resilience through seed provision (Krawchuk et al. 2016, Coop et al. 2019). Similar efforts to reduce fire severity in cool-moist subalpine and mixed-conifer forests, while impactful on post-fire microclimate, would have little ecological basis given a history of high-severity crown fire (e.g., Schoennagel et al. 2004). Further, our results imply that retaining standing dead trees after fires contributes to the moderation of microclimates and can thus indirectly support post-fire tree regeneration.

The inferences from this study apply most directly to the biophysical context of mixed-conifer and subalpine forests of the northern Rocky Mountains, which represent a small range of conditions relative to forests of western North America. In addition, it remains uncertain how microclimate conditions will change over time after fire in cool-wet and warm-dry forest types, which differ in rates of vegetation recovery. Future research should examine these relationships over a wider range of climate and forest conditions (e.g., structure, fire severity), and over longer

Chapter 1

timescales, to better understand the interactive effects of fire, vegetation, and local water balance on microclimatic buffering.

Literature Cited

- Abatzoglou, J. T. 2013. Development of gridded surface meteorological data for ecological applications and modelling. *International Journal of Climatology* 33:121–131.
- Abatzoglou, J. T., and A. P. Williams. 2016. Impact of anthropogenic climate change on wildfire across western US forests. *Proceedings of the National Academy of Sciences* 113:11770–11775.
- Anderson-Teixeira, K. J., A. D. Miller, J. E. Mohan, T. W. Hudiburg, B. D. Duval, and E. H. DeLucia. 2013. Altered dynamics of forest recovery under a changing climate. *Global Change Biology* 19:2001–2021.
- Andrus, R. A., B. J. Harvey, K. C. Rodman, S. J. Hart, and T. T. Veblen. 2018. Moisture availability limits subalpine tree establishment. *Ecology* 99:567–575.
- von Arx, G., E. Graf Pannatier, A. Thimonier, and M. Rebetez. 2013. Microclimate in forests with varying leaf area index and soil moisture: potential implications for seedling establishment in a changing climate. *Journal of Ecology* 101:1201–1213.
- Balch, J., T. Schoennagel, A. Williams, J. Abatzoglou, M. Cattau, N. Mietkiewicz, and L. St. Denis. 2018. Switching on the Big Burn of 2017. *Fire* 1:17.
- Bello-Rodríguez, V., L. A. Gómez, Á. Fernández López, M. J. Del-Arco-Aguilar, R. Hernández-Hernández, B. Emerson, and J. M. González-Mancebo. 2019. Short- and long-term effects of fire in subtropical cloud forests on an oceanic island. *Land Degradation & Development* 30:448–458.

Chapter 1

- De Boeck, H. J., F. E. Dreesen, I. A. Janssens, and I. Nijs. 2011. Whole-system responses of experimental plant communities to climate extremes imposed in different seasons. *New Phytologist* 189:806–817.
- Brown, C. D., J. Liu, G. Yan, and J. F. Johnstone. 2015. Disentangling legacy effects from environmental filters of postfire assembly of boreal tree assemblages. *Ecology* 96:3023–3032.
- Brown, D. J., I. Mali, and M. R. J. Forstner. 2014. Wildfire and Postfire restoration action effects on microclimate and seedling pine tree survivorship. *Journal of Fish and Wildlife Management* 5:174–182.
- Cardenas, M. B., and M. R. Kanarek. 2014. Soil moisture variation and dynamics across a wildfire burn boundary in a loblolly pine (*Pinus taeda*) forest. *Journal of Hydrology* 519:490–502.
- Certini, G. 2005. Effects of fire on properties of forest soils: a review. *Oecologia* 143:1–10.
- Chambers, S. D. 2005. Fire effects on net radiation and energy partitioning: Contrasting responses of tundra and boreal forest ecosystems. *Journal of Geophysical Research* 110:D09106.
- Coop, J. D., T. J. Delory, W. M. Downing, S. L. Haire, M. A. Krawchuk, C. Miller, M. A. Parisien, and R. B. Walker. 2019. Contributions of fire refugia to resilient ponderosa pine and dry mixed-conifer forest landscapes. *Ecosphere* 10:e02809.
- Coop, J. D., S. A. Parks, C. S. Stevens-Rumann, S. D. Crausbay, P. E. Higuera, M. D. Hurteau, A. Tepley, E. Whitman, T. Assal, B. M. Collins, K. T. Davis, S. Dobrowski, D. A. Falk, P. J. Fornwalt, P. Z. Fulé, B. J. Harvey, V. R. Kane, C. E. Littlefield, E. Q. Margolis, M.

Chapter 1

- North, M. A. Parisien, S. Prichard, and K. C. Rodman. 2020. Wildfire-Driven Forest Conversion in Western North American Landscapes. *BioScience* 70:659–673.
- Crotteau, J. S., J. Morgan Varner, and M. W. Ritchie. 2013. Post-fire regeneration across a fire severity gradient in the southern Cascades. *Forest Ecology and Management* 287:103–112.
- Davis, K. T., S. Z. Dobrowski, P. E. Higuera, Z. A. Holden, T. T. Veblen, M. T. Rother, S. A. Parks, A. Sala, and M. P. Maneta. 2019a. Wildfires and climate change push low-elevation forests across a critical climate threshold for tree regeneration. *Proceedings of the National Academy of Sciences of the United States of America* 116:6193–6198.
- Davis, K. T., S. Z. Dobrowski, Z. A. Holden, P. E. Higuera, and J. T. Abatzoglou. 2019b. Microclimatic buffering in forests of the future: the role of local water balance. *Ecography* 42:1–11.
- Davis, K. T., P. E. Higuera, and A. Sala. 2018. Anticipating fire-mediated impacts of climate change using a demographic framework. *Functional Ecology* 32:1729–1745.
- Donato, D. C., B. J. Harvey, and M. G. Turner. 2016. Regeneration of montane forests 24 years after the 1988 Yellowstone fires: A fire-catalyzed shift in lower treelines? *Ecosphere* 7:e01410.
- Flannigan, M. D., K. A. Logan, B. D. Amiro, W. R. Skinner, and B. J. Stocks. 2005. Future Area Burned in Canada. *Climatic Change* 72:1–16.
- Fontaine, J. B., D. C. Donato, J. L. Campbell, J. G. Martin, and B. E. Law. 2010. Effects of post-fire logging on forest surface air temperatures in the Siskiyou Mountains, Oregon, USA. *Forestry* 83:477–482.

Chapter 1

- De Frenne, P., F. Zellweger, F. Rodríguez-Sánchez, B. R. Scheffers, K. Hylander, M. Luoto, M. Vellend, K. Verheyen, and J. Lenoir. 2019. Global buffering of temperatures under forest canopies. *Nature Ecology & Evolution* 3:744–749.
- Frey, S. J. K., A. S. Hadley, S. L. Johnson, M. Schulze, J. A. Jones, and M. G. Betts. 2016. Spatial models reveal the microclimatic buffering capacity of old-growth forests. *Science Advances* 2:e1501392.
- Gillett, N. P., A. J. Weaver, F. W. Zwiers, and M. D. Flannigan. 2004. Detecting the effect of climate change on Canadian forest fires. *Geophysical Research Letters* 31:L18211.
- Hansen, W. D., and M. G. Turner. 2019. Origins of abrupt change? Postfire subalpine conifer regeneration declines nonlinearly with warming and drying. *Ecological Monographs* 89:e01340.
- Hesketh, M., D. F. Greene, and E. Pouden. 2009. Early establishment of conifer recruits in the northern Rocky Mountains as a function of postfire duff depth. *Canadian Journal of Forest Research* 39:2059–2064.
- Higuera, P. E., and J. T. Abatzoglou. 2021. Record-setting climate enabled the extraordinary 2020 fire season in the western United States. *Global Change Biology* 27:1–2.
- Hoecker, T. J., W. D. Hansen, and M. G. Turner. 2020. Topographic position amplifies consequences of short-interval stand-replacing fires on postfire tree establishment in subalpine conifer forests. *Forest Ecology and Management* 478:118523.
- Holden, Z. A., A. E. Klene, R. F. Keefe, and G. G. Moisen. 2013. Design and evaluation of an inexpensive radiation shield for monitoring surface air temperatures. *Agricultural and Forest Meteorology* 180:281–286.

Chapter 1

- Holden, Z. A., A. Swanson, A. E. Klene, J. T. Abatzoglou, S. Z. Dobrowski, S. A. Cushman, J. Squires, G. G. Moisen, and J. W. Oyler. 2016. Development of high-resolution (250 m) historical daily gridded air temperature data using reanalysis and distributed sensor networks for the US Northern Rocky Mountains. *International Journal of Climatology* 36:3620–3632.
- Holden, Z. A., A. Swanson, C. H. Luce, W. M. Jolly, M. Maneta, J. W. Oyler, D. A. Warren, R. Parsons, and D. Affleck. 2018. Decreasing fire season precipitation increased recent western US forest wildfire activity. *Proceedings of the National Academy of Sciences* 115:E8349–E8357.
- Jentsch, A., and C. Beierkuhnlein. 2008. Research frontiers in climate change: Effects of extreme meteorological events on ecosystems. *Comptes Rendus - Geoscience* 340:621–628.
- Johnson, D. M., K. A. McCulloh, and K. Reinhardt. 2011. The Earliest Stages of Tree Growth: Development, Physiology and Impacts of Microclimate. Pages 65–87 in F. C. Meinzer, B. Lachenbruch, and T. E. Dawson, editors. *Size- and Age-Related Changes in Tree Structure and Function*. Springer Netherlands, Dordrecht, Netherlands.
- Kemp, K. B., P. E. Higuera, P. Morgan, and J. T. Abatzoglou. 2019. Climate will increasingly determine post-fire tree regeneration success in low-elevation forests, Northern Rockies, USA. *Ecosphere* 10:e02568.
- Kolb, P. F., and R. Robberecht. 1996. High temperature and drought stress effects on survival of *Pinus ponderosa* seedlings. *Tree Physiology* 16:665–672.
- Kovács, B., F. Tinya, and P. Ódor. 2017. Stand structural drivers of microclimate in mature temperate mixed forests. *Agricultural and Forest Meteorology* 234–235:11–21.

Chapter 1

- Krawchuk, M. A., S. L. Haire, J. Coop, M. A. Parisien, E. Whitman, G. Chong, and C. Miller. 2016. Topographic and fire weather controls of fire refugia in forested ecosystems of northwestern North America. *Ecosphere* 7:e01632.
- Kuznetsova, A., P. B. Brockhoff, and R. H. B. Christensen. 2017. lmerTest Package: Tests in Linear Mixed Effects Models . *Journal of Statistical Software* 82:1–26.
- Liu, H. 2005. Changes in the surface energy budget after fire in boreal ecosystems of interior Alaska: An annual perspective. *Journal of Geophysical Research* 110:D13101.
- Liu, Z., A. P. Ballantyne, and L. A. Cooper. 2019. Biophysical feedback of global forest fires on surface temperature. *Nature Communications* 10:214.
- Ma, S., A. Concilio, B. Oakley, M. North, and J. Chen. 2010. Spatial variability in microclimate in a mixed-conifer forest before and after thinning and burning treatments. *Forest Ecology and Management* 259:904–915.
- Marshall, J. D., and R. H. Waring. 1984. Conifers and broadleaf species: stomatal sensitivity differs in western Oregon. *Canadian Journal of Forest Research* 14:905–908.
- McCune, B., and D. Keon. 2002. Equations for potential annual direct incident radiation and heat load. *Journal of Vegetation Science* 13:603–606.
- McKenzie, D., and J. S. Littell. 2017. Climate change and the eco-hydrology of fire: Will area burned increase in a warming western USA. *Ecological Applications* 27:26–36.
- Monteith, J., and M. Unsworth. 2013. *Principles of Environmental Physics: Plants, Animals, and the Atmosphere*. Page *Principles of Environmental Physics: Plants, Animals, and the Atmosphere: Fourth Edition*. Fourth. Elsevier Academic Press, Cambridge, MA, USA.
- Montes-Helu, M. C., T. Kolb, S. Dore, B. Sullivan, S. C. Hart, G. Koch, and B. A. Hungate. 2009. Persistent effects of fire-induced vegetation change on energy partitioning and

Chapter 1

- evapotranspiration in ponderosa pine forests. *Agricultural and Forest Meteorology* 149:491–500.
- MTBS Project (USDA Forest Service/U.S. Geological Survey). 2019. MTBS Data Access: Fire Level Geospatial Data. <http://mtbs.gov>.
- Parks, S. A., and J. T. Abatzoglou. 2020. Warmer and Drier Fire Seasons Contribute to Increases in Area Burned at High Severity in Western US Forests From 1985 to 2017. *Geophysical Research Letters* 47:e2020GL089858.
- PRISM Climate Group (Oregon State University). 2015. PRISM 30-Year Normals. Oregon State University. <http://prism.oregonstate.edu>.
- Rambo, T. R., and M. P. North. 2009. Canopy microclimate response to pattern and density of thinning in a Sierra Nevada forest. *Forest Ecology and Management* 257:435–442.
- Refsland, T., and J. Fraterrigo. 2018. Fire increases drought vulnerability of *Quercus alba* juveniles by altering forest microclimate and nitrogen availability. *Functional Ecology* 32:2298–2309.
- Reinhardt, K., M. J. Germino, L. M. Kueppers, J.-C. Domec, and J. Mitton. 2015. Linking carbon and water relations to drought-induced mortality in *Pinus flexilis* seedlings. *Tree Physiology* 35:771–782.
- Reyer, C. P. O., S. Leuzinger, A. Rammig, A. Wolf, R. P. Bartholomeus, A. Bonfante, F. de Lorenzi, M. Dury, P. Gloning, R. Abou Jaoudé, T. Klein, T. M. Kuster, M. Martins, G. Niedrist, M. Riccardi, G. Wohlfahrt, P. de Angelis, G. de Dato, L. François, A. Menzel, and M. Pereira. 2013. A plant's perspective of extremes: terrestrial plant responses to changing climatic variability. *Global Change Biology* 19:75–89.

Chapter 1

- Ripley, E. A., and O. W. Archibold. 1999. Effects of burning on prairie aspen grove microclimate. *Agriculture, Ecosystems and Environment* 72:227–237.
- Rother, M. T., T. T. Veblen, and L. G. Furman. 2015. A field experiment informs expected patterns of conifer regeneration after disturbance under changing climate conditions. *Canadian Journal of Forest Research* 45:1607–1616.
- Schoennagel, T., T. T. Veblen, and W. H. Romme. 2004. The Interaction of Fire, Fuels, and Climate across Rocky Mountain Forests. *BioScience* 54:661–676.
- Sedano, F., and J. T. Randerson. 2014. Multi-scale influence of vapor pressure deficit on fire ignition and spread in boreal forest ecosystems. *Biogeosciences* 11:3739–3755.
- Serra-Diaz, J. M., C. Maxwell, M. S. Lucash, R. M. Scheller, D. M. Laflower, A. D. Miller, A. J. Tepley, H. E. Epstein, K. J. Anderson-Teixeira, and J. R. Thompson. 2018. Disequilibrium of fire-prone forests sets the stage for a rapid decline in conifer dominance during the 21st century. *Scientific Reports* 8:6749.
- Stevens, J. T., H. D. Safford, S. Harrison, and A. M. Latimer. 2015. Forest disturbance accelerates thermophilization of understory plant communities. *Journal of Ecology* 103:1253–1263.
- Suggitt, A. J., P. K. Gillingham, J. K. Hill, B. Huntley, W. E. Kunin, D. B. Roy, and C. D. Thomas. 2011. Habitat microclimates drive fine-scale variation in extreme temperatures. *Oikos* 120:1–8.
- Tsuyuzaki, S., K. Kushida, and Y. Kodama. 2009. Recovery of surface albedo and plant cover after wildfire in a *Picea mariana* forest in interior Alaska. *Climatic Change* 93:517–525.

Chapter 1

- Turner, M. G., K. H. Braziunas, W. D. Hansen, and B. J. Harvey. 2019. Short-interval severe fire erodes the resilience of subalpine lodgepole pine forests. *Proceedings of the National Academy of Sciences* 116:11319–11328.
- Westerling, A. L. 2016. Increasing western US forest wildfire activity: sensitivity to changes in the timing of spring. *Philosophical transactions of the Royal Society of London. Series B, Biological sciences* 371:20150178.
- Westerling, A. L., M. G. Turner, E. A. H. Smithwick, W. H. Romme, and M. G. Ryan. 2011. Continued warming could transform Greater Yellowstone fire regimes by mid-21st century. *Proceedings of the National Academy of Sciences of the United States of America* 108:13165–70.
- Young, A. M., P. E. Higuera, P. A. Duffy, and F. S. Hu. 2017. Climatic thresholds shape northern high-latitude fire regimes and imply vulnerability to future climate change. *Ecography* 40:606–617.

CHAPTER 1

Tables

Table 1. Description of the response and predictor variables used in the statistical models.

Variable Name	Code	Units	Description
Response Variables			
Daily difference in maximum temperature	ΔT_{\max}	°C	Difference in daily maximum temperature between paired burned and unburned sites
Daily difference in maximum VPD	ΔV_{\max}	kPa	Difference in daily maximum vapor pressure deficit between paired burned and unburned sites
Explanatory Variables			
Ambient conditions			
GridMET daily maximum temperature	$T_{\max A}$	°C	daily maximum temperature derived from gridMET (4-km resolution; Abatzoglou 2013)
Biophysical site characteristics			
Climatic water deficit	DEF	cm	Mean annual climatic water deficit, a measure of unmet atmospheric demand for water, averaged over 1981-2015 for each burned site (250 m resolution)
Heat load index	HLI	unitless	Index of potential solar heating based on slope, aspect, and latitude of each burned site (c. 10 m resolution)
Field-based fire severity			
PCA Axis 1	Axis1	unitless	Index of fire severity based on plot-averaged tree mortality and live and dead canopy cover, derived from PCA (Fig. A.3)
PCA Axis 2	Axis2	unitless	Index of fire severity and vegetation regrowth based on plot-averaged ground cover, derived from PCA (Fig. A.3)
Site-difference variables			
Difference in canopy cover from unburned	ΔCanopy	%	Difference in total canopy cover directly over the sensor post between burned and unburned plots
Difference in DEF	ΔDEF	mm	Difference in climatic water deficit between burned and unburned plots
Difference in HLI	ΔHLI	unitless	Difference in heat load index between burned and unburned plots

Table 2. Comparison among candidate models, showing terms retained in final models and average cross-validated RMSE (\pm one standard deviation). Models include a null model (canopy cover only); a topo model (canopy cover + topographic variables), a fire model (canopy cover + fire severity variables), and a topo + fire model considering all potential predictors. Variable codes are described in Table 1. †Indicates selection as the final model reported on in the text.

Model	Predictors considered	Fixed effects terms	RMSE
Temperature (ΔT_{\max})			$^{\circ}\text{C}$
Null	$\Delta\text{Canopy}, T_{\max}A$	$\Delta\text{Canopy} + T_{\max}A$	2.82 \pm 1.23
Topo	$\Delta\text{Canopy}, T_{\max}A, \text{DEF}, \text{HLI}$	$\Delta\text{Canopy} + T_{\max}A + \text{DEF} + T_{\max}A:\text{DEF}$	2.80 \pm 0.96
Fire	$\Delta\text{Canopy}, T_{\max}A, \text{Axis1}, \text{Axis2}$	$\Delta\text{Canopy} + T_{\max}A + \text{Axis2} + T_{\max}A:\text{Axis2}$	2.75 \pm 1.01
Topo + Fire†	$\Delta\text{Canopy}, T_{\max}A, \text{DEF}, \text{HLI}, \text{Axis1}, \text{Axis2}$	$\Delta\text{Canopy} + T_{\max}A + \text{DEF} + \text{Axis2} + \text{HLI} + T_{\max}A:\text{DEF} + \text{HLI}:\text{DEF} + \text{HLI}:\text{Axis2}$	2.50 \pm 0.90
VPD (ΔV_{\max})			kPa
Null	$\Delta\text{Canopy}, T_{\max}A$	$\Delta\text{Canopy} + T_{\max}A + T_{\max}A^2$	0.67 \pm 0.36
Topo†	$\Delta\text{Canopy}, T_{\max}A, \text{DEF}, \text{HLI}$	$\Delta\text{Canopy} + T_{\max}A + T_{\max}A^2 + \text{DEF} + T_{\max}A:\text{DEF} + T_{\max}A^2:\text{DEF}$	0.62 \pm 0.25
Fire	$\Delta\text{Canopy}, T_{\max}A, \text{Axis1}, \text{Axis2}$	$\Delta\text{Canopy} + T_{\max}A + T_{\max}A^2 + \text{Axis2} + T_{\max}A:\text{Axis2} + T_{\max}A^2:\text{Axis2}$	0.65 \pm 0.32
Topo + Fire	$\Delta\text{Canopy}, T_{\max}A, \text{DEF}, \text{HLI}, \text{Axis1}, \text{Axis2}$	$\Delta\text{Canopy} + T_{\max}A + T_{\max}A^2 + \text{DEF} + \text{Axis2} + \text{HLI} + T_{\max}A:\text{DEF} + T_{\max}A^2:\text{DEF} + \text{HLI}:\text{DEF} + \text{HLI}:\text{Axis2}$	0.60 \pm 0.31

Figures

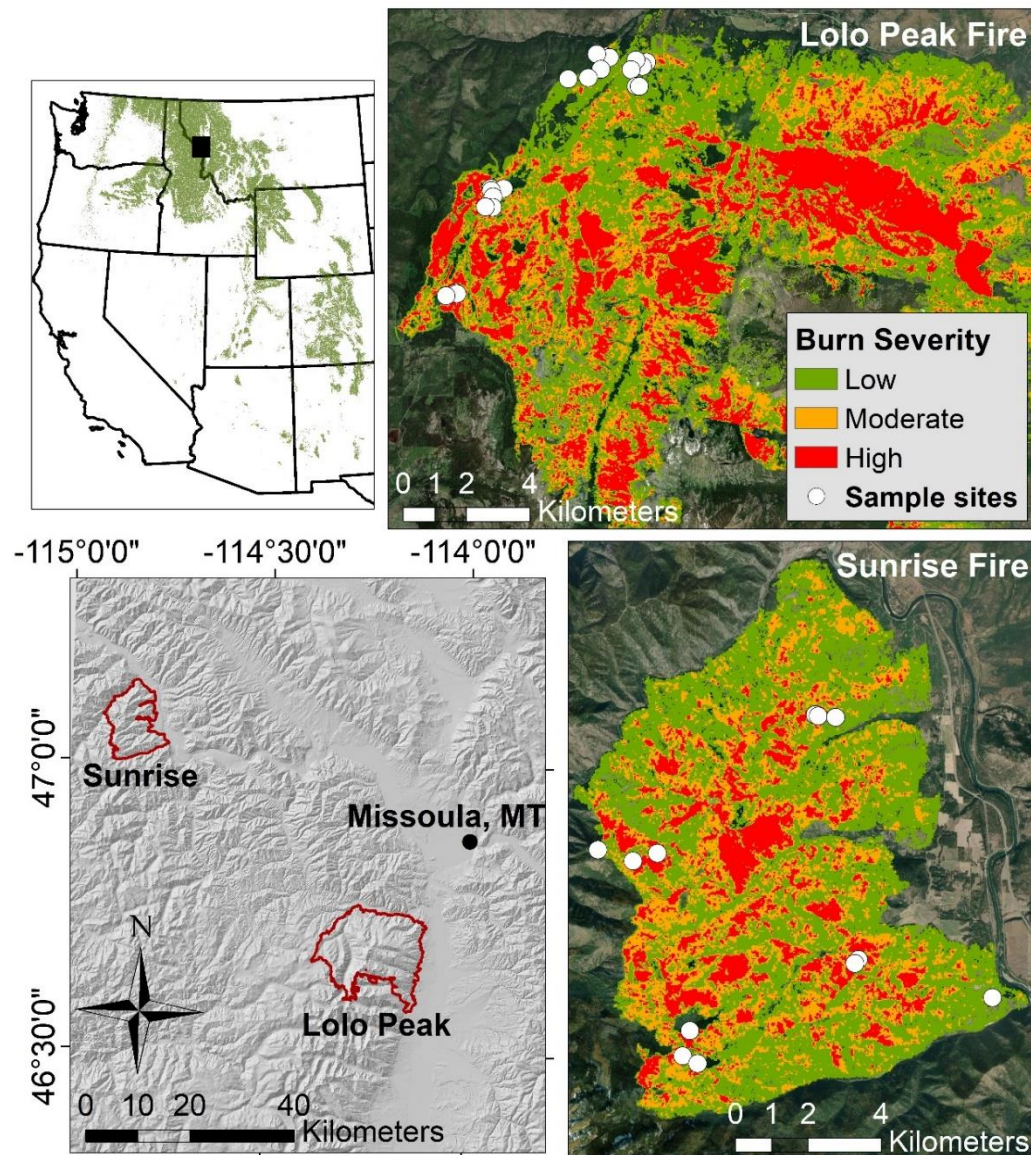


Figure 1. Map of sampling locations in the 2017 Sunrise ($n = 12$) and Lolo Peak ($n = 21$) fires, showing fire severity classifications obtained from the Monitoring Trends in Fire severity program (MTBS). Inset shows the location of study area (black square), with the green shaded area indicating the extent of Rocky Mountain mixed-conifer and subalpine forest classes mapped by the LANDFIRE program (landfire.gov).

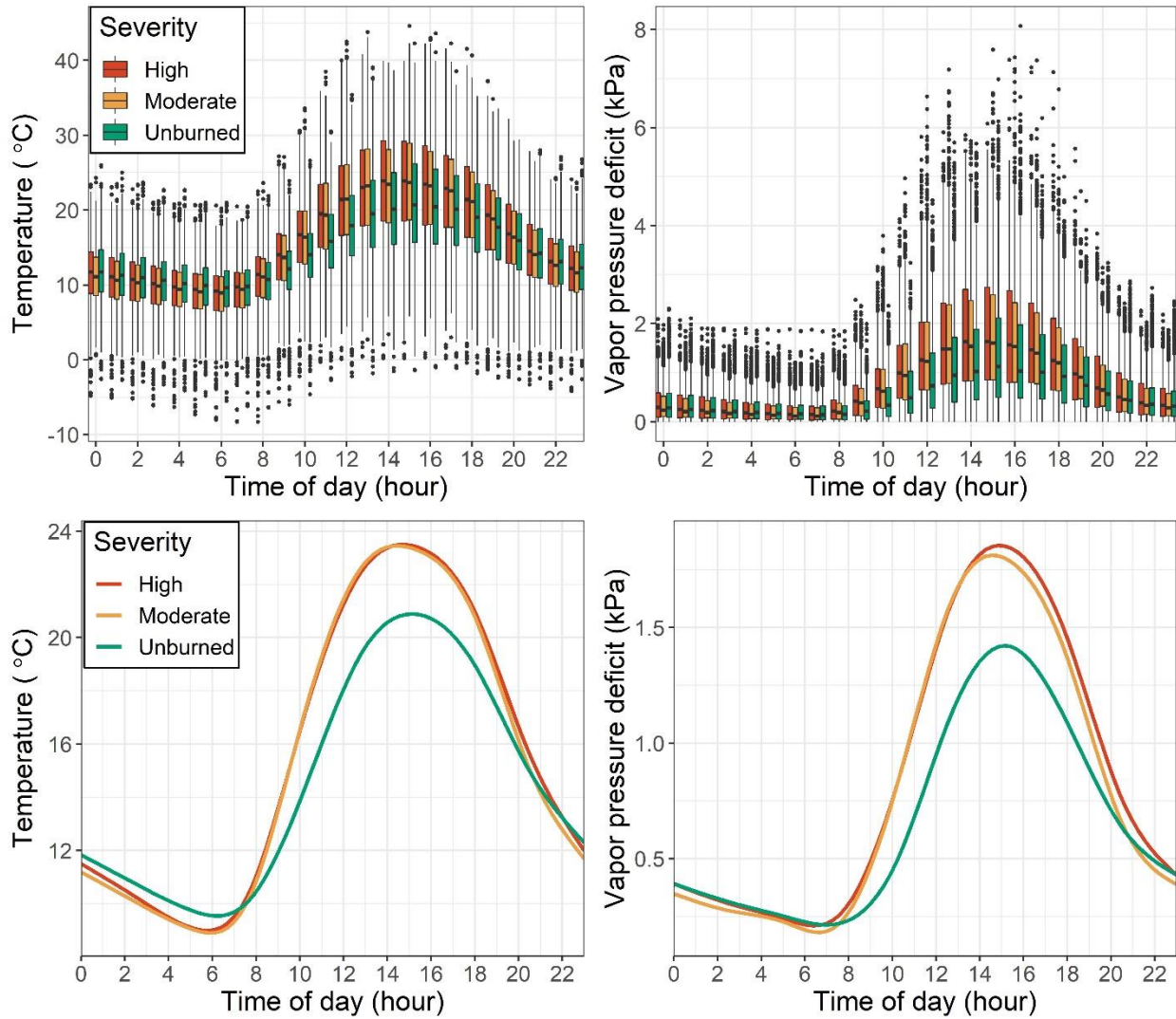


Figure 2. Diurnal variability in VPD (kPa) and temperature (°C) across all sensors and years, aggregated to hourly timesteps and displayed using boxplots (top panel) and curves fit by time of day (mgcv package in R) (bottom panel). Sensors are grouped by fire severity classifications (high, moderate, unburned) based on field measurements.

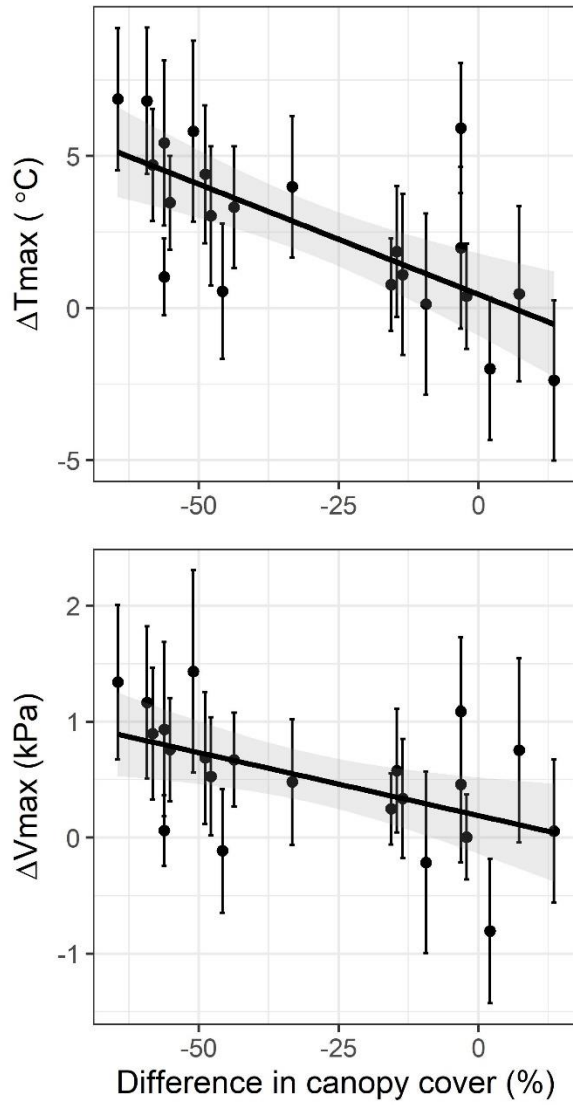


Figure 3. Bivariate relationship between the difference in canopy cover above the sensor in paired burned and unburned plots (ΔCanopy , x-axis) and ΔT_{\max} (top panel), and ΔV_{\max} (bottom panel). Positive ΔT_{\max} and ΔV_{\max} values indicate warmer/drier conditions in the burned plot than the unburned plot, and negative ΔCanopy values indicate less canopy cover in the burned plot than the unburned plot. Plot averages \pm two standard errors are shown, as well as a simple linear fit with 95% confidence intervals (shaded bands).

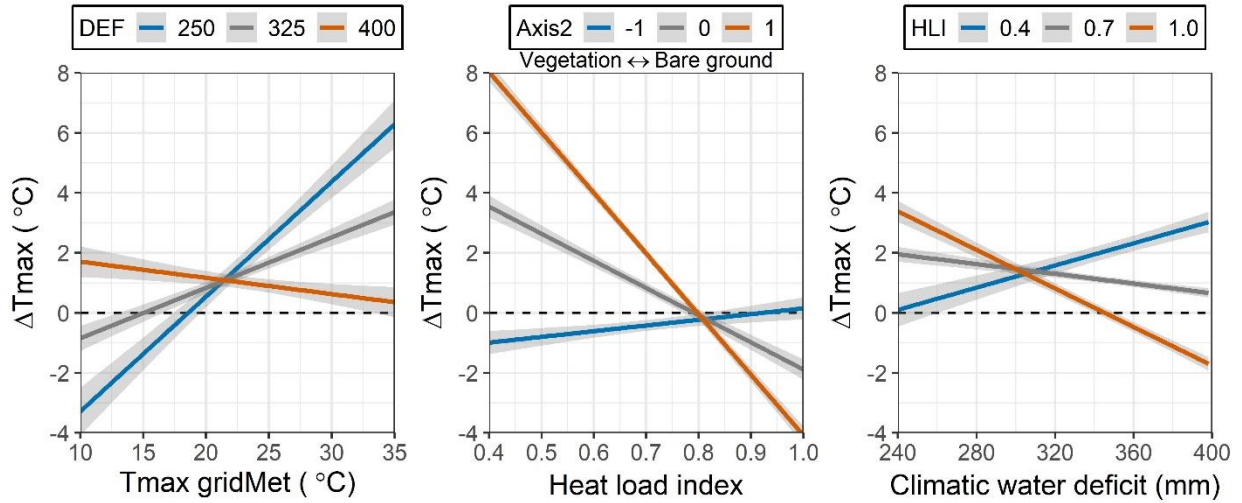


Figure 4. Model predictions of ΔT_{max} after controlling for differences in canopy cover between paired burned and unburned sites, where positive ΔT_{max} values indicate higher temperatures in the burned plot. Trends in ΔT_{max} are graphed to show the effects of interaction terms among ambient weather (T_{maxA}), mean annual climatic water deficit (DEF, mm), heat load index (HLI), and Axis2 (left panel to right panel). High DEF indicates lower long-term moisture availability. Negative Axis2 values indicate greater understory vegetation cover, while positive values indicate greater bare ground cover. High HLI indicates higher potential solar heating. Shaded bands show 95% confidence intervals for linear fits.

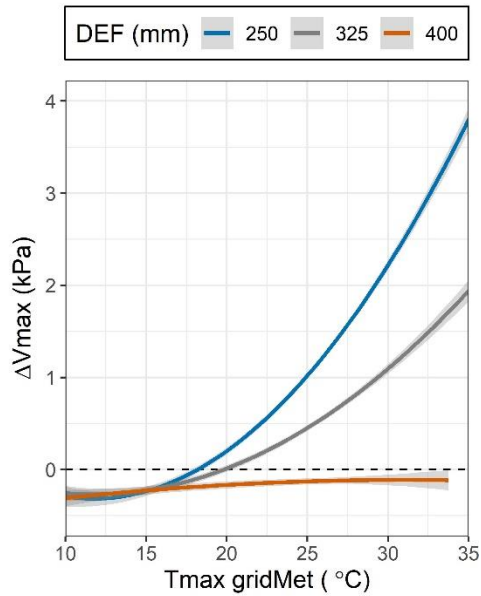


Figure 5. Model predictions of ΔV_{\max} after controlling for differences in canopy cover between paired burned and unburned sites, where higher ΔV_{\max} values indicate higher VPD in the burned plot. Trends in ΔV_{\max} are graphed against $T_{\max A}$ for varying levels of DEF, where high DEF indicates lower moisture availability. Shaded bands show 95% confidence intervals for quadratic fits.

CHAPTER 1
Supplementary Materials

Appendix A: Supplementary Methods

Table A.1. Site information, including year(s) sampled, distance between burned and unburned plots, elevation, plot-averaged dNBR values, live canopy cover above the sensor post (%), plot-averaged distance to the nearest live seed source (DSS, m), and plot-averaged bare ground cover (%). Rows within each site correspond to plots with different targeted fire severity classifications (i.e., high, moderate, unburned).

Site Code	Fire	Sampled:		Dist. from unburned (km)	Elev. (m)	dNBR	Live Canopy (%)	DSS (m)	Bare ground (%)
		2018	2019						
LPK_ HN1	Lolo	X	X	0.42	1834	881	0	49	54
	Peak			0.41	1840	672	0	16	30
						1799	2	98	2
LPK_ HN2	Lolo	X		0.33	1928	840	0	51	56
	Peak			0.37	1932	689	0	7	33
						1899	50	100	1
LPK_ HS1	Lolo		X	0.33	1720	885	0	44	83
	Peak			0.40	1749	601	22	3	6
						1821	-8	97	2
LPK_ LN1	Lolo		X	0.31	1302	322	0	69	5
	Peak			0.43	1284	189	11	5	1
						1266	-34	93	1
LPK_ LN2	Lolo	X		0.35	1312	629	0	38	6
	Peak			0.30	1321	302	12	3	0
						1293	90	80	1
LPK_ LS1	Lolo	X	X	1.39	1319	541	0	72	22
	Peak			0.49	1341	287	15	19	8
						1374	15	24	3
LPK_ LS2	Lolo	X		2.17	1394	604	0	68	27
	Peak			2.27	1395	266	36	2	3
						1445	-26	53	2
SUR _HN2	Sunrise		X	1.69	1566	901	0	51	50
				1.05	1604	568	6	5	17
					1654	38	98	2	0
	Sunrise		X	0.95	1970	924	0	84	82

SUR			0.47	1938	538	0	18	56
_HS3				1860	108	98	1	0
SUR	Sunrise	X	3.89	1204	852	0	38	20
_LN3			3.99	1255	545	3	10	12
				1035	83	74	4	0
SUR	Sunrise	X	0.48	1393	534	0	50	68
_LS2			0.56	1420	492	32	5	5
				1319	49	97	5	58

Sensor calibration and quality checking

All observations in 2018 used HOBO U23 Pro v2 data loggers (Onset Computer Corporation, Bourne, MA), while all observations in 2019 used LogTag HAXO-8 sensors (LogTag Recorders, Auckland, New Zealand). A laboratory calibration spanning the range of temperatures measured in the field was used to compare HOBO and LogTag sensors. The sensors performed similarly for measuring air temperature (< 2% average difference) but there was a consistent difference in relative humidity (RH) measurements (Fig. A.1). Based on this calibration, RH measurements from HOBO sensors were multiplied by a factor of 0.96 and increased by a constant value of 4.25% to be equivalent to RH measurements from LogTag sensors. After calibration, data were quality-checked by visually examining all measurements with a change of more than five degrees Celsius within a single timestep to look for potential sensor failures; less than 0.02% of data were excluded from analysis.

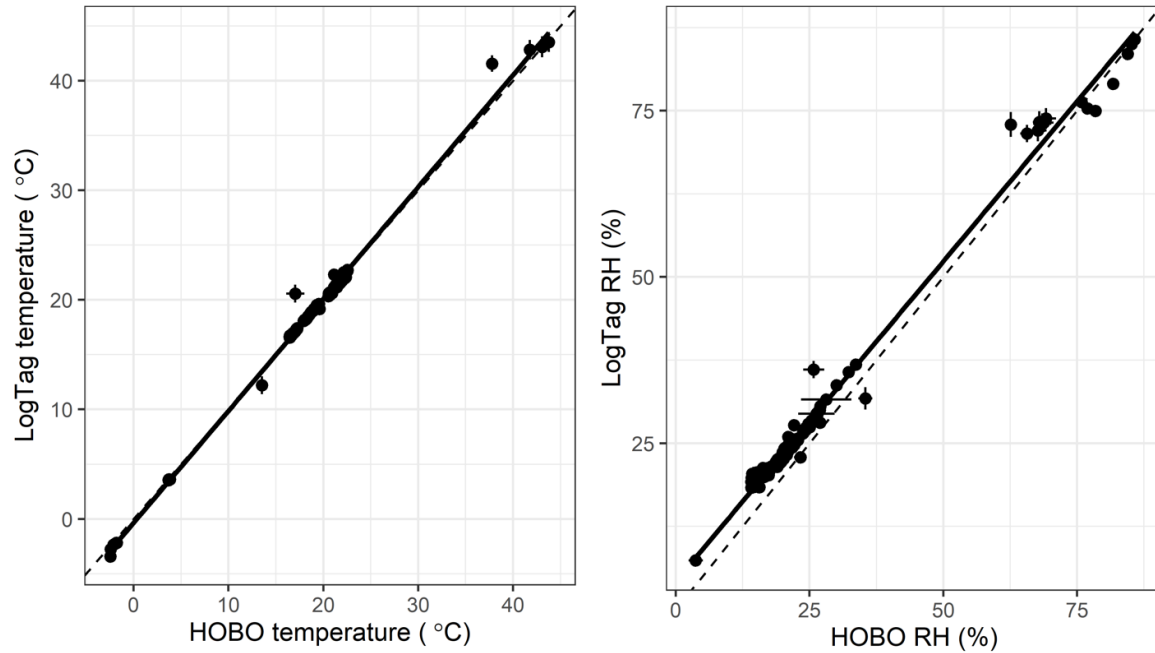


Fig. A.1. Results of laboratory calibration comparing LogTag HAXO-8 temperature and relative humidity (RH) sensors with HOBO U23 Pro v2 temperature and RH sensors. Three of each type of sensor recorded temperature and RH on the same half-hourly timesteps over three days, and were moved several times between a drying oven, refrigerator, freezer, and countertop to capture a wide range of temperatures; measured temperatures in the field ranged from -8 to 45 °C. Each point represents the average of the three sensors, with error bars showing standard deviations. Several outlier points with low agreement among sensors of the same type were removed from analysis (not shown). The solid line represents a linear fit of the data. The dashed line is the 1:1 line.

Daily differences in microclimate extremes between paired plots

We evaluated multiple methods for calculating daily differences in microclimate extremes between paired burned and unburned plots (Table A.2). First, as reported in the main text, we aggregated temperature and VPD measurement to the daily maximum values within each plot, regardless of the time it occurred, and calculated the difference in maxima between paired burned and unburned plots. For Method 2, we calculated differences between burned and unburned plots based on the timing of the maximum temperature and VPD at the unburned plot. For Method 3, we calculated the difference between burned and unburned plots based on the timing of the maximum temperature and VPD at the burned plot. Finally, for Method 4 we calculated the average daily temperature and VPD in each plot from 14:00 to 16:00 hr, and calculated the difference between these values. This time period in the afternoon is when 50% of the daily maximum temperature and VPD measurements occur among all sites. These four methods gave similar results, with a slightly larger average difference in temperature for Method 3 and slightly smaller average difference for Method 2 relative to what is reported in the main text, due to a median lag in timing of the maxima between paired burned and unburned plots of c. 0.5 hours (Fig. A.2).

Table A.2. Results for the four alternative methods for calculating daily differences in microclimate extremes between paired burned and unburned plots. The mean ΔT_{\max} and ΔV_{\max} across all plots is reported for each method, plus or minus one standard deviation.

	Differencing method	ΔT_{\max} (°C)	ΔV_{\max} (kPa)
Method 1:	Difference in site-specific daily maximum T and VPD, regardless of time	2.62 ± 2.68	0.52 ± 0.54
Method 2:	Difference at the time of the maximum values in the unburned plot	1.39 ± 2.81	0.28 ± 0.55
Method 3:	Difference at the time of the maximum values in the burned plot	4.21 ± 2.21	0.81 ± 0.50
Method 4:	Difference between the daily average between 14:00 and 16:00 hr	3.00 ± 2.20	0.56 ± 0.52

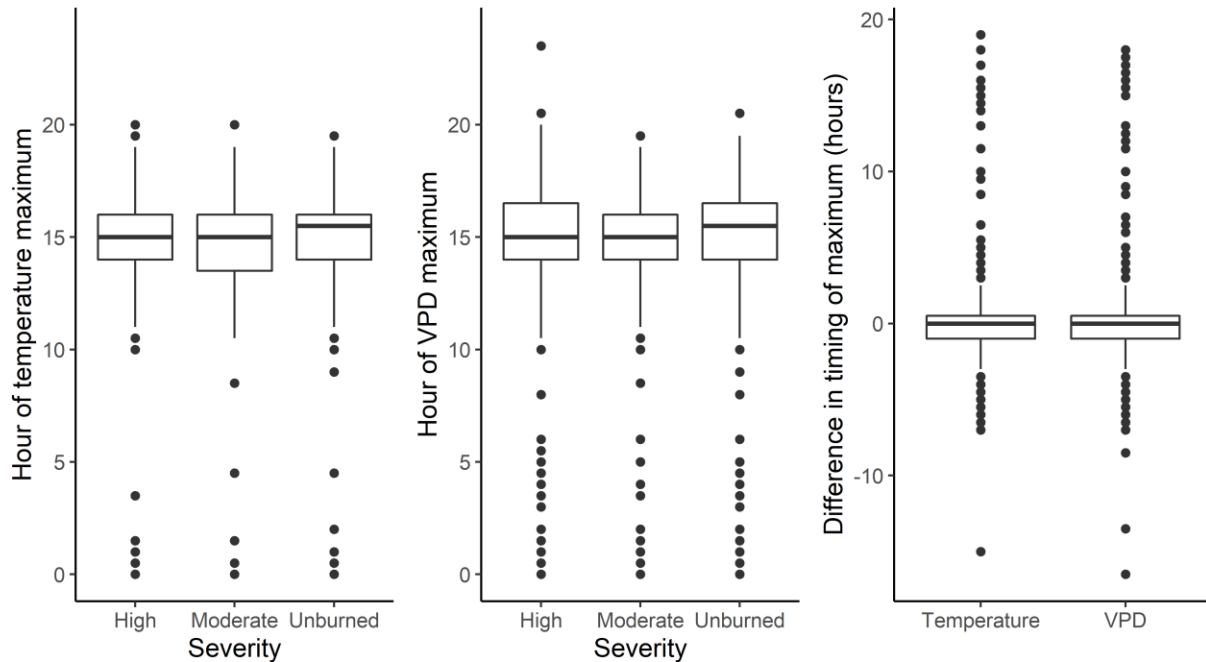


Fig. A.2. Timing of daily maxima in temperature (left) and VPD (center) across all plots and observation days ($n = 3471$), and daily difference in timing of maxima between paired burned and unburned plots (right), where negative values indicate that the unburned plot experienced its daily maximum temperature or VPD later than the paired burned plot. Plots are grouped by field-identified fire severity classifications. The median timing of daily temperature and VPD maxima in burned plots is 15:00, whereas the median timing in unburned plots is 15:30.

Principal Components Analysis

To characterize fire severity using field measurements, we conducted a principal components analysis (PCA) using the *ade4* package in R (Fig. A.3). Variables included in the PCA were plot-averaged values of: live and dead canopy cover, live and dead basal area, percent overstory mortality, scorch height, the distance to the nearest live tree, and percent ground cover of bare ground or rock, understory vegetation, and litter. Where necessary, variables were square-root or $\log(x+1)$ transformed prior to PCA, to reduce skewness and conform to assumptions of normality. The first two principal components (Axis1 and Axis2) account for 72.1% and 12.6%, respectively, of the variability in the dataset. Plot-averaged dNBR is significantly correlated with values of Axis1 ($r = -0.68$; $p = 0.0005$, $t = -4.1$, $df = 20$) and Axis2 ($r = 0.72$; $p = 0.0002$, $t = 4.6$, $df = 20$); thus, Axis1 and Axis2 are interpreted as metrics of fire severity.

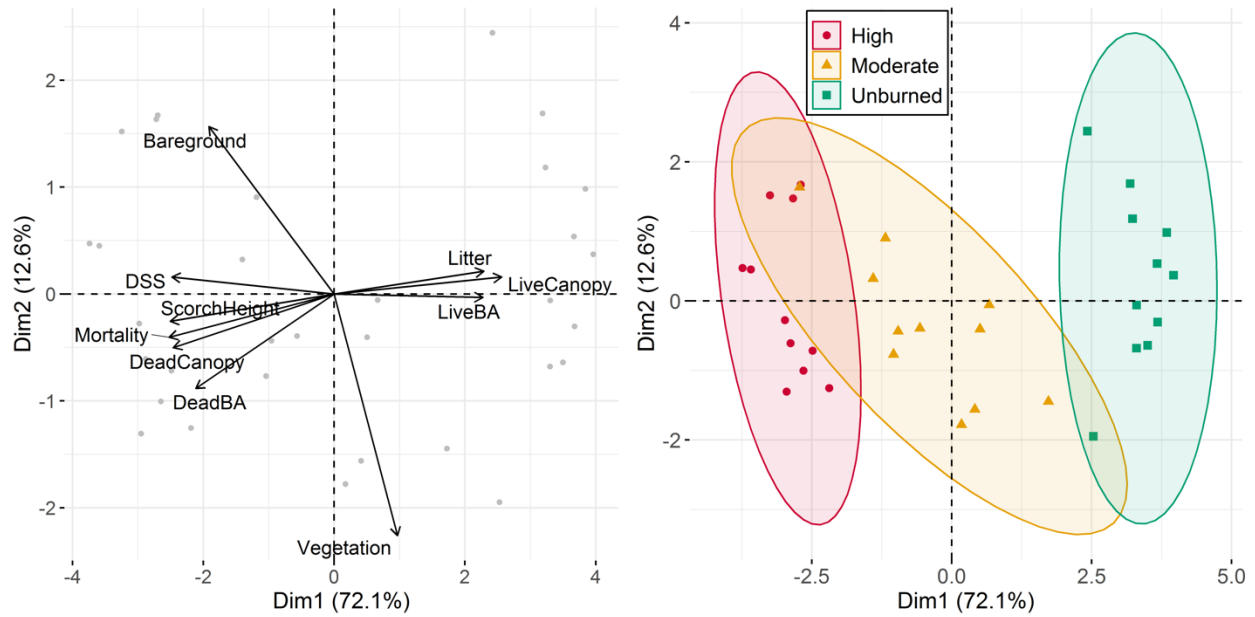


Fig. A.3. PCA biplots showing variability in field measurements on two axes which describe the fire severity of sampling sites. Axis loadings of each variable are shown in the left-hand figure. Variable names are: Bareground = bare ground and rock cover (%); Litter = litter cover (%); Vegetation = cover of grasses, forbs, & shrubs (%); Canopy = canopy cover (%), live or dead; BA = basal area, live or dead; Mortality = fire-caused mortality of trees >1.37 m height (%); ScorchHeight = average height of bole scorch (m); DSS = distance to the nearest live mature tree (m). The right-hand figure shows sites grouped by field-identified classifications of fire severity, which were based on tree mortality.

Appendix B: Supplementary Results**Table B.1.** Final fitted models for ΔT_{\max} and ΔV_{\max} , with mean cross-validated RMSE \pm one standard deviation. Note that predictors are not on the same scale.

Predictor	Estimate	T value	P value
Final model for ΔT_{\max} (RMSE = 2.50 \pm 0.90)			
Δ Canopy	-0.075	-5.45	<0.0001
$T_{\max}A$	0.979	6.38	<0.0001
DEF	20.9	5.15	<0.0001
Axis2	8.38	3.78	0.0012
HLI	71.1	3.75	0.0013
DEF : $T_{\max}A$	-0.240	-5.54	<0.0001
HLI : DEF	-22.2	-4.00	0.0007
HLI : Axis2	-10.5	-3.31	0.0035
Final model for ΔV_{\max} (RMSE = 0.62 \pm 0.25)			
Δ Canopy	-0.013	-3.25	0.0041
$T_{\max}A$	33.06	8.80	<0.0001
$T_{\max}A^2$	12.09	3.48	0.0006
DEF	-0.62	-3.32	0.0033
DEF : $T_{\max}A$	-7.90	-7.59	<0.0001
DEF : $T_{\max}A^2$	-2.98	-3.07	0.0024

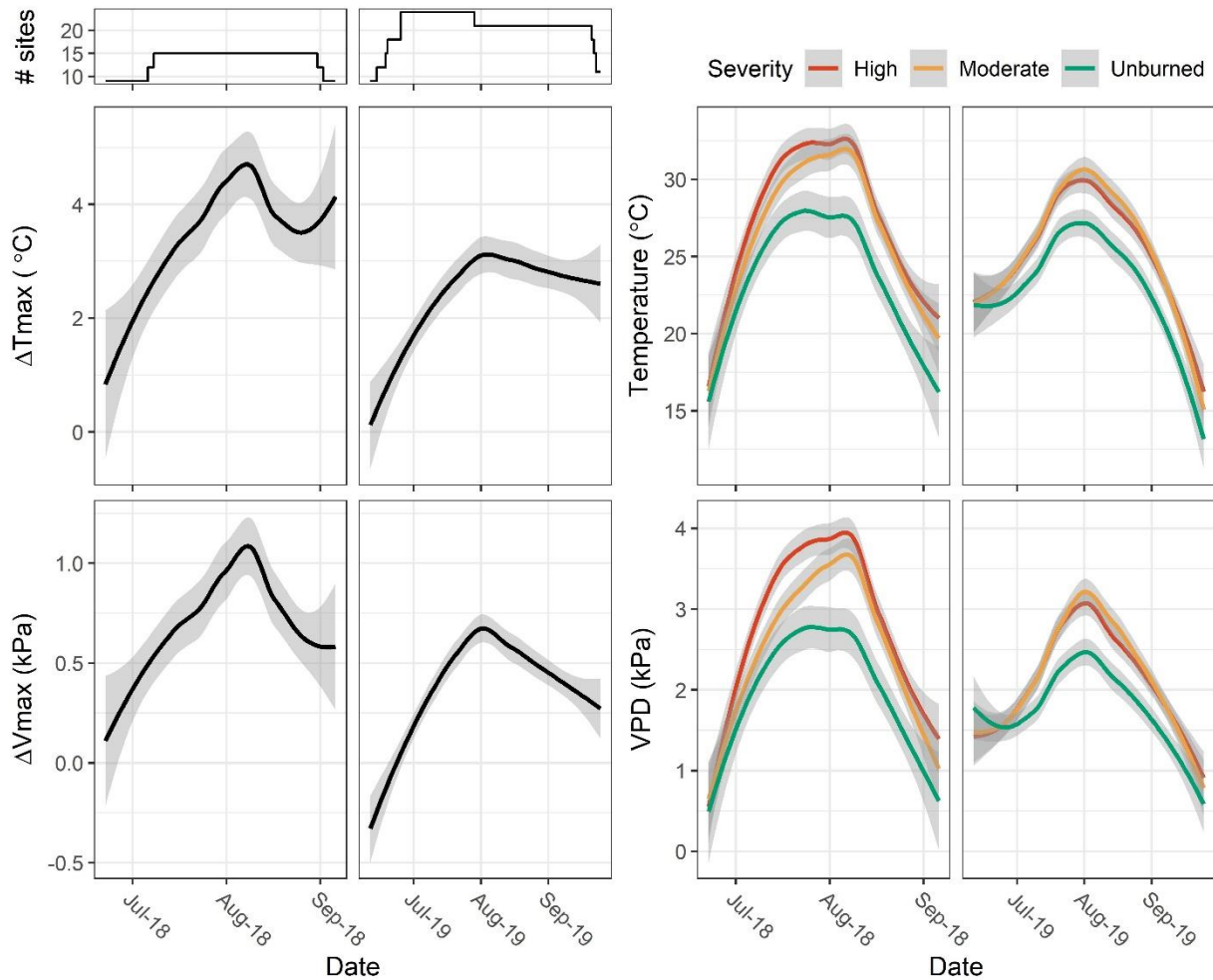


Fig. B.1. Seasonal patterns in near-ground microclimate conditions in 2018 and 2019, showing the number of plots recording throughout each season (left top), daily differences in maximum temperature and VPD between paired burned and unburned plots (left), and raw daily maximum temperature and VPD at plots grouped according to field-based fire severity classifications (right). Curves are fit by date using a LOESS smoother to capture seasonal trends across plots, with shaded bands showing 95% confidence intervals.

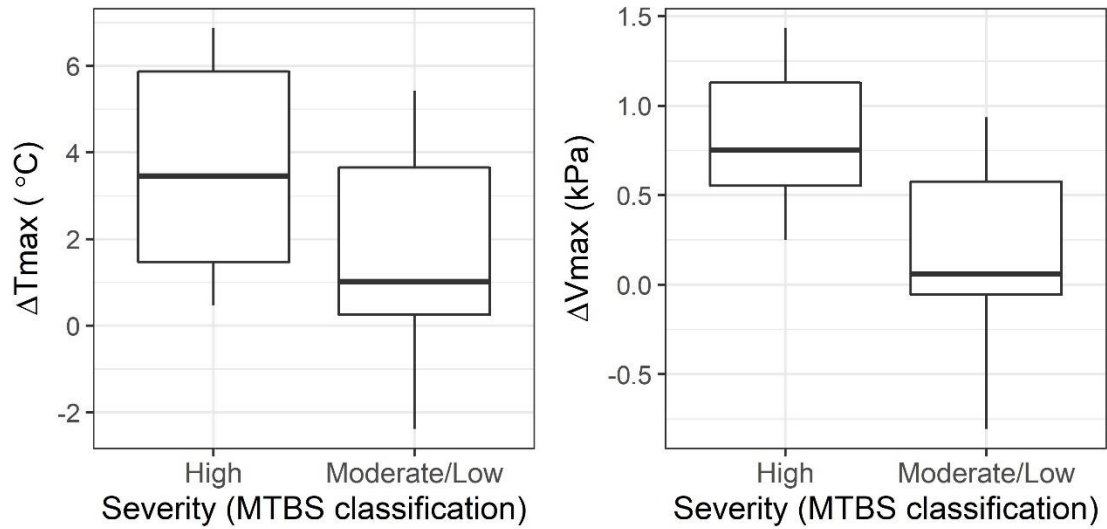


Fig. B.2. Boxplot of average ΔT_{\max} and ΔV_{\max} values for plots classified as high severity (n=11) or moderate/low severity (n=11) based on dNBR values using MTBS classifications. The difference in median ΔV_{\max} of 0.57 kPa is significant ($p = 0.010$, $W = 22$, $n = 11$), while the difference in median ΔT_{\max} of 2.17 is marginally significant ($p = 0.065$, $W = 32$, $n = 11$). Several plots (n=5) classified as moderate severity in the field had dNBR values in the range of low fire severity; these are grouped with the moderate-severity plots.

CHAPTER 2: Conifer seedling demography reveals mechanisms of initial forest resilience to wildfires in the northern Rocky Mountains

*This chapter is published with the following co-authors and citation:

Clark-Wolf, K., P. E. Higuera, and K. T. Davis. 2022. Conifer seedling demography reveals mechanisms of initial forest resilience to wildfires in the northern Rocky Mountains. *Forest Ecology and Management* 523:120487. doi: 10.1016/j.foreco.2022.120487.

Abstract

Climate warming and an increased frequency and severity of wildfires is expected to transform forest ecosystems, in part through altered post-fire vegetation trajectories. Such a loss of forest resilience to wildfires arises due to a failure to pass through one or more critical demographic stages, or “filters,” including seed availability, germination, establishment, and survival. Here we quantify the relative influence of microclimate and microsite conditions on key stages of post-fire seedling demography in two large, lightning-ignited wildfires from the regionally extensive fire season of 2017 in the northern Rocky Mountains, U.S.A. We tracked conifer seedling density, survival, and growth in the first three years post-fire in 69 plots spanning gradients in fire severity, topography, and climate; all plots were limited to within 100 m of a seed source to assure seed availability. Microclimate conditions were inferred based on measurements in a subset of 46 plots. We found abundant post-fire conifer regeneration, with a median of 2,633 seedlings per hectare after three years, highlighting early resilience to wildfire. This robust regeneration was due in part to moderate post-fire climate conditions, supporting high survivorship (>50% on average) of all seedlings tracked over the study period (n = 763). A statistical model based on variables describing potential seed availability, microclimate, fire severity, understory vegetation, and soil nitrogen availability explained 75% of the variability in seedling density among plots. This analysis highlights the overarching importance of fine-scale heterogeneity in fire effects, which determine microclimate conditions and create diverse

Chapter 2

microsites for seedlings, ultimately facilitating post-fire tree regeneration. Our study elucidates mechanisms of forest resilience to wildfires and demonstrates the utility of a demographic perspective for anticipating forest responses to future wildfires under changing environmental conditions.

Introduction

Forest ecosystems and the services they provide are changing due to the combined impacts of warmer, drier climate conditions from anthropogenic climate change and increased wildfire frequency and severity, driven strongly by anthropogenic climate change (Abatzoglou and Williams 2016, Holden et al. 2018, Parks and Abatzoglou 2020). These changes stem in part from altered patterns of post-fire tree regeneration, which is a critical stage of community re-organization affecting forest composition and structure for decades to centuries (Tepley et al. 2013, Turner et al. 2016). Across western North America, numerous studies document a decline in post-fire tree regeneration in the 21st century (e.g., Stevens-Rumann et al. 2018, Turner et al. 2019, Coop et al. 2020), a trend expected to continue under climate warming (Kemp et al. 2019, Davis et al. 2020). These changes can indicate a loss of resilience to wildfire, used here to reflect the capacity of an ecosystem to recover following a disturbance and retain fundamental structures and functions (Gunderson 2000). Forest resilience to wildfire is ultimately governed by complex interactions among climate, disturbance regimes, and species-specific responses to biophysical conditions (e.g., Rammer et al. 2021). Ongoing warming and increasing fire activity highlight the pressing need to understand mechanisms of forest resilience to wildfires, how these mechanisms vary among species and across biophysical gradients, and if, when, and where forest resilience to wildfire will be overcome in the future.

Chapter 2

Anticipating forest resilience to wildfires is aided by considering key demographic filters that control fire-caused tree mortality and post-fire tree regeneration (Davis et al. 2018). Tree regeneration is the net result of mechanisms influencing seed production and dispersal, and seedling germination, establishment, and survival over multiple years after a fire (Karavani et al. 2018, Davis et al. 2018, Falk et al. 2022). The combined impacts of these processes depend on a suite of biotic and abiotic factors at each demographic stage, summarized by a demographic framework (Fig. 1).

Climate warming and changing fire regimes have the potential to impede post-fire tree regeneration by altering these biotic and abiotic factors that govern seedling demography. For example, numerous studies highlight fire effects on availability of viable seeds as a primary mechanism shaping post-fire seedling establishment (e.g., Kemp et al. 2016, Rodman et al. 2020b, Peeler and Smithwick 2020, Stewart et al. 2021). Seed availability may become more limiting in the future due to shorter intervals between fires and thus time for trees to produce viable seed; through increased fire severity, which leaves fewer surviving seed trees; or through climate-driven reductions in tree fecundity (Enright et al. 2015, Clark et al. 2021, Gill et al. 2022). Vulnerability to these changes varies as a function of species traits. For example, species with serotinous cones can regenerate in the absence of surviving trees from seeds stored in an aerial seed bank, but the production of serotinous cones is constrained by short fire-return intervals (Buma et al. 2013, Hansen et al. 2018).

Where seeds are available for post-fire germination, variability in fire effects and climate interact to shape the microclimate conditions experienced by seedlings. Post-fire climate conditions have well-recognized effects on tree regeneration (Fig. 1), with relatively cool, moist conditions most favorable (e.g., Harvey et al. 2016b, Andrus et al. 2018, Davis et al. 2019a,

Chapter 2

Rodman et al. 2020b). These regional climate conditions are mediated by local factors, including topography, forest structure and productivity, and understory vegetation (Dobrowski 2011, De Frenne et al. 2019), which shape local microclimate conditions in post-fire environments (Ma et al. 2010, Carlson et al. 2020b, Crockett and Hurteau 2022). With climate warming and increased fire activity, reductions in canopy cover and evapotranspiration are expected to result in less microclimatic buffering by vegetation in recently burned areas (Davis et al. 2019b, Wolf et al. 2021), increasing exposure to microclimatic extremes that inhibit regeneration (Carlson et al. 2020a, Hoecker et al. 2020).

Changes in fire severity can also alter microsite factors that influence seedling demography, independent of microclimate. Fires shape the competitive environment and increase the short-term availability of resources such as light, soil nutrients, and seed beds through changes in overstory, understory, and soil conditions (Fig. 1), which can play an important role in providing regeneration opportunities (Johnstone and Chapin 2006, Parra and Moreno 2017, Steed and Goeking 2020). Responses to these varying factors differ among species and are difficult to tease apart, making it challenging to anticipate the impacts of changing fire severity (Urza and Sibold 2017, Hill and Ex 2020). For example, high-severity fire results in more stressful, warm-dry microclimate conditions (Wolf et al. 2021), but also a pulse of nutrient availability (Smithwick et al. 2005); sensitivity to these changes will depend on species traits (e.g., drought tolerance). The effects of fires on seed availability, microclimate, and other microsite factors can thus have contrasting effects on seedling demography, complicating our understanding of the influence of fire severity on post-fire tree regeneration.

Among recent work documenting tree regeneration in North America (see reviews by Stevens-Rumann and Morgan 2019, Coop et al. 2020), post-fire demographic processes have

Chapter 2

rarely been tracked over time during the first several years after a wildfire, which is often a critical period for setting up long-term vegetation trajectories (e.g., through “priority” effects *sensu* Fukami 2015; Tepley et al. 2013, 2017, Urza and Sibold 2017). This leaves a key research gap making it challenging to disentangle the relative importance of biophysical factors at early life stages and how these factors are impacted by changing climate and fire activity.

In this study, we use a demographic filter framework (Davis et al. 2018) to help elucidate mechanisms of forest resilience to two large wildfires in mid-elevation to lower subalpine conifer-dominated forests (hereafter “mixed-conifer” forests) of the northern Rocky Mountains, U.S.A. (Fig. 1). We build on prior research documenting post-fire near-ground atmospheric conditions (Wolf et al. 2021) to quantify the impacts of fire severity on regeneration through its effects on microclimate and other microsite factors, at sites where seed availability was not limiting. Specifically, we tracked seedlings in two wildfires in western Montana over three years post-fire, and estimated species-specific rates of seedling establishment, survival, and growth in study sites stratified by topographical position and fire severity to capture a range of abiotic and biotic conditions. Our objectives were to: 1) quantify the relative importance of climate, microclimate and fire severity at key seedling demographic stages for dominant conifer species; 2) disentangle the varying impacts of fire severity on seedling demography, including through changes in overstory and understory vegetation composition and structure and soil conditions; and 3) place our findings into the demographic framework to help assess what these examples imply about future forest resilience under climate change. Our results provide a detailed example of contemporary forest response to wildfire, and, more broadly, help to anticipate how ongoing climate warming and changing fire regimes will alter future forest resilience to wildfire.

Methods

We characterized post-fire seedling demography by tracking seedling density, survival, and vertical growth in the first three years after fire occurrence to elucidate controls of post-fire tree regeneration. We monitored seedling regeneration in 69 sites across two fires. These include a subset of sites (22 burned and 11 unburned) from a previous study where we monitored microclimate to quantify the impacts of moderate- and high-severity fire on below-canopy atmospheric conditions (Wolf et al. 2021). Our study sites were located using a stratified sampling design to capture a range of biophysical settings (via elevation and aspect) and fire severity (unburned, moderate, high), as described by Wolf et al. (2021).

Study area

We studied conifer regeneration in mixed-conifer forests within two large wildfires in the Bitterroot Mountains of Montana (Fig. 2). The study area spans forests dominated by ponderosa pine (*Pinus ponderosa*), Douglas-fir (*Pseudotsuga menziesii*), and western larch (*Larix occidentalis*) at low to mid elevations (i.e., <1500 m) and xeric aspects, and lodgepole pine (*Pinus contorta* var. *latifolia*), subalpine fir (*Abies lasiocarpa*), and Engelmann spruce (*Picea engelmannii*) at mid to high elevations (c. 1500 - 2200 m). Soils are primarily gravelly, well-drained inceptisols derived from volcanic ash overlying metasedimentary, granitic, or mica schist parent material (Soil Survey Staff 2017). Mean annual temperature at our sites averaged 5.1 °C and total annual precipitation averaged 986 mm from 1981-2010, with 22% of precipitation occurring during the growing season of June to September (PRISM Climate Group 2015).

The Lolo Peak and Sunrise fires burned across c. 22,000 and 11,000 ha, respectively, from July to September, 2017, with 15-20% of the burned area classified as high severity (MTBS Project 2019). Across both fires, > 88% of the area burned was within 100 m of a non-high-

Chapter 2

severity burn patch, where live trees likely provide seed sources (Fig. A.5). In addition, most of the area in the Lolo Peak (91%) and Sunrise (56%) fires that was more than 100 m from a non-severe patch fell within the elevational range of *Pinus contorta*, which exhibits cone serotiny in this region (personal observation; Harvey et al. 2016b). This spatial patterning of burn severity is consistent with similar wildfires across the northern Rocky Mountains: among a random subset of 30 large fires (>5000 ha) in the region that burned under unusually hot, dry conditions in the regional fire years of 2000, 2003, 2007, 2012, 2015, and 2017, an average of 86% of the area burned was within 100 m of a non-severe patch (Appendix A). Thus, the Lolo Peak and Sunrise fires are representative of other large wildfires in the region that burned during regional fire years with warm, dry summer climate conditions (Morgan et al. 2008).

Field measurements

We sampled field sites in the first three years after fire (2018-2020) to measure aspects of seeding demography and vegetation change (Table A.1). Seedling density, overstory tree density (defined as trees >1.37 m height), and live and dead basal area were measured within 60-m-long belt transects that varied from 1 to 10 m in width, with the goal of sampling at least 25-50 seedlings per transect while balancing our ability to accurately search the transect area. To minimize uncertainty from age estimates (Hankin et al. 2018), we focused our analyses on total seedling density in the final sampling year in burned sites (i.e., pooling all post-fire seedlings). Post-fire seedlings were easily determined in burned sites, given near-complete surface fire. We restricted seedling counts in unburned sites to post-2017 individuals based on age estimates using height, presence of cotyledons, and bud scars (Urza and Sibold 2013). We grouped seedlings of *Abies grandis* and *A. lasiocarpa* together in our analyses because *A. grandis* was rare, and distinguishing between germinant seedlings of these species was not always possible.

Chapter 2

Post-fire planting by USFS overlapped with seven of the 69 sites (10%); planted seedlings were easily distinguishable from natural regeneration based on size and were excluded from analyses.

Within each transect, we established 6-10 permanent 1-m² subplots for repeat sampling. Live and dead canopy cover and the distance to the nearest live tree were measured at each subplot, and ocular ground cover measurements were taken to estimate cover of bare ground or rock, litter, coarse woody debris, moss or lichen, forbs, grasses, and shrubs to the nearest five percent. We monitored individual seedlings within 2-10 subplots, with the goal of tracking 10-100 seedlings per site. A total of 1253 seedlings were identified in subplots over the three years, with 212 and 617 in sites that burned at high and moderate severity, respectively, and 424 in unburned sites. We marked seedlings and measured height to track annual survivorship and vertical growth (Table 1).

Seed source

We used two metrics of potential seed availability: field-measured distance to seed source (*DSS*), and a distance-weighted propagule pressure metric (*PP*) based on post-fire imagery (Table 2). Presence of live trees after fire was identified visually in post-fire imagery in 10 x 10 m grid cells within a 200 m radius circle centered on each site, using post-fire satellite imagery in ESRI basemaps (Environmental Systems Research Institute; 0.5-m resolution) and aerial imagery from NAIP (National Agriculture Imagery Program; 1-m resolution). To account for declining seed dispersal with greater distance from a seed source, live tree cover was distance weighted (i.e., 1 / m from site center) using methods from Coop et al. (2019) to create the *PP* metric.

Topoclimate Metrics

Chapter 2

We used a suite of long-term topoclimate metrics with fine spatial resolution (<1 km) to characterize the biophysical setting of each site (Table 2). Heat load index (*HLI*), calculated at 1/3 arc-second resolution, integrates aspect, slope, and latitude into an index of potential solar heating (McCune and Keon 2002). Water balance was represented by climatic water deficit (*DEF*, mm), averaged for 1981-2015 from a downscaled (250-m) climate product (Holden et al. 2018). Annual precipitation (*ppt_{ann}*, mm) and growing-season precipitation (*ppt_{JJAS}*, mm) were averaged for 1981-2015 from the ClimateWNA product, which interpolates 800-m PRISM grids and adjusts for elevation to generate scale-free climate data (Wang et al. 2016).

Microclimate Metrics

To characterize near-ground microclimate experienced by seedlings, we used field-based measurements from a subset of sites to create a statistical model predicting daily microclimate based on topoclimate, canopy cover, and fire severity variables. The model was based on field measurements at 46 of the 69 sites. To extrapolate beyond these 46 sites, we used linear mixed effects models to predict daily microclimate conditions in all sites over the three study years (Appendix A). Daily predictions were aggregated to the absolute (T_{max}) and the average (T_{avg}) maximum daily temperature over the growing season in each site and year (Table 2).

Site-level metrics of fire severity

We developed continuous metrics of fire severity at each site, by using a PCA to summarize a suite of field measurements of fire effects, as described by Wolf et al. (2021) and detailed in Appendix A. We interpreted the first two principal components to reflect distinct aspects of fire severity, and use these as predictor variables in statistical models of seedling density (Table 2). PCA Axis 1 (*Axis1*) reflects overstory fire effects, with positive values associated with high tree mortality and char height. PCA Axis 2 (*Axis2*) reflects understory

Chapter 2

conditions, with positive values associated with greater bare ground cover and negative values associated with greater moss and forb cover.

Soil inorganic nitrogen

To measure soil inorganic nitrogen content in the first and second year after fire, we collected soil samples at 0, 30, and 60 m along each transect in August-September of 2018 and 2019. To obtain a time-integrated measure of inorganic nitrogen availability, we deployed mesh capsules containing ion-exchange resin (Unibest, Walla Walla, WA, USA), which adsorb ammonium (NH_4^+) and nitrate (NO_3^-) ions in soil solution (Binkley and Matson 1983). These were placed at c. 5-cm depth in the mineral soil at 0, 30, and 60 m along each transect in August-September 2018, and were allowed to incubate in the field until June 2019 to capture post-thaw N mineralization. See Appendix A for detailed sampling and laboratory analyses.

Hypothesis testing to evaluate controls of post-fire regeneration

We used statistical models to assess the effects of potential seed sources, microclimate, and fire severity on total seedling density after three years of regeneration, reflecting the net result of germination, establishment, and survivorship (Table 1). We conducted model selection to obtain a best-fit model, and tested the relative influence of controls of regeneration (Fig. A.4). Statistical analyses were conducted in R v. 4.0.4 (R Core Team 2020).

Seedling counts were modeled separately in burned and unburned sites using negative binomial models with a log link. A model was created for all species combined, and a second set of species-specific models was created for *P. menziesii*, *L. occidentalis*, and *P. contorta* individually. For each model, the random structure was determined by using AICc to compare generalized linear mixed models including a random intercept of fire (i.e., Lolo or Sunrise fire) to generalized linear models with no random effects. We included an offset of $\log(\text{area})$ to

Chapter 2

account for transect size. Fixed-effects predictors were square-root transformed when necessary to reduce skewness, and standardized (z-scores) to facilitate direct comparison among coefficients. We grouped predictors into three broad categories describing fundamental controls of post-fire regeneration: potential seed availability, climate, and fire effects. Each category included subcategories of correlated variables describing distinct aspects of the fundamental controls (Table 2).

To identify an initial set of predictor variables for the statistical models, we first selected one predictor from within each of the eight subcategories of variables; species-specific models included an additional indicator variable for species presence (Table 2). Within each subcategory, we considered the best predictor variable as that with the lowest AICc, and we restricted variables to those with variance inflation factor less than five. The resulting predictors were used for best-fit model selection and hypothesis testing, described below (Fig. A.4).

Using this initial set of predictors, we proceeded with model selection to obtain final, best-fit models for inferring controls of seedling density. We dropped terms that did not significantly improve fit ($\Delta\text{AICc} < 2$), and added quadratic terms and two-way interaction terms describing plausible ecological relationships if they improved fit. Model skill was evaluated using AICc, marginal pseudo- R^2 values (Bartoń 2022), and raw (ρ) and cross-validated ($\rho\text{-CV}$) Spearman correlations between observed and predicted values (details in Appendix A). We conducted k-fold cross-validation by holding out 25% of the data for validation, training the model on the remaining data, and averaging ρ over 1000 repetitions. We assessed residuals visually and used semivariograms to evaluate spatial autocorrelation. Partial effects and 95% confidence intervals were calculated using the *effects* package (Fox and Weisberg 2018).

To explicitly test the relative influence of the varying controls of post-fire regeneration predicted by a demographic framework (Fig. 1), we used the initial set of variables to compare models containing subsets of predictors describing seed sources, climate, and fire severity (Table B.1). Each subset model was compared with the next-simplest model using log-likelihood ratio tests to assess the added explanatory power of sets of variables in each category. To evaluate different climate metrics, we compared models including microclimate variables in place of climatic water deficit (*DEF*, Table 2); microclimate and *DEF* were not included in the same models because they were well-correlated ($r = 0.61$, $p < 0.001$; $t = 6.3$, $df = 69$).

Seedling demographic stages: annual recruitment, survivorship, & growth

We utilized annual seedling recruitment, survivorship, and height data to assess the influence of biotic and abiotic factors at each demographic stage (Table 1). To evaluate temporal as well as spatial variability in regeneration, we built statistical models of annual recruitment in burned sites, defined as the density of germination-year seedlings alive in August-September of each sampling year at each site. We avoided problems of aging uncertainty by restricting this analysis to germination-year seedlings (identified based on the presence of cotyledons).

Recruitment was modeled using the same methods as for seedling density to obtain a best-fit model. We included a random intercept of site to account for repeated measurements, and predictor variables included those in Table 2 and post-fire year.

To evaluate the influence of microclimate and microsite factors on seedling survivorship, we used binomial mixed effects models with a logit link. To account for lack of independence among observations from repeat sampling, and among observations from subplots within the same site, we restricted our analysis to year three after fire and included a random effect of site. The binomial response variable was the count of marked seedlings in each subplot that survived

Chapter 2

or died between the 2019 and 2020 measurements (Table 1). Fixed-effects predictors included seedling age and those described in Table 2 under the broad categories of climate and fire effects. We used annual subplot-specific (i.e., not site-averaged) measurements of canopy and ground cover as predictors, to assess the influence of microsite conditions on survivorship. We calculated area under the receiver operating curves (AUC) using the *pROC* package (Robin et al. 2011; see Appendix A). Simulation-based tests of residuals from the *DHARMA* package (Hartig 2021) were used to assess dispersion.

To evaluate the effects of species, age, and site characteristics on growth, we built a generalized linear mixed-effects model of seedling height. We restricted our analysis to data from year three after fire and used random effects of subplot nested within site to conform to assumptions of independence. A gamma distribution with a log link was used to account for greater variance in height among taller seedlings. Predictors included species, seedling age, and climate variables and fire-effects variables described in Table 2.

Results

Regeneration was abundant by the third year after fire, with a median density among all sites of 2,633 seedlings per hectare (IQR 750 to 7500 ha⁻¹). All burned sites (n=47) had at least one live seedling, four sites (8.5%) had densities < 100 ha⁻¹, and 12 sites (26%) had densities > 10,000 ha⁻¹. Seedling density was significantly greater in burned than unburned sites on average for *P. contorta*, *P. ponderosa*, and *L. occidentalis* (Fig. 3). Comparing post-fire seedling densities with reconstructed pre-fire tree densities, two-thirds of burned sites were at or above replacement density three years post-fire, and species composition of seedlings generally reflected pre-fire composition of mature trees (Fig. B.1, B.2). The most common species pre- and post-fire were *P. menziesii* and *P. contorta*, present in >50% of sites.

Relative influence of potential seed availability, climate, and fire severity on seedling densities

The best-fit model for total seedling density in burned sites accounted for c. 75% of the variability among sites (marginal pseudo- R^2), and had a high cross-validated correlation between predicted and observed values (ρ -CV = 0.63). Seedling density was negatively related with distance to seed source, negatively related with T_{max} , representing microclimate, and varied with *Axis1*, *Axis2*, and *soilN*, reflecting distinct aspects of fire severity (Fig. B.3). Total seedling density increased with overstory fire severity (*Axis1*) and moss and forb cover (*Axis2*), and decreased with greater soil nitrogen availability (*soilN*). These general patterns were largely consistent among species, although the specific variables retained and their relative influence differed (Fig. 4; Table B.2). In particular, the effects of fire severity metrics were not uniform, indicating that the influence of microsite conditions on regeneration varied among species. Notably, *P. menziesii* seedling density had a negative relationship with fire severity and no relationship with soil nitrogen variables, in contrast to overall trends with species combined, while *P. contorta* density was positively related with coarse wood cover (Fig. 4). Some relationships of seedling density with microsite variables also differed between burned and unburned sites (Fig. B.3, B.4).

Variables describing seed source proximity or density explained 50% of the total variability in seedling densities among sites (Table B.1). Total density was greater at sites closer to live seed sources and with a greater abundance of pre-fire *P. contorta* (*BAPICO*), representing a proxy for seeds from serotinous cones. *P. contorta* also had the highest median (25,270 ha⁻¹) and maximum (>500,000 ha⁻¹) post-fire seedling density among all species. After accounting for potential seed availability, the addition of variables describing topoclimate improved model fit, resulting in an increase in the marginal pseudo- R^2 from 50% (“Seed” model) to 62%

(“Seed+Clim” model; Fig. 4, Table B.1). The further addition of microclimate information slightly improved model fit (“Seed+MC” model, Fig. 4; marginal pseudo- $R^2 = 64\%$), indicating that the influence of spatial climate variability on seedling density was largely captured by topoclimate metrics. Finally, after accounting for potential seed availability and microclimate, variables describing fire severity substantially improved model fit (“Seed+MC+Fire” model, Fig. 4; marginal pseudo- $R^2 = 78\%$).

Seedling demographic stages: annual recruitment, survivorship, & vertical growth

Annual recruitment in burned sites varied among species and declined over time, with greater recruitment in the first year (median 1292 ha⁻¹) compared to the second (850 ha⁻¹) and third (417 ha⁻¹) year post-fire (Fig. 3). Annual recruitment was largely influenced by the same variables that influenced total seedling density, but with added nuance from an interaction between post-fire year and basal area of *P. contorta*, and interactions involving HLI, precipitation, and forb cover (Table B.3, Fig. 5).

Seedling survival was high, with a median of 66% (IQR 46 – 82%) cumulative survivorship of all seedlings tracked during the study period. Overall survivorship was higher on average in burned sites (median 73%, IQR 50-84%) compared to unburned sites (median 50%, IQR 24- 65%; Fig. 3). Among sites in which survivorship could be estimated for each species, overall survival was highest (>80%) for *P. contorta* (22 sites), *L. occidentalis* (14 sites), and *Abies spp.* (4 sites), with lower survival (averaging 50%) survival for *P. menziesii* (31 sites), *P. ponderosa* (7 sites), and *P. engelmannii* (5 sites). At annual timescales, survivorship varied with seedling age, with the lowest survival within the germination year (Fig. 3). In burned sites, annual seedling survivorship between the second and third year after fire was positively related to seedling age, canopy cover (*Canopy*, subplot scale), and total moss and forb cover (*Moss &*

Forb, subplot scale), and negatively related to *DEF* and resin nitrate (*NO3*), with a model AUC of 0.77 (Fig. 6). Expected probability of survival decreased with higher *DEF*, but only for seedlings of younger ages (Fig. 6A).

Seedling height after three years was positively related to microclimate (T_{avg}) and moss and forb cover (*Axis2*), with the most pronounced growth in sites with warm, dry microclimate (Fig. B.5). Seedling height also varied among species ($p < 0.001$, Kruskal-Wallis $X^2 = 43.2$, $df = 5$). *P. engelmannii* seedlings were the smallest on average after three years, while *L. occidentalis* and *P. ponderosa* were the largest on average (Fig. 3). *L. occidentalis* grew fastest over the three-year period, with median height of 11.5 cm (IQR 8 – 18 cm) at age three and a maximum of 42 cm.

Discussion

Our findings of abundant tree regeneration provide an important example of how forests can exhibit early resilience to contemporary fire activity, even in the context of increasingly stressful climate conditions for post-fire tree regeneration over the 21st century (e.g., Davis et al. 2019a). Biophysical aspects of the pre- and post-fire environments helped explain over 75% of the variability observed in post-fire conifer density in the two large fires we studied, supporting predictions based on the demographic framework used to frame our study (Fig. 1). This understanding elucidates the relative importance of fire effects on microclimate and microsite factors that influence recruitment, survival, and growth, and helps anticipate how forest resilience to wildfires may change under changing climate.

Evidence of forest resilience to wildfire

Mixed-conifer forests at our sites exhibited signs of resilience to recent moderate- and high-severity wildfire. Given abundant natural post-fire regeneration (Fig. 3, Fig. B.1), we expect

Chapter 2

these sites to develop species composition and stand characteristics broadly similar to pre-fire conditions. The regeneration observed in these individual fires contrasts with recent observations of declines in post-fire conifer regeneration at larger regional scales in the northern Rocky Mountains and across the West (Donato et al. 2016, Stevens-Rumann et al. 2018, Davis et al. 2019a, Rodman et al. 2020a). We attribute this robust regeneration in part to moderate post-fire climate conditions experienced from 2018-2020, which supported high rates of seedling survival (Fig. 3). Growing-season (June-September) daily maximum temperatures in 2018-2020 averaged only 0.3 °C (0.21 sd) above the 1981-2020 mean in Missoula, Montana, with precipitation only 32 mm (0.63 sd) below average (Western Regional Climate Center 2021); these values varied little among the three study years (Fig. A.1). Similarly, recent studies in the eastern Cascade Mountains of Washington state provide examples of robust conifer regeneration under mild post-fire climate conditions (Littlefield 2019, Povak et al. 2020).

Importantly, all of our sites were within 100 m of a live seed source, by design, so our findings apply to locations where dispersal distance is not severely limiting to seed availability (e.g., Kemp et al. 2016, Chambers et al. 2016, Littlefield 2019, Peeler and Smithwick 2020). Although we did not sample across a full range of distance-to-seed-source values, the fires studied here are characterized by complex spatial patterns of fire severity, as is common within even large fires in the region (e.g., Turner et al. 1994, Harvey et al. 2016a). As such, our sites are representative of the majority of burned areas within these fires, which are proximate to potential seed sources (Fig. A.5).

A key uncertainty in our ability to anticipate forest resilience to these wildfires is whether the initial patterns of regeneration observed here will be maintained, to ultimately determine longer-term trajectories in tree densities and species composition (Gill et al. 2017). Given the

Chapter 2

context of directional climate warming, it is possible that the observed early resilience could be undermined by future tree mortality events. For example, *P. ponderosa* seedlings in northern Arizona experienced substantial mortality (65%) due to drought conditions five years after cohort initiation (Kolb et al. 2020). Nevertheless, our finding of increasing survival with seedling age (Fig. 3) suggests that only a severe drought or subsequent disturbance would alter the successional trajectories established thus far. While the long-term fate of these forests is unknown, our findings exemplify mechanisms of post-fire forest recovery that are likely operating within the “safe operating space” defined by the historical range of variability (Johnstone et al. 2016).

Mechanisms of forest resilience to wildfires

We identify three key mechanisms of resilience to moderate- and high-severity wildfires in these mixed-conifer forests. First, the availability of viable seeds consistently serves as the first biotic filter to overcome for post-fire tree regeneration (Davis et al. 2018, Stevens-Rumann and Morgan 2019) (Fig. 4, 5). While we used distance to seed source as a coarse metric for seed rain, its importance in our statistical models highlights the need to account for potential seed availability when evaluating the influence of other factors on post-fire regeneration (e.g., fire severity). Secondly, our results demonstrate how post-fire regeneration depends on microclimate conditions, reflecting an interaction between climate and fire severity. Finally, our results underscore that fire itself facilitates tree regeneration, with heterogeneity in fire effects at multiple scales supporting regeneration via seed provision and microsite diversity. Our results are consistent with demographic predictions and observational studies from conifer forests across the West highlighting seed dispersal and climate as key filters on post-fire regeneration (e.g., Harvey et al. 2016b, Stevens-Rumann et al. 2018, Kemp et al. 2019, Rodman et al. 2020b, Busby

and Holz 2022; Fig. 1). Further, this study provides an example revealing how microsite factors affected by fire severity can either facilitate or limit regeneration.

Our findings highlight important influences of post-fire microclimate conditions on seedling establishment and survival. Total seedling densities, annual recruitment, and annual survivorship were all higher in relatively cool-wet sites (Fig. 4-6), indicating that regeneration was sensitive to near-ground microclimate conditions. The impacts of microclimate on regeneration are strongest in early life stages, when juveniles are vulnerable to desiccation or heat-induced mortality from warm, dry atmospheric or soil conditions (Kolb and Robberecht 1996, Johnson et al. 2011, Miller and Johnson 2017). We found that seedling survival was most sensitive to climate between the germination year and the second year of life (Fig. 6A), supporting the idea that weather and climate conditions during the germination year serve as an important mortality filter affecting forest regeneration (Stein and Kimberling 2003).

Our results further demonstrate how fire plays a vital role in facilitating regeneration in these forests. Seedling recruitment was strongly predicted by the basal area of *P. contorta* in the first year after fire, demonstrating the likely importance of serotiny in driving initial post-fire regeneration where *P. contorta* was present (Fig. 5A). Further, initial recruitment and survival were greater on average in burned sites compared to unburned sites, implying more favorable site conditions for seedlings after fire (Fig. 3). Moderate- and high-severity wildfire increase the availability of resources such as light, favorable seed beds, and growth-limiting nutrients (e.g., Pausas et al. 2002, Urza and Sibold 2017), which limit regeneration in unburned forest (Fig. B.4, B.6). Declining recruitment by the third year after fire implies that such favorable conditions are short-lived, with initial patterns of establishment during this “window of opportunity” ultimately shaping forest trajectories (Karavani et al. 2018).

The contrasting impacts of recent wildfire on regeneration – through both increased resource availability and exposure to microclimatic extremes – illustrates how high-severity fire creates trade-offs that govern post-fire conifer seedling demography. For example, seedling recruitment was higher in sites with greater tree mortality given similar distance to seed source (Fig. 5D). This implies that while some remaining canopy cover, even dead, supports regeneration through microclimatic buffering, overstory mortality also supports regeneration, via greater light availability and/or increased soil moisture due to reduced canopy interception and evapotranspiration (Ma et al. 2010, Parra and Moreno 2017, Rodman et al. 2020b, Kolb et al. 2020). Responses to this trade-off varied among species; for instance, *P. menziesii* seedling density was greater in sites that burned at lower severity (Fig. 4A), indicating greater germination and survival in cooler, more shaded environments. This pattern is consistent with prior studies and the greater shade-tolerance of *P. menziesii* compared to *P. contorta*, *L. occidentalis*, or *P. ponderosa* (Minore 1979, Rodman et al. 2020b).

Fire severity thus alters biophysical factors in ways that both promote and impede the regeneration of each conifer species. Our findings imply that soil nitrogen availability represents another such trade-off. Consistent with a widely-observed short-term N pulse after fire (Smithwick et al. 2005), nitrogen availability was elevated in burned soils (Fig. B.6). High post-fire soil inorganic nitrogen was associated with low seedling recruitment and survival (Fig. 5G, 6D), with the exception of *P. menziesii*. High N supply could stimulate aboveground growth without commensurate root development, potentially inhibiting seedling drought resistance and survival (Isaac and Hopkins 1937, Benseid 1943, Nilsen 1995). Alternatively, elevated soil inorganic nitrogen may be associated with other changes, such as reduced mycorrhizal abundance and diversity (Taudière et al. 2017, Remke et al. 2020) or enhanced erosion (Certini

2005). Additional research is needed to evaluate how fire effects on soil physical properties, biogeochemical processes, and biota affect seedling physiology and demography. Nevertheless, our results imply that while some N availability and exposure of mineral seed beds may generally benefit seedlings (Fig. B.4), severe soil impacts likely inhibit regeneration.

These multifaceted effects of fire severity highlight how burn mosaics can promote forest resilience. At patch scales (e.g., 10^2 - 10^4 m²; Coop et al. 2019), heterogeneity in tree mortality provides seed sources, while at finer microsite scales, heterogeneous canopy and understory environments facilitate regeneration. For example, *P. menziesii* and *L. occidentalis* seedling densities (Fig. 4) and all-species density, survival, and growth (Fig. 6, Fig. B.5) were higher in sites with greater moss and forb cover and less bare ground cover. Moss and forb cover could serve as a proxy for greater surface soil moisture or less competition from shrubs and grasses (Wagner et al. 1989, Landhausser et al. 1996, Plamboeck et al. 2008, Kolb et al. 2020, Carlson et al. 2020a). Indeed, forb cover (mostly *Chamaenerion angustifolium*) had a larger positive effect on recruitment on south- than north-facing sites (Fig. 5E), suggesting a potential facilitative effect through microclimatic buffering. This finding is consistent with studies demonstrating how shrubs can facilitate seedling establishment in semiarid environments (Urza et al. 2019, Crockett and Hurteau 2022), and it highlights the possibility that forbs could play a similar role as nurse plants in more mesic sites in the northern Rocky Mountains. Conversely, extensive bare soil may be associated with high surface temperatures or vulnerability to erosion (Certini 2005). While sites burned at higher severity had more bare ground and less forb cover ($\rho = 0.67$ and $\rho = -0.47$, respectively; $p < 0.001$, $n = 47$), moss and coarse wood cover did not differ with fire severity, suggesting that high-severity patches can harbor favorable below-canopy microsites. Thus, fine-scale heterogeneity in fire effects promotes resilience even within areas of stand-replacing fire.

Several limitations to this study highlight priorities for continued research. Most critically, the regeneration patterns observed here could be altered by continued recruitment or mortality (Gill et al. 2017, Kolb et al. 2020). Future research should quantify changes in climate sensitivity as seedlings age, to evaluate vulnerability to climatic extremes over time. Additional research priorities include investigating what drives differing sensitivity among species, for example the contrasting responses to soil nitrogen availability and overstory fire severity in *P. menziesii* compared with general trends (Fig. 4, Table B.4). In addition, our study did not consider post-fire contingencies of seed masting in conifers; *P. ponderosa* recruitment was low in our sites relative to co-occurring species, and it is unclear if this is due to environmental drivers or a lack of mast years during the sampling window (Keyes et al. 2015). Regeneration was likely also influenced by unmeasured factors, including soil moisture, seed predation, and herbivory (Fig. 1). Although our interpretations are limited to a narrow range of conditions, our findings demonstrate the utility of a demographic framework for predicting the dominant controls of post-fire conifer regeneration.

Implications for forest management

Our findings support three important management approaches used to promote or maintain forest resilience to wildfires. First, a diversity of microsite conditions supported regeneration, implying that heterogeneity in pre-fire forest structure, fire severity, and post-fire understory communities can create microrefugia for tree seedlings. Our results thus support the use of fuel treatments in low- and mixed-severity fire regimes, under the goal of promoting patch and microsite diversity (Prichard et al. 2021). While fuels management is less effective in subalpine forests with high-severity fire regimes (Halofsky et al. 2018), allowing fires to burn

under moderate fire weather could achieve similar goals by promoting heterogeneity in fire effects.

Second, our results bolster the understanding that post-fire planting is most effective in areas lacking seed sources and in relatively cool-wet topographical settings, with residual structures to provide shading, and with little competition from shrubs and grasses (e.g., Stevens-Rumann and Morgan 2019) (Fig. 5-6). Finally, our results support the utility of predictive spatial models for reforestation planning (Holden et al. 2021). Despite the importance of field-based microclimate metrics, our statistical models also did an excellent job explaining seedling density based on topoclimate and fire severity alone (Fig. 4, Table B.1), suggesting that fine-scale (250-m) climate data capture spatial variation in microclimate that is useful in management contexts.

Anticipating forest resilience under changing climate and fire regimes

Climate change over the remainder of the 21st century has the potential to undermine the forest resilience observed in this study, directly via more stressful climate conditions, indirectly via higher fire activity, and through interactions between climate and fire that alter local microclimate conditions (Fig. 5F). Our results imply that fire-caused canopy loss can amplify the impacts of climate warming on regeneration by increasing exposure to warm-dry extremes (Zellweger et al. 2020), particularly in the first few years after fire prior to vegetation recovery, and in relatively cool-wet forests where canopy loss has a larger absolute effect on microclimate (Davis et al. 2019b, Wolf et al. 2021). Indeed, other studies from the Rocky Mountains highlight the potential for short-interval severe fire to sharply curtail regeneration via seed limitation and stressful post-fire microclimate and soil conditions (e.g., Turner et al. 2019, Hoecker et al. 2020, Rammer et al. 2021). Forest development will thus depend on microclimate conditions and the frequency, severity, and spatial patterning of fire.

Finally, varied responses to fire severity among species (Fig. 4A) suggest that fire-relevant traits will govern post-fire seedling demography, ultimately driving changes in species composition anticipated under climate change. For example, our finding of greater *P. menziesii* recruitment in sites with remaining canopy cover (Fig. 4, Table B.3) suggests that it may be particularly vulnerable to increased fire severity. In contrast, we found that *L. occidentalis* was fast-growing (Fig. B.5) and regenerated at greater densities in areas of high overstory fire severity (Fig. 4), implying that it may be well-suited to take advantage of high-light, recently disturbed areas (Steed and Goeking 2020). In contrast to regeneration failures expected at lower-treeline ecotones where warming exceeds species tolerances (Davis et al. 2019a), wildfires in mid- and high-elevation forests have the potential to catalyze shifts in relative abundances in areas of overlapping species distributions (Hoecker and Turner 2022).

Literature Cited

- Abatzoglou, J. T., and A. P. Williams. 2016. Impact of anthropogenic climate change on wildfire across western US forests. *Proceedings of the National Academy of Sciences* 113:11770–11775.
- Andrus, R. A., B. J. Harvey, K. C. Rodman, S. J. Hart, and T. T. Veblen. 2018. Moisture availability limits subalpine tree establishment. *Ecology* 99:567–575.
- Bartoń, K. 2022, February 24. MuMIn: Multi-Model Inference.
- Bensend, D. W. 1943. Effect of Nitrogen on Growth and Drouth Resistance of Jack Pine Seedlings.
- Binkley, D., and P. Matson. 1983. Ion Exchange Resin Bag Method for Assessing Forest Soil Nitrogen Availability. *Soil Science Society of America Journal* 47:1050–1052.

Chapter 2

- Buma, B., C. D. Brown, D. C. Donato, J. B. Fontaine, and J. F. Johnstone. 2013. The Impacts of Changing Disturbance Regimes on Serotinous Plant Populations and Communities. *BioScience* 63:866–876.
- Busby, S. U., and A. Holz. 2022. Interactions Between Fire Refugia and Climate-Environment Conditions Determine Mesic Subalpine Forest Recovery After Large and Severe Wildfires. *Frontiers in Forests and Global Change* 5.
- Carlson, A. R., J. S. Sibold, and J. F. Negrón. 2020a. Canopy structure and below-canopy temperatures interact to shape seedling response to disturbance in a Rocky Mountain subalpine forest. *Forest Ecology and Management* 472:118234.
- Carlson, A. R., J. S. Sibold, and J. F. Negrón. 2020b. Wildfire and spruce beetle outbreak have mixed effects on below-canopy temperatures in a Rocky Mountain subalpine forest. *Journal of Biogeography*:jbi.13994.
- Certini, G. 2005. Effects of fire on properties of forest soils: a review. *Oecologia* 143:1–10.
- Chambers, M. E., P. J. Fornwalt, S. L. Malone, and M. A. Battaglia. 2016. Patterns of conifer regeneration following high severity wildfire in ponderosa pine – dominated forests of the Colorado Front Range. *Forest Ecology and Management* 378:57–67.
- Clark, J. S., R. Andrus, M. Aubry-Kientz, Y. Bergeron, M. Bogdziewicz, D. C. Bragg, D. Brockway, N. L. Cleavitt, S. Cohen, B. Courbaud, R. Daley, A. J. Das, M. Dietze, T. J. Fahey, I. Fer, J. F. Franklin, C. A. Gehring, G. S. Gilbert, C. H. Greenberg, Q. Guo, J. HilleRisLambers, I. Ibanez, J. Johnstone, C. L. Kilner, J. Knops, W. D. Koenig, G. Kunstler, J. M. LaMontagne, K. L. Legg, J. Luongo, J. A. Lutz, D. Macias, E. J. B. McIntire, Y. Messaoud, C. M. Moore, E. Moran, J. A. Myers, O. B. Myers, C. Nunez, R. Parmenter, S. Pearse, S. Pearson, R. Poulton-Kamakura, E. Ready, M. D. Redmond, C.

Chapter 2

- D. Reid, K. C. Rodman, C. L. Scher, W. H. Schlesinger, A. M. Schwantes, E. Shanahan, S. Sharma, M. A. Steele, N. L. Stephenson, S. Sutton, J. J. Swenson, M. Swift, T. T. Veblen, A. V. Whipple, T. G. Whitham, A. P. Wion, K. Zhu, and R. Zlotin. 2021. Continent-wide tree fecundity driven by indirect climate effects. *Nature Communications* 12:1242.
- Coop, J. D., T. J. Delory, W. M. Downing, S. L. Haire, M. A. Krawchuk, C. Miller, M. A. Parisien, and R. B. Walker. 2019. Contributions of fire refugia to resilient ponderosa pine and dry mixed-conifer forest landscapes. *Ecosphere* 10:e02809.
- Coop, J. D., S. A. Parks, C. S. Stevens-Rumann, S. D. Crausbay, P. E. Higuera, M. D. Hurteau, A. Tepley, E. Whitman, T. Assal, B. M. Collins, K. T. Davis, S. Dobrowski, D. A. Falk, P. J. Fornwalt, P. Z. Fulé, B. J. Harvey, V. R. Kane, C. E. Littlefield, E. Q. Margolis, M. North, M. A. Parisien, S. Prichard, and K. C. Rodman. 2020. Wildfire-Driven Forest Conversion in Western North American Landscapes. *BioScience* 70:659–673.
- Crockett, J. L., and M. D. Hurteau. 2022. Post-fire early successional vegetation buffers surface microclimate and increases survival of planted conifer seedlings in the southwestern United States. *Canadian Journal of Forest Research* 52:416–425.
- Davis, K. T., S. Z. Dobrowski, P. E. Higuera, Z. A. Holden, T. T. Veblen, M. T. Rother, S. A. Parks, A. Sala, and M. P. Maneta. 2019a. Wildfires and climate change push low-elevation forests across a critical climate threshold for tree regeneration. *Proceedings of the National Academy of Sciences* 116:6193–6198.
- Davis, K. T., S. Z. Dobrowski, Z. A. Holden, P. E. Higuera, and J. T. Abatzoglou. 2019b. Microclimatic buffering in forests of the future: the role of local water balance. *Ecography* 42:1–11.

Chapter 2

- Davis, K. T., P. E. Higuera, S. Dobrowski, S. Parks, J. T. Abatzoglou, M. Rother, and T. Veblen. 2020. Fire-catalyzed vegetation shifts in ponderosa pine and Douglas-fir forests of the western United States. *Environmental Research Letters* 15:1040–1048.
- Davis, K. T., P. E. Higuera, and A. Sala. 2018. Anticipating fire-mediated impacts of climate change using a demographic framework. *Functional Ecology* 32:1729–1745.
- De Frenne, P., F. Zellweger, F. Rodríguez-Sánchez, B. R. Scheffers, K. Hylander, M. Luoto, M. Vellend, K. Verheyen, and J. Lenoir. 2019. Global buffering of temperatures under forest canopies. *Nature Ecology & Evolution* 3:744–749.
- Dobrowski, S. Z. 2011. A climatic basis for microrefugia: the influence of terrain on climate. *Global Change Biology* 17:1022–1035.
- Donato, D. C., B. J. Harvey, and M. G. Turner. 2016. Regeneration of montane forests 24 years after the 1988 Yellowstone fires: A fire-catalyzed shift in lower treelines? *Ecosphere* 7:e01410.
- Enright, N. J., J. B. Fontaine, D. M. J. S. Bowman, R. A. Bradstock, and R. J. Williams. 2015. Interval squeeze: Altered fire regimes and demographic responses interact to threaten woody species persistence as climate changes. *Frontiers in Ecology and the Environment* 13.
- Falk, D. A., P. J. van Mantgem, J. E. Keeley, R. M. Gregg, C. H. Guiterman, A. J. Tepley, D. JN Young, and L. A. Marshall. 2022. Mechanisms of forest resilience. *Forest Ecology and Management* 512:120129.
- Fox, J., and S. Weisberg. 2018. Visualizing fit and lack of fit in complex regression models with predictor effect plots and partial residuals. *Journal of Statistical Software* 87.

Chapter 2

- Fukami, T. 2015. Historical Contingency in Community Assembly: Integrating Niches, Species Pools, and Priority Effects. *Annual Review of Ecology Evolution and Systematics* 46:1–23.
- Gill, N. S., D. Jarvis, T. T. Veblen, S. T. A. Pickett, and D. Kulakowski. 2017. Is initial post-disturbance regeneration indicative of longer-term trajectories? *Ecosphere* 8:e01924.
- Gill, N. S., M. G. Turner, C. D. Brown, S. I. Glassman, S. L. Haire, W. D. Hansen, E. R. Pansing, S. B. St Clair, and D. F. Tomback. 2022. Limitations to Propagule Dispersal Will Constrain Postfire Recovery of Plants and Fungi in Western Coniferous Forests. *BioScience:biab139*.
- Gunderson, L. H. 2000. Ecological Resilience—In Theory and Application. *Annual Review of Ecology and Systematics* 31:425–439.
- Halofsky, J. S., D. C. Donato, J. F. Franklin, J. E. Halofsky, D. L. Peterson, and B. J. Harvey. 2018. The nature of the beast: examining climate adaptation options in forests with stand-replacing fire regimes. *Ecosphere* 9:e02140.
- Hankin, L. E., P. E. Higuera, K. T. Davis, and S. Z. Dobrowski. 2018. Accuracy of node and bud-scar counts for aging two dominant conifers in western North America. *Forest Ecology and Management* 427:365–371.
- Hansen, W. D., K. H. Braziunas, W. Rammer, R. Seidl, and M. G. Turner. 2018. It takes a few to tango: changing climate and fire regimes can cause regeneration failure of two subalpine conifers. *Ecology* 99:966–977.
- Hartig, F. 2021. Residual Diagnostics for Hierarchical (Multi-Level / Mixed) Regression Models [R package DHARMA version 0.4.1]. Comprehensive R Archive Network (CRAN).

Chapter 2

- Harvey, B. J., D. C. Donato, and M. G. Turner. 2016a. Drivers and trends in landscape patterns of stand-replacing fire in forests of the US Northern Rocky Mountains (1984–2010). *Landscape Ecology*.
- Harvey, B. J., D. C. Donato, and M. G. Turner. 2016b. High and dry: post-fire tree seedling establishment in subalpine forests decreases with post-fire drought and large stand-replacing burn patches. *Global Ecology and Biogeography* 25:655–669.
- Hill, E. M., and S. Ex. 2020. Microsite conditions in a low-elevation Engelmann spruce forest favor ponderosa pine establishment during drought conditions. *Forest Ecology and Management* 463:118037.
- Hoecker, T. J., W. D. Hansen, and M. G. Turner. 2020. Topographic position amplifies consequences of short-interval stand-replacing fires on postfire tree establishment in subalpine conifer forests. *Forest Ecology and Management* 478:118523.
- Hoecker, T. J., and M. G. Turner. 2022. A short-interval reburn catalyzes departures from historical structure and composition in a mesic mixed-conifer forest. *Forest Ecology and Management* 504:119814.
- Holden, Z. A., A. Swanson, C. H. Luce, W. M. Jolly, M. Maneta, J. W. Oyler, D. A. Warren, R. Parsons, and D. Affleck. 2018. Decreasing fire season precipitation increased recent western US forest wildfire activity. *Proceedings of the National Academy of Sciences* 115:E8349–E8357.
- Holden, Z., A. Warren, E. Jungck, M. Maneta, S. Dobrowski, K. Davis, V. Archer, and S. Fox. 2021. *Topofire -- Regeneration Mapper*. University of Montana, Missoula.
- Isaac, L. A., and H. G. Hopkins. 1937. The Forest Soil of the Douglas Fir Region, and Changes Wrought Upon it by Logging and Slash Burning. *Ecology* 18:264–279.

Chapter 2

- Johnson, D. M., K. A. McCulloh, and K. Reinhardt. 2011. The Earliest Stages of Tree Growth: Development, Physiology and Impacts of Microclimate. Pages 65–87 in F. C. Meinzer, B. Lachenbruch, and T. E. Dawson, editors. *Size- and Age-Related Changes in Tree Structure and Function*. Springer Netherlands, Dordrecht, Netherlands.
- Johnstone, J. F., C. D. Allen, J. F. Franklin, L. E. Frelich, B. J. Harvey, P. E. Higuera, M. C. Mack, R. K. Meentemeyer, M. R. Metz, G. L. W. Perry, T. Schoennagel, and M. G. Turner. 2016. Changing disturbance regimes, ecological memory, and forest resilience. *Frontiers in Ecology and the Environment* 14:369–378.
- Johnstone, J. F., and F. S. Chapin. 2006. Effects of Soil Burn Severity on Post-Fire Tree Recruitment in Boreal Forest. *Ecosystems* 9:14–31.
- Karavani, A., M. M. Boer, M. Baudena, C. Colinas, R. Díaz-Sierra, J. Pemán, M. de Luis, Á. Enríquez-de-Salamanca, and V. Resco de Dios. 2018. Fire-induced deforestation in drought-prone Mediterranean forests: drivers and unknowns from leaves to communities. *Ecological Monographs* 88:141–169.
- Kemp, K. B., P. E. Higuera, and P. Morgan. 2016. Fire legacies impact conifer regeneration across environmental gradients in the U.S. northern Rockies. *Landscape Ecology* 31:619–636.
- Kemp, K. B., P. E. Higuera, P. Morgan, and J. T. Abatzoglou. 2019. Climate will increasingly determine post-fire tree regeneration success in low-elevation forests, Northern Rockies, USA. *Ecosphere* 10:e02568.
- Keyes, C. R., R. Manso Gonzalez, and R. M. Gonzalez. 2015. Climate-influenced ponderosa pine (*Pinus ponderosa*) seed masting trends in western Montana, USA.

Chapter 2

- Kolb, P. F., and R. Robberecht. 1996. High temperature and drought stress effects on survival of *Pinus ponderosa* seedlings. *Tree Physiology* 16:665–672.
- Kolb, T. E., K. Flathers, J. B. Bradford, C. Andrews, L. A. Asherin, and W. K. Moser. 2020. Stand Density, Drought and Herbivory Constrain Ponderosa Pine Regeneration Pulse. *Canadian Journal of Forest Research*:cjfr-2019-0248.
- Landhausser, S. M., K. J. Stadt, and V. J. Lieffers. 1996. Screening for Control of a Forest Weed: Early Competition Between Three Replacement Species and *Calamagrostis canadensis* of *Picea glauca*. *Journal of Applied Ecology* 33:1517–1526.
- Littlefield, C. E. 2019. Topography and post-fire climatic conditions shape spatio-temporal patterns of conifer establishment and growth. *Fire Ecology* 15.
- Ma, S., A. Concilio, B. Oakley, M. North, and J. Chen. 2010. Spatial variability in microclimate in a mixed-conifer forest before and after thinning and burning treatments. *Forest Ecology and Management* 259:904–915.
- McCune, B., and D. Keon. 2002. Equations for potential annual direct incident radiation and heat load. *Journal of Vegetation Science* 13:603–606.
- Miller, M. L., and D. M. Johnson. 2017. Vascular development in very young conifer seedlings: Theoretical hydraulic capacities and potential resistance to embolism. *American Journal of Botany* 104:979–992.
- Minore, D. 1979. Comparative autoecological characteristics of northwestern tree species - a literature review. Portland, OR.
- Morgan, P., E. K. Heyerdahl, and C. E. Gibson. 2008. Multi-season climate synchronized fires throughout the 20th century, northern Rockies, USA. *Ecology* 89:717–728.

Chapter 2

MTBS Project (USDA Forest Service/U.S. Geological Survey). 2019. MTBS Data Acces: Fire Level Geospatial Data. <http://mtbs.gov>.

Nilsen, P. 1995. Effect of nitrogen on drought strain and nutrient uptake in Norway spruce *Picea abies* (L.) Karst.) trees. *Plant and Soil* 172:73–85.

Parks, S. A., and J. T. Abatzoglou. 2020. Warmer and Drier Fire Seasons Contribute to Increases in Area Burned at High Severity in Western US Forests From 1985 to 2017. *Geophysical Research Letters* 47:e2020GL089858.

Parra, A., and J. M. Moreno. 2017. Post-fire environments are favourable for plant functioning of seeder and resprouter Mediterranean shrubs, even under drought. *New Phytologist* 214:1118–1131.

Pausas, J. G. G., N. Ouadah, A. Ferran, T. Gimeno, and R. Vallejo. 2002. Fire severity and seedling establishment in *Pinus halepensis* woodlands, eastern Iberian Peninsula. *Plant Ecology* 169:205–213.

Peeler, J. L., and E. A. H. Smithwick. 2020. Seed source pattern and terrain have scale-dependent effects on post-fire tree recovery. *Landscape Ecology* 35:1945–1959.

Plamboeck, A. H., M. North, and T. E. Dawson. 2008. Conifer Seedling Survival Under Closed-Canopy And Manzanita Patches In the Sierra Nevada. *Madroño* 55:191–201.

Povak, N. A., D. J. Churchill, C. A. Cansler, P. F. Hessburg, V. R. Kane, J. T. Kane, J. A. Lutz, and A. J. Larson. 2020. Wildfire severity and postfire salvage harvest effects on long-term forest regeneration. *Ecosphere* 11.

Prichard, S. J., P. F. Hessburg, R. K. Hagmann, N. A. Povak, S. Z. Dobrowski, M. D. Hurteau, R. V. Kane, R. E. Keane, L. N. Kobziar, C. A. Kolden, M. North, S. A. Parks, H. D. Safford, J. T. Stevens, L. L. Yocom, D. J. Churchill, R. W. Gray, D. W. Huffman, F. K.

Chapter 2

- Lake, and P. Khatri-Chhetri. 2021. Adapting western North American forests to climate change and wildfires: ten common questions. *Ecological Applications*:e02433.
- PRISM Climate Group (Oregon State University). 2015. PRISM 30-Year Normals. Oregon State University. <http://prism.oregonstate.edu>.
- R Core Team. 2020. R: A language and environment for statistical computing. R Foundation for Statistical Computing, Vienna, Austria.
- Rammer, W., K. H. Braziunas, W. D. Hansen, Z. Ratajczak, A. L. Westerling, M. G. Turner, and R. Seidl. 2021. Widespread regeneration failure in forests of Greater Yellowstone under scenarios of future climate and fire. *Global Change Biology* 00:gcb.15726.
- Remke, M. J., T. Hoang, T. Kolb, C. Gehring, N. C. Johnson, and M. A. Bowker. 2020. Familiar soil conditions help *Pinus ponderosa* seedlings cope with warming and drying climate. *Restoration Ecology* 28:S344–S354.
- Robin, X., N. Turck, A. Hainard, N. Tiberti, F. Lisacek, J. Sanchez, and M. Muller. 2011. pROC: an open-source package for R and S+ to analyze and compare ROC curves.
- Rodman, K. C., T. T. Veblen, M. A. Battaglia, M. E. Chambers, P. J. Fornwalt, Z. A. Holden, T. E. Kolb, J. R. Ouzts, and M. T. Rother. 2020a. A changing climate is snuffing out post-fire recovery in montane forests. *Global Ecology and Biogeography*.
- Rodman, K. C., T. T. Veblen, T. B. Chapman, M. T. Rother, A. P. Wion, and M. D. Redmond. 2020b. Limitations to recovery following wildfire in dry forests of southern Colorado and northern New Mexico, USA. *Ecological Applications* 30:e02001.
- Smithwick, E. A. H., M. G. Turner, M. C. Mack, and F. S. Chapin. 2005. Postfire Soil N Cycling in Northern Conifer Forests Affected by Severe, Stand-Replacing Wildfires. *Ecosystems* 8:163–181.

Chapter 2

Soil Survey Staff. 2017. SSURGO Web Soil Survey. Natural Resources Conservation Service, USDA.

Steed, J. E., and S. A. Goeking. 2020. Western larch regeneration responds more strongly to site and indirect climate factors than to direct climate factors. *Forests* 11.

Stein, S. J., and D. N. Kimberling. 2003. Germination, establishment, and mortality of naturally seeded Southwestern ponderosa pine. *Western Journal of Applied Forestry* 18:109–114.

Stevens-Rumann, C. S., K. B. Kemp, P. E. Higuera, B. J. Harvey, M. T. Rother, D. C. Donato, P. Morgan, and T. T. Veblen. 2018. Evidence for declining forest resilience to wildfires under climate change. *Ecology Letters* 21:243–252.

Stevens-Rumann, C. S., and P. Morgan. 2019, December 1. Tree regeneration following wildfires in the western US: a review. SpringerOpen.

Stewart, J. A. E., P. J. van Mantgem, D. J. N. Young, K. L. Shive, H. K. Preisler, A. J. Das, N. L. Stephenson, J. E. Keeley, H. D. Safford, M. C. Wright, K. R. Welch, and J. H. Thorne. 2021. Effects of postfire climate and seed availability on postfire conifer regeneration. *Ecological Applications* 31:e02280.

Taudière, A., F. Richard, and C. Carcaillet. 2017. Review on fire effects on ectomycorrhizal symbiosis, an unachieved work for a scalding topic. *Forest Ecology and Management* 391:446–457.

Tepley, A. J., F. J. Swanson, and T. A. Spies. 2013. Fire-mediated pathways of stand development in Douglas-fir/western hemlock forests of the Pacific Northwest, USA. *Ecology* 94:1729–1743.

Chapter 2

- Tepley, A. J., J. R. Thompson, H. E. Epstein, and K. J. Anderson-Teixeira. 2017. Vulnerability to forest loss through altered postfire recovery dynamics in a warming climate in the Klamath Mountains. *Global Change Biology* 23:4117–4132.
- Turner, M. G., K. H. Braziunas, W. D. Hansen, and B. J. Harvey. 2019. Short-interval severe fire erodes the resilience of subalpine lodgepole pine forests. *Proceedings of the National Academy of Sciences of the United States of America* 166:11319–11328.
- Turner, M. G., W. W. Hargrove, R. H. Gardner, and W. H. Romme. 1994. Effects of fire on landscape heterogeneity in Yellowstone National Park, Wyoming. *Journal of Vegetation Science* 5:731–742.
- Turner, M. G., T. G. Whitby, D. B. Tinker, and W. H. Romme. 2016. Twenty-four years after the Yellowstone Fires: Are postfire lodgepole pine stands converging in structure and function? *Ecology* 97:1260–1273.
- Urza, A. K., and J. S. Sibold. 2013. Nondestructive Aging of Postfire Seedlings for Four Conifer Species in Northwestern Montana. *Western Journal of Applied Forestry* 28:22–29.
- Urza, A. K., and J. S. Sibold. 2017. Climate and seed availability initiate alternate post-fire trajectories in a lower subalpine forest. *Journal of Vegetation Science* 28:43–56.
- Urza, A. K., P. J. Weisberg, J. C. Chambers, and B. W. Sullivan. 2019. Shrub facilitation of tree establishment varies with ontogenetic stage across environmental gradients. *New Phytologist* 223:1795–1808.
- Wagner, R. G., T. D. Petersen, D. W. Ross, and S. R. Radosevich. 1989. Competition thresholds for the survival and growth of ponderosa pine seedlings associated with woody and herbaceous vegetation. *New Forests* 3:151–170.

Chapter 2

Wang, T., A. Hamann, D. Spittlehouse, and C. Carroll. 2016. Locally downscaled and spatially customizable climate data for historical and future periods for North America. *PLoS ONE* 11:e0156720.

Western Regional Climate Center. 2021. Western U.S. Climate Historical Summaries. NOAA.

Wolf, K. D., P. E. Higuera, K. T. Davis, and S. Z. Dobrowski. 2021. Wildfire impacts on forest microclimate vary with biophysical context. *Ecosphere* 12:e03467.

Zellweger, F., P. D. Frenne, J. Lenoir, P. Vangansbeke, K. Verheyen, M. Bernhardt-Römermann, L. Baeten, R. Hédl, I. Berki, J. Brunet, H. V. Calster, M. Chudomelová, G. Decocq, T. Dirnböck, T. Durak, T. Heinken, B. Jaroszewicz, M. Kopecký, F. Máliš, M. Macek, M. Malicki, T. Naaf, T. A. Nagel, A. Ortmann-Ajkai, P. Petřík, R. Pielech, K. Reczyńska, W. Schmidt, T. Standovár, K. Świerkosz, B. Teleki, O. Vild, M. Wulf, and D. Coomes. 2020. Forest microclimate dynamics drive plant responses to warming. *Science* 368:772–775.

CHAPTER 2

Tables

Table 1. Description of the four sets of models used to understand controls of post-fire demographic processes, including the response variables, their scale of measurement, model family, link function, and potential random intercept terms. Sample sizes are reported for regeneration of all species in burned sites. Note that separate models of density, recruitment, and survivorship were built for all species together and for species individually, whereas the growth model included species as a categorical variable.

	<i>Response</i>	<i>Scale of measurement</i>	<i>Sample size</i>	<i>Model family</i>	<i>Link function</i>	<i>Random effects</i>
Density	Net regeneration after 3 yr post-fire	Transect	47 sites	Negative binomial	log	Fire
Recruitment	Annual seedling establishment	Transect	128 site-yr combinations	Negative binomial	log	Fire Site
Survivorship	Inter-annual survival between yr 2 & 3 post-fire	Subplot	186 subplots	Binomial	logit	Fire Site
Growth	Seedling height after 3 yr post-fire	Individual	582 seedlings	Gamma	log	Fire Site Subplot

Table 2. Predictors of seedling regeneration considered in statistical models. Predictors are grouped into broad categories describing key controls of regeneration: potential seed availability, topoclimate/microclimate, and fire effects, each of which includes several subcategories of related variables describing distinct aspects of the three broad controls. Model selection initially included one variable from each subcategory of predictors. Water balance and microclimate variables were not included in the same models because they covaried.

Category	Subcategory	Candidate Variable	Units	Description
Seed availability	Seed source proximity	<i>PP_dWt</i>		Propagule pressure, defined as distance-weighted live tree cover in a 200-m radius around site center.
		<i>DSS</i>	m	Plot-averaged distance to the nearest live tree of any species, measured in the field.
		<i>BA_{Spp_L}</i>		Live basal area of focal species, used only in species-specific models.
	Serotiny	<i>BA_{PICO}</i>		Plot-averaged basal area of <i>P. contorta</i> , used as a proxy for potential release of serotinous cones. Used only in all-species and PICO models.
	Forest type	<i>Spp_{present}</i>	1/0	Binary: 1 if focal species is present in overstory or as a seed source, 0 otherwise. Used only in species-specific models.
(Micro) climate	Topoclimate	<i>HLI</i>		Unitless index of potential solar heating.
	Precipitation	<i>ppt_{ann}</i>	mm	35-year average annual precipitation.
		<i>ppt_{JJAS}</i>	mm	35-year average growing-season precipitation.
		<i>ppt_{pf}</i>	mm	2-year postfire average growing-season precipitation.
	Water balance vs. Microclimate	<i>DEF</i>	mm	35-year average climatic water deficit (250 m).
		<i>T_{max}</i>	°C	Modeled post-fire absolute maximum JJAS temperature.
	<i>T_{avg}</i>	°C	Modeled post-fire average daily maximum JJAS temperature.	
Fire effects	Overstory	<i>Axis1</i>		First principle component of field measurements describing fire severity, with positive values reflecting greater overstory mortality and loss of live canopy cover.
		<i>dnbr</i>		Delta Normalized Burn Ratio: satellite-derived metric of fire severity.
		<i>Canopy</i>	%	Live + dead canopy cover, averaged to site scale for models of seedling density.
	Understory	<i>Axis2</i>		Second principle component of field measurements describing fire severity, with positive values reflecting greater bare ground cover and negative values reflecting greater moss and forb cover.
		<i>Cover</i>	%	Six variables describing ground cover in subplots of different vegetation types (Moss, Forb, Grass, Shrub),

Chapter 2

			coarse woody debris (Wood), and bare ground (Bare), which are averaged to site scale for models of seedling density.
Soil	<i>soilN</i> <i>NO3</i> <i>NH4</i>	$\mu\text{g N}$ day^{-1}	Three variables describing resin-capsule inorganic nitrogen (NO_3 , NH_4 , or total), an integrated measure of nitrogen availability in years 1-2 post-fire.

Figures

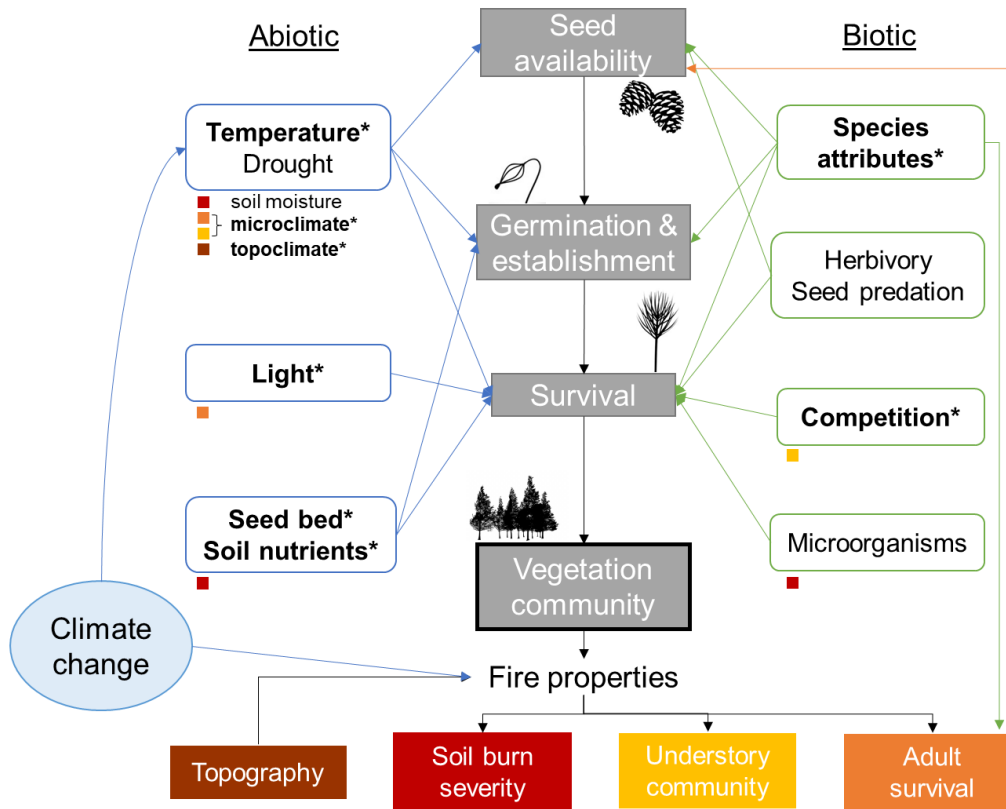


Figure 1. Demographic filter framework predicting key factors governing post-fire tree regeneration in the context of climate change, adapted from Davis et al. (2018). Conifer regeneration requires passing through three demographic stages (grey rectangles), which are affected by varying abiotic (blue rectangles) and biotic (green rectangles) factors. Fire properties (e.g., intensity, size, spatial patterns) influence these abiotic and biotic conditions in the post-fire environment, and are in turn influenced by climate (and climate change), the vegetation community, and topography. Factors that are bold with asterisks are accounted for, directly or indirectly, in this study.

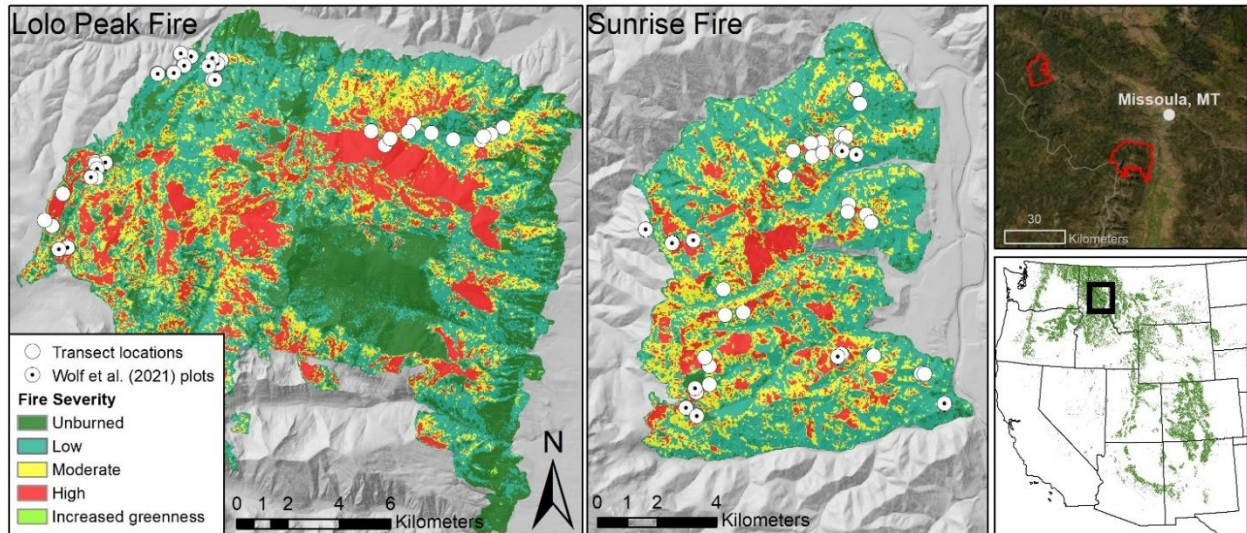


Figure 2. Map of study area and sample sites in the Lolo Peak ($n = 35$ sites) and Sunrise fires ($n = 34$). Sample sites include those that are unique to this study (white circles) and those which also have microclimate measurements published in Wolf et al. (2021) (white circles with black dots). Fire severity classifications are from the Monitoring Trends in Burn Severity project (MTBS Project (USDA Forest Service/U.S. Geological Survey) 2019), and satellite imagery is from Esri. The green area in the lower right panel delineates the extent of Rocky Mountain forest cover, defined by LANDFIRE’s National Vegetation Classification product (landfire.gov).

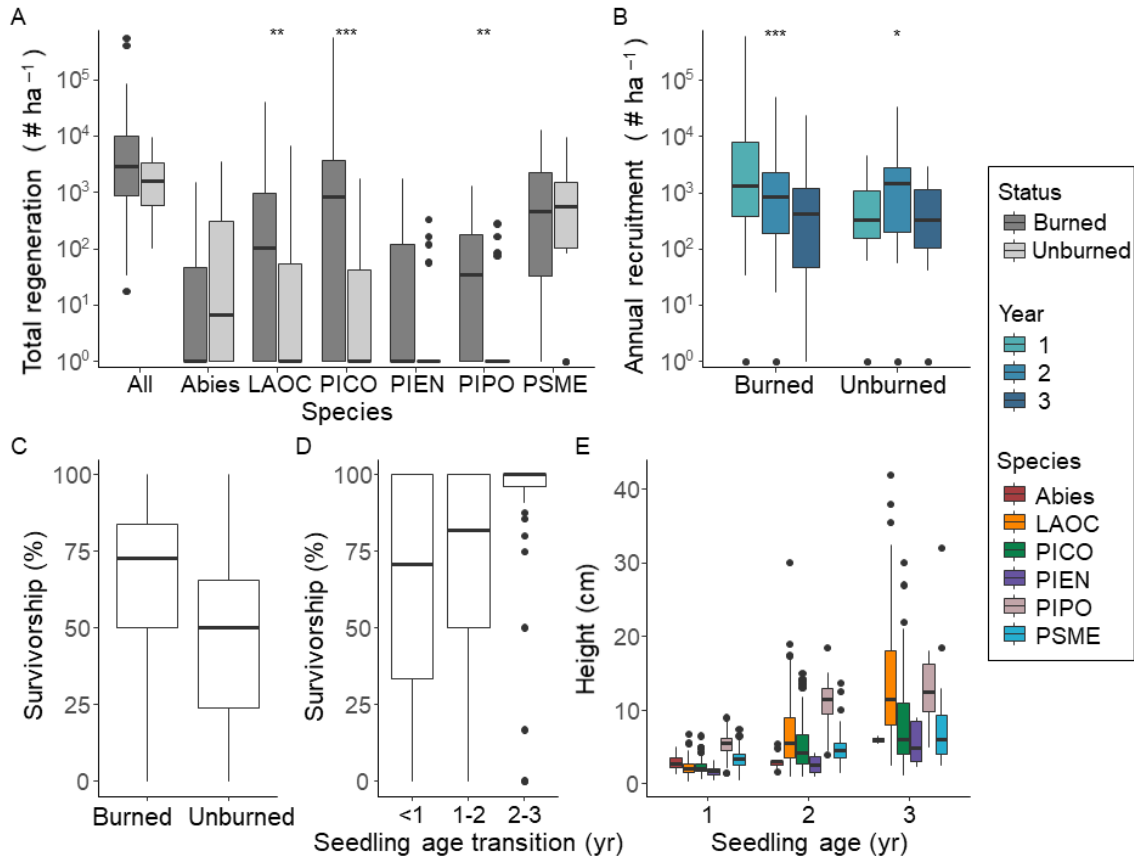


Figure 3. Estimates of total regeneration, annual recruitment, seedling survivorship, and height measurements over the first three years after fire. **A:** Total regeneration of all species and individual species in burned and unburned sites. **B:** Annual recruitment (density of germination-year seedlings) in burned and unburned sites. A constant of 1 was added to seedling density values to allow them to be represented on a log scale. Asterisks indicate statistical significance of nonparametric Wilcoxon rank-sum tests comparing burned and unburned sites (A), and Friedman tests comparing years (B) [$* p < 0.05$, $** p < 0.01$, $*** p < 0.001$]. **C:** Total percent survivorship of all marked seedlings over 2018-2020 in burned and unburned sites. **D:** Annual survivorship of marked seedlings across different age transitions: < 1 yr is intra-annual survival of germination-year seedlings; 1-2 is inter-annual survival from the first to the second growing season of life; and 2-3 is inter-annual survival from the second to the third growing season. Survivorship values

Chapter 2

for each age transition differ in the sampling window over which they were measured, and not all age-sampling year combinations are represented in the dataset; intra-annual survivorship of germinant seedlings was only measured once, from June to August/September 2019. **E:** Seedling height measurements grouped by age and species. Boxes enclose the central 50% of data, dark horizontal lines indicate medians, and upper and lower vertical lines extend to the largest/smallest observation that is less than or equal to 1.5 times the interquartile range outside of the box; dots indicate outliers.

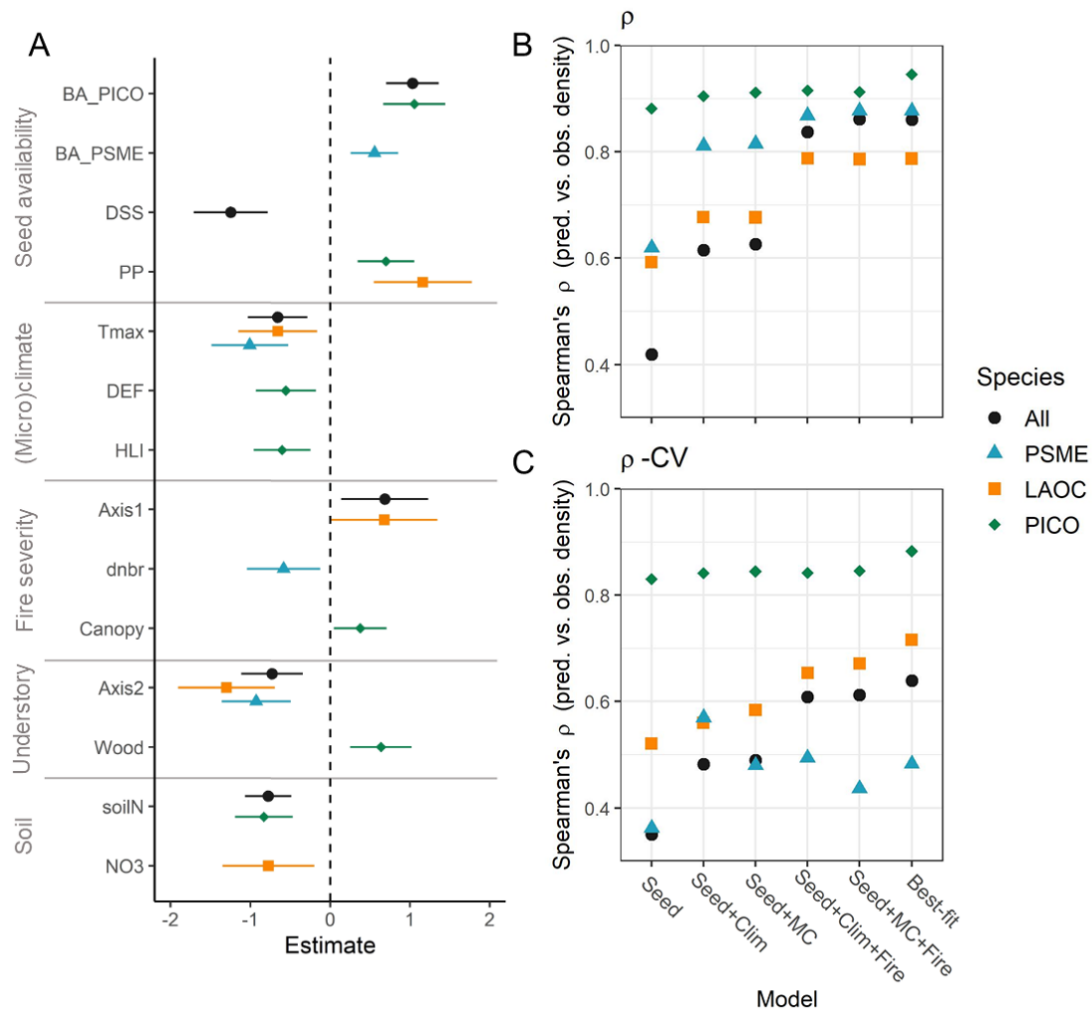


Figure 4. Best-fit models of seedling density in year three after fire in burned sites, and the relative influence of (micro)climate and fire severity on regeneration after accounting for factors that influence seed availability. Results are presented for models of total (all-species) seedling density and for individual species: *P. menziesii* (PSME), *L. occidentalis* (LAOC), *P. contorta* (PICO). Predictors are grouped into categories describing potential seed availability (“Seed”), fire effects (“Fire”), and microclimate (“MC”) or topoclimate (“Clim”), described in Table 2. **A:** Estimates of main effects and 95% confidence intervals for best-fit models. **B, C:** Comparison of models including subsets of predictors, showing correlations between observed and predicted values (B) and cross-validation results (C).

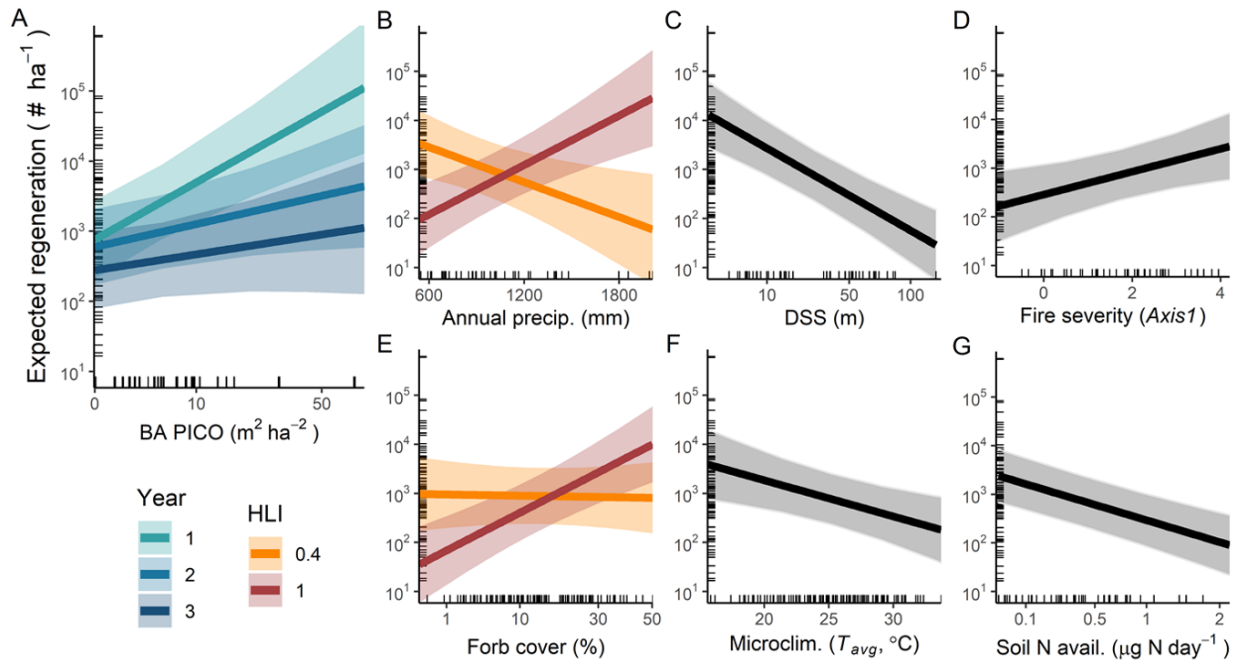


Figure 5. Partial effects plots for best-fit model of annual seedling recruitment in burned sites (all species), with 95% confidence intervals. Legend text: “Year” is years since fire; “HLI” is heat load index. Variables include (A) total basal area of *P. contorta* (“BA PICO”); (B) 30-yr average total annual precipitation; (C) distance to potential seed source (“DSS”); (D) fire severity, as represented by PCA Axis 1 scores (see methods); (E) forb cover (annual); (F) microclimate, represented by average daily summer temperature (annual); and (G) soil nitrogen availability. Note that x-axis scales are back-transformed from z-scores used in model fitting to represent predictor variables in their native units, and x-axis scales in panels A, C, E, and G also reflect a square-root transformation. Ticks on the x- and y-axes represent the observed values.

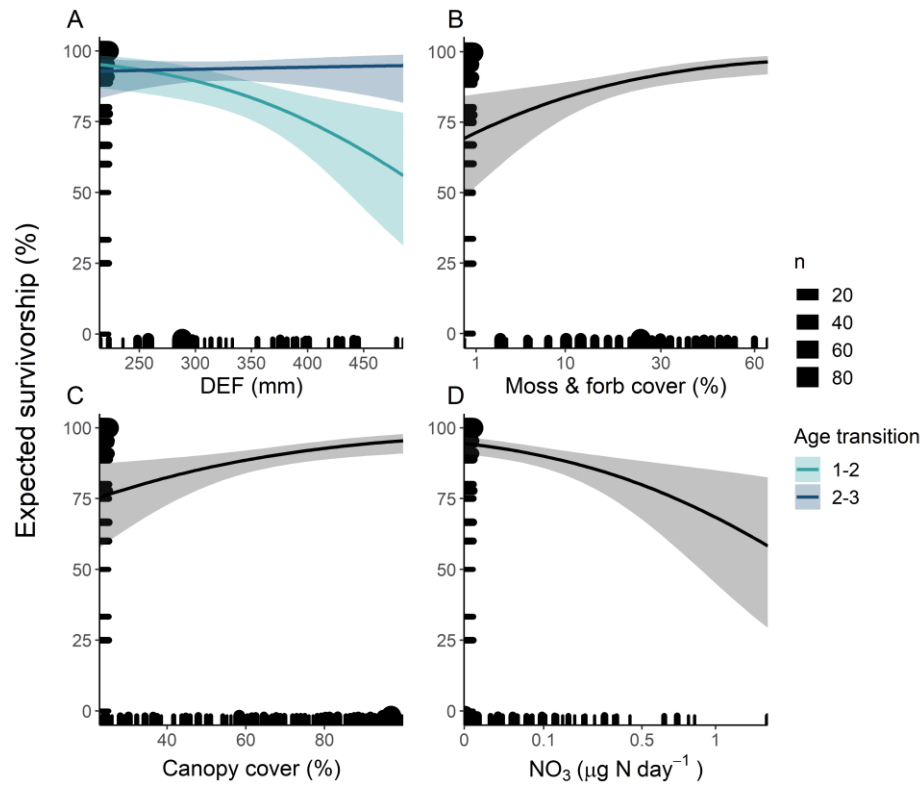


Figure 6. Partial effects plots for best-fit model of seedling survivorship (all species) between post-fire years 2 and 3 in subplots within burned sites, with 95% confidence intervals. Marker sizes on axes indicate the number of seedlings (n) represented by the survivorship estimate in each subplot (Table 1); only subplots with marked seedlings alive in post-fire year 2 are included. Seedling age transitions are given in years: 1-2 is inter-annual survival from the first to the second growing season of life; 2-3 is inter-annual survival from the second to the third growing season of life. Variables include (A) 30-yr average climatic water deficit (“DEF”); (B) average of moss and forb cover at each subplot; (C) total canopy cover at each subplot; (D) nitrate (NO_3) availability estimated using resin capsules (Table 2). Note that x-axis scales are back-transformed from z-scores used in model fitting to represent predictor variables in their native units, and x-axis scales in panels B and D also reflect a square-root transformation.

CHAPTER 2 Supplementary Materials

Appendix A: Supplementary Methods

Sampling timeline

Twenty sites were first established in June of 2018, while the remaining 49 were established in August-September of 2018. All 69 sites were revisited both in June and August/September of 2019, and again in August/September of 2020 (Table A.1). To account for differing sampling times, the 2018 data from the 20 sites originally established in June 2018 are excluded from annual seedling recruitment and survivorship estimates, which are based on the number of seedlings alive in August/September of each sampling year.

Table A.1. Sampling timeline, including when each site was visited and what measurements were taken: total seedling density within belt transects, and seedling presence, survival, and growth within subplots along transects.

Year	Sampling time	Total seedling density	Seedlings in subplots	# sites
2018	June	X	X	20 [†]
	August/September	X	X	49
2019	June		X	all
	August/September	X	X	all
2020	August/September	X	X	all

[†]2018 data not included in mortality estimates or annual recruitment models.

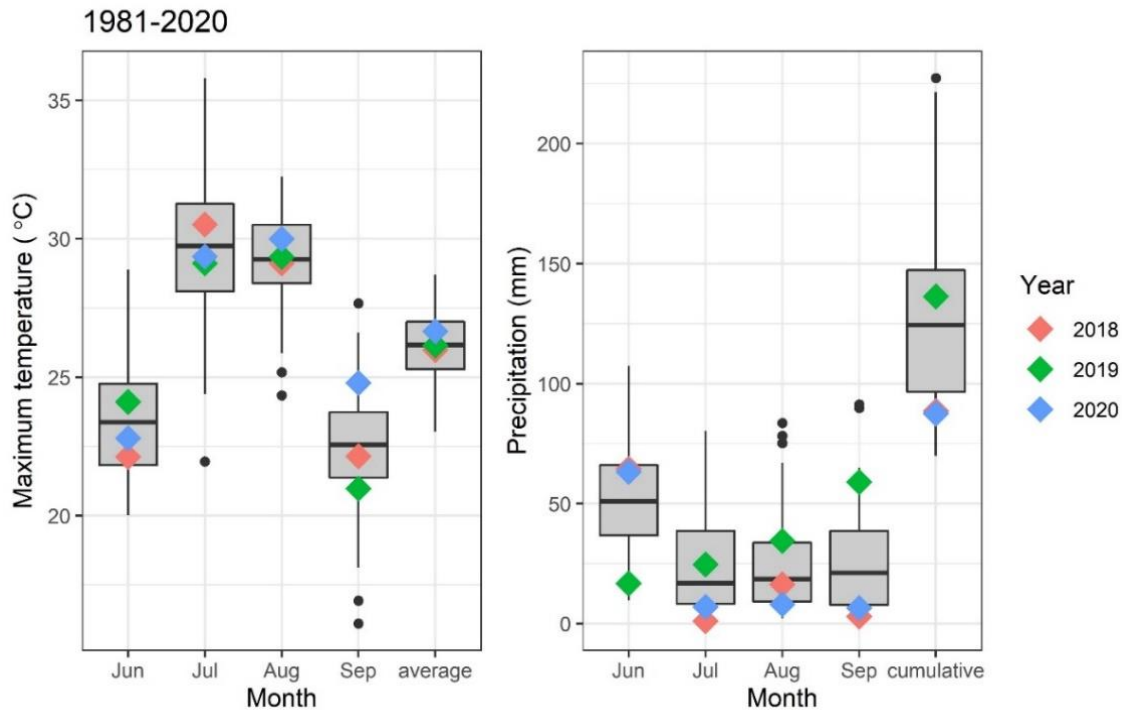
Post-fire climate

Figure A.1. June-September average daily maximum temperature and total precipitation in Missoula, Montana, from 1981-2020 (boxplots) and during each of the three study years (colored squares; wrcc.dri.edu).

Predictive models of post-fire growing-season microclimate

Predictive models were built using growing-season microclimate data from 46 of our 69 sites, including data from the 33 sites published in Wolf et al. (2021). Microclimate data were collected from June through September in the first two years after fire, with 15 sites monitored in 2018 and 40 monitored in 2019. These include 23 moderate-severity sites, 12 high-severity sites, and 11 unburned sites, and span the full range of biophysical gradients represented by the study. Data collection, aggregation, and quality-checking are described in Wolf et al. (2021).

The 2019 microclimate data were used to train the models, and the 2018 data were withheld as an independent validation data set. The training data were subset to retain one day out of every six to account for temporal autocorrelation, yielding an average of 15 days of observations from each of 40 sites over June-September 2019. A random effect of site was included to account for repeat measurements. The models included predictors describing the biophysical setting and fire severity of each site: elevation, climatic water deficit (*DEF*), heat load index (*HLI*), total canopy cover above the sensor post (%), and field-based fire severity metrics (*Axis1* and *Axis2*, see below). Daily maximum temperature from the gridMET climate product (4-km resolution; Abatzoglou 2013) was included as a proxy for daily ambient weather. A quadratic term of gridMET temperature was considered to allow a flexible relationship between gridded and measured climate variables, and all possible two-way interaction terms were considered.

Models were selected initially through automated backward elimination to retain all significant terms based on F-tests ($p < 0.05$) using the *lmerTest* package in R (Kuznetsova et al. 2017). To avoid overfitting the data, we dropped additional terms based on cross-validated root mean squared error (RMSE). Two cross-validation procedures were used to select the final model. First, a leave-one-out cross-validation procedure was used to evaluate model skill across the full biophysical and fire-severity gradients represented by the training data. We held out data from one site and trained the model on the data from the remaining sites, and then predicted on the holdout data and calculated the RMSE; this was repeated for all 40 sites in the training data set to obtain an average. Second, we predicted on the temporally independent validation data from the 15 sites with microclimate measurements in 2018 and calculated a cross-validated RMSE from data not used in model selection.

The fully-reduced temperature model retained canopy cover, elevation, heat load index, and a quadratic term of gridMET temperature as predictors. For the temperature model, the leave-one-out cross-validated RMSE was 3.0 °C and the independent cross-validated RMSE was 2.6 °C. The final VPD model retained canopy cover, field-based fire severity (*Axis1* and *Axis2*), heat load index, elevation, and a quadratic term of gridMET temperature as predictors, with a leave-one-out cross-validated RMSE of 0.69 kPa and an independent cross-validated RMSE of 0.86 kPa. Average maximum daily VPD was highly correlated with temperature ($r = 0.92$, $p < 0.001$; $t = 19.5$, $df = 69$) and not used in further analyses.

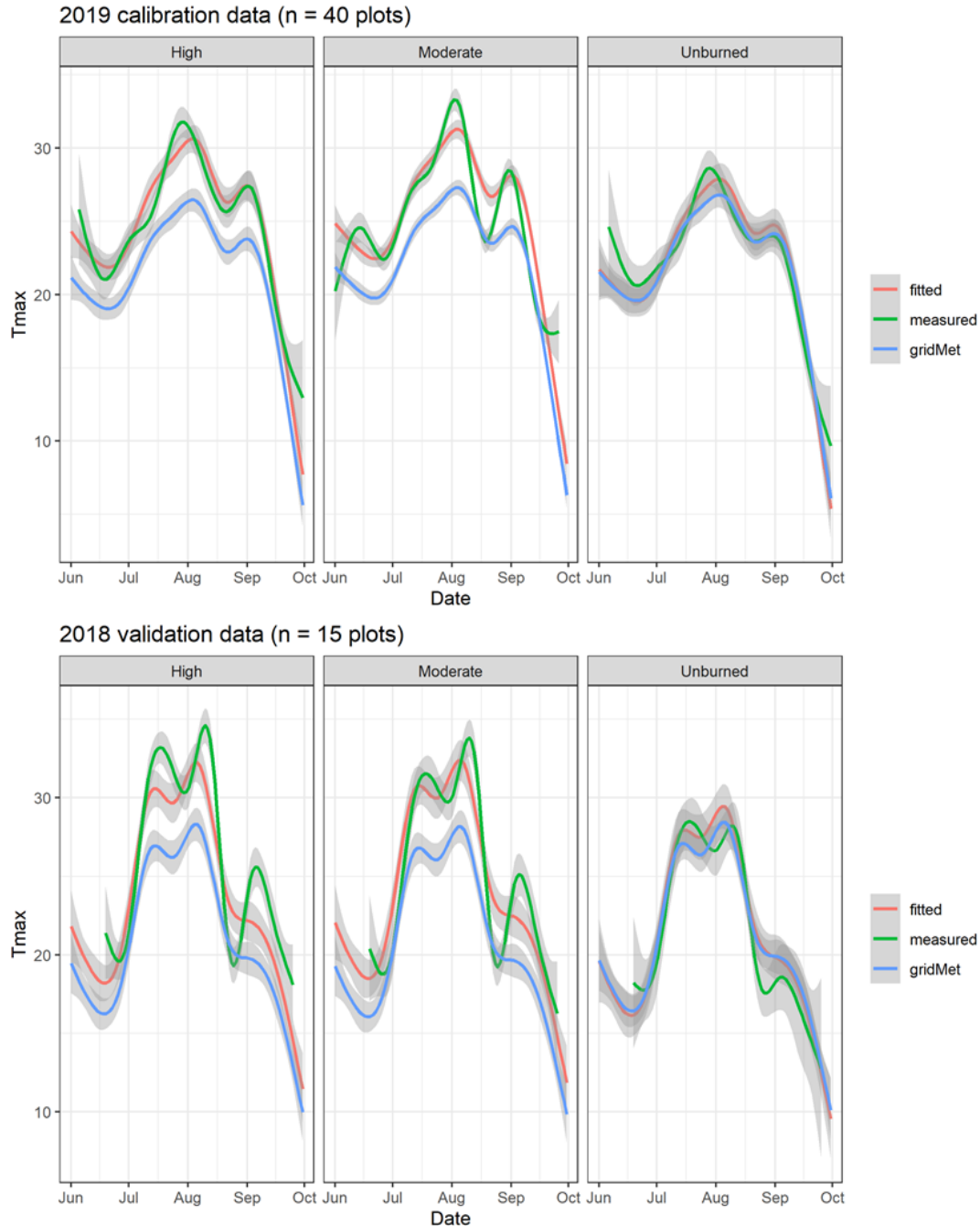


Figure A.2. Daily maximum temperature at study sites during June-Oct. 2018 ($n = 15$ sites) and 2018 ($n = 40$ sites). Comparison between coarse-scale gridded climate data (gridMet), field-measured near-ground microclimate data (measured), and model predictions of near-ground microclimate conditions (fitted), displayed using GAM smoothers of daily data from sites grouped by fire severity class with 95% confidence intervals.

Principal components analysis of field-based fire severity

We conducted a principal components analysis (PCA) using the *ade4* package in R (Dray and Dufour 2007) following methods from Wolf et al. (2021) to characterize fire severity using a suite of field measurements. These field measurements included site-averaged values of live and dead canopy cover and basal area, percent tree mortality (*mort*), scorch height (*SH*), propagule pressure (*PP*), and percent cover of bare ground or rock (*BG*), understory vegetation (*Shrub*, *Grass*, *Forb*, *Moss*), and litter (Fig. A.3). Variables were square-root transformed where necessary to reduce skewness prior to PCA. The first two principal components (Axis1 and Axis2) account for 53.5% and 12.1%, respectively, of the variability among sites. The Axis1 metric is significantly correlated with site-averaged dNBR ($r = 0.91$, $p < 0.001$; $t = 18.2$, $df = 67$); it therefore represents a metric of fire severity and distinguishes between burned and unburned sites. The Axis2 metric does not separate between burned and unburned sites, but among burned sites only, Axis2 is correlated with dNBR ($r = 0.56$, $p < 0.001$; $t = 4.63$, $df = 45$) and represents a metric of understory conditions that are affected by fire.

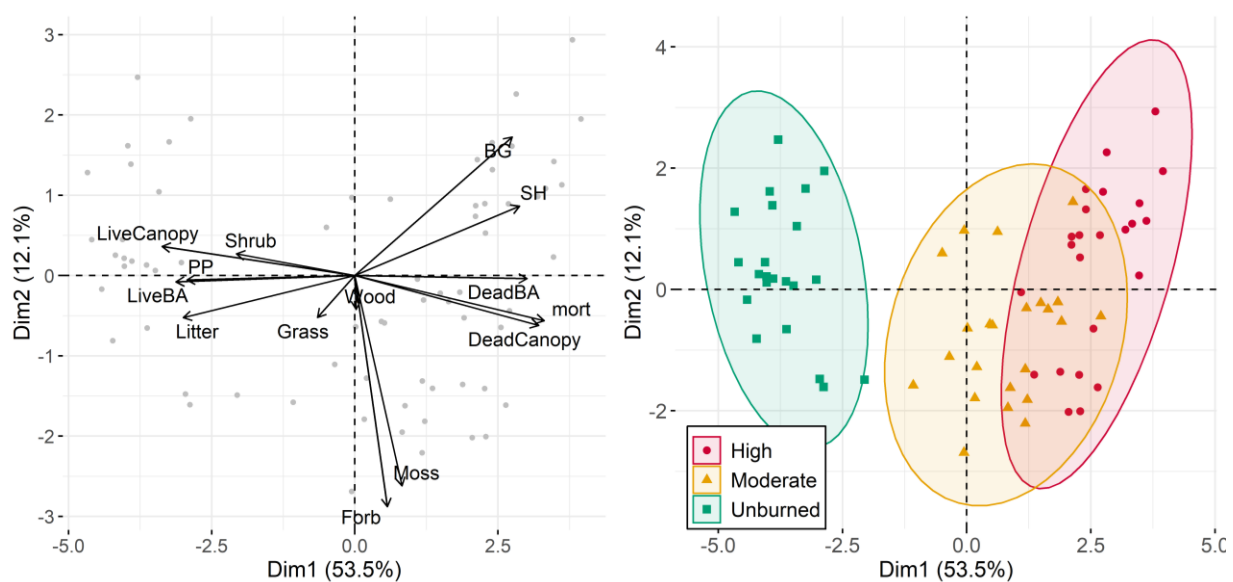


Figure A.3. PCA biplots describing field-based fire severity metrics.

Soil sampling and laboratory analyses

Soil samples were collected and ion-exchange resin capsules were incubated at 0, 30, and 60 m along each transect. Mineral soils were sampled to 10-cm depth using a 2-cm diameter soil probe. The forest floor was sampled using a 10-cm diameter PVC ring to collect undecomposed and partially decomposed litter and roots comprising the organic horizon, and the depth of this layer was measured. Samples were combined and homogenized in the laboratory to yield one composite mineral and organic soil sample from each site in each year (2018 and 2019). Soils were sorted using a 2-mm sieve to remove stones and roots and extracted within 48 hours of collection.

Inorganic nitrogen was extracted from soil samples by shaking c. 9 g of fresh soil in 40 mL of 2 mol/L KCl solution for one hour. Samples were centrifuged, decanted, and filtered through Whatman #1 filter paper using a vacuum manifold. Resin-sorbed inorganic nitrogen was extracted by shaking resin capsules with 10 mL of 2 mol/L KCl solution for 30 minutes and repeating three times, decanting the extract each time to create a total extract volume of 30 mL (DeLuca and Sala 2006), which was filtered using the same method. Concentrations of NH_4^+ and NO_3^- were analyzed colorimetrically on a microplate reader using the salicylate-hypochlorite method (Weatherburn 1967) and vanadium reduction method (Doane and Horwath 2003), respectively. Measured concentrations were used to calculate $\mu\text{g N}$ per gram of soil, and $\mu\text{g N}$ per day of incubation for resin capsules. Total C and N in mineral soil were measured using an elemental analyzer on oven-dried and finely ground composite soil samples collected in 2018, and mineral soil pH was measured on an air-dried subsample using a 2:1 (solution:soil) slurry of 0.01 mol/L CaCl_2 .

Additional statistical methods

Model selection followed the steps shown in Fig. A.4. To evaluate the skill of our statistical models of seedling density, we conducted k -fold cross-validation by holding out 25% of the data and training the model on the remaining data, predicting on the hold-out data, and calculating the Spearman correlation; this was repeated 1000 times to obtain an average cross-validated correlation (ρ -CV). For glmms, we also calculated the marginal pseudo- R^2 (trigamma method) using the *MuMin* package in R, which represents the variance explained by the fixed-effects predictors (Bartoń 2022), while for glms, we calculated percent deviance explained. For binomial glmms of seedling survival, we calculated the area under the Receiver Operating Curve as a measure of model accuracy (AUC), where a value of 0.5 indicates that the model performs no better than random, while a value of 1 indicates perfect prediction (Robin et al. 2011). To compare the dominant controls of regeneration in burned and unburned sites, we built separate models of seedling density in 2020 in all sites ($n = 69$), in unburned sites ($n = 22$), and in burned sites ($n = 47$, presented in the main text).

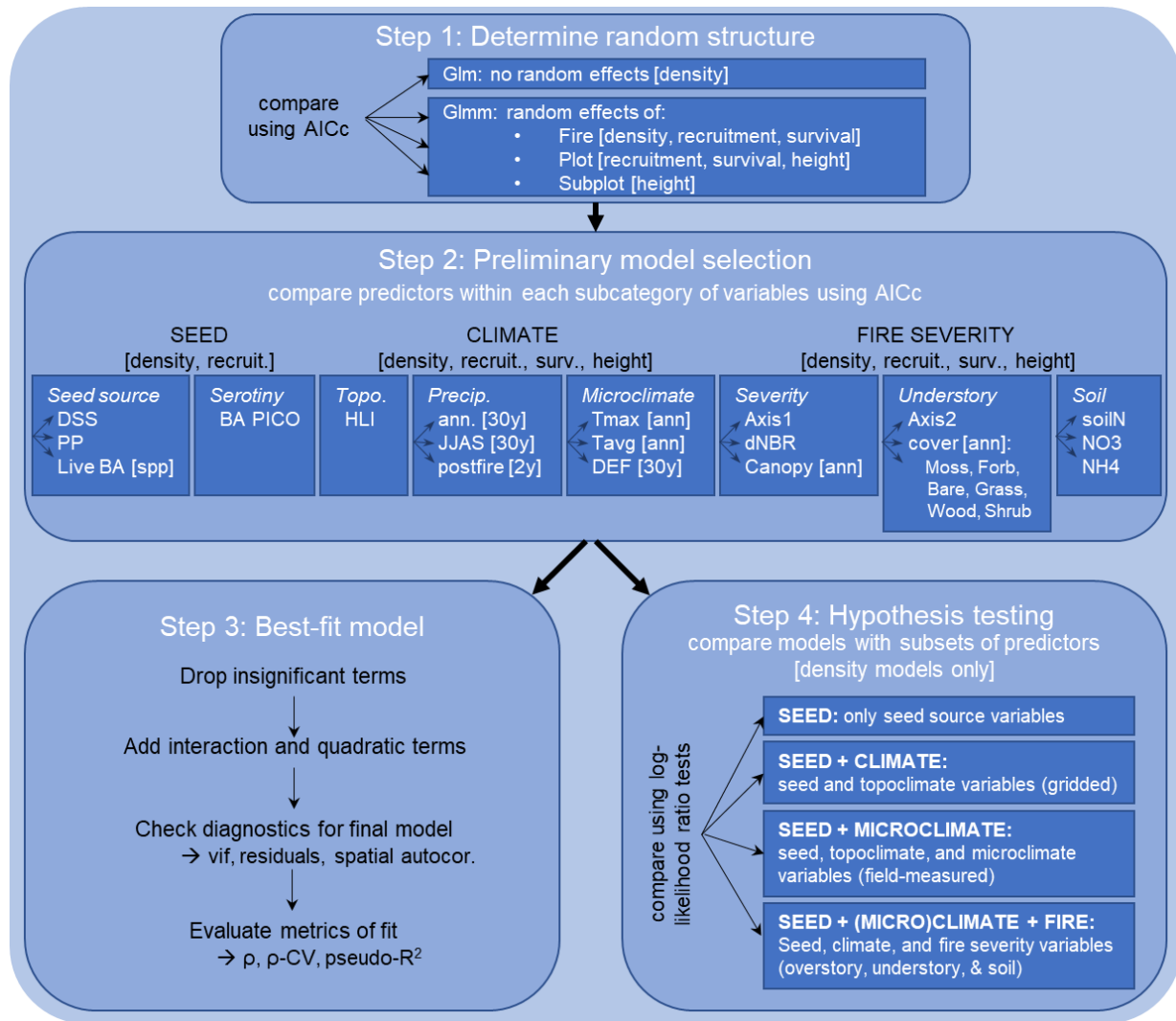


Figure A.4. Schematic showing the model selection workflow for statistical models of total seedling density, annual seedling recruitment, survivorship, and height. All model types were built for total (all species) responses and individual species (*P. contorta*, *P. menziesii*, *L. occidentalis*) as sample size allowed, and burned and unburned sites were modeled separately. Random effects only apply to certain model types, as described using brackets. Each model started with an arbitrary set of initial variables, which were refined in Step 2 by comparing models that substituted variables from within the same subcategory. Fixed-effects variables are described in detail in Table 1 in the main text, and vary in spatial/temporal domain.

Supplementary analysis of distance-to-non-severe

The RegenMapper tool (Holden et al. 2021) was used to calculate the area of each fire burned at high severity that was >100 m from a low- or moderate-severity or unburned patch based on MTBS classifications of fire severity (Fig. A.5). Approximately 12% of the area of the Lolo Peak Fire and 8% of the Sunrise fire was >100 m from a non-severe patch. These maps were overlaid with Digital Elevation Models to quantify the area of each fire that was both >100 m from a non-severe patch and within the approximate range of subalpine forest in this region (1500-2400 m elevation), representing areas of high-severity fire with the potential for serotinous *P. contorta* regeneration. Of the burned area >100 m from a non-severe patch, 91% and 56% in the Lolo Peak and Sunrise fires, respectively, is within the range of *P. contorta*.

To provide additional context for these two fires, which burned under unusually hot, dry conditions during the summer of 2017 (Balch et al. 2018), we also conducted a similar analysis with 30 randomly-selected similar large wildfires. We selected a random subset of five wildfires >5000 ha in size from each regional fire year in the northern Rocky Mountains over the 21st century (2000, 2003, 2007, 2012, 2015, 2017), for a total of 30 fires. We calculated the percent of the area of each fire burned at high-severity and the percent of area >100 m from a non-severe patch. Across the 30 wildfires, the average area of high-severity fire was $20\% \pm 11\%$ (sd) and the average area >100 m from non-severe was $14\% \pm 9\%$. Therefore, the spatial pattern of high-severity fire within the Lolo Peak and Sunrise fires is within the range of similar large wildfires during regional fire years characterized by warm, dry conditions over the past two decades.

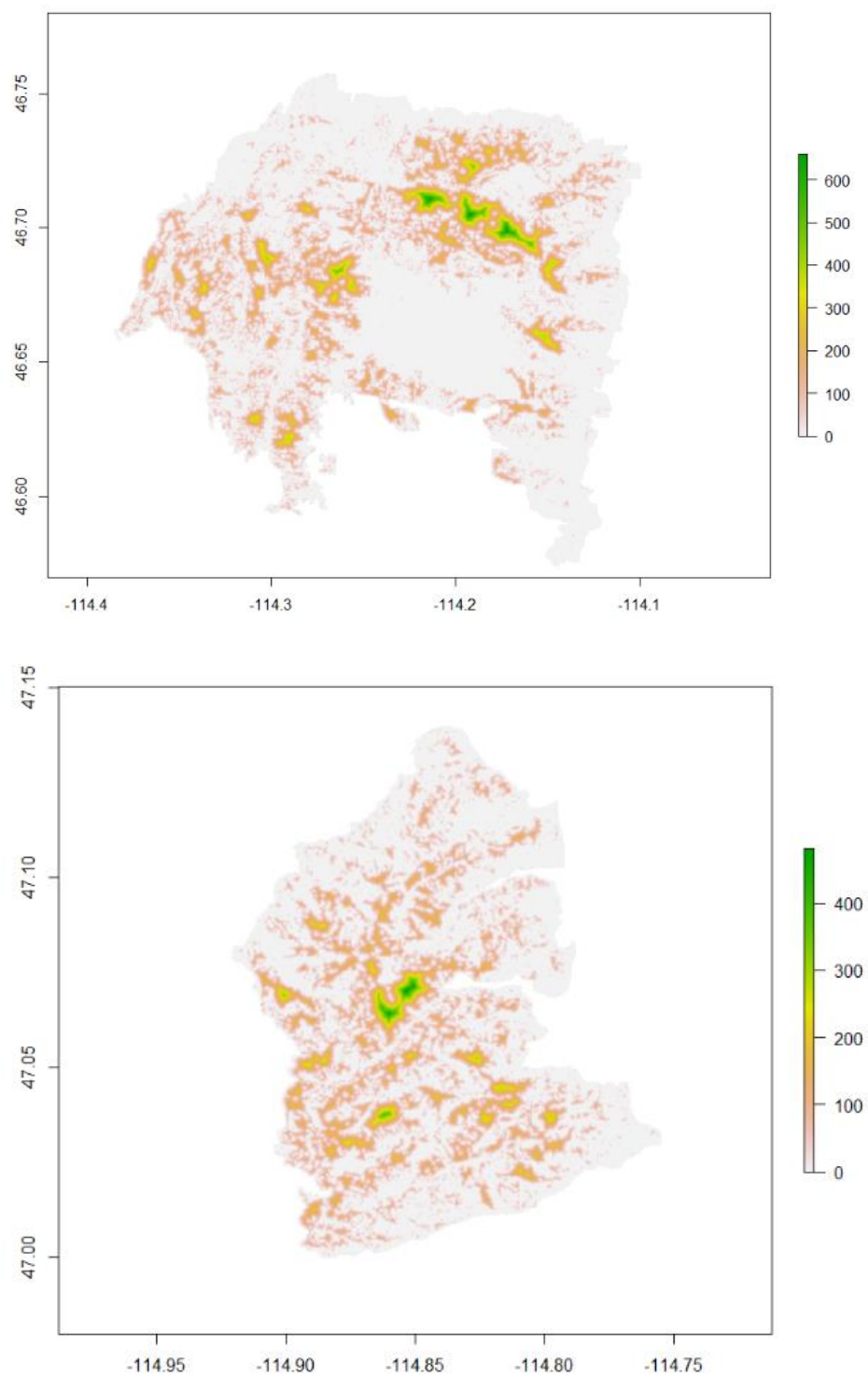


Figure A.5. Footprint of the Lolo Peak (top) and Sunrise (bottom) fires, with a colormap representing the distance to a non-severe patch in meters. Pixels are 30-m resolution, with data calculated in the RegenMapper tool (Holden et al. 2021).

Appendix B: Supplementary Results

Table B.1. Results of hypothesis testing to evaluate controls of post-fire seedling regeneration. Each model includes all original model terms and added terms, and is compared with the next-simpler model including only the original model terms using a log-likelihood ratio test.

Category	Original model terms	Added terms	Log-lik p-value	AICc	BIC	ρ (obs~pred)	ρ-CV (obs~pred)	Marginal pseudo-R² (trigamma)
Seed	Intercept	DSS ba_PICO	<0.001	588	595	0.42	0.35	0.50
Seed + Climate	Intercept DSS ba_PICO	HLI ppt_JJAS DEF	0.006	583	594	0.62	0.49	0.62
Seed + Microclimate	Intercept DSS ba_PICO	HLI ppt_post Tmax	0.003	582	593	0.63	0.50	0.64
Seed + Climate + Fire Severity	Intercept DSS ba_PICO HLI ppt DEF	Axis1 Axis2 soilN	<0.001	566	580	0.84	0.60	0.78
Seed + Microclimate + Fire Severity	Intercept DSS ba_PICO HLI ppt Tmax	Axis1 Axis2 soilN	<0.001	564	577	0.86	0.61	0.76
Best-fit model		DSS ba_PICO soilN Axis2 Axis1 Tmax		559	570	0.84	0.63	0.75

Table B.2. Species-specific models of total regeneration density three years post-fire in burned sites.

Species	Random effects terms	Fixed effects terms	Estimate	z-value	p-value	ρ	ρ -CV	R-sq [†]	% dev [†]
All	Fire	DSS	-1.246	-5.29	<0.001	0.84	0.63	0.75	
		ba_PICO	1.032	6.13	<0.001				
		soilN	-0.776	-5.28	<0.001				
		Axis2	-0.729	-3.70	<0.001				
		Axis1	0.685	2.46	0.014				
		Tmax	-0.657	-3.45	<0.001				
PSME	Fire	Present	2.030	3.61	<0.001	0.88	0.50	0.56	
		Tmax	-1.052	-4.58	<0.001				
		Axis2	-0.917	-4.72	<0.001				
		Axis2 ²	-0.459	-3.00	0.003				
		dnbr	-0.601	-2.66	0.008				
		BA _{PSME_L}	0.459	3.71	<0.001				
PICO	none	Present	3.111	4.99	<0.001	0.95	0.89	0.95	
		BA _{PICO}	0.963	6.32	<0.001				
		PP_dWt	0.745	5.24	<0.001				
		Wood	0.665	4.25	<0.001				
		Canopy	0.516	3.97	<0.001				
		Canopy ²	0.484	4.60	<0.001				
		soilN	-0.487	-3.28	0.001				
		HLI	-0.479	-3.38	<0.001				
		DEF	-0.363	-2.34	0.019				
		DEF:Wood	0.437	3.67	<0.001				
LAOC	none	Present	2.301	4.96	<0.001	0.79	0.72	0.74	
		NO ₃	-0.941	-3.23	0.001				
		Axis2	-0.938	-3.34	<0.001				
		PP_dWt	0.783	3.13	0.002				
		Tmax	-0.679	-2.74	0.006				

†A glmm was fit if a random effect of fire improved AIC, and the marginal pseudo-R² is reported; otherwise, a glm was fit and the ratio of residual to null deviance is reported.

Table B.3. Species-specific models of annual recruitment in burned sites.

Species	Random effects terms	Fixed effects terms	Estimate	z-value	p-value	ρ	ρ -CV	Marginal pseudo-R ²
All	Fire Plot	BA _{PICO}	1.033	4.43	<0.001	0.89	0.60	0.72
		DSS	-1.425	-5.67	<0.001			
	HLI	-0.106	-0.69	0.490				
	ppt_ann	0.234	1.00	0.317				
	T _{ann}	-0.656	-2.86	0.004				
	Axis1	0.671	2.52	0.012				
	Forb	0.608	4.95	<0.001				
	soilN	-0.861	-5.50	<0.001				
	Year2	-0.743	-3.74	<0.001				
	Year3	-1.609	-7.90	<0.001				
	HLI:ppt	0.683	4.10	<0.001				
	HLI:Forb	0.355	2.83	0.005				
	BA _{PICO} :Y2	-0.626	-3.47	<0.001				
	BA _{PICO} :Y3	-0.741	-3.30	<0.001				
PSME	Fire Plot	Present	1.438	2.49	0.013	0.88	0.62	0.52
		DSS	-0.565	-3.56	<0.001			
	Canopy	0.577	4.07	<0.001				
	Axis2	-1.155	-6.29	<0.001				
	Year2	0.735	3.06	0.002				
	Year3	-0.958	-3.59	<0.001				
PICO	Plot	BA _{PICO}	1.464	7.93	<0.001	0.84	0.79	0.77
		DSS	-0.492	-3.02	0.003			
		HLI	-0.722	-3.96	<0.001			
		DEF	-0.622	-3.16	0.002			
		Wood	0.672	3.78	<0.001			
		soilN	-0.912	-5.23	<0.001			
		Year2	-2.300	-7.90	<0.001			
		Year3	-2.548	-8.65	<0.001			
		HLI:DEF	-0.435	-2.41	0.016			
LAOC	Plot	Present	2.17	2.99	0.003	0.90	0.68	0.71
		Bare	-1.949	-4.56	<0.001			
		PP_dWt	1.724	3.53	<0.001			
		Axis1	1.472	2.58	0.010			
		Tmax	-0.725	-2.10	0.036			

Table B.4. Models of seedling survivorship from 2019-2020 in burned sites. Only *P. menziesii* and *P. contorta* had sufficient data for species-specific models.

Species	Random effects terms	Fixed effects terms	Estimate	z-value	p-value	AUC
All	Plot	DEF	-2.139	-2.49	0.013	0.77
		Age	1.096	2.78	0.005	
		Moss+Forb	0.639	2.87	0.004	
		NO ₃	-0.590	-2.72	0.006	
		Canopy	0.589	2.87	0.004	
		DEF:Age	0.691	2.04	0.041	
PSME	Plot	BG	-1.331	-3.09	0.002	0.80
		NH4	1.270	2.17	0.030	
		HLI	-0.839	-2.16	0.031	
PICO	Plot	Moss	1.049	2.31	0.021	0.71
		Canopy	0.621	1.96	0.050	

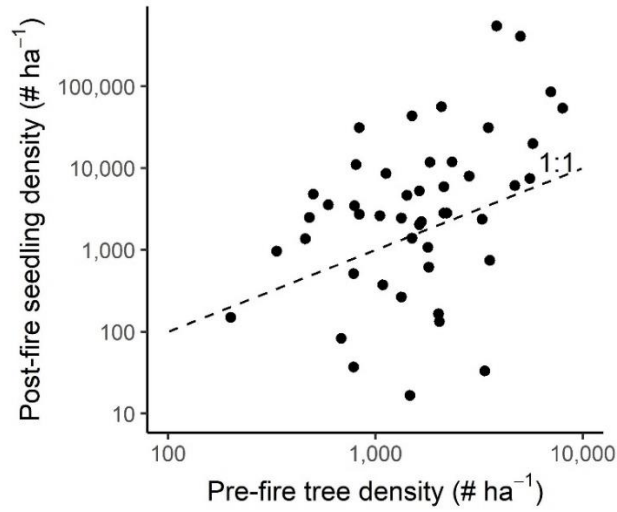


Figure B.1. Total seedling density in year three after fire, plotted against reconstructed pre-fire mature tree density for all burned sites ($n = 47$). The dashed line shows a 1:1 relationship, where sites on or above that line have the number of seedlings present after fire equal to or greater than the number of adult trees present before fire.

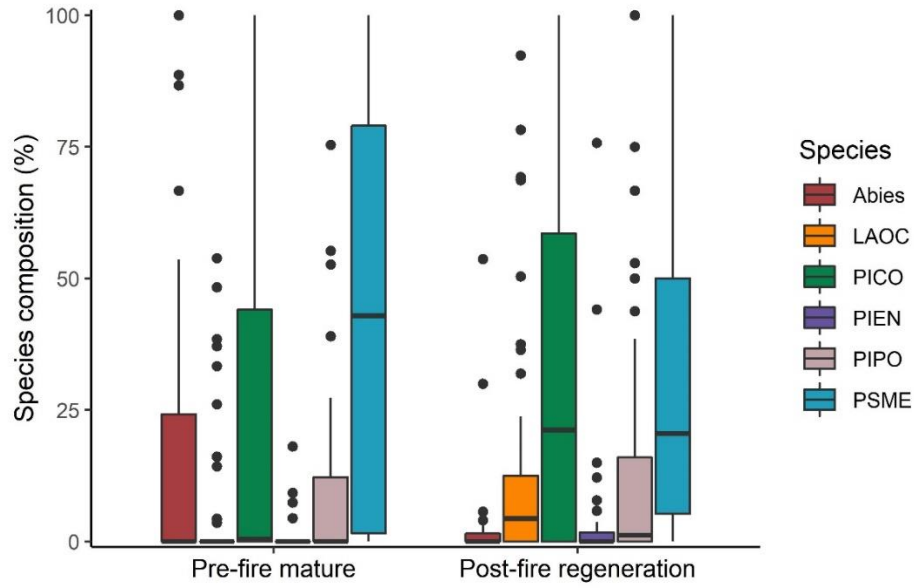


Figure B.2. Boxplots of pre- and post-fire species composition in burned sites (n = 47). Pre-fire composition includes all trees >1.37 m height, while post-fire includes all seedlings that regenerated after the fire and were alive three years post-fire.

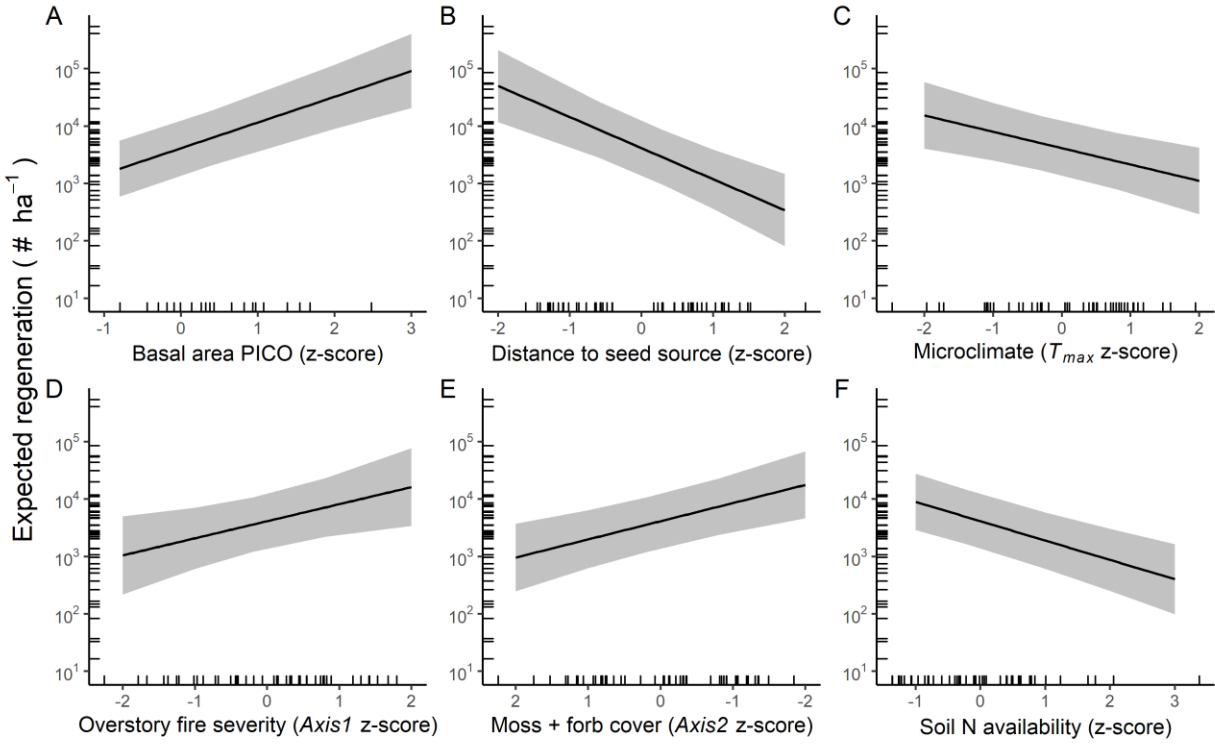


Figure B.3. Partial effects of covariates in the all-species seedling density model for burned sites alone ($n = 47$) in year three after fire, with 95% confidence intervals. Predictor variables are represented as z-scores, with ticks on the axes displaying the observed values.

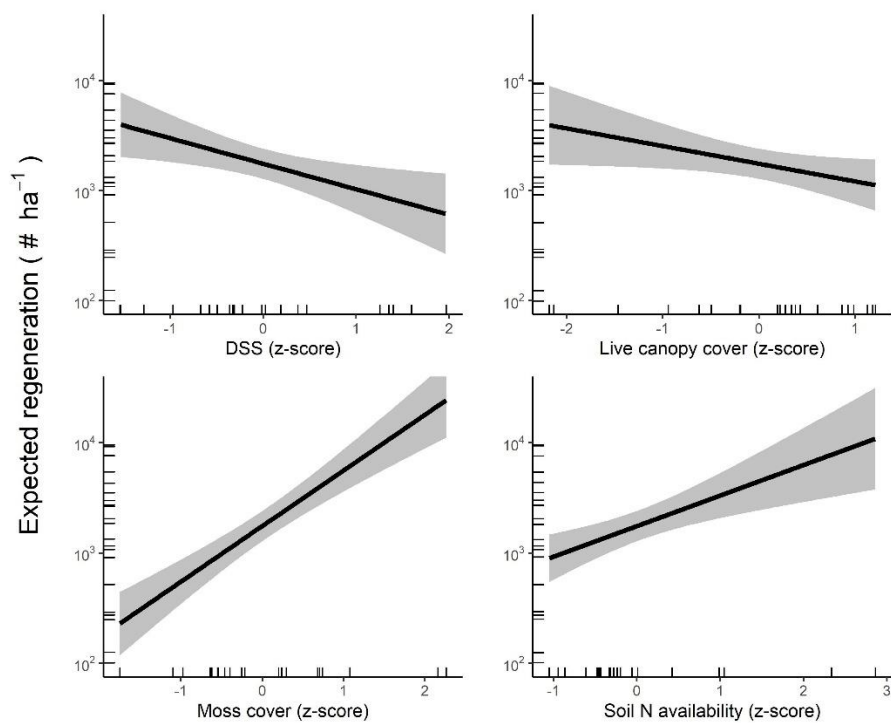


Figure B.4. Partial effects of covariates in the all-species seedling density model for unburned sites alone ($n = 22$) in year three after fire, with 95% confidence intervals. Predictor variables are represented as z-scores, with ticks on the axes displaying the observed values.

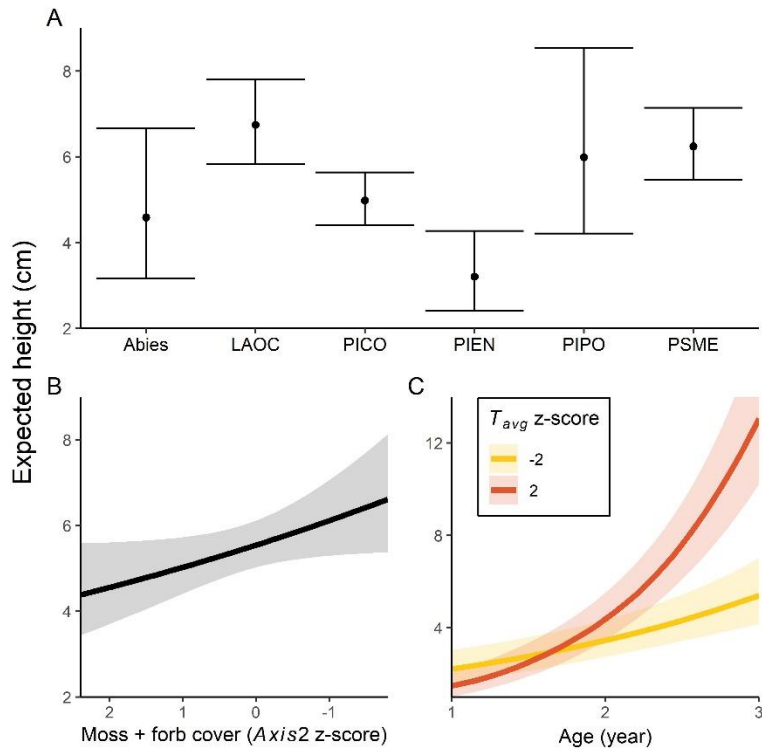


Figure B.5. Partial effects of covariates in the model of seedling height for seedlings in all plots (n=69) in year three after fire, with 95% confidence intervals. Predictor variables are represented as z-scores.

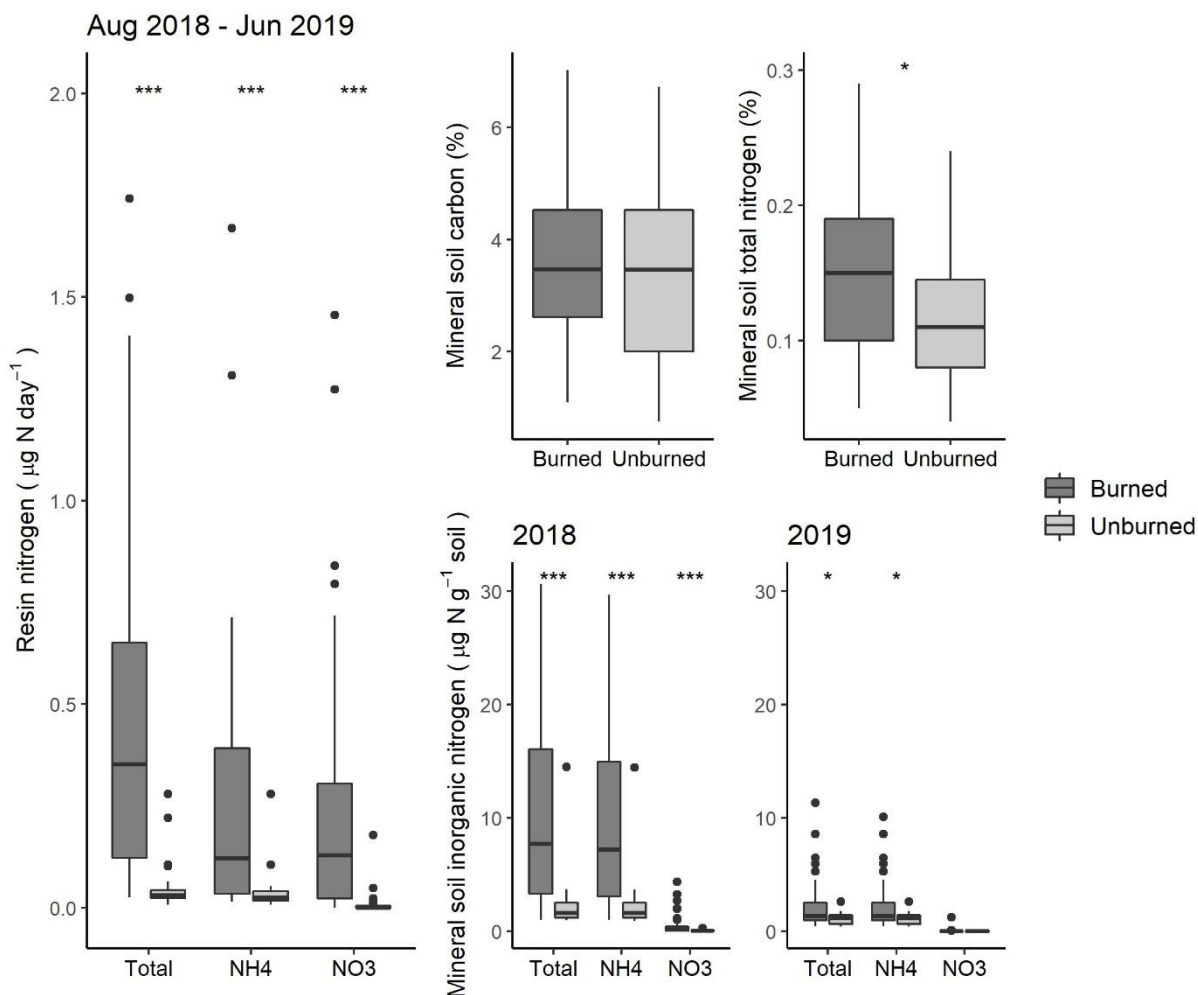


Figure B.6. Boxplots of soil nitrogen measurements. Left: resin-sorbed inorganic nitrogen from 2018-2019. Upper right: mineral soil total carbon and nitrogen in 2018 (% by mass). Lower right: mineral soil inorganic nitrogen concentration in 2018 and 2019. Statistical significance of nonparametric Wilcoxon rank-sum tests comparing burned and unburned soils are reported (* $p < 0.05$, ** $p < 0.01$, *** $p < 0.001$).

Literature Cited

- Abatzoglou, J. T. 2013. Development of gridded surface meteorological data for ecological applications and modelling. *International Journal of Climatology* 33:121–131.
- Balch, J., T. Schoennagel, A. Williams, J. Abatzoglou, M. Cattau, N. Mietkiewicz, and L. St. Denis. 2018. Switching on the Big Burn of 2017. *Fire* 1:17.
- Bartoń, K. 2022, February 24. MuMIn: Multi-Model Inference.
- DeLuca, T. H., and A. Sala. 2006. Frequent fire alters nitrogen transformations in ponderosa pine stands of the Inland Northwest. *Ecology* 87:2511–2522.
- Doane, T. A., and W. R. Horwath. 2003. Spectrophotometric Determination of Nitrate with a Single Reagent. *Analytical Letters* 36:2713–2722.
- Dray, S., and A.-B. Dufour. 2007. The ade4 Package: Implementing the Duality Diagram for Ecologists. 2007 22:20.
- Holden, Z., A. Warren, E. Jungck, M. Maneta, S. Dobrowski, K. Davis, V. Archer, and S. Fox. 2021. Topofire -- Regeneration Mapper. University of Montana, Missoula.
- Kuznetsova, A., P. B. Brockhoff, and R. H. B. Christensen. 2017. lmerTest Package: Tests in Linear Mixed Effects Models . *Journal of Statistical Software* 82:1–26.
- Robin, X., N. Turck, A. Hainard, N. Tiberti, F. Lisacek, J. Sanchez, and M. Muller. 2011. pROC: an open-source package for R and S+ to analyze and compare ROC curves.
- Weatherburn, M. W. 1967. Phenol-hypochlorite reaction for determination of ammonia. *Analytical chemistry* 39:971–974.
- Wolf, K. D., P. E. Higuera, K. T. Davis, and S. Z. Dobrowski. 2021. Wildfire impacts on forest microclimate vary with biophysical context. *Ecosphere* 12:e03467.

CHAPTER 3: Climate change, pyrodiversity, and ecosystem resilience to wildfire over the past 4800 years in a Rocky Mountain forest

*This chapter is prepared as a manuscript that has been submitted for publication with the following authors: Kyra D. Clark-Wolf¹, Philip E. Higuera¹, Kendra K. McLauchlan², Bryan N. Shuman³, Meredith C. Parish⁴

¹ Department of Ecosystem and Conservation Sciences, University of Montana, Missoula, MT

² Division of Environmental Biology, National Science Foundation, Alexandria, VA

³ Department of Geology and Geophysics, University of Wyoming, Laramie, WY

⁴ Department of Earth, Environmental, and Planetary Sciences, Brown University, Providence, RI

Abstract

Wildfires strongly influence forest ecosystem processes, including carbon and nutrient cycling and vegetation dynamics. As fire activity increases under changing climate conditions, the ecological and biogeochemical resilience of many forest ecosystems remains unknown. To investigate the resilience of forest ecosystems to wildfires and climatic change on decadal to millennial timescales, we developed a 4800-yr high-resolution lake-sediment record from Silver Lake, Montana, USA (47.360° N, 115.566° W). Charcoal particles, pollen grains, element concentrations, and stable isotopes of carbon and nitrogen serve as proxies of past changes in fire, vegetation, and ecosystem processes, respectively, within a small subalpine forest watershed. A previously published lake-level history from Silver Lake provides a local record of paleohydrology. A trend toward increased effective moisture over the late Holocene coincided with a distinct shift in the pollen assemblage c. 1900 yr BP, reflecting increasing subalpine conifer abundance. Fire activity, inferred from peaks in macroscopic charcoal, decreased significantly after 1900 yr BP, from one fire event every 126 yr (83-184 yr, 95% CI) from 4800-1900 yr BP, to one event every 223 yr (175-280 yr) from 1900 yr BP to present. Biogeochemical proxies likewise reveal a long-term trend in watershed response to late-Holocene climatic changes, reflecting a shift in within-lake processes. Across the entire record, individual fire events were followed by two distinct decadal-scale biogeochemical responses characterized by

contrasting changes in multiple proxies, reflecting differences in ecosystem impacts of paleofires on watershed processes. These distinct biogeochemical responses were interpreted as relating to fire severity, highlighting (i) erosion, likely from large or high-severity fires, and (ii) nutrient transfers and enhanced within-lake productivity, likely from lower-severity or patchier fires. This variation characterizes pyrodiversity, defined as heterogeneity in fire behavior and fire effects over space and time. Regardless of the nature of fire effects, biogeochemical and vegetation proxies returned to pre-fire values within decades, revealing forest ecosystem resilience to wildfire across long-term variability in climate and fire activity. Higher fire frequencies in past millennia relative to the 20th-21st century suggests that northern Rocky Mountain subalpine ecosystems could remain resilient to future increases in fire activity, provided continued ecosystem recovery within decades.

Introduction

Wildfire activity is increasing across western North America, enabled in part by anthropogenic climate change (Abatzoglou and Williams 2016, Kirchmeier-Young et al. 2017, Zhuang et al. 2021), and is in some regions exceeding the historical range of variability of recent millennia (Kelly et al. 2013, Higuera et al. 2021). In forests of the western United States, abundant fuels are expected to support continued climate-enabled increases in area burned through mid-century (Abatzoglou et al. 2021). Climate-driven shifts in fire regimes may impact forest ecosystems through vegetation transformations (Coop et al. 2020) and changes in carbon (C) and nitrogen (N) cycling (Kelly et al. 2015, Pellegrini et al. 2018, Walker et al. 2019). For example, an increase in fire-caused losses of C and nutrients has the potential to intensify nutrient limitation and alter forest recovery trajectories (Anderson-Teixeira et al. 2013, Tierney et al. 2019). These feedbacks are complex and operate over decadal to millennial timescales, making it difficult to accurately predict ecosystem response to changing fire activity.

Anticipating future changes in forest ecosystems, therefore, requires understanding the biogeochemical implications of shifting fire regimes.

A key organizing concept in disturbance ecology is resilience, or the capacity of an ecosystem to recover following a disturbance and retain fundamental processes, structures, and species composition (Gunderson 2000, Falk et al. 2022). Biogeochemical states and processes are a component of system resilience, and are sensitive to fire (Smithwick 2011). The direct and indirect effects of prescribed and wildland fires on C and nutrient stocks and fluxes have been well-documented through experimental and observational studies (reviewed in Wan et al. 2001, Certini 2005, Smithwick et al. 2005, Boerner et al. 2009, Li et al. 2021). Most studies report changes in nutrient availability and biogeochemical processes lasting months to years after fire. However, multidecadal biogeochemical legacies have been observed following high-severity fires in forest ecosystems (Smithwick et al. 2009, Kashian et al. 2013, Bowd et al. 2019, Dove et al. 2020, Li et al. 2021). During post-fire succession, biogeochemical cycles are generally tightly linked with vegetation via plant-soil interactions and C fluxes (Hart et al. 2005), but such linkages are not universally evident (Dove et al. 2020). Biogeochemical responses to fire are partly a function of the behavior and subsequent severity of fire, site characteristics and prior disturbance history, and post-fire ecological trajectories (Romme et al. 2011, McLauchlan et al. 2014, Kranabetter et al. 2016). Understanding and anticipating biogeochemical resilience to changing fire regimes – or lack thereof – requires disentangling these factors.

Over centennial and millennial time scales, long-term climatic changes can alter fire regimes (Whitlock et al. 2010), and have the potential to influence biogeochemical states and processes across multiple disturbance intervals (McLauchlan et al. 2014). Climate-driven changes in vegetation or weathering rates can directly influence biogeochemical cycling

(Schaller et al. 2010, Peltzer et al. 2010, Zhou et al. 2021), while variation in fire frequency and severity can shift the balance between accumulation and losses of carbon and nutrients over time (Pellegrini et al. 2018, 2020b, 2020a, Tierney et al. 2019, Walker et al. 2019). However, much of this understanding comes from ecosystems that experience frequent fire (i.e., on average every several years to decades). The biogeochemical implications of fire-regime changes are less well-constrained in ecosystems where fires historically occurred once every century or more on average due to a lack of long-term empirical datasets. High-resolution paleoecological records help fill this knowledge gap by revealing long-term patterns and resolving the impacts of individual disturbances, which ultimately scale up to shape biogeochemical changes over millennia (Kelly et al. 2015, Hudiburg et al. 2017). Such retrospective information provides context for anticipating the effects of anthropogenic climate change and shifting fire regimes on element cycling in forests with infrequent high-severity fire regimes.

Existing long-term paleoecological records reveal diverse impacts of wildfires on terrestrial and aquatic ecosystems, leaving many different signals integrated through proxy measures in lake sediments. For example, high-severity fires in a subalpine forest in Colorado resulted in losses of plant nutrients, as well as enhanced post-fire erosion spanning several decades (Dunnette et al. 2014, Leys et al. 2016). However, records from other subalpine forests and boreal regions reveal varying post-fire changes in lake-sediment geochemistry (Chipman and Hu 2019, Pompeani et al. 2020), arising in part from differences in topography, organic matter sources, and sample resolution (Morris et al. 2015). Thus, site-specific biophysical factors help determine biogeochemical responses to fire, and sampling methodologies determine to what extent those responses are detectable in paleoenvironmental records (Morris et al. 2015, Pompeani et al. 2020). These processes may also be superimposed upon directional trends in

climate conditions, adding further complexity. Variation in ecosystem responses to fires have not been evaluated within a single multi-millennial record, which makes it challenging to separate the relative influences of site characteristics, fire severity, and longer-term climatic- or fire-regime change on ecosystem processes.

To evaluate the impacts of millennial-scale climatic changes on fire regimes and subalpine forest ecosystems of the northern Rocky Mountains, we developed a 4800-yr multiproxy biogeochemical, vegetation, and fire-history record from Silver Lake, Montana, USA. The study site is located in a forested subalpine cirque in the northern Bitterroot Mountains, and has previously been used to reconstruct paleoclimate using lake-level variations (Parish et al. 2022). We used this record to answer two research questions: (1) How did millennial-scale climatic changes affect the vegetation community, watershed biogeochemistry, and fire regime?; and (2) How did the vegetation community and watershed biogeochemistry vary over successional timescales in response to individual fire events? Using past climate variability as a natural experiment, we aimed to test the influence of climate on fire-ecosystem interactions. We anticipated that a trend toward cooler, wetter climate conditions over the late Holocene would result in an increase in the abundance of subalpine forest species, and a decline in fire frequency due to higher summer fuel moisture and shorter fire seasons. Shifts in decadal-scale biogeochemical and vegetation impacts tightly associated with changes in fire activity would indicate that ecosystem responses to climate were indirectly mediated by changing fire regimes. Conversely, millennial-scale biogeochemical shifts in the absence of changing impacts of fires could indicate strong direct climatic control of ecosystem processes, depending upon the relationship of the vegetation and biogeochemical history to past climate changes. We identify distinct ecosystem impacts of past fires and draw comparisons between the late Holocene record

described here and changes expected over the 21st century to help anticipate the potential resilience of subalpine forest ecosystems to shifting fire regimes.

Study area and site description

Silver Lake is located in the northern Bitterroot Mountains in the Lolo National Forest, Montana, USA (Fig. 1). The lake has a surface area of 5.26 ha and a maximum water depth of 18.8 m. Silver Lake lies at 1623 m elevation in a c. 100-ha cirque basin dammed by a glacial moraine, with no significant inlet streams and a seasonal outlet. The lake basin lies on the Proterozoic Wallace Formation, which is composed of dolomitic quartzite and siltite capped by black argillite, and is locally intersected by diorite (Vuke et al. 2007). Soils in the watershed are deep, well-drained andisols and inceptisols derived from glacial till overlain by volcanic ash, both of which were deposited since the Last Glacial Maximum ~18,000 years ago (USDA-NRCS 2019).

Subalpine forests occupy the Silver Lake watershed, and are dominated by subalpine fir (*Abies lasiocarpa*) and Engelmann spruce (*Picea engelmannii*), with smaller components of mountain hemlock (*Tsuga mertensiana*), lodgepole pine (*Pinus contorta* var. *latifolia*), and western larch (*Larix occidentalis*). Broadleaf taxa are not a significant component of subalpine forests in the region. Alder trees (*Alnus rubra*) and shrubs (*Alnus sinuata*) are common in riparian and disturbed areas, respectively, within the region. The site burned most recently in 1918, but not in the regionally extensive fire year of 1910 (Gibson et al. 2014). Total annual precipitation averaged 1306 mm and mean annual temperature averaged 4.43 °C from 1981-2010 (PRISM Climate Group 2015). Precipitation is snow-dominated, with less than 50 mm of rain during the driest months of July and August.

Local paleoclimate history

We characterized late-Holocene climatic and vegetation changes in the study region by drawing on existing paleohydrology and paleovegetation records. Paleohydrology at Silver Lake is well-resolved from a lake-level reconstruction of past variation in effective moisture (Parish et al. 2022). The lake-level record provides evidence of increased effective moisture c. 2800 calibrated years before present (hereafter yr BP, with present defined as 1950 CE), with modern levels reached c. 1800 yr BP. Vegetation shifts at other sites within the study region corroborate the timing of hydroclimate changes reconstructed at Silver Lake. For example, a pollen and macrofossil-based vegetation reconstruction at Dismal Lake represents a similar elevation and forest type as Silver Lake (Fig. 1; Herring et al. 2018). The Dismal Lake vegetation reconstruction is broadly consistent with paleoclimate becoming cooler and wetter, based on the establishment of *T. mertensiana* after c. 800 yr BP, and distinct shifts in forest vegetation from *P. menziesii* to *L. occidentalis* c. 3450 yr BP, and from *A. grandis* to *A. lasiocarpa* after c. 1950 yr BP (Fig. 2).

Methods

Identifying distinct time periods of paleoclimate a priori from existing records

To test for changes in late-Holocene fire regimes in the Silver Lake record, we identified the timing of regional climatic and vegetation changes based on previously published records. Specifically, we compared the timing of climatic changes in the paleohydrology record from Silver Lake (Parish et al. 2022) to changes in paleovegetation inferred from a stratigraphically constrained cluster analysis performed on a macrofossil record from nearby Dismal Lake (c. 27 km southwest, Herring et al. 2018; Fig. A.2). Dismal Lake represents a similar climatic and ecological setting as Silver Lake, and it resolves sub-genus shifts in plant abundance not evident in pollen records, independently of the Silver Lake pollen record developed here. The two

significant zone breaks in the Dismal Lake macrofossil record corresponded to lake-level changes in the Silver Lake paleohydrology record (Fig. 2), at c. 1950 and 3450 yr BP. These two dates were used to identify three distinct periods – here after “zones” – used to test for significant changes in fire frequency at Silver Lake (see *Fire history* below).

Lake sediment sampling

Two overlapping sediment cores were collected from the deepest part of the lake in September 2017 using a 7.62-cm diameter, 1-m long modified Livingstone piston corer (Wright et al. 1984). A total of c. 8 m of sediment were recovered, terminating in a thick tephra layer inferred to be the Mount Mazama tephra (c. 7631 cal yr BP; Egan et al. 2015). A short core was collected in June 2018 using a polycarbonate tube piston corer, and the upper c. 30 cm of sediment were extruded vertically in the field at 0.5-cm intervals. Deeper cores were extruded horizontally in the lab, split lengthwise, and photographed.

Magnetic susceptibility (MS) was measured on core surfaces at 0.5-cm intervals using a Bartington MS3 Meter and MS2E Core Logging Sensor (Bartington Instruments, Oxford, UK). The record was characterized by uniform dark brown gyttja with fine laminations in the uppermost c. 21 cm, and intermittent laminations throughout the deeper sediments. Cores were correlated based on visual stratigraphy and MS measurements and combined with overlapping sections to produce a continuous record. Cores were sliced at 0.5-cm intervals for subsequent proxy development.

Chronology

Sediment ages were inferred based on 15 ^{210}Pb activity measurements in the upper 40 cm of sediments, 14 AMS ^{14}C ages of terrestrial macrofossils or charcoal in deeper sediments, and three estimated ages of tephra layers. Measurements of ^{210}Pb activity were obtained from Flett

Research Ltd. (Manitoba, Canada), and two measurements of ^{226}Ra activity were used to confirm estimated supported ^{210}Pb activity. Ages were estimated using the constant rate of supply model (Binford 1990). Tephra layers were identified visually and corroborated by MS measurements, and ages were inferred based on known tephra deposits at Silver Lake (Parish et al. 2022). Radiocarbon dating was conducted at the Lawrence Livermore National Laboratory Center for Accelerator Mass Spectrometry, and ^{14}C ages were calibrated using IntCal20 (Reimer et al. 2020). An age-depth relationship was built using the R package *rbacon* with flexible priors to allow a range of sediment accumulation rates (Fig. A.1; Blaauw and Christen 2011). Two ^{14}C dates were excluded from the chronology, given age estimates > 1000 years older than those from samples within c. 50 cm: a wood macrofossil at 204 cm, and a needle macrofossil at 520 cm, assumed to be material with long terrestrial residence times (Gavin 2001, Oswald et al. 2005).

Fire history

For charcoal analysis, sediment subsamples of 3 cm³ were taken from continuous 0.5-cm slices and soaked in a 5% sodium metaphosphate solution for 72 hours before gently wet sieving through a 125- μm wire mesh sieve. Samples were soaked in a 2% sodium hypochlorite solution for an additional 24 hours and sieved again, and charcoal particles were identified visually under a stereomicroscope and counted at 10-40x magnification. The number of particles in each sample was converted to charcoal concentration in units of pieces cm⁻³ of sediment.

To identify peaks in charcoal accumulation inferred as local fire events, charcoal data were analyzed using *CharAnalysis* (v. 1.1, Higuera 2009) in MATLAB (MathWorks 2021). Prior to peak detection, charcoal concentrations (pieces cm⁻³) were interpolated to a constant timestep of 10 years and multiplied by sediment accumulation (cm yr⁻¹) to calculate charcoal

accumulation rate (CHAR, pieces $\text{cm}^{-2} \text{yr}^{-1}$). Low-frequency trends in CHAR ('background') were estimated with a 500-year locally-weighted regression robust to outliers (Cleveland 1979), which was subtracted from the CHAR timeseries to produce a residual timeseries. Peaks in residual CHAR that exceeded the 99th percentile of a locally-fit Gaussian mixture model were interpreted as local fire events (i.e. within 1 km of the lake, Higuera et al. 2007, 2011, Kelly et al. 2013). Charcoal peaks were screened using a minimum-count test (Higuera et al. 2010); a peak was retained if it had less than a 5% probability of coming from the same Poisson distribution as the minimum charcoal count within the 75 years prior.

We characterized the frequency component of the fire regime within three time periods (zones) identified based on paleoclimate and paleovegetation records (Fig. 2, see *Identifying zones* above). The timing of fire events was used to calculate fire return intervals (FRIs), and the mean fire return interval (mFRI) was summarized for each zone. We estimate 95% confidence intervals around the mFRI from 1000 bootstrapped samples of FRIs within each zone. To detect potential changes in fire regimes, a two-parameter Weibull model was fit to the FRIs from each zone using maximum likelihood (*fitdistrplus* package in R). We tested the null hypotheses that FRIs did not differ between adjacent zones using a likelihood-ratio test, following methods described by Higuera et al. (2009). Zones that did not differ ($p > 0.05$) were pooled together in further analyses.

Vegetation history

Vegetation was inferred from pollen analyses from 68 sediment samples spanning the upper 600 cm of core depth, corresponding to one sample every 96 yr on average ($\text{sd} = 36$), extending back to 6400 yr BP. Subsamples were processed using standard methods (Faegri and Iversen 1989), and pollen was counted at 400x magnification by Erin Herring (EMH Consulting,

LLC). Pollen was identified to the lowest taxonomic level possible using published keys and the modern reference collection at the University of Oregon. A minimum of 300 terrestrial pollen grains were identified in each sample, averaging 366 grains (sd = 16). *Cyperaceae* was excluded from pollen sums due to its very high abundance in some samples (up to 90%), likely originating from wetland taxa along the lake margin. Pollen concentration was determined by adding a known concentration of an exotic tracer (*Lycopodium*) and used to calculate pollen accumulation rate (PAR).

Pollen abundances were summarized as percentages of the terrestrial sum. Pollen types present in at least 50% of samples and with a maximum abundance of at least 1% were considered major taxa (Chileen et al. 2020); these taxa were further grouped into three categories: conifer (trees), broadleaf (trees and shrubs), and herbaceous (understory grasses and forbs). The ratio of overstory to understory taxa (AP:NAP) was calculated using the equation $[a - b] / [a + b]$, where a is the sum of arboreal pollen counts (conifer and deciduous), and b is the sum of non-arboreal pollen counts (shrubs and herbaceous plants). We also calculated a ratio of major conifer to broadleaf pollen taxa (conifer:broadleaf) using the same equation.

To assess decadal-scale vegetation responses to fire, pollen samples were classified based on time-since-fire (Chileen et al. 2020). Pollen samples within 10 yr of a CHAR peak or up to 40 yr after were considered “fire-associated” (n = 15), to account for potentially imprecise alignment between charcoal peaks, fire timing, and pollen samples. Fire-associated samples were compared to samples coming after charcoal peaks (“post-fire”), between 41-80 yr (n = 7), 81-120 yr (n = 11), and >120 yr (n = 20). We compared pollen ratios from among these four sets of samples using nonparametric Wilcoxon rank-sum and Kruskal-Wallis tests.

Sediment biogeochemistry

Biogeochemical proxies were analyzed from each 0.5-cm-interval sample spanning the past c. 4800 years, totaling 861 samples. Subsamples of 0.5-1 cm³ were oven dried at 65 °C for at least 48 hours and homogenized. Dried samples were weighed prior to geochemical analyses to calculate bulk density (g dry mass cm⁻³). The concentrations of 10 elements (Al, Ca, Fe, K, Mg, Mn, P, S, Si, Ti) were measured using X-ray fluorescence (XRF) at the Paleoenvironmental Lab at Kansas State University. Samples were measured using a handheld Bruker Tracer 5i wavelength-dispersive XRF analyzer for 300 seconds, and the concentration of each element (% dry mass) was calculated using a soil calibration. Analytical precision was estimated by conducting at least three repeat measurements on a set of 60 samples spanning the core, with an average coefficient of variation of approximately 3-9%.

Sediment C, N and isotopic composition were measured on the same sediment samples using a Costech 4010 Elemental Analyzer and a Thermo Finnigan Delta V Plus XP mass spectrometer at the University of Wyoming Stable Isotope Facility. Sediment C and N are reported in % dry mass. Isotope ratios are reported relative to VPDB for carbon and atmospheric N₂ for nitrogen, using standard delta notation ($\delta^{13}\text{C}$, $\delta^{15}\text{N}$, ‰). Analytical precision was estimated via repeat measurements for 56 samples spanning the core. Precision was $\pm 0.07\text{‰}$ and $\pm 0.04\text{‰}$ for $\delta^{15}\text{N}$ and $\delta^{13}\text{C}$, and $\pm 0.14\%$ and $\pm 0.01\%$ for C and N, respectively. A correction was applied to $\delta^{13}\text{C}$ measurements younger than 1800 CE to account for the Suess effect (Dombrosky 2020).

To help infer the composition of potential organic matter sources to lake sediments, a set of 43 modern terrestrial samples were collected from the watershed surrounding Silver Lake (Fig. B.1). These included 14 foliage samples of overstory conifers and understory shrubs, and eight litter and 21 soil samples (0-30 cm depth). Samples were analyzed for element

concentrations and isotopes using the same methods, except that a separate foliar method and calibration was used for XRF analysis.

Statistical analyses of biogeochemical proxies

Statistical analyses were conducted in R (v. 4.1.1, R Core Team 2021), and significance is reported using a “language of evidence” (Muff et al. 2021). Dominant modes of variation in elemental concentrations and isotopic composition of sediments (C, N, S, P, Ca, K, Al, Ti, Si, Mg, C:N, $\delta^{13}\text{C}$, $\delta^{15}\text{N}$) were summarized via a principle component analysis (PCA) using the *ade4* package in R (Dray and Dufour 2007). Biogeochemical data were log-transformed prior to PCA as needed to reduce skewness, based on a visual inspection of histograms. Row weights were used to ensure that the influence of each sample was equally distributed across sample ages.

To quantify the impacts of individual fire events on sediment geochemistry, we used a compositing technique derived from superposed epoch analysis (SEA; Adams et al. 2003, Dunnette et al. 2014). Biogeochemical proxies were interpolated to 10-yr timesteps, detrended, and averaged over a pre-fire baseline of 20-40 yr before each charcoal peak, and again over 0-20, 30-50, and 60-80 yr after each charcoal peak. To produce a composite record summarizing changes in biogeochemical proxies before and after fire events, values in each time lag were averaged across all inferred fire events in the record. A Monte Carlo randomization method was used to generate confidence intervals for the mean response (Appendix A).

Upon initial inspection of the composite records, at least two distinct patterns emerged. To quantify and evaluate the robustness of these patterns, *a posteriori*, we used hierarchical cluster analysis to identify sets of fire events with similar post-fire biogeochemical patterns. For each fire event, values of each element or isotope were extracted and averaged over 0-30 yr and over 40-70 yr following the fire; this differed from the compositing described above, to avoid

excess complexity while capturing the initial magnitude and the duration of responses. Post-fire averages for each variable were scaled (by z-scores) and used to calculate squared-chord distances among all fire events. A hierarchical cluster analysis using Ward's method was performed, identifying two distinct sets of post-fire responses (Fig. A.3). Finally, given the expectation that some charcoal peaks recorded in sediment records result from low-severity or extra-local fires and thus would not influence catchment biogeochemistry (Dunnette et al. 2014), we conducted an additional step to identify fires with no detectable biogeochemical response (Appendix A). Fire events that lacked a significant biogeochemical response were removed from each cluster and placed into an additional category, "unresponsive." To characterize the average biogeochemical impacts of these different populations of fire events, we conducted separate composite analyses, as described above, using each of the three distinct sets of fire events.

Results

Chronology

The Silver Lake record reported here begins c. 4800 yr BP. Each ½-cm sample represents a median of 5 yr (range: 1-18), corresponding to a median sediment accumulation rate of 0.13 cm yr⁻¹ (Fig. 3). Although the core we retrieved extends to deeper and older sediment, we restricted our analyses to sediments younger than 4800 yr BP, due to a distinct increase in sediment accumulation rate over approximately 500-600 cm depth relative to the rest of the core.

Fire history

Charcoal particles were abundant in the sediment samples, with a median concentration throughout the 4800-yr record of 25 charcoal pieces cm⁻³ and median accumulation rate of 2.4 pieces cm⁻² yr⁻¹. The record-wide median signal-to-noise index was 4.3 and varied from 3.0 to 10.0, indicating strong separation of charcoal peaks from noise and the suitability of the record

for charcoal peak analysis (*cf.* Kelly et al. 2011). Charcoal peak analysis identified 31 peaks over the past 4800 yr (Fig. 4), interpreted as fire events (i.e., one or more local fires within the 10-year sampling interval). Mean fire return intervals (mFRIs) for Zones 1 (1950 yr BP - present), 2 (3450-1950 yr BP), and 3 (4760-3450 yr BP) were 223 yr (95% CI: 175-280), 137 yr (60-255), and 117 yr (80-152), respectively (Table 1). Likelihood ratio tests provide moderate evidence that the FRI distribution in Zone 1 differed from Zone 2 and Zone 3 ($p = 0.01$ and 0.04 , respectively). There is not sufficient evidence to support a difference in FRIs between Zones 2 and 3 ($p = 0.26$). This suggests a single shift in fire frequency over the record, near 1950 yr BP.

Vegetation history

Pollen assemblages were dominated by coniferous tree taxa, with a median (IQR) abundance of major conifer taxa of 70% (64-77%) over the past 4800 yr, with 35% (33-40%) from *Pinus* pollen types. Diploxylon *Pinus* pollen types are interpreted as originating from *P. contorta*, while haploxylon pollen types are interpreted as originating from *P. albicaulis* or *P. monticola*. *Picea* pollen types (*P. engelmannii*) and *Abies* pollen types (*A. lasiocarpa* and *A. grandis*) had median abundances of 12% (8-16%) and 11% (10-15%), respectively.

Pseudotsuga-Larix-type, *Tsuga*, and *Cupressaceae* pollen types each had median abundances of <5%. Among non-conifer taxa, *Alnus rubra* pollen types were the most abundant, with a median of 14% (9-16%). Dominant pollen types from understory taxa included *Alnus sinuata*, *Poaceae*, and *Artemisia*, each averaging 3% abundance.

Millennial-scale changes in pollen abundance were summarized using cluster analysis, which revealed one significant shift in the pollen assemblage at c. 1900 yr BP (Fig 5), consistent with the Dismal Lake macrofossil record (Fig. 2). The change in macrofossil assemblage identified in the Dismal Lake record c. 3450 yr BP was not evident in the Silver Lake record,

although the percentage of *Picea* pollen types increased to >10% at approximately this time. At Silver Lake, the AP:NAP ratio was relatively constant over millennial timescales, averaging 0.75 (IQR: 0.66-0.81), but the relative abundances of arboreal pollen taxa shifted over time (Fig. 5). *Pinus* pollen types increased in abundance from a median of 34% between 4800-1900 yr BP to 41% after 1900 yr BP ($p < 0.001$), in part driven by an increase in haploxylon-type pollen from 1% to 4% ($p < 0.001$). Concurrently, median abundance of *Tsuga mertensiana* pollen types increased from 1% to 3% ($p < 0.001$) and *Abies* pollen abundance increased from 11 to 14% ($p = 0.03$), while percentages of *Alnus rubra* and *Alnus sinuata* pollen types decreased substantially from 19% to 8% median abundance ($p < 0.001$) and from 5% to 2% ($p = 0.002$), respectively.

Biogeochemical proxies and organic matter sources

The elemental composition and stable isotope ratios of Silver Lake sediments were broadly consistent with expected values for lacustrine sediments, integrating terrestrial and aquatic organic matter sources, allochthonous clastic material, and organic matter processing (Meyers 1997, Talbot 2001). Here we report elemental concentrations and stable isotope values, and briefly highlight their associations with primary biogeochemical signals from watershed processes to aid in interpretation. See Appendix A for additional details on interpretation of biogeochemical proxies.

Sediments were moderately organic, with median C and N concentrations of 16% (13.6 – 17.2%) and 1.1% (1.0 – 1.2%), respectively. Si was the most abundant element in the sediment, with a median (IQR) concentration of 25% (23.3 – 26.3%), followed by C, Al (median 4.2%; 3.6 – 4.7%), and Fe (median 2.4%; 2.0 – 3.5), while P and Mn were the least abundant (median 0.05%, Fig. 6). The median (IQR) molar C:N ratio of 14.4 (13.5-15.3) was lower than the C:N of

terrestrial soil and foliar samples (median 18.8 and 43.9, respectively; Fig. B.1) but higher than that expected of algal biomass (c. 4-10; Meyers 1994), implying a mix of sources. Sedimentary $\delta^{15}\text{N}$ values averaged 0.65‰ (IQR: 0.46 – 0.85‰), representing an integrator of catchment N-cycle processes (Robinson 2001). Sedimentary $\delta^{13}\text{C}$ values averaged -27.6‰ (IQR: -29.8 – -26.7‰) and varied as much as 3-5‰ over multidecadal timescales throughout the record (Fig. 6), providing information about within-lake production.

Principal components (PC) analysis explained 67.6% of the variability in element concentration and stable isotope data with the first two axes (Fig. 7). PC1 accounted for 42.2% of the variability and was positively associated with $\delta^{13}\text{C}$, $\delta^{15}\text{N}$, C:N, and concentrations of minerogenic elements and base cations (K, Si, Ti, Ca). PC1 was negatively associated with concentrations of redox-sensitive elements and those associated with organic matter, including C, N, P, S, Fe, and Mn. PC2 accounted for 25.4% of the variability in the data and was positively correlated with Mg, reflecting an antiphase between Mg concentrations compared to Al and other elements.

Centennial and millennial-scale variability in sediment geochemistry

Sedimentary elemental concentrations and isotopes exhibited notable low-frequency variability. Millennial-scale trends in biogeochemical proxies were summarized by applying a 1000-yr loess smoother to PC1 and PC2 (Fig. 7). PC1 reached a maximum at c. 2500 yr BP and generally declined toward present, reflecting a long-term shift in the elemental and isotopic composition of the lake sediment. PC2 varied throughout the record, increasing modestly between c. 4800 – 3600 yr BP, and decreasing slightly between c. 2200 – 700 yr BP.

Trends in PC1 and PC2 integrated variation in individual proxies, many of which covaried (Fig. 6). For example, concentrations of Si, Ti, Ca, and K displayed similar low-

frequency changes, declining slightly over the past 4800 years, while concentrations of P, S, Mn, and Fe increased between c. 2500 - 150 yr BP. C concentration increased slightly after 2500 yr BP before declining over the past 500 years, while N concentration did not display a clear long-term trend, resulting in a subtle long-term increase in sedimentary C:N to a maximum of 18 c. 750 yr BP and a subsequent decline to <10 today. Lake-sediment $\delta^{13}\text{C}$ values declined from a maximum of -26.3‰ between 3100 – 2600 yr BP to a minimum of -34.2‰ today (after Suess correction), while $\delta^{15}\text{N}$ values varied only slightly throughout the record.

Decadal-scale post-fire variations in sediment geochemistry and pollen assemblage

We termed the two distinct patterns of post-fire biogeochemical responses identified via cluster analysis “erosion-associated” (Type 1, n = 10) and “non-erosional” (Type 2, n = 10) based on the dominant biogeochemical response (Fig. 8; *cf.* Leys et al. 2016). For consistency, we use these terms throughout; see Discussion for interpretation of post-fire biogeochemical responses. A third category lacked post-fire changes in any geochemical proxy besides $\delta^{13}\text{C}$, which we termed “non-responsive” (n = 9). There was no evidence that the average charcoal peak magnitude differed between the three populations (Kruskal-Wallis $p = 0.23$), although the three peaks with the highest peak magnitude were of Type 1 (Fig. B.2). Additionally, there was no evidence that the frequency of each post-fire response type changed over the record (Fig. B.2).

The average response following erosion-associated (Type 1) fires was characterized by an initial increase in the concentrations of minerogenic elements, summarized by an increase in PC1 values and a decrease in PC2 values relative to pre-fire (Fig. 8). The composite analysis for erosion-associated (Type 1) fires showed strong evidence of an increase in mean values of Ti, $\delta^{15}\text{N}$, Al, K, and Si and a decline in C relative to the long-term average over 0-20 yr after fire

($p < 0.01$). There was moderate evidence of initial increases in sediment bulk density, Ca, and $\delta^{13}\text{C}$, and a decline in N over 0-20 yr following fire events ($p < 0.05$), although the responses in C, N, $\delta^{13}\text{C}$, Al, K, Si, and Ca were not significant when medians were considered (Fig. 8).

Geochemical responses following these erosion-associated fire events persisted for 30-50 yr for all proxies except $\delta^{15}\text{N}$ and C, which returned to pre-fire values on average within c. 20 yr after fire. All geochemical responses were recovered to baseline or reversed in sign by 60-80 yr after fire.

The average response following non-erosional (Type 2) fires was characterized by opposing responses in many proxies compared with Type 1 fires, summarized by an initial decrease in PC1 values and an increase in PC2 values relative to pre-fire (Fig. 8). There was strong evidence of an initial increase in sediment N concentration and a decrease in Ti, $\delta^{13}\text{C}$, $\delta^{15}\text{N}$, C:N, sediment bulk density, Al, K, and Ca 0-20 yr after non-erosional (Type 2) fires ($p < 0.01$). Additionally, there was weak to moderate evidence that non-erosional fires were followed by increases in average sediment C and S concentrations and decreases in Si ($p < 0.10$), although these responses and those in Al, K, and Ca were not significant when medians were considered (Fig. 8). All geochemical proxies returned to baseline values within c. 50 yr post-fire on average (Fig. 8).

Pollen assemblages varied significantly based on time-since-fire (Fig. 9). Fire effects on vegetation were most evident within 40 yr after fire, and pollen assemblages typically returned to pre-fire values within c. 80 yr after fire (Fig. 9B). There was moderate evidence that conifer pollen concentrations decreased and broadleaf pollen concentrations increased initially after fire ($p < 0.05$), while AP:NAP and herbaceous pollen percentages did not change after fire (Fig. 9A). Post-fire changes in pollen abundances were, in large part, driven by initial decreases in

percentages of *Pinus* and *Abies* pollen types and increases in percentages of *Alnus* pollen types, and were broadly similar throughout the record (Fig. B.4). Changes in pollen assemblages were generally of higher magnitude following erosion-associated (Type 1) fires compared with non-erosional (Type 2) fires, but very small sample sizes limit our ability to interpret those differences (Fig. B.4).

Discussion

The ecosystems in the watershed of Silver Lake, Montana experienced long-term changes in vegetation and fire activity over the past 4800 yr consistent with our expectations of a shift toward subalpine forest composition and decreased fire frequency as climate became cooler and wetter toward present. On decadal timescales, fire events recorded in the sedimentary record had distinct and diverse biogeochemical impacts throughout the past five millennia. The discovery of qualitative variability in fire severity provides a relatively rare example of heterogeneity in fire effects – pyrodiversity – as seen in this paleorecord. Overall, the Silver Lake record underscores the overarching influence of climate conditions (through temperature and moisture) on both fire regimes and ecosystem processes over centuries to millennia. Further, throughout repeated wildfire events, the ecosystems surrounding Silver Lake demonstrate consistent biogeochemical resilience to wildfires spanning millennia, across variation in climate, fire frequency, and fire effects.

Vegetation and fire regimes were sensitive to regional climatic changes

Our results indicate that coniferous forest vegetation and fire frequency have been sensitive to millennial-scale climatic changes over the late Holocene. Increased pollen abundances of conifer taxa after 1900 yr at Silver Lake (Fig. 5), and particularly of *T. mertensiana* (Fig. 4), are consistent with vegetation changes inferred from the Dismal Lake

macrofossil record and regional pollen records indicating the development of modern subalpine forests between 2000 – 4000 yr BP (Brunelle et al. 2005, Herring et al. 2018). Increased dominance of subalpine conifer species was likely facilitated by declining summer insolation and greater effective moisture over the past two millennia (Herring et al. 2018, Parish et al. 2022). The vegetation shift c. 1900 yr BP also reflects a long-term decline in *Alnus* pollen (Fig. 5), which is consistent with other regional records and likely reflects increased forest density reducing non-local pollen delivery of *Alnus*, originating from disturbed and riparian areas within the broader landscape (Brunelle et al. 2005). Alternatively, the increase in lake level could have altered habitat along the lake margin, reducing the local abundance of *Alnus*. We attribute the lack of a distinct change in pollen assemblages at Silver Lake c. 3400 yr BP, contrasting with a vegetation shift inferred at nearby Dismal Lake (Fig. 2), to the lower taxonomic resolution of pollen compared with macrofossil data. Specifically, the Dismal Lake macrofossil record highlights a shift from *P. menziesii* to *L. occidentalis* c. 3400 yr BP, which is undetectable with pollen (i.e., *Pseudotsuga* and *Larix* pollen types are indistinguishable).

Fire frequency decreased as effective moisture increased to near modern after c. 2000 yr BP (Parish et al. 2022), reflecting a 77% increase in the mean fire return interval (mFRI). The estimated mFRI of 222 yr (95% CI: 173-276 yr, Table 1) for the past 2000 years aligns well with regional tree-ring and contemporary records from subalpine forests in the northern Rocky Mountains. Tree-ring estimated mFRIs range from 140-240 yr (Kipfmeuller 2003), and the 1900-2021 fire rotation period in the study area was 215 yr, based on documented burning in subalpine forests (Gibson et al. 2014). Under climate conditions of recent decades to centuries, widespread fire activity in the northern Rocky Mountains occurs in years with relatively warm and dry spring and summer conditions, which lowers fuel moisture and facilitates fire ignition and spread

(Heyerdahl et al. 2008, Morgan et al. 2008, Higuera et al. 2015). Decreased fire activity in the past two millennia is attributable to increased snowpack and later snowmelt from late-Holocene climatic changes, which would favor higher summer fuel moisture and/or shorter fire seasons (Westerling 2016).

Results from Silver Lake are broadly consistent with existing paleoecological records from the northern Rocky Mountains highlighting strong links between climate and fire activity over the Holocene. Hoodoo Lake, Idaho, the geographically closest paleofire record to Silver Lake (c. 135 km south) and representing a similar climatic regime, also revealed a decline in fire frequency during the past 2000 yr, inferred as a response to late-Holocene cooling (Brunelle et al. 2005). Among other paleofire records across a broader region, variability in the timing and patterns of changes in fire-event frequency likely reflect spatial variation in climate and local controls of fire activity (Brunelle et al. 2005, Whitlock et al. 2008, 2011). Overall, paleofire records from across the northwestern United States display a modest decline in charcoal accumulation within the past 2000 yr, implying a reduction in overall biomass burning during the late Holocene (Whitlock et al. 2008).

While a shift toward cooler and wetter climate conditions was likely the overarching driver of the observed vegetation change at c. 1900 yr BP at Silver Lake, vegetation changes were also consistent with the direct impacts of lower fire frequencies within the past two millennia. Specifically, longer fire-free intervals would favor relatively slow-growing, shade-tolerant species such as *T. mertensiana* and *A. lasiocarpa* (Fig. 5). Additionally, broadleaf taxa were positively associated with fire activity on decadal timescales (Fig. 9), implying that changing fire frequency could have contributed to the decline in the abundance of *Alnus* pollen types over the past 2000 yr (Fig. 10). While changes in *Alnus* pollen abundance likely reflect, in

large part, variation in local conifer density determining the signal of non-local pollen, a reduction in fire activity may also have reduced the landscape prevalence of N-fixing *A. sinuata*, which grows in disturbed sites and requires high-light environments (Yelenik et al. 2013).

The shift in fire frequency detected at c. 1900 yr BP at Silver Lake contrasts with the lack of a distinct change in fire frequency as effective moisture increased c. 3400 yr BP (Fig. 10). This complacency of the fire-history record may be due to changes in climatic variability that enabled similar fire activity despite wetter annual climate overall. For example, if increased effective moisture c. 3400 primarily derived from winter precipitation, this may not have translated to greater summer fuel moisture, particularly because summer insolation was higher than present at that time (Hostetler et al. 2018). Further, wildfire spread is a non-linear process, such that a given change in climate may not be expected to result in a change in fire activity of similar magnitude (Young et al. 2017, Juang et al. 2022). Finally, with only one record, we have low statistical power to detect subtle changes in fire frequency (Higuera 2006).

Biogeochemical responses to millennial-scale variations in climate and fire regimes

Millennial-scale climate change exerted a strong influence on catchment biogeochemistry, independent of changing fire activity. The dominant temporal trend in catchment biogeochemistry is characterized by the decline in PC1 over the past 2500 yr BP, likely attributable to the shift toward greater effective moisture, revealed by increasing lake level beginning by 2800 yr BP and reaching near-modern after c. 1800 yr BP (Fig. 10). A wetter climate could promote influxes of materials from the surrounding watershed; for example, increased delivery of isotopically light DIC from terrestrial runoff is consistent with the observed decline in sedimentary $\delta^{13}\text{C}$ values (Meyers and Teranes 2001). Changes in the quantity and/or

type of precipitation, such as those that would be reflected in a higher lake level, would seem to increase the hydrological connections between the catchment and the lake at this site.

In addition, wetter conditions within the past two millennia altered within-lake processes. Increasing concentrations of redox-sensitive elements (S, Mn, Fe) likely reflect a shift in redox conditions in the water column or upper sediments of Silver Lake (Boyle 2001). Given that Mn reduction proceeds more rapidly under anoxic conditions, an increase in the ratio of Fe to Mn in the sediment after c. 1900 yr BP implies a decline in oxygen availability (Fig. B.5; Hu et al. 2001, Naeher et al. 2013). This interpretation is consistent with a rise in lake level, which could have strengthened seasonal stratification and reduced hypolimnetic oxygen (Boehrer and Schultze 2008), although the net change in water depth over the last several millennia was only slight due to rapid sediment accumulation (Fig. B.5). Shifts in within-lake circulation or seasonal turnover, possibly as a result of millennial-scale changes in atmospheric circulation (Stone et al. 2016), may have also intensified geochemical focusing of fine-textured Mn and Fe precipitates to deeper waters (Naeher et al. 2013). There is little evidence that reduced fire frequency in the past two millennia influenced long-term variation in sediment geochemistry. The predominant trend in PC1 – largely driven by changes in Mn, Fe, and $\delta^{13}\text{C}$ – mainly reflects within-lake processes, and we found no strong evidence of post-fire responses in Mn or Fe. Therefore, the millennial-scale trends in PC1 were most likely related to climatic changes.

Disturbance processes or sub-millennial scale climate variations may have played a role in multidecadal or century-scale fluctuations in biogeochemical proxies, reflecting variation in lake thermal structure or element cycling within the lake or surrounding watershed (McCullough et al. 2019). For example, the amplitude of high-frequency variations in sedimentary concentrations of S, Fe, Mn, and P increased over the past 2000 yr (Fig. 6), potentially due to

shorter-term climate variability undetected through lake-level changes. Additionally, a c. 600-yr fire-free interval c. 3000-2400 yr BP was associated with distinct trends in several proxies (Fig. 6-7), suggesting that the lack of fire altered century-scale biogeochemical processes. Declines in fire-caused mobilization of C and other elements may have progressively reduced terrestrial subsidies to the lake, consistent with paleo-informed ecosystem modeling highlighting the accumulation of soil carbon during long fire-free intervals (Hudiburg et al. 2017, Bartowitz et al. 2019). Alternatively, a shift in the depositional environment due to a fluctuation in lake level could account for changes in sediment geochemistry (Fig. 10), but the precise timing of the lake-level shift is not clear, and we found no evidence of a change in sediment accumulation rate or stratigraphy during this particular fire-free interval.

Fire severity and ecosystem impacts of wildfires

The Silver Lake record usefully records multiple distinct biogeochemical impacts of past wildfires, revealing diversity in fire effects rarely discernable in paleo-fire records. Sediment biogeochemistry changed distinctly in response to fire events, representing varying fire effects related to fire behavior and severity (i.e., direct, or first-order fire effects), as well as ecosystem dynamics over successional timescales after fire (i.e., indirect, or second-order fire effects; Higuera 2020). Given the decadal-scale resolution of the record, we cannot distinguish between direct and indirect fire effects. Nonetheless, we frame our discussion in the context of inferred fire severity and subsequent biogeochemical responses over successional timescales.

Nearly half of fire events reconstructed ($n = 10$) had biogeochemical responses consistent with an influx of material from post-fire soil erosion, which were likely spatially extensive, high-severity fires that burned in the watershed. Fire-related erosion is supported by initial increases in the concentration of minerogenic elements (Fig. 8), similar to the biogeochemical impacts of

lake-sediment-inferred high-severity fires in a subalpine watershed in Colorado (Dunnette et al. 2014, Leys et al. 2016). Intense and spatially continuous burning enhances erosion via reduced interception and increased soil water repellency, resulting in greater overland flows and a redistribution of topsoil and associated elements within the watershed (Shakesby and Doerr 2006, Larsen et al. 2009, Vieira et al. 2015, Berhe et al. 2018). Elevated erosion can persist for several years (Larson-Nash et al. 2018), and is consistent with diluted organic content in the sediment (Fig. 8). Additionally, initial increases in sedimentary $\delta^{15}\text{N}$ values after fires implies isotopic enrichment of residual forest N pools, attributable to volatile N losses during fire and, possibly, subsequent leaching losses, consistent with a more “open” N cycle initially following fire (LeDuc et al. 2013, Dunnette et al. 2014, Perakis et al. 2015). High-severity wildfires can increase the $\delta^{15}\text{N}$ of terrestrial N via preferential volatilization of the lighter isotope, combustion of isotopically depleted foliar and litter N pools, as well as elevated nitrification and nitrate leaching after fire, given that nitrification strongly discriminates against the heavier isotope (Hoberg 1997). In turn, changes in the size and isotopic makeup of terrestrial N pools alter the N budget and sedimentary $\delta^{15}\text{N}$ values of closely linked lacustrine systems (Hu et al. 2001, Dunnette et al. 2014, Morris et al. 2015, Kim et al. 2016).

An equal number of fire events ($n = 10$) were associated with increased organic inputs and nutrient subsidies to the lake, lacking any indications of fire-caused soil erosion (Fig. 8). The lack of erosion associated with these events is corroborated by magnetic susceptibility, which provides an additional proxy for allochthonous clastic material (Whitlock and Larsen 2001): of the 10 fires classed as Type 2, none were associated with a peak in MS (Fig. B.3). We interpret non-erosional fire events as non-stand-replacing fires or high-severity fires that burned a lesser proportion of the catchment. Importantly, these events were still impactful enough to influence

biogeochemical processes. For example, some amount of the plant nutrients such as N, S, and P that are released from organic tissues by combustion can be delivered to lakes via ash deposition and riverine and subsurface flows (Spencer et al. 2003, Murphy et al. 2006, Rhoades et al. 2011, Gustine et al. 2022), and soil ammonium and nitrate pools often increase dramatically following wildfire (Wan et al. 2001, Smithwick et al. 2005, Turner et al. 2007). An influx of leached N could stimulate within-lake algal production (Morris and Lewis 1988, McCullough et al. 2019), as implied by low sediment bulk density and C:N, and high C and N concentrations observed after fires (Fig. 8). Indeed, elevated lake-sediment N 0-20 yr after paleofires at Gold Creek Lake, Colorado, was interpreted as evidence of aquatic productivity (Pompeani et al. 2020), a pattern also evident in Silver Lake (Fig. 8). However, post-fire pulses in N availability typically last months to years, in contrast to the decadal-scale biogeochemical responses observed here. Growth of N-fixing plant species (e.g., *Alnus*) and other non-symbiotic N-fixers during early successional stages could increase nutrient subsidies to the lake while lowering the $\delta^{15}\text{N}$ of terrestrial N pools, highlighting biotic controls on catchment biogeochemistry (Fig. 9; Yelenik et al. 2013, Perakis et al. 2015, Cleveland et al. 2022). The decline in $\delta^{15}\text{N}$ after non-erosional fires contrasts with post-fire increases in lake-sediment $\delta^{15}\text{N}$ in two records from northern Colorado, where *Alnus* is less abundant (Chickaree, Hinman Lake; Dunnette et al. 2014, Calder et al. 2019, Pompeani et al. 2020). Future research is needed to fully understand the role of biological N fixation, in shaping catchment N-cycle dynamics over successional timescales following wildfire.

Finally, nearly an equal proportion of fire events ($n = 9$) were associated with a lack of significant biogeochemical responses. We interpret these as reflecting lower-severity, spatially variable fires within the watershed, or fires burning nearby but outside of the watershed (e.g., 1-2

km). Evidence of changes in pollen assemblages following these fire events indicate that they indeed represent burning within the pollen and charcoal source areas of Silver Lake (Fig. B.4). The only distinct change in biogeochemical proxies after these fires was an initial decrease in $\delta^{13}\text{C}$ (Fig. 8), which may simply reflect the influx of charcoal itself (Fig. B.6), given that partial combustion can deplete wood $\delta^{13}\text{C}$ by up to 1.6‰ (Ascough et al. 2008).

Ecosystem resilience to wildfires over millennia

Our results highlight consistent ecosystem resilience to wildfires throughout the past 4800 years, despite variations in climate, vegetation, and fire activity (Fig. 10). Regardless of the type of post-fire response, biogeochemical proxies and pollen assemblages recovered to pre-fire values within c. 50-80 yr (Fig. 8-9), consistent with expectations that re-establishment and growth of forest vegetation would stabilize soils and conserve nitrogen through increased demand (Cerdà et al. 2005, Turner et al. 2007, Kim et al. 2016, 2021). Evidence of ecosystem resilience to wildfires at Silver Lake is also consistent with several records from subalpine and boreal forest sites (Leys et al. 2016, Chipman and Hu 2019, Pompeani et al. 2020, Chileen et al. 2020), and highlights tight linkages between vegetation and biogeochemical processes over successional timescales (Smithwick 2011). Additionally, a diversity of fire effects were evident even across the shift to lower fire frequency in the past two millennia, demonstrating how distinct components of a fire regime can vary independently (e.g., Higuera et al. 2014), and providing support for ecosystem resilience to a variety of disturbance processes.

Pyrodiversity

The varying direction and magnitude of decadal-scale biogeochemical changes following fire events provide an example of pyrodiversity in the paleo-record, defined as spatial or temporal variability in fire effects within a given fire regime, and hypothesized to promote

biodiversity (Martin and Sapsis 1992, Jones and Tingley 2022). Large and severe wildfires caused a loss of N and base cations from the terrestrial environment (e.g., Bormann et al. 2008), whereas shifts in nutrient cycling were evident following lower-severity or patchier fires lacking significant soil erosion. Similar changes could also occur following severe fires but may be diluted or obscured by eroded material, such that the dominant processes preserved in lake sediments differ among fires. Our results thus underscore the importance of fire intensity and severity as key controls of fire effects on the amounts and fluxes of C and other elements (Raison 1979, Smithwick et al. 2005, Adkins et al. 2019, Li et al. 2021). Importantly, this pyrodiversity occurred throughout the past 4800 yr at Silver Lake, within multi-millennial periods characterized by the same general climate and vegetation conditions, as well as fire frequency (Fig. 10), indicating that multiple types of fires can occur within a single fire regime and climate.

The diversity of fire severity and fire effects revealed over the past 4800 years is analogous to spatial variability in fire severity observed within contemporary wildfires. Approximately one third of fire events identified in the Silver Lake record fell into the categories of erosion-associated, non-erosional, or non-responsive, reflecting differences in fire severity likely resulting from variation in pre-fire vegetation and fire weather (e.g., Evers et al. 2022). Within contemporary wildfires, 34% of forest fire area over 1984-2010 across the northern Rocky Mountains burned at high severity, with the remainder in areas of moderate- or low-severity fire (Harvey et al. 2016). Thus, even in forest types characterized by infrequent high-severity fire regimes – where many fires kill nearly 100% of trees – patches of non-stand-replacing fire contribute to spatial and temporal complexity in forest structure and species composition (Jones and Tingley 2022), and have done so consistently for millennia. Future research is needed to elucidate how variation in the timing and severity of past fires (e.g.,

historical contingencies) interact with climate variability to shape ecological trajectories and biogeochemical processes over decades to centuries (e.g., Turner et al. 2020). While not possible within a single record, bringing together high-resolution geochemical proxies and reconstructed fire histories from multiple sites would support greater statistical power for evaluating how variation in fire frequency and severity influence ecosystem dynamics.

Implications for future ecosystem change

The strong control of climate on disturbance and ecosystem processes across the Silver Lake record implies that ongoing and future climate change will likewise impact disturbance and ecosystem processes. Fire activity in the study region is projected to nearly double by the late 21st century under high emissions scenarios relative to the 1979-2000 baseline (Gao et al. 2021), in line with broader predictions of increased atmospheric aridity resulting in higher fuel aridity and fire activity across the West (Ficklin and Novick 2017, Abatzoglou et al. 2021). A close-to-doubling of contemporary fire activity is consistent with the higher fire frequency observed at Silver Lake between 4800-1900 yr BP, providing an imperfect analog for ecological dynamics with more frequent fire in the future. Our results suggest that ecosystem resilience could be maintained if fire-free periods at the forest stand level remain on average > 100 years, within the range of variability characterizing the past 4800 years (i.e., mFRI between c. 115-223 yr). However, if fire-free intervals are shorter than our estimated biogeochemical recovery time of c. 50 yr, then this resilience would be compromised. Additionally, warmer and drier conditions and more severe fire could increase the time needed to recover, or alter post-fire ecological trajectories, further undermining the longstanding ecosystem resilience revealed in the paleorecord (McLauchlan et al. 2014, Johnstone et al. 2016, Turner et al. 2019).

Feedbacks between shifting fire activity and ecosystem changes may also emerge. Our results indicate that non-stand-replacing fires have been an important component of the fire regime for millennia at Silver Lake, including during a period of drier conditions characterized by more frequent burning and likely lower forest density c. 4800-1900 yr BP (Fig. 10). We expect that with ongoing climate change, increasing area burned and shifts in forest composition or structure could in turn lead to feedbacks whereby fuel types or availability mitigate fire severity and C emissions (Parks et al. 2016, e.g., Walker et al. 2020, Mack et al. 2021), potentially supporting a range of fire severities and biogeochemical impacts even under warmer and drier climate conditions. Such feedbacks are unlikely to manifest in the near-term of the next several decades (Abatzoglou et al. 2021), but could ultimately promote forest resilience over centennial timescales. Still, it remains unclear how ecosystem transformations will unfold under rapid climate change, particularly given the possibility for hysteresis in ecological systems, which limits our ability to use the past as an analog to inform future changes (Scheffer et al. 2001, Anderson-Teixeira et al. 2013). Research to further clarify feedbacks among fire regimes, vegetation, and forest biogeochemistry will help anticipate impacts of ongoing warming and drying and serve to inform management agendas (Crausbay et al. 2022).

Literature Cited

Abatzoglou, J. T., D. S. Battisti, A. P. Williams, W. D. Hansen, B. J. Harvey, and C. A. Kolden. 2021. Projected increases in western US forest fire despite growing fuel constraints. *Communications Earth & Environment* 2:1–8.

- Abatzoglou, J. T., and A. P. Williams. 2016. Impact of anthropogenic climate change on wildfire across western US forests. *Proceedings of the National Academy of Sciences* 113:11770–11775.
- Adams, J. B., M. E. Mann, and C. M. Ammann. 2003. Proxy evidence for an El Niño-like response to volcanic forcing. *Nature* 426:274–278.
- Adkins, J., J. Sanderman, and J. Miesel. 2019. Soil carbon pools and fluxes vary across a burn severity gradient three years after wildfire in Sierra Nevada mixed-conifer forest. *Geoderma* 333:10–22.
- Anderson-Teixeira, K. J., A. D. Miller, J. E. Mohan, T. W. Hudiburg, B. D. Duval, and E. H. DeLucia. 2013. Altered dynamics of forest recovery under a changing climate. *Global Change Biology* 19:2001–2021.
- Ascough, P. L., M. I. Bird, P. Wormald, C. E. Snape, and D. Apperley. 2008. Influence of production variables and starting material on charcoal stable isotopic and molecular characteristics. *Geochimica et Cosmochimica Acta* 72:6090–6102.
- Bailey, R. G. 1995. Descriptions of the ecoregions of the United States: US Department of Agriculture. Forest Service, Miscellaneous Publication 1391:108.
- Bartowitz, K. J., P. E. Higuera, B. N. Shuman, K. K. McLauchlan, and T. W. Hudiburg. 2019. Post-Fire Carbon Dynamics in Subalpine Forests of the Rocky Mountains. *Fire* 2:58.
- Berhe, A. A., R. T. Barnes, J. Six, and E. Marín-Spiotta. 2018. Role of Soil Erosion in Biogeochemical Cycling of Essential Elements: Carbon, Nitrogen, and Phosphorus. *The Annual Review of Earth and Planetary Sciences* is online at earth.annualreviews.org 46:521–569.

- Binford, M. W. 1990. Calculation and uncertainty analysis of ^{210}Pb dates for PIRLA project lake sediment cores. *Journal of Paleolimnology* 3:253–267.
- Blaauw, M., and J. A. Christen. 2011. Flexible paleoclimate age-depth models using an autoregressive gamma process. *Bayesian Analysis* 6:457–474.
- Boehrer, B., and M. Schultze. 2008. Stratification of lakes. *Reviews of Geophysics* 46.
- Boerner, R. E. J., J. Huang, and S. C. Hart. 2009. Impacts of Fire and Fire Surrogate treatments on forest soil properties: a meta-analytical approach. *Ecological Applications* 19:338–358.
- Bormann, B. T., P. S. Homann, R. L. Darbyshire, and B. A. Morrisette. 2008. Intense forest wildfire sharply reduces mineral soil C and N: the first direct evidence. *Canadian Journal of Forest Research* 38:2771–2783.
- Bowd, E. J., S. C. Banks, C. L. Strong, and D. B. Lindenmayer. 2019. Long-term impacts of wildfire and logging on forest soils. *Nature Geoscience* 12:113–118.
- Boyle, J. 2001. Inorganic geochemical methods in paleolimnology. Pages 83–141 *Tracking Environmental Change Using Lake Sediments: Physical and Geochemical Methods*. First edition. Kulwer Academic Publishers, Dordrecht, Netherlands.
- Brunelle, A., C. Whitlock, P. Bartlein, and K. Kipfmüller. 2005. Holocene fire and vegetation along environmental gradients in the Northern Rocky Mountains. *Quaternary Science Reviews* 24:2281–2300.
- Calder, W. J., I. Stefanova, and B. Shuman. 2019. Climate-fire-vegetation interactions and the rise of novel landscape patterns in subalpine ecosystems, Colorado. *Journal of Ecology*.

- Cerdà, A., S. H. Doerr, A. Cerdà, and S. H. Doerr. 2005. Influence of vegetation recovery on soil hydrology and erodibility following fire: an 11-year investigation. *International Journal of Wildland Fire* 14:423–437.
- Certini, G. 2005. Effects of fire on properties of forest soils: a review. *Oecologia* 143:1–10.
- Chileen, B. V., K. K. McLauchlan, P. E. Higuera, M. Parish, and B. N. Shuman. 2020. Vegetation response to wildfire and climate forcing in a Rocky Mountain lodgepole pine forest over the past 2500 years. *The Holocene* 30:1493–1503.
- Chipman, M. L., and F. S. Hu. 2019. Resilience of lake biogeochemistry to boreal-forest wildfires during the late Holocene. *Biology Letters* 15:20190390.
- Cleveland, C. C., C. R. G. Reis, S. S. Perakis, K. A. Dynarski, S. A. Batterman, T. E. Crews, M. Gei, M. J. Gundale, D. N. L. Menge, M. B. Peoples, S. C. Reed, V. G. Salmon, F. M. Soper, B. N. Taylor, M. G. Turner, and N. Wurzburger. 2022. Exploring the Role of Cryptic Nitrogen Fixers in Terrestrial Ecosystems: A Frontier in Nitrogen Cycling Research. *Ecosystems*.
- Cleveland, W. S. 1979. Robust Locally Weighted Regression and Smoothing Scatterplots. *Journal of the American Statistical Association* 74:829–836.
- Coop, J. D., S. A. Parks, C. S. Stevens-Rumann, S. D. Crausbay, P. E. Higuera, M. D. Hurteau, A. Tepley, E. Whitman, T. Assal, B. M. Collins, K. T. Davis, S. Dobrowski, D. A. Falk, P. J. Fornwalt, P. Z. Fulé, B. J. Harvey, V. R. Kane, C. E. Littlefield, E. Q. Margolis, M. North, M. A. Parisien, S. Prichard, and K. C. Rodman. 2020. Wildfire-Driven Forest Conversion in Western North American Landscapes. *BioScience* 70:659–673.
- Crausbay, S. D., H. R. Sofaer, A. E. Cravens, B. C. Chaffin, K. R. Clifford, J. E. Gross, C. N. Knapp, D. J. Lawrence, D. R. Magness, A. J. Miller-Rushing, G. W. Schuurman, and C.

- S. Stevens-Rumann. 2022. A Science Agenda to Inform Natural Resource Management Decisions in an Era of Ecological Transformation. *BioScience* 72:71–90.
- Dombrosky, J. 2020. A ~1000-year ^{13}C Suess correction model for the study of past ecosystems. *The Holocene* 30:474–478.
- Dove, N. C., H. D. Safford, G. N. Bohlman, B. L. Estes, and S. C. Hart. 2020. High-severity wildfire leads to multi-decadal impacts on soil biogeochemistry in mixed-conifer forests. *Ecological Applications*.
- Dray, S., and A.-B. Dufour. 2007. The ade4 Package: Implementing the Duality Diagram for Ecologists. 2007 22:20.
- Dunnette, P. V., P. E. Higuera, K. K. McLauchlan, K. M. Derr, C. E. Briles, and M. H. Keefe. 2014. Biogeochemical impacts of wildfires over four millennia in a Rocky Mountain subalpine watershed. *New Phytologist* 203:900–912.
- Egan, J., R. Staff, and J. Blackford. 2015. A high-precision age estimate of the Holocene Plinian eruption of Mount Mazama, Oregon, USA. *The Holocene* 25:1054–1067.
- Evers, C., A. Holz, S. Busby, and M. Nielsen-Pincus. 2022. Extreme Winds Alter Influence of Fuels and Topography on Megafire Burn Severity in Seasonal Temperate Rainforests under Record Fuel Aridity. *Fire* 5:41.
- Faegri, K., and J. Iversen. 1989. Textbook of pollen analysis (4th edn by Faegri, K., Kaland, PE & Krzywinski, K.). Wiley, Chichester.
- Falk, D. A., P. J. van Mantgem, J. E. Keeley, R. M. Gregg, C. H. Guiterman, A. J. Tepley, D. JN Young, and L. A. Marshall. 2022. Mechanisms of forest resilience. *Forest Ecology and Management* 512:120129.

- Ficklin, D. L., and K. A. Novick. 2017. Historic and projected changes in vapor pressure deficit suggest a continental-scale drying of the United States atmosphere. *Journal of Geophysical Research: Atmospheres* 122:2061–2079.
- Gao, P., A. J. Terando, J. A. Kupfer, J. Morgan Varner, M. C. Stambaugh, T. L. Lei, and J. Kevin Hiers. 2021. Robust projections of future fire probability for the conterminous United States. *Science of The Total Environment* 789:147872.
- Gavin, D. G. 2001. Estimation of inbuilt age in radiocarbon ages of soil charcoal for fire history studies. *Radiocarbon* 43:27–44.
- Gibson, C. E., P. Morgan, and A. M. Wilson. 2014. Atlas of digital polygon fire extents for Idaho and western Montana (2nd Edition). Forest Service Research Data Archive, Fort Collins, CO.
- Gunderson, L. H. 2000. Ecological Resilience—In Theory and Application. *Annual Review of Ecology and Systematics* 31:425–439.
- Gustine, R. N., E. J. Hanan, P. R. Robichaud, and W. J. Elliot. 2022. From burned slopes to streams: how wildfire affects nitrogen cycling and retention in forests and fire-prone watersheds. *Biogeochemistry* 157:51–68.
- Hart, S. C., T. H. DeLuca, G. S. Newman, M. D. MacKenzie, and S. I. Boyle. 2005. Post-fire vegetative dynamics as drivers of microbial community structure and function in forest soils. *Forest Ecology and Management* 220:166–184.
- Harvey, B. J., D. C. Donato, and M. G. Turner. 2016. Drivers and trends in landscape patterns of stand-replacing fire in forests of the US Northern Rocky Mountains (1984–2010). *Landscape Ecology*.

- Herring, E. M., D. G. Gavin, S. Z. Dobrowski, M. Fernandez, and F. S. Hu. 2018. Ecological history of a long-lived conifer in a disjunct population. *Journal of Ecology* 106:319–332.
- Heyerdahl, E. K., P. Morgan, and J. P. Riser. 2008. Multi-season climate synchronized historical fires in dry forests (1650-1900) northern Rockies, USA. *Ecology* 89:705–716.
- Higuera, P. 2006. Detecting changes in fire-frequency regimes: sample size & statistical power. Pages 154–171 *Late Glacial and Holocene Fire History in the Southcentral Brooks Range, Alaska: Direct and Indirect Impacts of Climatic Change on Fire Regimes*. University of Washington.
- Higuera, P. 2009. CharAnalysis 0.9: diagnostic and analytical tools for sedimentcharcoal analysis. User's Guide, Montana State University, Bozeman, MT.
- Higuera, P. E. 2020. First- and Second-Order Fire Effects. Pages 461–463 *in* S. L. Manzello, editor. *Encyclopedia of Wildfires and Wildland-Urban Interface (WUI) Fires*. Springer International Publishing, Cham.
- Higuera, P. E., J. T. Abatzoglou, J. S. Littell, and P. Morgan. 2015. The Changing Strength and Nature of Fire-Climate Relationships in the Northern Rocky Mountains, U.S.A., 1902-2008. *PLOS ONE* 10:e0127563.
- Higuera, P. E., C. E. Briles, and C. Whitlock. 2014. Fire-regime complacency and sensitivity to centennial-through millennial-scale climate change in Rocky Mountain subalpine forests, Colorado, USA. *Journal of Ecology* 102:1429–1441.
- Higuera, P. E., L. B. Brubaker, P. M. Anderson, F. S. Hu, and T. A. Brown. 2009. Vegetation mediated the impacts of postglacial climate change on fire regimes in the south-central Brooks Range, Alaska. *Ecological Monographs* 79:201–219.

- Higuera, P. E., D. G. Gavin, P. J. Bartlein, and D. J. Hallett. 2010. Peak detection in sediment–charcoal records: impacts of alternative data analysis methods on fire-history interpretations. *International Journal of Wildland Fire* 19:996–1014.
- Higuera, P. E., M. E. Peters, L. B. Brubaker, and D. G. Gavin. 2007. Understanding the origin and analysis of sediment-charcoal records with a simulation model. *Quaternary Science Reviews* 26:1790–1809.
- Higuera, P. E., B. N. Shuman, and K. D. Wolf. 2021. Rocky Mountain subalpine forests now burning more than any time in recent millennia. *Proceedings of the National Academy of Sciences* 118:e2103135118.
- Higuera, P. E., C. Whitlock, and J. A. Gage. 2011. Linking tree-ring and sediment-charcoal records to reconstruct fire occurrence and area burned in subalpine forests of Yellowstone National Park, USA. *The Holocene* 21:327–341.
- Hoberg, P. 1997. Tansley Review No. 95 15N natural abundance in soil-plant systems. *New Phytologist* 137:179–203.
- Hostetler, S. W., P. J. Bartlein, and J. R. Alder. 2018. Atmospheric and Surface Climate Associated With 1986–2013 Wildfires in North America. *Journal of Geophysical Research: Biogeosciences* 123:1588–1609.
- Hu, F. S., B. P. Finney, and L. B. Brubaker. 2001. Effects of Holocene *Alnus* Expansion on Aquatic Productivity, Nitrogen Cycling, and Soil Development in Southwestern Alaska. *Ecosystems* 4:358–368.
- Hudiburg, T. W., P. E. Higuera, and J. A. Hicke. 2017. Fire-regime variability impacts forest carbon dynamics for centuries to millennia. *Biogeosciences* 14:3873–3882.

- Johnstone, J. F., C. D. Allen, J. F. Franklin, L. E. Frelich, B. J. Harvey, P. E. Higuera, M. C. Mack, R. K. Meentemeyer, M. R. Metz, G. L. W. Perry, T. Schoennagel, and M. G. Turner. 2016. Changing disturbance regimes, ecological memory, and forest resilience. *Frontiers in Ecology and the Environment* 14:369–378.
- Jones, G. M., and M. W. Tingley. 2022. Pyrodiversity and biodiversity: A history, synthesis, and outlook. *Diversity and Distributions* 28:386–403.
- Juang, C. S., A. P. Williams, J. T. Abatzoglou, J. K. Balch, M. D. Hurteau, and M. A. Moritz. 2022. Rapid Growth of Large Forest Fires Drives the Exponential Response of Annual Forest-Fire Area to Aridity in the Western United States. *Geophysical Research Letters* 49:e2021GL097131.
- Kashian, D. M., W. H. Romme, D. B. Tinker, M. G. Turner, and M. G. Ryan. 2013. Postfire changes in forest carbon storage over a 300-year chronosequence of *Pinus contorta* - dominated forests. *Ecological Monographs* 83:49–66.
- Kelly, R., M. L. Chipman, P. E. Higuera, I. Stefanova, L. B. Brubaker, and F. S. Hu. 2013. Recent burning of boreal forests exceeds fire regime limits of the past 10,000 years. *Proceedings of the National Academy of Sciences* 110:13055–13060.
- Kelly, R. F., P. E. Higuera, C. M. Barrett, and F. S. Hu. 2011. A signal-to-noise index to quantify the potential for peak detection in sediment–charcoal records. *Quaternary Research* 75:11–17.
- Kelly, R., H. Genet, A. D. McGuire, and F. S. Hu. 2015. Palaeodata-informed modelling of large carbon losses from recent burning of boreal forests. *Nature Climate Change* 6:79.

- Kim, S. L., B. N. Shuman, T. A. Minckley, and J. P. Marsicek. 2016. Biogeochemical Change During Climate-Driven Afforestation: A Paleocological Perspective from the Rocky Mountains. *Ecosystems* 19:615–624.
- Kim, Y., C.-G. Kim, K. S. Lee, and Y. Choung. 2021. Effects of Post-Fire Vegetation Recovery on Soil Erosion in Vulnerable Montane Regions in a Monsoon Climate: A Decade of Monitoring. *Journal of Plant Biology* 64:123–133.
- Kipfmeuller, K. F. 2003. Fire-climate-vegetation interactions in subalpine forests of the Selway-Bitterroot Wilderness Area, Idaho and Montana, United States. The University of Arizona.
- Kirchmeier-Young, M. C., F. W. Zwiers, N. P. Gillett, and A. J. Cannon. 2017. Attributing extreme fire risk in Western Canada to human emissions. *Climatic Change* 144:365–379.
- Kranabetter, J. M., K. K. McLaughlan, S. K. Enders, J. M. Fraterrigo, P. E. Higuera, J. L. Morris, E. B. Rastetter, R. Barnes, B. Buma, D. G. Gavin, L. M. Gerhart, L. Gillson, P. Hietz, M. C. Mack, B. McNeil, and S. Perakis. 2016. A Framework to Assess Biogeochemical Response to Ecosystem Disturbance Using Nutrient Partitioning Ratios. *Ecosystems* 19:387–395.
- Larsen, I. J., L. H. MacDonald, E. Brown, D. Rough, M. J. Welsh, J. H. Pietraszek, Z. Libohova, J. de Dios Benavides-Solorio, and K. Schaffrath. 2009. Causes of Post-Fire Runoff and Erosion: Water Repellency, Cover, or Soil Sealing? *Soil Science Society of America Journal* 73:1393–1407.
- Larson-Nash, S. S., P. R. Robichaud, F. B. Pierson, C. A. Moffet, J. Williams, K. Spaeth, R. E. Brown, and S. A. Lewis. 2018. Recovery of small-scale infiltration and erosion after wildfires. *Journal of Hydrology and Hydromechanics* 66:261–270.

- LeDuc, S. D., D. E. Rothstein, Z. Yermakov, and S. E. Spaulding. 2013. Jack pine foliar $\delta^{15}\text{N}$ indicates shifts in plant nitrogen acquisition after severe wildfire and through forest stand development. *Plant and soil* 373:955–965.
- Leys, B. A., P. E. Higuera, K. K. McLauchlan, and P. V. Dunnette. 2016. Wildfires and geochemical change in a subalpine forest over the past six millennia. *Environmental Research Letters* 11:125003.
- Li, J., J. Pei, J. Liu, J. Wu, B. Li, C. Fang, and M. Nie. 2021. Spatiotemporal variability of fire effects on soil carbon and nitrogen: A global meta-analysis. *Global Change Biology* 27:4196–4206.
- Mack, M. C., X. J. Walker, J. F. Johnstone, H. D. Alexander, A. M. Melvin, M. Jean, and S. N. Miller. 2021. Carbon loss from boreal forest wildfires offset by increased dominance of deciduous trees. *Science* 372:280–283.
- Martin, R., and D. Sapsis. 1992. Fires as agents of biodiversity: pyrodiversity promotes biodiversity. Cooperative Extension, University of California, Berkeley.
- McCullough, I. M., K. S. Cheruvilil, J. Lapierre, N. R. Lottig, M. A. Moritz, J. Stachelek, and P. A. Soranno. 2019. Do lakes feel the burn? Ecological consequences of increasing exposure of lakes to fire in the continental United States. *Global Change Biology* 25:2841–2854.
- McLauchlan, K. K., P. E. Higuera, D. G. Gavin, S. S. Perakis, M. C. Mack, H. Alexander, J. Battles, F. Biondi, B. Buma, D. Colombaroli, S. K. Enders, D. R. Engstrom, F. S. Hu, J. R. Marlon, J. Marshall, M. McGlone, J. L. Morris, L. E. Nave, B. Shuman, E. A. H. Smithwick, D. H. Urrego, D. A. Wardle, C. J. Williams, and J. J. Williams. 2014.

- Reconstructing Disturbances and Their Biogeochemical Consequences over Multiple Timescales. *BioScience* 64:105–116.
- Meyers, P. A. 1994. Preservation of elemental and isotopic source identification of sedimentary organic matter. *Chemical Geology* 114:289–302.
- Meyers, P. A. 1997. Organic geochemical proxies of paleoceanographic, paleolimnologic, and paleoclimatic processes. Pages 213–250 *Organic Geochemistry*. Pergamon.
- Meyers, P. A., and J. L. Teranes. 2001. Sediment Organic Matter. Pages 239–269 *Tracking Environmental Change Using Lake Sediments: Physical and Geochemical Methods*. First edition. Kluwer Academic Publishers, Dordrecht, Netherlands.
- Morgan, P., E. K. Heyerdahl, and C. E. Gibson. 2008. Multi-season climate synchronized fires throughout the 20th century, northern Rockies, USA. *Ecology* 89:717–728.
- Morris, D. P., and W. M. Lewis. 1988. Phytoplankton nutrient limitation in Colorado mountain lakes. *Freshwater Biology* 20:315–327.
- Morris, J. L., K. K. McLauchlan, and P. E. Higuera. 2015. Sensitivity and complacency of sedimentary biogeochemical records to climate-mediated forest disturbances. *Earth-Science Reviews* 148:121–133.
- Muff, S., E. B. Nilsen, R. B. O'Hara, and C. R. Nater. 2021. Rewriting results sections in the language of evidence. *Trends in Ecology & Evolution*.
- Murphy, J. D., D. W. Johnson, W. W. Miller, R. F. Walker, E. F. Carroll, and R. R. Blank. 2006. Wildfire Effects on Soil Nutrients and Leaching in a Tahoe Basin Watershed. *Journal of Environmental Quality* 35:479–489.

- Naeher, S., A. Gilli, R. P. North, Y. Hamann, and C. J. Schubert. 2013. Tracing bottom water oxygenation with sedimentary Mn/Fe ratios in Lake Zurich, Switzerland. *Chemical Geology* 352:125–133.
- Oswald, W. W., P. M. Anderson, T. A. Brown, L. B. Brubaker, F. S. Hu, A. V. Lozhkin, W. Tinner, and P. Kaltenrieder. 2005. Effects of sample mass and macrofossil type on radiocarbon dating of arctic and boreal lake sediments. *The Holocene* 15:758–767.
- Parish, M. C., K. D. Wolf, P. E. Higuera, and B. N. Shuman. 2022. Holocene water levels of Silver Lake, Montana, and the hydroclimate history of the Inland Northwest. *Quaternary Research*.
- Parks, S. A., C. L. Miller, J. Abatzoglou, L. M. Holsinger, M. A. Parisien, and S. Dobrowski. 2016. How will climate change affect wildland fire severity in the western US? *Environmental Research Letters* 11:35002.
- Pellegrini, A. F. A., A. Ahlström, S. E. Hobbie, P. B. Reich, L. P. Nieradzik, A. C. Staver, B. C. Scharenbroch, A. Jumpponen, W. R. L. Anderegg, J. T. Randerson, and R. B. Jackson. 2018. Fire frequency drives decadal changes in soil carbon and nitrogen and ecosystem productivity.
- Pellegrini, A. F. A., S. E. Hobbie, P. B. Reich, A. Jumpponen, E. N. J. Brookshire, A. C. Caprio, C. Coetsee, and R. B. Jackson. 2020a. Repeated fire shifts carbon and nitrogen cycling by changing plant inputs and soil decomposition across ecosystems. *Ecological Monographs* 90:e01409.
- Pellegrini, A. F. A., K. K. McLauchlan, S. E. Hobbie, M. C. Mack, A. L. Marcotte, D. M. Nelson, S. S. Perakis, P. B. Reich, and K. Whittinghill. 2020b. Frequent burning causes

- large losses of carbon from deep soil layers in a temperate savanna. *Journal of Ecology* 108:1426–1441.
- Peltzer, D. A., D. A. Wardle, V. J. Allison, W. T. Baisden, R. D. Bardgett, O. A. Chadwick, L. M. Condon, R. L. Parfitt, S. Porder, S. J. Richardson, B. L. Turner, P. M. Vitousek, J. Walker, and L. R. Walker. 2010. Understanding ecosystem retrogression. *Ecological Monographs* 80:509–529.
- Perakis, S. S., A. J. Tepley, and J. E. Compton. 2015. Disturbance and Topography Shape Nitrogen Availability and $\delta^{15}\text{N}$ over Long-Term Forest Succession. *Ecosystems* 18:573–588.
- Pompeani, D. P., K. K. McLauchlan, B. V. Chileen, W. J. Calder, B. N. Shuman, and P. E. Higuera. 2020. The biogeochemical consequences of late Holocene wildfires in three subalpine lakes from northern Colorado. *Quaternary Science Reviews* 236:106293.
- PRISM Climate Group (Oregon State University). 2021. PRISM 30-Year Normals. Oregon State University.
- R Core Team. 2021, August 10. R: A language and environment for statistical computing.
- Raison, R. J. 1979. Modification of the soil environment by vegetation fires, with particular reference to nitrogen transformations: a review. *Plant and soil* 51:73–108.
- Reimer, P. J., W. E. N. Austin, E. Bard, A. Bayliss, P. G. Blackwell, C. B. Ramsey, M. Butzin, H. Cheng, R. L. Edwards, M. Friedrich, P. M. Grootes, T. P. Guilderson, I. Hajdas, T. J. Heaton, A. G. Hogg, K. A. Hughen, B. Kromer, S. W. Manning, R. Muscheler, J. G. Palmer, C. Pearson, J. van der Plicht, R. W. Reimer, D. A. Richards, E. M. Scott, J. R. Southon, C. S. M. Turney, L. Wacker, F. Adolphi, U. Büntgen, M. Capano, S. M. Fahrni, A. Fogtmann-Schulz, R. Friedrich, P. Köhler, S. Kudsk, F. Miyake, J. Olsen, F. Reinig,

- M. Sakamoto, A. Sookdeo, and S. Talamo. 2020. The IntCal20 Northern Hemisphere Radiocarbon Age Calibration Curve (0–55 cal kBP). *Radiocarbon* 62:725–757.
- Rhoades, C. C., D. Entwistle, and D. Butler. 2011. The influence of wildfire extent and severity on streamwater chemistry, sediment and temperature following the Hayman Fire, Colorado. *International Journal of Wildland Fire* 20:430–442.
- Robinson, D. 2001. $\delta^{15}\text{N}$ as an integrator of the nitrogen cycle. *Trends in Ecology & Evolution* 16:153–162.
- Romme, W. H., M. S. Boyce, R. Gresswell, E. H. Merrill, G. W. Minshall, C. Whitlock, and M. G. Turner. 2011. Twenty Years After the 1988 Yellowstone Fires: Lessons About Disturbance and Ecosystems. *Ecosystems* 14:1196–1215.
- Schaller, M., J. D. Blum, S. P. Hamburg, and M. A. Vadeboncoeur. 2010. Spatial variability of long-term chemical weathering rates in the White Mountains, New Hampshire, USA. *Geoderma* 154:294–301.
- Scheffer, M., S. Carpenter, J. A. Foley, C. Folke, and B. Walker. 2001. Catastrophic shifts in ecosystems. *Nature* 413:591–596.
- Shakesby, R. A., and S. H. Doerr. 2006. Wildfire as a hydrological and geomorphological agent. *Earth-Science Reviews* 74:269–307.
- Smithwick, E. A. H. 2011. Pyrogeography and Biogeochemical Resilience. Pages 143–163 in D. McKenzie, C. Miller, and D. A. Falk, editors. *The Landscape Ecology of Fire*. Springer Netherlands, Dordrecht.
- Smithwick, E. A. H., D. M. Kashian, M. G. Ryan, and M. G. Turner. 2009. Long-Term Nitrogen Storage and Soil Nitrogen Availability in Post-Fire Lodgepole Pine Ecosystems. *Ecosystems* 12:792–806.

- Smithwick, E. A. H., M. G. Turner, M. C. Mack, and F. S. Chapin. 2005. Postfire Soil N Cycling in Northern Conifer Forests Affected by Severe, Stand-Replacing Wildfires. *Ecosystems* 8:163–181.
- Spencer, C. N., K. O. Gabel, and F. R. Hauer. 2003. Wildfire effects on stream food webs and nutrient dynamics in Glacier National Park, USA. *Forest Ecology and Management* 178:141–153.
- Stone, J. R., J. E. Saros, and G. T. Pederson. 2016. Coherent late-Holocene climate-driven shifts in the structure of three Rocky Mountain lakes. *The Holocene* 26:1103–1111.
- Talbot, M. R. 2001. Nitrogen isotopes in palaeolimnology. Pages 401–439 *Tracking Environmental Change Using Lake Sediments: Physical and Geochemical Methods*. First edition. Kluwer Academic Publishers, Dordrecht, Netherlands.
- The MathWorks, Inc. 2021. MATLAB.
- Tierney, J. A., L. O. Hedin, and N. Wurzburger. 2019. Nitrogen fixation does not balance fire-induced nitrogen losses in longleaf pine savannas. *Ecology* 100.
- Turner, M. G., K. H. Braziunas, W. D. Hansen, and B. J. Harvey. 2019. Short-interval severe fire erodes the resilience of subalpine lodgepole pine forests. *Proceedings of the National Academy of Sciences of the United States of America* 166:11319–11328.
- Turner, M. G., W. J. Calder, G. S. Cumming, T. P. Hughes, A. Jentsch, S. L. LaDeau, T. M. Lenton, B. N. Shuman, M. R. Turetsky, Z. Ratajczak, J. W. Williams, A. P. Williams, and S. R. Carpenter. 2020. Climate change, ecosystems and abrupt change: science priorities. *Philosophical Transactions of the Royal Society B: Biological Sciences* 375:20190105.

- Turner, M. G., E. A. H. Smithwick, K. L. Metzger, D. B. Tinker, and W. H. Romme. 2007. Inorganic nitrogen availability after severe stand-replacing fire in the Greater Yellowstone ecosystem. *Proceedings of the National Academy of Sciences* 104:4782–4789.
- USDA-NRCS, C. S. R. L. University of California, Davis, and D. of A. and N. R. University of California. 2019. SoilWeb: Online Soil Survey. University of California; Natural Resources Conservation Service.
- Vieira, D. C. S., C. Fernández, J. A. Vega, and J. J. Keizer. 2015. Does soil burn severity affect the post-fire runoff and interrill erosion response? A review based on meta-analysis of field rainfall simulation data. *Journal of Hydrology* 523:452–464.
- Vuke, S. M., K. W. Porter, J. D. Lonn, and D. A. Lopez. 2007. Geologic Map of Montana. Geologic Map, U.S. Geological Survey, Montana Bureau of Mines and Geology.
- Walker, X. J., J. L. Baltzer, S. G. Cumming, N. J. Day, C. Ebert, S. Goetz, J. F. Johnstone, S. Potter, B. M. Rogers, E. A. G. Schuur, M. R. Turetsky, and M. C. Mack. 2019. Increasing wildfires threaten historic carbon sink of boreal forest soils. *Nature* 572:520–523.
- Walker, X. J., B. M. Rogers, S. Veraverbeke, J. F. Johnstone, J. L. Baltzer, K. Barrett, L. Bourgeau-Chavez, N. J. Day, W. J. de Groot, C. M. Dieleman, S. Goetz, E. Hoy, L. K. Jenkins, E. S. Kane, M.-A. Parisien, S. Potter, E. a. G. Schuur, M. Turetsky, E. Whitman, and M. C. Mack. 2020. Fuel availability not fire weather controls boreal wildfire severity and carbon emissions. *Nature Climate Change* 10:1130–1136.
- Wan, S., D. Hui, and Y. Luo. 2001. Fire effects on nitrogen pools and dynamics in terrestrial ecosystems: a meta-analysis. *Ecological Applications* 11:1349–1365.

- Westerling, A. L. 2016. Increasing western US forest wildfire activity: sensitivity to changes in the timing of spring. *Philosophical transactions of the Royal Society of London. Series B, Biological sciences* 371:20150178.
- Whitlock, C., C. E. Briles, M. C. Fernandez, and J. Gage. 2011. Holocene vegetation, fire and climate history of the Sawtooth Range, central Idaho, USA. *Quaternary Research* 75:114–124.
- Whitlock, C., P. E. Higuera, D. B. McWethy, and C. E. Briles. 2010. Paleocological Perspectives on Fire Ecology: Revisiting the Fire-Regime Concept. *The Open Ecology Journal* 3:6–23.
- Whitlock, C., and C. Larsen. 2001. Charcoal as a fire proxy. Pages 75–97 in J. P. Smol Birks, HJB and Last, WM., editor. *Tracking environmental change using lake sediments. Volume 3: terrestrial, algal, and siliceous indicators.* Kluwer Academic Publishers.
- Whitlock, C., J. Marlon, C. Briles, A. Brunelle, C. Long, and P. Bartlein. 2008. Long-term relations among fire, fuel, and climate in the north-western US based on lake-sediment studies. *International Journal of Wildland Fire* 17:72–83.
- Wright, H. E., D. H. Mann, and P. H. Glaser. 1984. Piston corers for peat and lake sediments. *Ecology* 65:657–659.
- Yelenik, S., S. Perakis, and D. Hibbs. 2013. Regional constraints to biological nitrogen fixation in post-fire forest communities. *Ecology* 94:739–750.
- Young, A. M., P. E. Higuera, P. A. Duffy, and F. S. Hu. 2017. Climatic thresholds shape northern high-latitude fire regimes and imply vulnerability to future climate change. *Ecography* 40:606–617.

Zhou, Y., R. J. Taylor, and T. W. Boutton. 2021. Divergent Patterns and Spatial Heterogeneity of Soil Nutrients in a Complex and Dynamic Savanna Landscape. *Journal of Geophysical Research: Biogeosciences* 126:e2021JG006575.

Zhuang, Y., R. Fu, B. D. Santer, R. E. Dickinson, and A. Hall. 2021. Quantifying contributions of natural variability and anthropogenic forcings on increased fire weather risk over the western United States. *Proceedings of the National Academy of Sciences* 118:e2111875118.

CHAPTER 3

Tables

Table 1. Zones used to test changes in fire frequency, giving estimated mean fire return intervals (mFRI) and 95% confidence intervals for the mean, fitted Weibull b and c parameters, and log-likelihood p-values comparing FRI distributions among zones.

	<i>Time (cal yr BP)</i>	<i>mFRI</i>	<i>95% CI</i>	<i>n FRI</i>	<i>Wbl b, c</i>	<i>Comparison</i>	<i>P-val</i>
<i>Zone 1</i>	1950 – -68	223	175 - 280	8	244, 2.95	1 vs. 2	0.009
<i>Zone 2</i>	3450 – 1950	137	60 - 255	10	127, 0.93	2 vs. 3	0.255
<i>Zone 3</i>	4760 – 3450	117	80 - 152	10	124, 2.11	1 vs. 2-3	0.018
<i>Zone 2-3</i>	4760 – 1950	126	83 - 184	21	128, 1.18		

CHAPTER 3

Figures

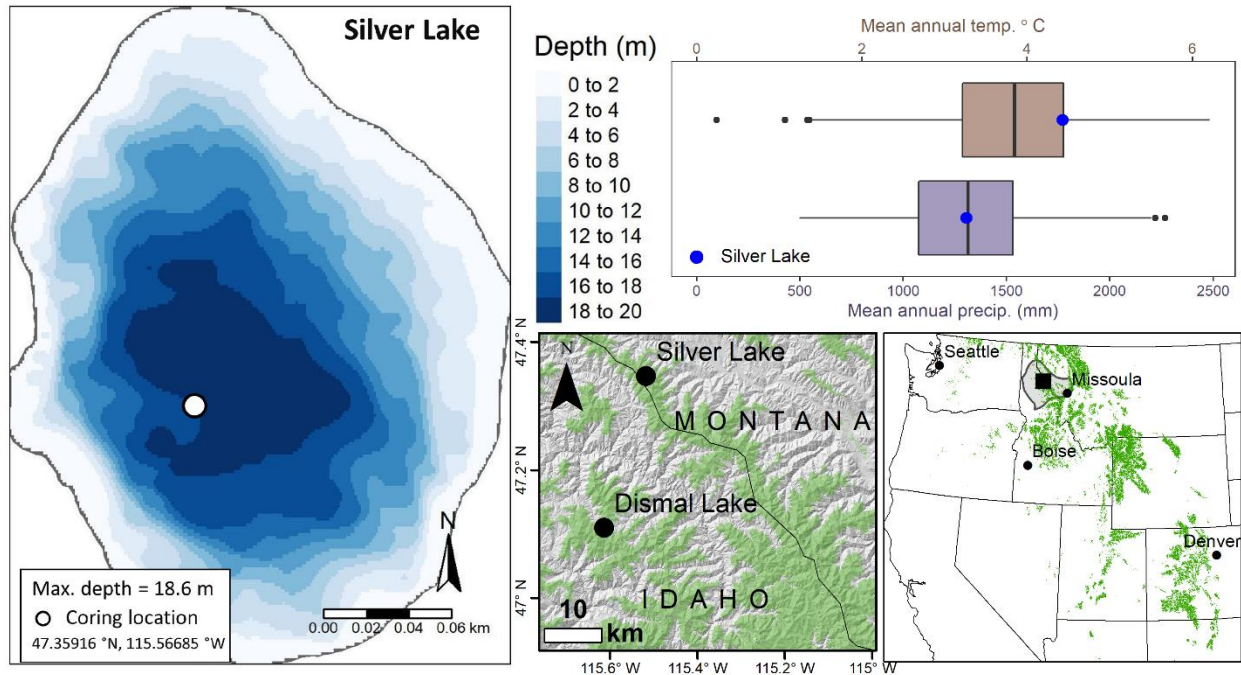


Figure 1. Site map showing the location of Silver Lake and its bathymetry. Boxplots display the regional climate (30-yr normal mean annual temperature and precipitation) of subalpine forests within the Bitterroot Mountains ecoregion (Bailey 1995), compared with the climate of Silver Lake (blue dot). On the map, the Bitterroot Mountains ecoregion is shown in grey, while the location of the study area is represented by a square. The green area delineates the potential extent of Rocky Mountain subalpine forest based on LandFire Environmental Site Potential (landfire.gov).

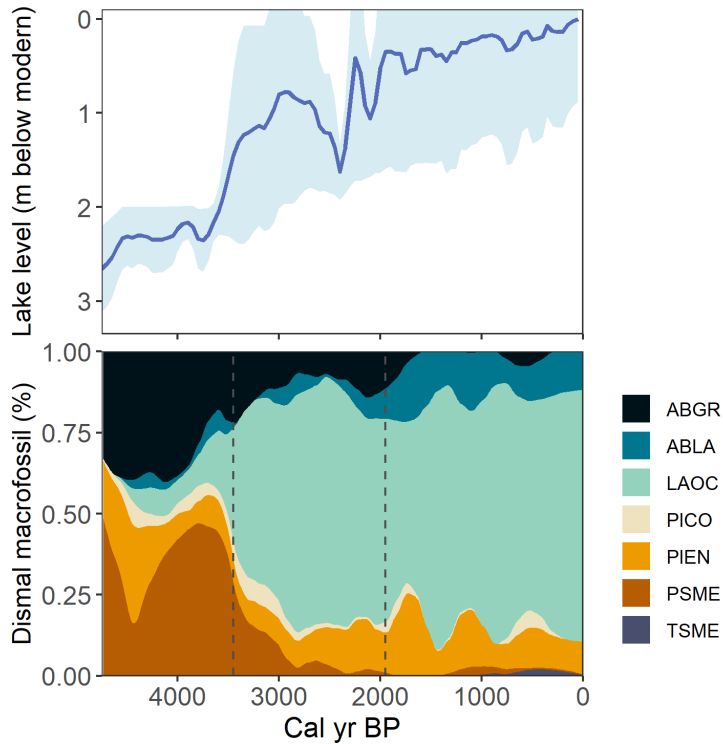


Figure 2. Local paleoclimate and regional vegetation history, which provide a foundation for the study design. *Top:* Reconstructed lake level anomalies in meters below modern, with 95% confidence bands (replotted from Parish et al. 2022). *Bottom:* Reconstructed vegetation history from Dismal Lake, ID, showing proportions of total macrofossil counts (needle equivalents) smoothed to 1,000-year trends, replotted using data from Herring et al. (2018). Vertical dashed lines delineate breaks between Dismal Lake vegetation zones (identified via cluster analysis using macrofossil counts) that correspond with lake-level changes at Silver Lake, which were used to test for shifts in fire frequency. Species codes: *A. grandis* (ABGR), *A. lasiocarpa* (ABLA), *L. occidentalis* (LAOC), *P. contorta* (PICO), *P. engelmannii* (PIEN), *P. menziesii* (PSME), *T. mertensiana* (TSME).

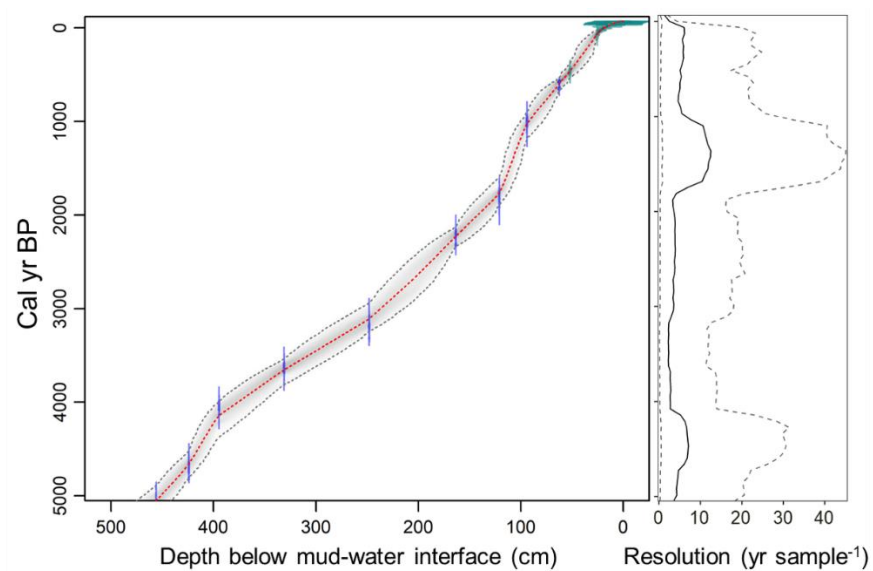


Figure 3. Age-depth relationship over the past 5,000 years for the Silver Lake record, modeled using *rbacon*. Purple shows the distribution of ages for calibrated radiocarbon dates, while green shows additional dates (tephra layers and Pb^{210} -inferred ages). The red curve is the median estimated age for each depth, and the shaded area shows the 95% confidence intervals. Average sample resolution with confidence intervals is shown on the right.

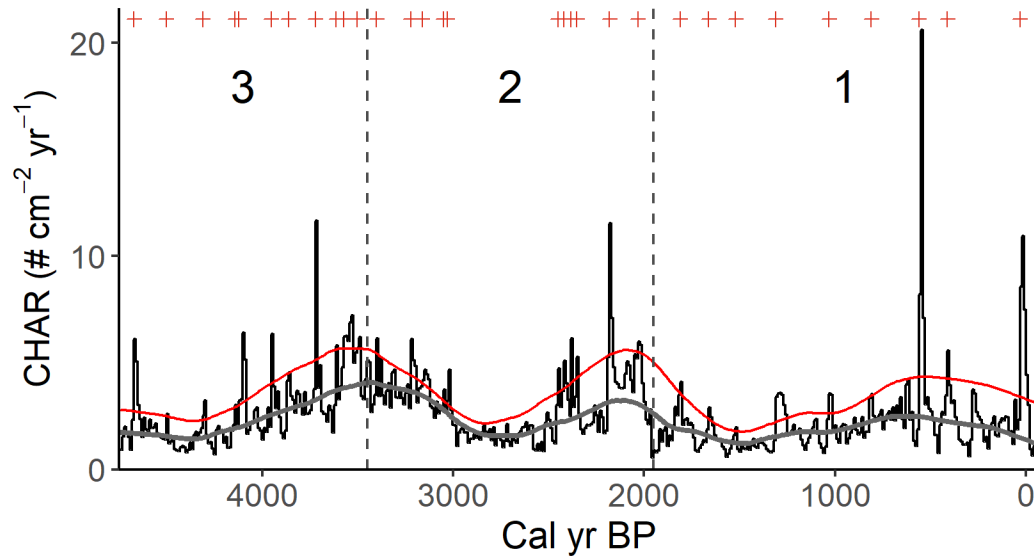


Figure 4. Fire history from Silver Lake over the past 4800 yr. The y-axis displays charcoal accumulation rate (CHAR), interpolated to a constant interval of 10 yr. Vertical dashed lines delineate breaks between zones used to test for fire-regime changes, identified *a priori* from local paleoclimate and a regional vegetation record (see Table 1). The grey and red curves display 500-yr smoothed estimates of background CHAR and the threshold used in peak detection analysis, respectively, with points above the graph corresponding to the timing of significant charcoal peaks.

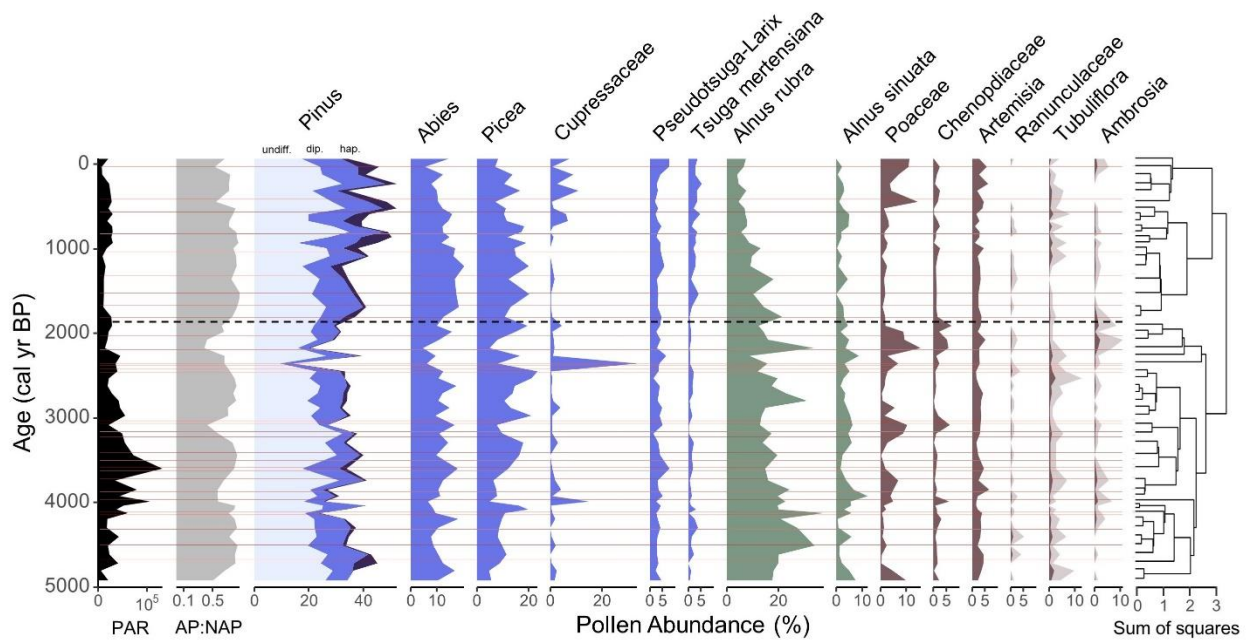


Figure 5. Pollen diagram, showing percent abundance of major pollen taxa, pollen accumulation rate (grains cm⁻² yr⁻¹), and the ratio of arboreal to non-arboreal pollen (AP:NAP). The results of hierarchical cluster analysis are displayed, with two significant pollen zones identified and delineated using a dashed line (break at c. 1900 BP). The shaded area on the rightmost three pollen panels shows a 5x magnification of pollen percentages, to highlight changes over time in taxa with low abundance. Colors denote major pollen types (blue = coniferous trees; green = broadleaf trees and shrubs; brown = herbaceous understory plants). Horizontal lines indicate the timing of inferred fire events.

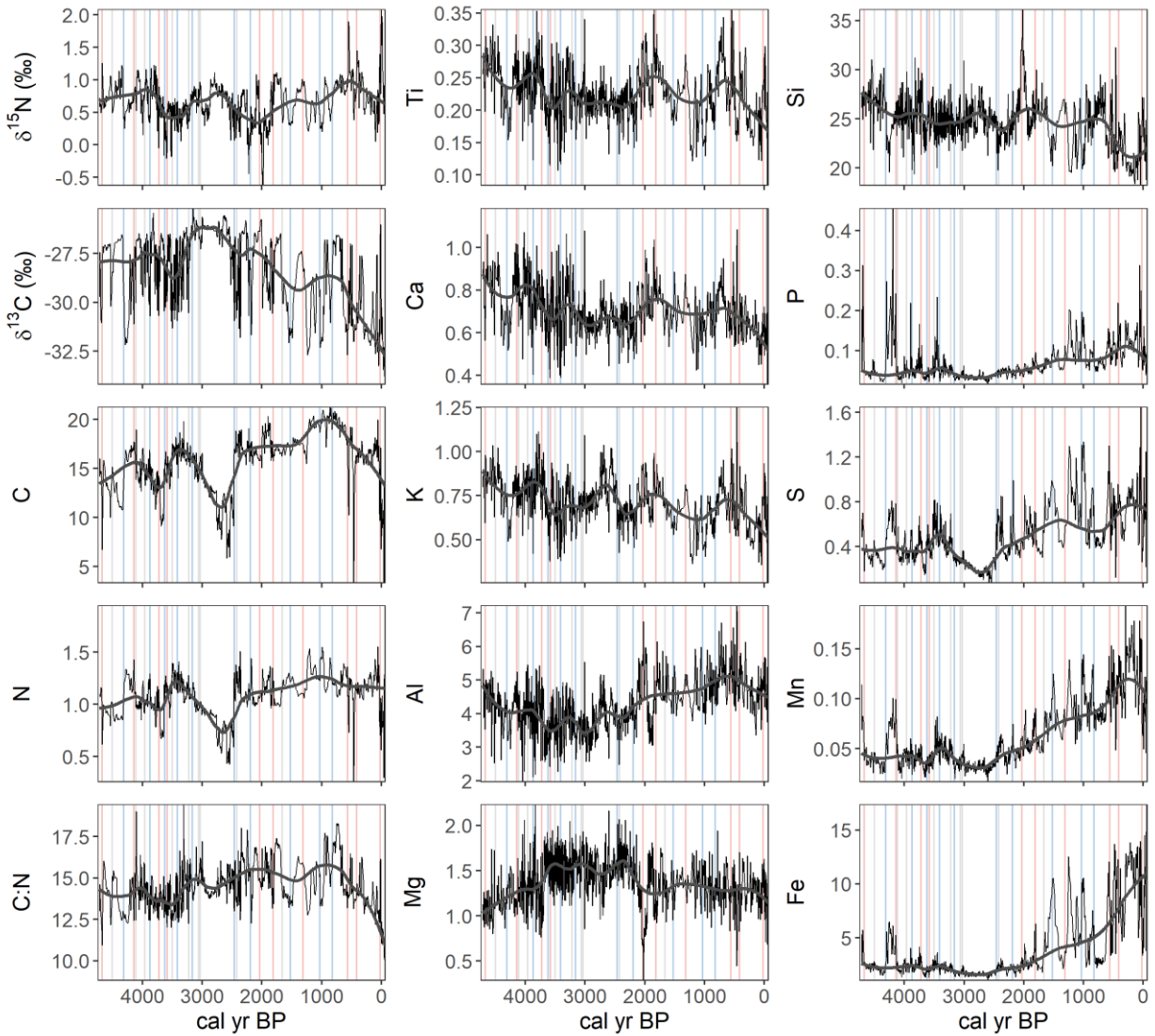


Figure 6. Timeseries of isotope values ($\delta^{13}\text{C}$ and $\delta^{15}\text{N}$, ‰), C:N values, and elemental concentrations (%), showing high-frequency variation and low-frequency (1000-year) trends using a loess smoother robust to outliers. Vertical lines denote the timing of inferred fire episodes, with red for Type 1 (erosion-associated) fires, blue for Type 2 (non-erosional) fires, and grey for non-responsive fires.

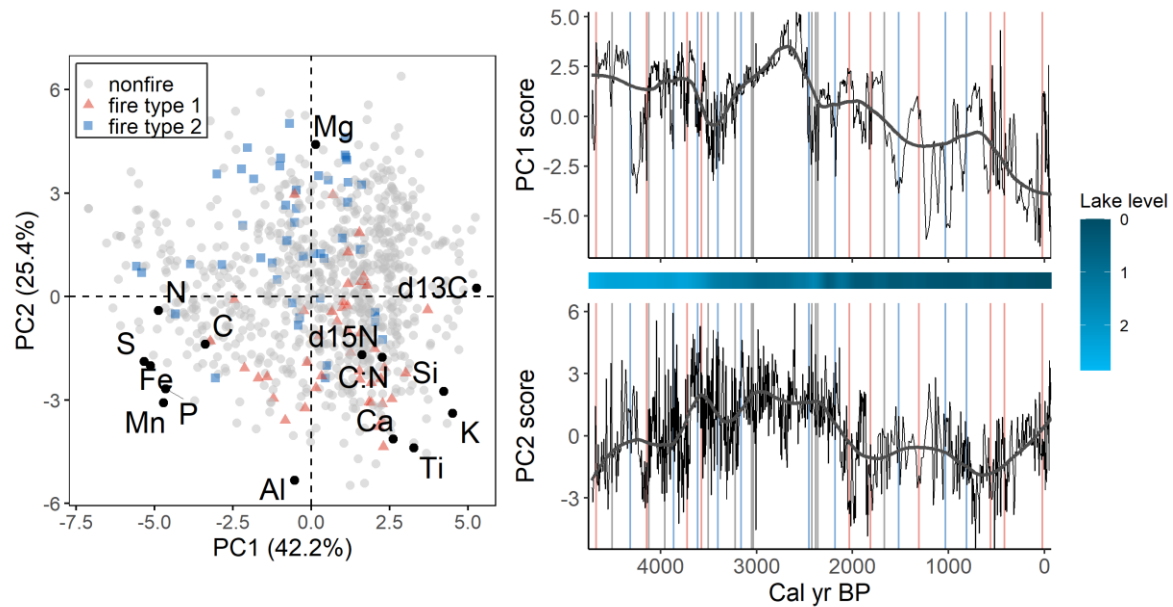


Figure 7. Principal components analysis summarizing variation in biogeochemical proxies. Left: biplot showing the location of each element and the axis scores of individual lake-sediment samples, which are displayed based on association with charcoal-inferred fire events. Samples during or within 20 years following a biogeochemically-responsive fire are shown in color and non-fire samples are shown in grey. Right: timeseries displaying short-term variation (raw data) and long-term trends (1000-year loess) in the first two principal components (PC1 and PC2), with vertical lines indicating the timing of inferred fire events. Red = Type 1 (erosion-associated) fires; blue = Type 2 (non-erosional) fires; grey = non-responsive fires. The shaded bar shows variation in effective moisture at the site, represented using reconstructed lake level anomalies in meters below modern (Parish et al. 2022).

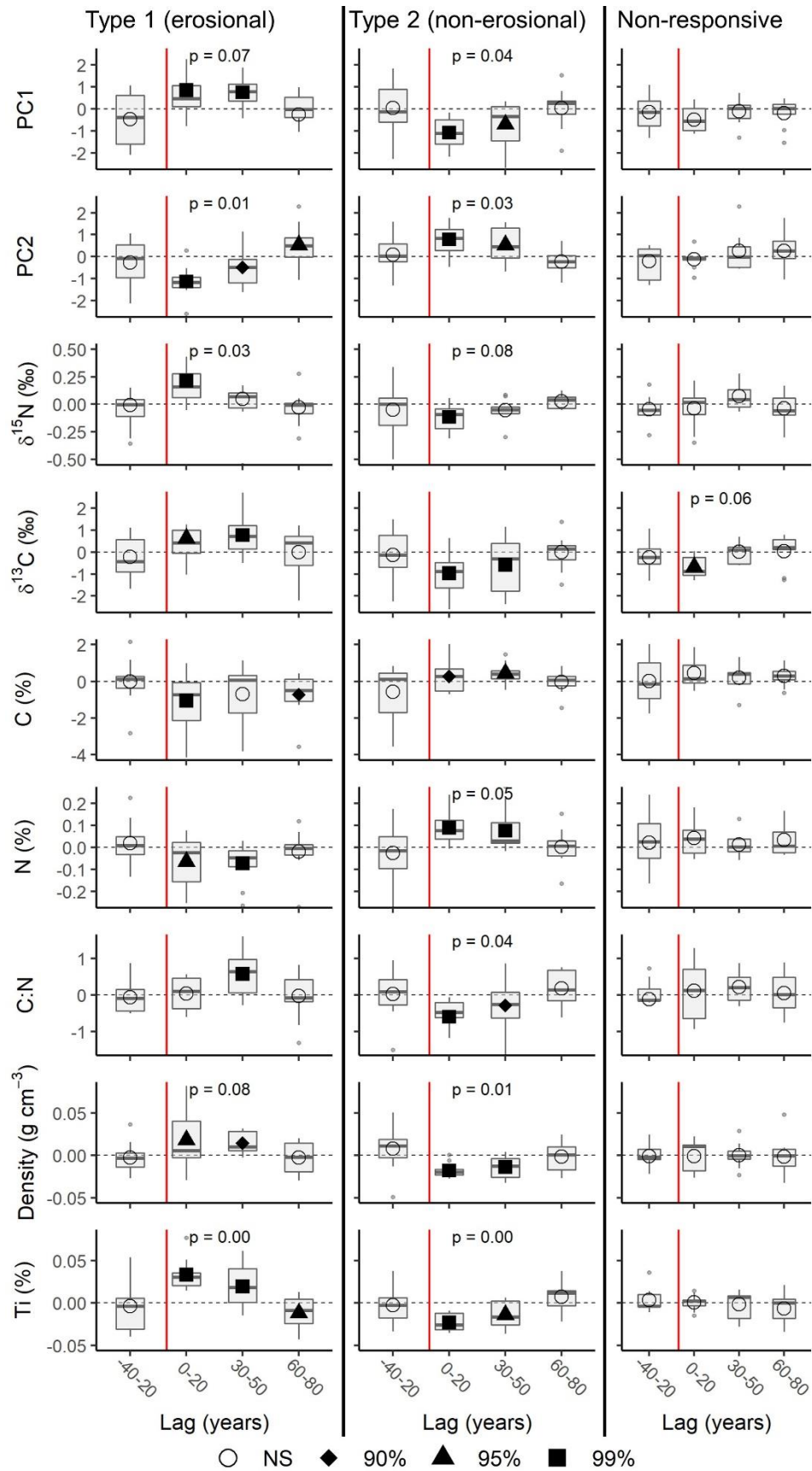


Figure 8. Post-fire responses of select geochemical proxies for Type 1 (erosion-associated, n = 10), Type 2 (non-erosional, n = 10), and non-responsive (n =9) fires, which were identified using hierarchical cluster analysis and screening for a post-fire Ti response. Geochemical proxies are plotted as anomalies around the locally-weighted mean. To show the range of post-fire responses following individual fires, boxplots display average values for a baseline of 20-40 years before each fire, and for 30-year time lags spanning 0-80 years following fire. P-values above plots give the result of Kruskal-Wallis tests, to evaluate the null hypothesis that the samples did not differ among lags before and after fire. To show the average response across fires, mean values for each time lag are displayed using points, with colors of post-fire mean values denoting significant differences from the pre-fire mean (90, 95, and 99% confidence based on 10,000 permutations).

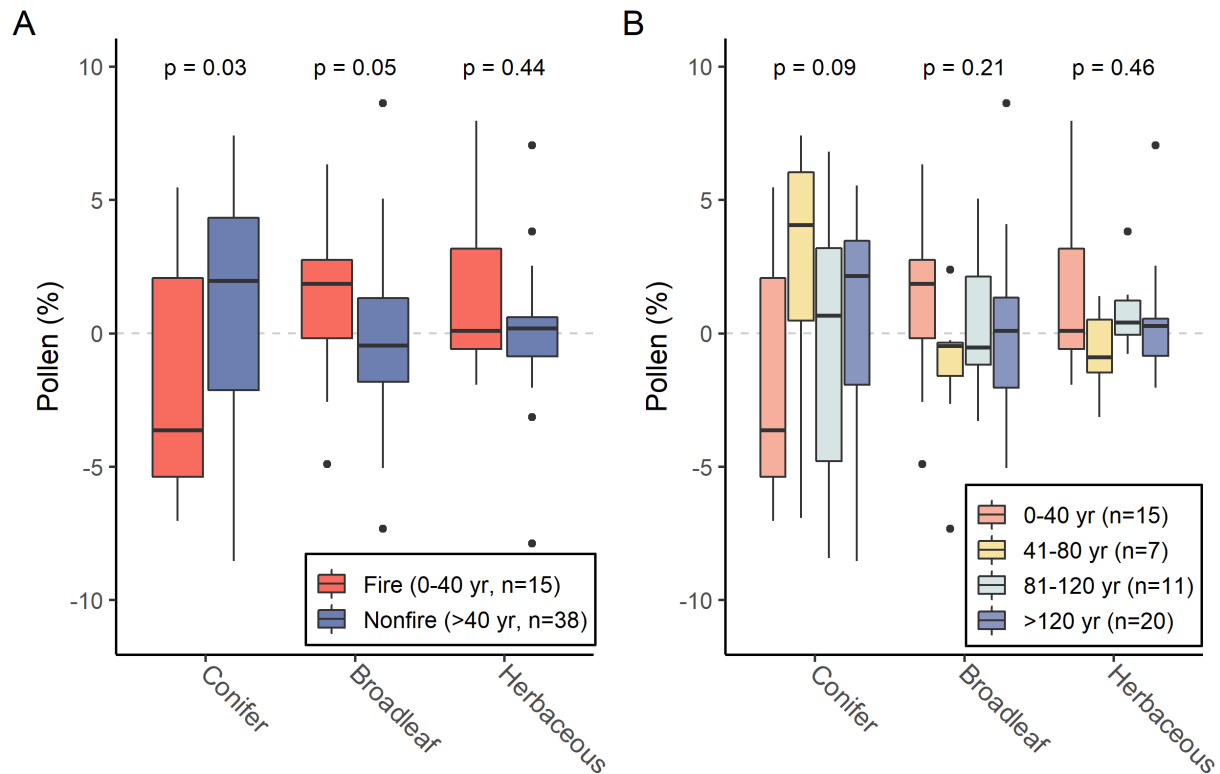


Figure 9. Boxplots comparing pollen abundance of major taxa among samples with differing time since fire, represented as anomalies from the locally weighted mean. **A:** Grouped by fire status, where fire-associated pollen samples are those that were within 10 yr of to 40 yr after a CHAR peak; **B:** same, with additional grouping by fire type (T1 = erosion-associated, T2 = non-erosional) inferred from geochemical proxy data; **C:** grouped by time window after fire. P-values report the results of nonparametric Wilcoxon rank-sum tests (A) or Kruskal-Wallis tests (B, C). Major pollen taxa are summarized by dominant groups as in Fig. 4: Conifer (*Abies*, *Pinus*, *Picea*, *Tsuga mertensiana*, *Pseudotsuga-Larix*, *Cupressaceae*); Broadleaf (*Alnus rubra*, *Alnus sinuata*); and Herbaceous (*Poaceae*, *Artemisia*, *Tubuliflorea*, *Ambrosia*, *Ranunculaceae*, *Chenopodiaceae*).

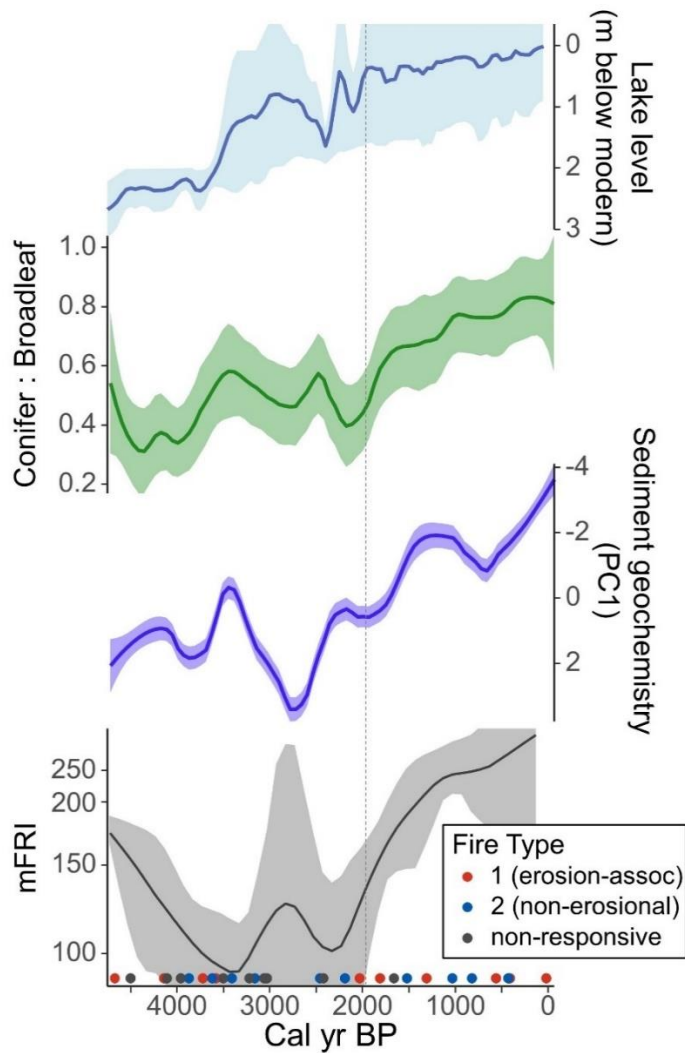


Figure 10. Fire, geochemical, vegetation, and paleoclimate history over the past 4800 yr at Silver Lake. Millennial-scale trends in fire frequency are represented using a smoothed estimate of the mean fire-return interval (mFRI). Points below the timeseries display the timing of charcoal peaks (red = Type 1, erosion-associated fires; blue = Type 2, non-erosional fires; grey = no biogeochemical response). Long-term variation in sediment geochemistry is summarized by *PC1* values, and the vegetation history is represented using the pollen ratio of major conifer to broadleaf pollen types, smoothed to show 1000-yr trends with 95% confidence bands. Positive values of *PC1* are associated with higher concentrations of minerogenic elements, and negative values are associated with redox-sensitive elements (see Fig. 7). Paleoclimate was inferred from

Chapter 3

a previously published lake-level reconstruction (Parish et al. 2022). The vertical dotted line delineates the zone break identified as a significant change in fire frequency.

CHAPTER 3
Supplementary Materials

Appendix A: Supplementary Methods

Chronology

Table A.1. Dates used to construct the Silver Lake chronology, including core depths and ages of 12 ²¹⁰Pb-inferred dates in the uppermost sediments, three tephra layers, and 15 radiocarbon dates of terrestrial macrofossils or charcoal. Estimated ¹⁴C ages are presented for radiocarbon dates, and calibrated ages are presented in cal. yr BP with error expressed using the 95% CI of ages for each date. Confidence intervals for ²¹⁰Pb dates and tephra layers are based on a normal distribution of age uncertainty.

Laboratory ID¹	Material	Depth (cm)	¹⁴C age (yr BP)²	1 σ	cal. age (yr BP)³	cal. 5%	cal. 95%
210Pb.90808	bulk sediment	0	–	–	-68	-70	-66
210Pb.90809	bulk sediment	1.5	–	–	-66	-68	-64
210Pb.90811	bulk sediment	3.5	–	–	-60	-62	-58
210Pb.90814	bulk sediment	6.5	–	–	-53	-55	-51
210Pb.90816	bulk sediment	8.5	–	–	-47	-49	-45
210Pb.90817	bulk sediment	9.5	–	–	-43	-45	-41
–	Mt. St. Helens tephra	10	–	–	-30	-32	-28
210Pb.90818	bulk sediment	10.5	–	–	-37	-39	-35
210Pb.90820	bulk sediment	12.5	–	–	-27	-31	-23
210Pb.90823	bulk sediment	15.5	–	–	-10	-14	-6
210Pb.90826	bulk sediment	18.5	–	–	8	0	16
210Pb.90829	bulk sediment	21.5	–	–	29	17	41
210Pb.90833	bulk sediment	25.5	–	–	89	39	139
–	Mt. St. Helens tephra	52	–	–	470	410	530
CAMS.179896	needle macrofossil	62.5	660	30	613	562	670
CAMS.185640	concentrated charcoal	94	1095	40	1004	937	1134
CAMS.179897	needle macrofossil	121	1915	40	1861	1741	1950
CAMS.179898	needle macrofossil	163.5	2245	35	2231	2158	2337
CAMS.179899	wood macrofossil	204	5920	30	6739	6673	6830
CAMS.179900	needle macrofossil	248	3005	35	3192	3078	3326
CAMS.179901	needle macrofossil	331	3390	35	3633	3564	3738
CAMS.179902	needle macrofossil	394.5	3700	30	4037	3939	4140
CAMS.179903	needle macrofossil	424	4165	30	4710	4587	4823
CAMS.179904	needle macrofossil	456	4495	40	5163	4988	5293

Chapter 3 Supplementary Material

<i>CAMS.185641</i>	cone macrofossil	500	4680	30	5395	5324	5566
<i>CAMS.179905</i>	needle macrofossil	519.5	5615	35	6386	6314	6472
<i>CAMS.179906</i>	wood macrofossil	571.5	4800	80	5519	5333	5692
<i>CAMS.179925</i>	wood macrofossil	632	5875	30	6698	6640	6769
<i>CAMS.179907</i>	needle macrofossil	674.5	6310	45	7237	7159	7366
–	Mt. Mazama tephra	692.5	–	–	7631	7579	7683

¹ ²¹⁰Pb: ids from Flett Research Ltd., Winnipeg, MB, Canada. CAMS: Center for Accelerator Mass Spectrometry, Lawrence Livermore National Laboratory, Livermore, CA.

² Conventional radiocarbon years before present (CE 1950).

³ Calendar years before present (CE 1950).

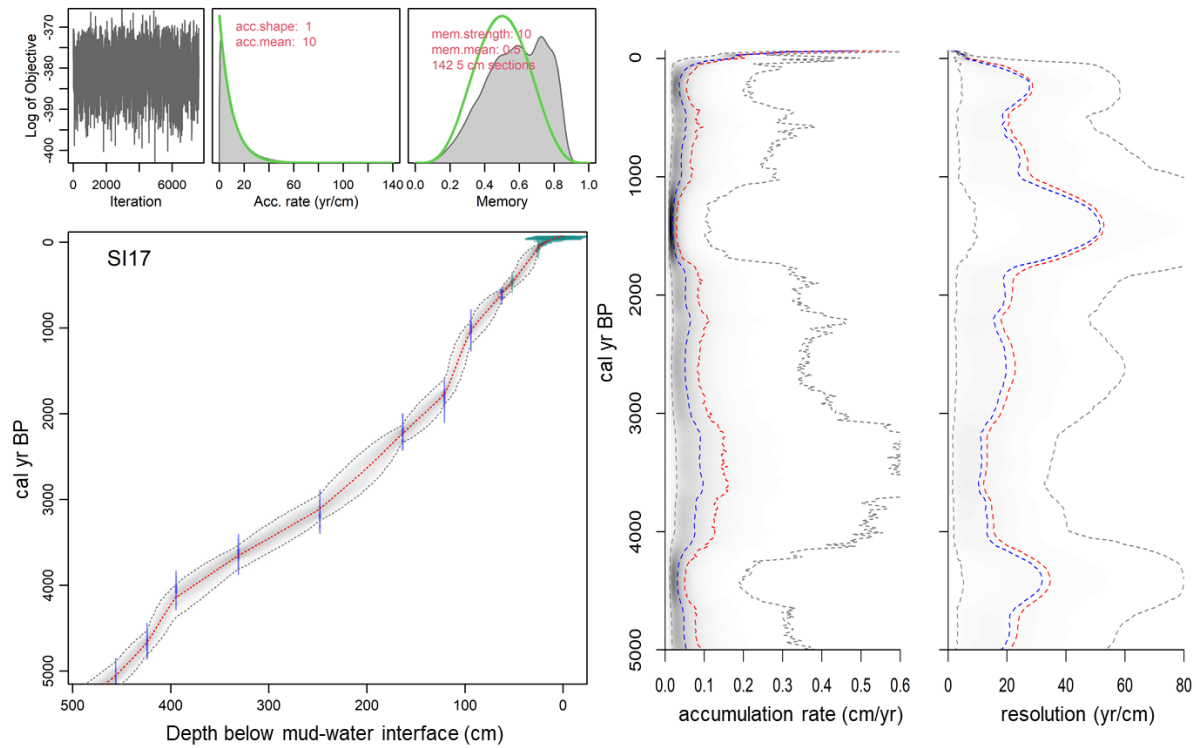


Fig. A.1. Age-depth relationship over the past 5,000 years for the Silver Lake core, modeled using *rbacon*. Purple ranges show the distribution of ages for calibrated radiocarbon dates, while green shows additional dates (tephra layers and Pb^{210} -inferred ages), and the curve shows median and 95% confidence intervals for the estimated age at each core depth. Prior and posterior distributions for parameters are shown at the top. The graphs on the right give the estimated accumulation rates and sample resolution, with red for medians, blue for means, and shaded areas for 95% confidence intervals. Ash samples from shallower cores used to reconstruct past lake-level changes at Silver Lake were previously analyzed (Parish et al. 2022), and we assumed that the same tephra were represented in our deep-water core.

Identification of time periods (“zones”) used to test changes in fire frequency

A high-resolution macrofossil record from Dismal Lake, Idaho (Herring et al. 2018) was analyzed in conjunction with the Silver Lake paleohydrology record to identify, *a priori*, climate/vegetation zones which were subsequently used to test changes in fire frequency at Silver Lake. The macrofossil record was used because it resolved sub-genus shifts in plant abundance not evident in pollen records, and helped verify the timing of local climatic changes. The timing of vegetation changes at Dismal Lake were identified via stratigraphically constrained cluster analysis using the *rioja* package in R. Prior to clustering, macrofossil counts, originally produced for contiguous 1-cm intervals, were aggregated to 5-cm intervals. Squared-chord distances were calculated and clustered using the *coniss* method. Zone breaks that corresponded to lake-level changes were used to test for fire-regime shifts at Silver Lake.

Vegetation shifts at Dismal Lake, Idaho, and other regional sites corroborate the timing of hydroclimate changes at Silver Lake. Evidence of increased effective moisture at Silver Lake during the late Holocene is consistent with declining summer insolation, and likely reflects greater frequency or intensity of atmospheric river events bringing Pacific moisture to western Montana (Parish et al. 2022). Increased dominance of *A. lasiocarpa* after c. 1850 BP and the establishment of *T. mertensiana* after c. 800 BP at Dismal Lake are consistent with a trend toward cooler regional climate conditions during the late Holocene (Herring et al. 2018). Additional regional sites show a decrease in *Alnus* pollen over the past several millennia, implying an increase in forest density (of conifer taxa) obscuring non-local pollen delivery of broadleaf species (Brunelle et al. 2005).

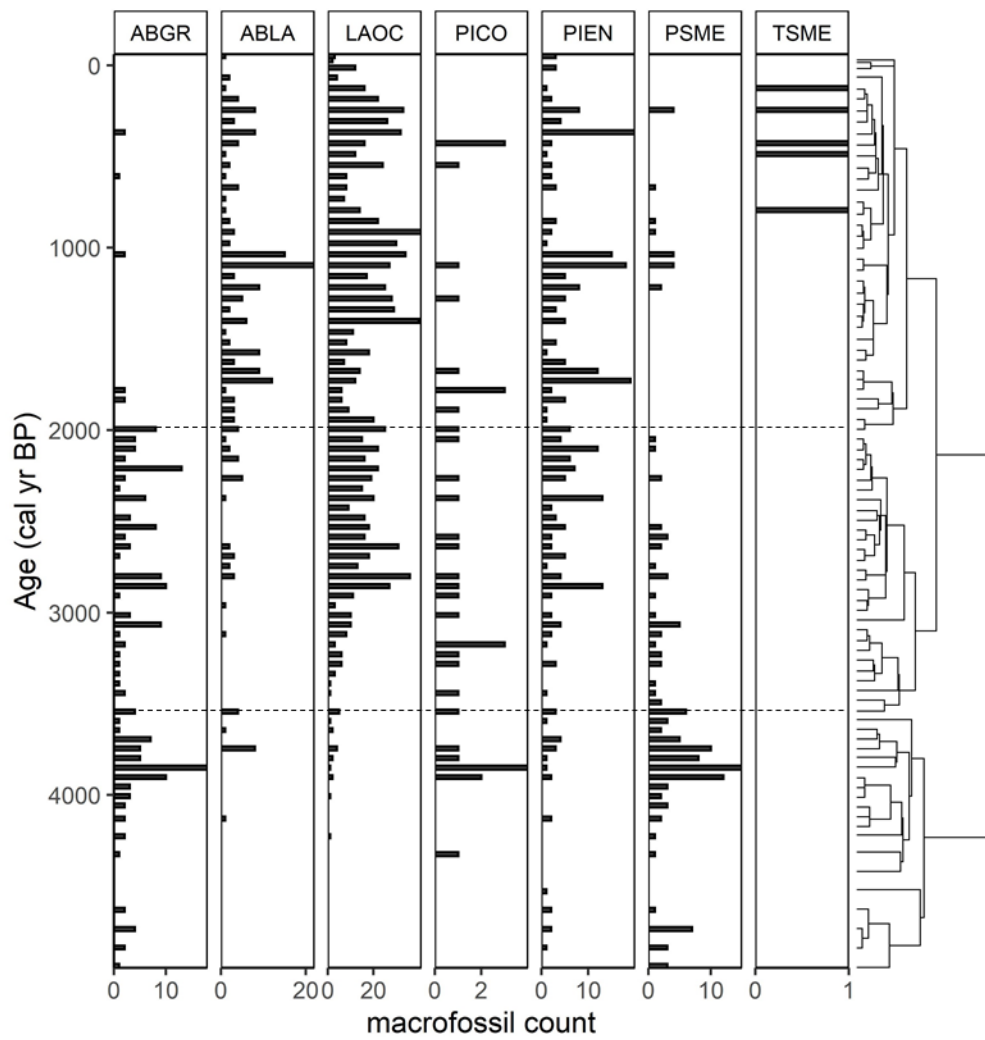


Fig. A.2. Macrofossil counts of needle-equivalents from Dismal Lake, ID (Herring et al. 2018) aggregated to 5-cm intervals, showing the results of stratigraphically constrained hierarchical cluster analysis.

Compositing and cluster analysis of post-fire biogeochemical responses

A composite timeseries of average biogeochemical responses to fire was generated using the biogeochemical proxy data. Prior to analysis, the timing of individual fire episodes, identified in CharAnalysis using a constant interpolation, was refined to correspond precisely to the sample with the maximum charcoal concentration contributing to each CHAR peak. Two CHAR peaks that occurred only 20 yr apart were excluded from analysis, yielding a total of 29 fire events included in the analysis. Elemental concentrations and biogeochemical data were interpolated to a constant 10-year timestep, and low-frequency trends were removed by subtracting a 500-year loess smoother robust to outliers, yielding anomalies representing high-frequency variation in each proxy. The resulting detrended biogeochemical data were averaged over 30-year lags before and after the charcoal peak, excluding the prior sample to account for a degree of uncertainty in precise fire timing. This resulted in average values for a baseline of 20-40 years before each fire, and for periods of 0-20, 30-50, and 60-80 years after each fire, providing a measure of the direction, magnitude, and duration of change following inferred fire events. To develop a composite record summarizing changes across all fires in the record, mean values were calculated for each time lag.

To assess the significance of post-fire changes in each element or isotope, confidence intervals were generated using a Monte Carlo randomization method akin to Superposed Epoch Analysis. Randomized time series of each response variable were created by shuffling blocks equal to a 125-year window (e.g., 50 years before and 75 years after a fire) to preserve temporal autocorrelation in the data. For each of 10,000 randomized time series of each response variable, with the reconstructed timing of fires remaining the same, the compositing analysis described above was repeated. We used quantiles of these random composites to construct 90%, 95%, and

99% confidence intervals for the mean response. In addition, to guard against composite mean values being driven by extreme values, we used a nonparametric Kruskal-Wallis test to test the null hypothesis that the set of pre- and post-fire values for all fires at each time lag did not differ.

We applied this compositing analysis separately to each of the two populations of fire events identified by the cluster analysis. Additionally, we screened each individual fire event based on the post-fire pattern in T_i , an indicator for clastic inputs (Kylander et al. 2011, Leys et al. 2016), based on the initial observation that an increase or decrease in T_i was a dominant pattern following each set of fires identified by the cluster analysis. This resulted in a third category of fire events with no significant post-fire biogeochemical response, which we then analyzed separately.

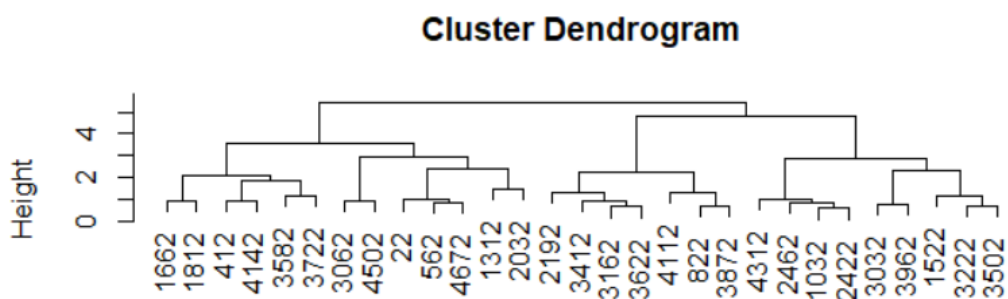


Fig. A.3. Cluster dendrogram of inferred fire events, based on average geochemical responses 0-30 and 40-70 years after fire. Two primary clusters were optimal, and thus are used to identify Type 1 and Type 2 patterns of fire responses. Two charcoal peaks that were 20 years apart were excluded from analysis; a total of 29 inferred fire events were used.

Appendix B: Supplementary Results

Biogeochemical proxies and interpretation

Average sedimentary C:N (median 14.4, IQR 13.3-15.3) was below that of soil and foliage from the surrounding watershed (median 18.8 and 43.9, respectively; Fig. B.1), but higher than expected values of algal organic matter (c. 4-10; Meyers and Teranes 2001), suggesting that the sediment composition reflects both terrestrial and aquatic organic matter inputs. High sediment accumulation rates and a positive correlation between sedimentary C and N ($r = 0.83$; $p < 0.001$, $df = 859$) suggest that organic matter was fairly well-preserved, perhaps due to rapid burial of sediment (Meyers and Teranes 2001). A lack of correlation between sedimentary $\delta^{15}\text{N}$ and C:N ($r = 0.08$), indicates that preferential degradation of labile, N-enriched material in oxic surface sediments was probably not a dominant process, providing further support that the sediment composition largely reflects primary biogeochemical signals (Lehmann et al. 2002).

Sedimentary $\delta^{15}\text{N}$ values integrate whole-ecosystem N availability, with higher values broadly interpreted as being associated with a more “open” N cycle (i.e., more fractionating losses from the catchment), and lower values being associated with a more closed cycle (Robinson 2001). At Silver Lake, sedimentary $\delta^{15}\text{N}$ values varied over a narrow range of values, and likely reflect the influence of terrestrial dissolved organic N (DON) inputs. The Silver Lake sediments were depleted in ^{15}N relative to mineral soil from the surrounding watershed (median $\delta^{15}\text{N}$ 4.49‰) and enriched relative to tree and shrub foliage (median $\delta^{15}\text{N}$ -2.75‰; Fig. B.1). Average sediment $\delta^{15}\text{N}$ values from Silver Lake (mean 0.65‰) were broadly similar to a set of subalpine lakes in the Canadian Rockies (mean 0.97‰; Bunting et al. 2010), and a small subalpine lake in Colorado (mean 0.96‰; Dunnette et al. 2014). The authors interpreted the average $\delta^{15}\text{N}$ at that

site as a result of substantial inputs of DON from the forest floor (which tends to be isotopically depleted) driving within-lake N cycling (Dunnette et al. 2014). Alternatively, relatively low average $\delta^{15}\text{N}$ values close to atmospheric N_2 (0‰) could imply a role of N-fixing cyanobacteria in lacustrine production at Silver Lake (e.g., Talbot and Lærdal 2000); indeed, *Pediastrum* (green algae) cells were identified in some pollen slides from the Silver Lake sediments (Jankovská and Komárek 2000).

While $\delta^{13}\text{C}$ often correlates with lake productivity (Brenner et al. 1999), its interpretation is not unambiguous at this site. Approximately a quarter of lake-sediment samples from Silver Lake had $\delta^{13}\text{C}$ values less than -30‰, which was below the range of values from terrestrial soil and foliar samples (Fig. B.1). The lowest $\delta^{13}\text{C}$ measurements were below the range of expected values for C3 plants or lacustrine algae (~ 25-30‰; Meyers and Teranes 2001), and sediment $\delta^{13}\text{C}$ was moderately positively correlated with C:N throughout the record ($r = 0.64$; $df=859$, $p<0.001$), which is inconsistent with $\delta^{13}\text{C}$ enrichment of algal biomass during periods of high lake productivity and associated depletion of dissolved inorganic carbon (DIC) pools. Rather, low sediment $\delta^{13}\text{C}$ likely results from fixation of isotopically depleted DIC by lacustrine algae, which can derive from soil or within-lake respiration, producing isotopically depleted algal biomass (Rau 1978). Thus, variation in $\delta^{13}\text{C}$ values at Silver Lake may be influenced by sources of DIC or rates of within-lake respiration. Alternatively, in some lakes, algae may be more depleted in ^{13}C than terrestrial organic matter (Hu et al. 2001), such that lower sediment $\delta^{13}\text{C}$ and C:N values could indicate greater relative contributions of aquatic biomass. Differential contributions of pelagic, profundal, and benthic algae with varying $\delta^{13}\text{C}$ signatures could also account for some of the variation in sediment $\delta^{13}\text{C}$ values throughout the record (Vander Zanden et al. 2006).

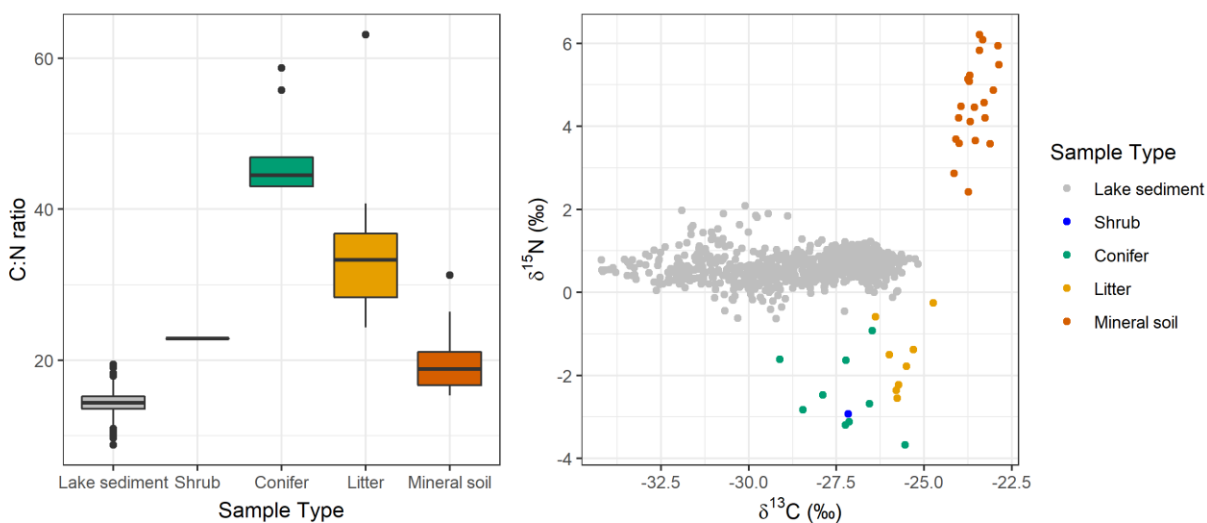


Fig. B.1. C:N ratios and stable isotope measurements of lake-sediment samples spanning the past 4,800 years at Silver Lake, and modern terrestrial soil and foliar samples from the surrounding watershed. Modern terrestrial samples include shrub foliage (*Menzisia ferruginea*, n=1), conifer foliage (*A. lasiocarpa*, n= 4; *P. engelmannii*, n= 4; *T. mertensiana*, n= 1), litter (n=8), and mineral soil (0-10 cm depth, n = 8; 10-20 cm depth, n = 8; 20-30 cm depth, n=5). Modern samples and $\delta^{13}\text{C}$ measurements from recent lake-sediment samples have been adjusted for the Suess effect (Dombrosky 2020).

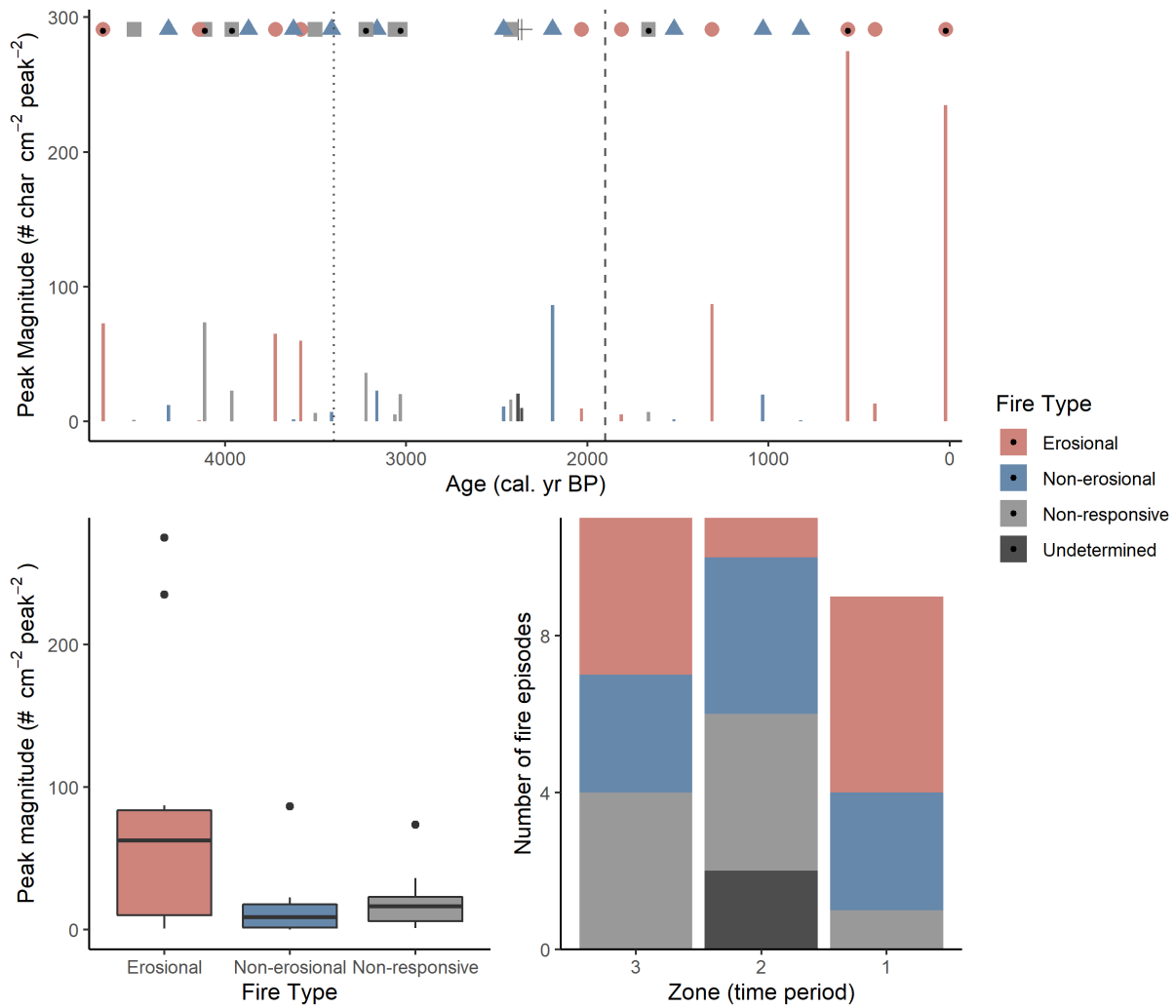


Fig. B.2. Peak magnitude (number of charcoal pieces cm⁻² peak⁻¹) and fire type over time. Black dots indicate the timing of charcoal peaks that corresponded with peaks in magnetic susceptibility (<20 yr apart). Peak magnitude is compared between the three fire response types using boxplots; there is no evidence that medians differed between the groups ($p = 0.23$). Bar plots show the distribution of fire episodes of each response type in each zone.

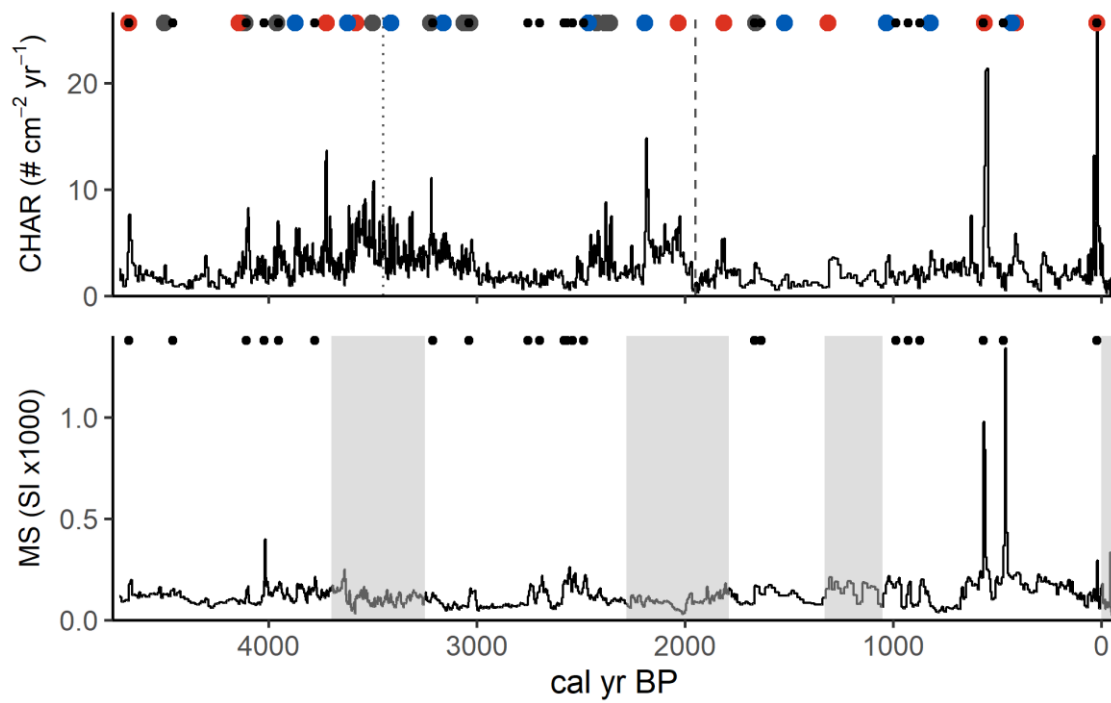


Fig. B.3. Timeseries of charcoal accumulation and magnetic susceptibility. The timing of charcoal peaks are displayed using red (Type 1, erosion-associated fires), blue (Type 2, non-erosional fires), and grey (non-responsive or undetermined), while MS peaks are displayed using black dots. Grey bands show areas of the MS timeseries with signal to noise index less than 3, which were excluded from peak detection analysis (Kelly et al. 2011).

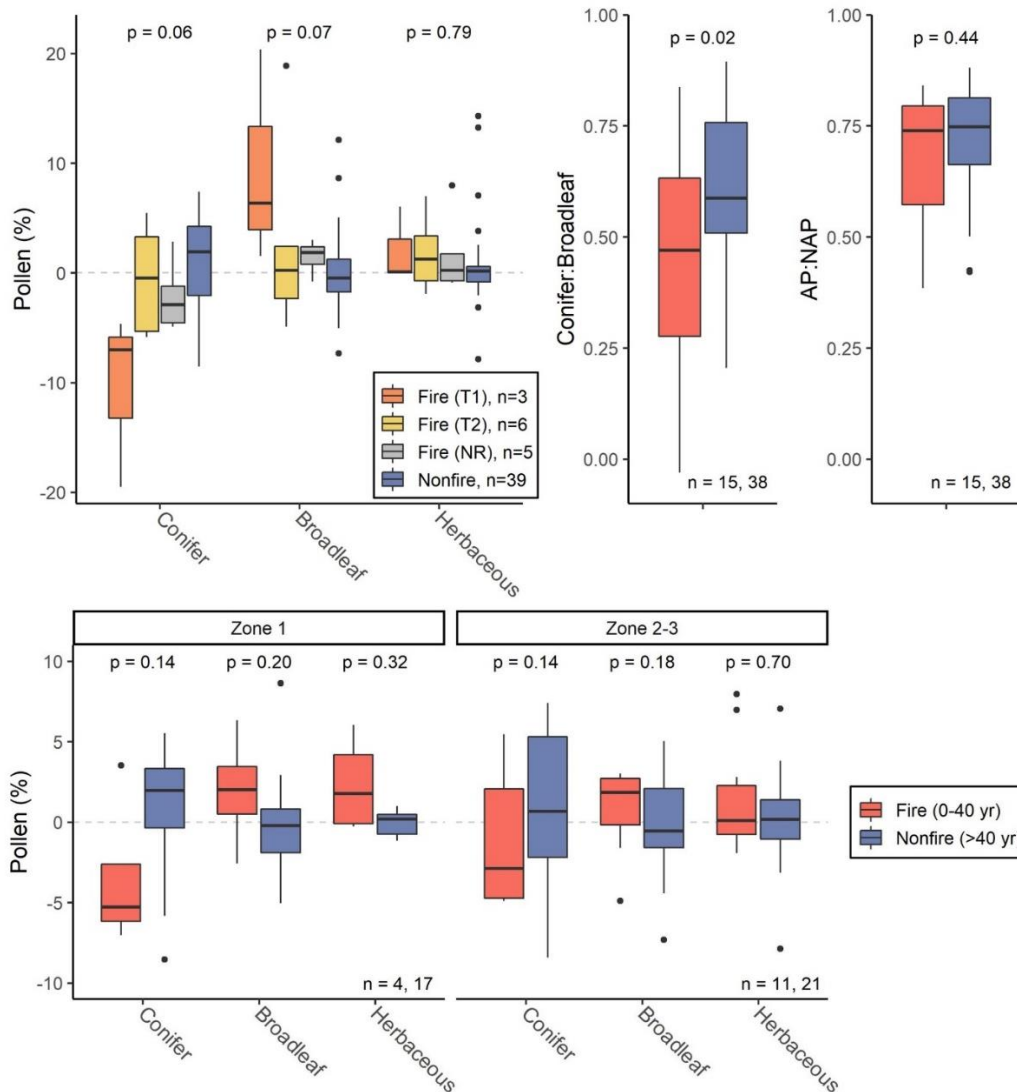


Fig. B.4. Boxplots comparing pollen ratios and pollen abundances of major taxa among samples grouped by association with fire (“Fire” = within 10 yr of a fire event to 40 yr after; “Nonfire” = >40 yr after fire). Pollen abundances are expressed as anomalies from the locally-weighted mean. Top left: fire-associated samples are further grouped based on the average post-fire biogeochemical response: T1 = erosion-associated; T2 = non-erosional; NR = non-responsive. Bottom: fire-associated and non-fire samples are separated by fire-regime zone. P-values give the results of nonparametric tests, either Kruskal-Wallis for comparisons with more than two groups, or Wilcoxon rank-sum for comparisons with two groups. Sample sizes (n) are the number of pollen samples represented in each of the fire and non-fire categories.

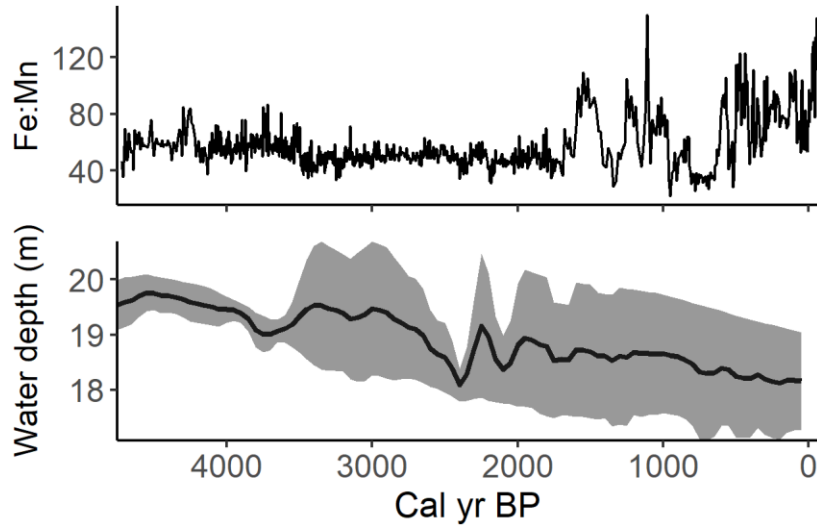


Fig. B.5. Ratio of Fe to Mn in lake sediments from Silver Lake, and lake-level reconstruction from Parish et al. (2022) corrected for sediment accumulation rate at the coring location (in the deepest part of the lake) to display long-term changes in water depth, with bands showing 95% confidence intervals.

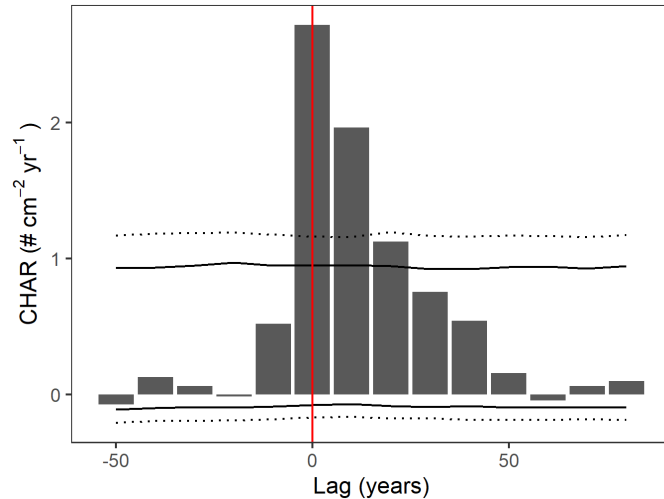


Fig. B.6. Superposed epoch analysis showing the average charcoal accumulation rate (CHAR) surrounding charcoal peaks in the sedimentary record, indicating that elevated charcoal influx typically spans one to several samples after the inferred event timing. Solid and dotted lines display 95% and 99% confidence intervals for significant excursions from baseline CHAR values based on 10,000 permutations. Year 0 is the inferred fire year.

Literature Cited

- Brenner, M., T. J. Whitmore, J. H. Curtis, D. A. Hodell, and C. L. Schelske. 1999. Stable isotope ($\delta^{13}\text{C}$ and $\delta^{15}\text{N}$) signatures of sedimented organic matter as indicators of historic lake trophic state. *Journal of Paleolimnology* 22:205–221.
- Brunelle, A., C. Whitlock, P. Bartlein, and K. Kipfmüller. 2005. Holocene fire and vegetation along environmental gradients in the Northern Rocky Mountains. *Quaternary Science Reviews* 24:2281–2300.
- Bunting, L., P. R. Leavitt, R. P. Weidman, and R. D. Vinebrooke. 2010. Regulation of the nitrogen biogeochemistry of mountain lakes by subsidies of terrestrial dissolved organic

- matter and the implications for climate studies. *Limnology and Oceanography* 55:333–345.
- Dombrosky, J. 2020. A ~1000-year ^{13}C Suess correction model for the study of past ecosystems. *The Holocene* 30:474–478.
- Dunnette, P. V., P. E. Higuera, K. K. McLauchlan, K. M. Derr, C. E. Briles, and M. H. Keefe. 2014. Biogeochemical impacts of wildfires over four millennia in a Rocky Mountain subalpine watershed. *New Phytologist* 203:900–912.
- Herring, E. M., D. G. Gavin, S. Z. Dobrowski, M. Fernandez, and F. S. Hu. 2018. Ecological history of a long-lived conifer in a disjunct population. *Journal of Ecology* 106:319–332.
- Hu, F. S., B. P. Finney, and L. B. Brubaker. 2001. Effects of Holocene *Alnus* Expansion on Aquatic Productivity, Nitrogen Cycling, and Soil Development in Southwestern Alaska. *Ecosystems* 4:358–368.
- Jankovská, V., and J. Komárek. 2000. Indicative Value of *Pediastrum* and Other Coccal Green Algae in Palaeoecology. *Folia Geobotanica* 35:59–82.
- Kelly, R. F., P. E. Higuera, C. M. Barrett, and F. S. Hu. 2011. A signal-to-noise index to quantify the potential for peak detection in sediment–charcoal records. *Quaternary Research* 75:11–17.
- Kylander, M. E., L. Ampel, B. Wohlfarth, and D. Veres. 2011. High-resolution X-ray fluorescence core scanning analysis of Les Echets (France) sedimentary sequence: new insights from chemical proxies. *Journal of Quaternary Science* 26:109–117.
- Lehmann, M. F., S. M. Bernasconi, A. Barbieri, and J. A. McKenzie. 2002. Preservation of organic matter and alteration of its carbon and nitrogen isotope composition during

- simulated and in situ early sedimentary diagenesis. *Geochimica et Cosmochimica Acta* 66:3573–3584.
- Leys, B. A., P. E. Higuera, K. K. McLauchlan, and P. V. Dunnette. 2016. Wildfires and geochemical change in a subalpine forest over the past six millennia. *Environmental Research Letters* 11:125003.
- Meyers, P. A., and J. L. Teranes. 2001. Sediment Organic Matter. Pages 239–269 *Tracking Environmental Change Using Lake Sediments: Physical and Geochemical Methods*. First edition. Kulwer Academic Publishers, Dordrecht, Netherlands.
- Parish, M. C., K. D. Wolf, P. E. Higuera, and B. N. Shuman. 2022. Holocene water levels of Silver Lake, Montana, and the hydroclimate history of the Inland Northwest. *Quaternary Research*.
- Rau, G. 1978. Carbon-13 Depletion in a Subalpine Lake: Carbon Flow Implications. *Science* 201:901–902.
- Robinson, D. 2001. $\delta^{15}\text{N}$ as an integrator of the nitrogen cycle. *Trends in Ecology & Evolution* 16:153–162.
- Talbot, M. R., and T. Lærdal. 2000. The Late Pleistocene - Holocene palaeolimnology of Lake Victoria, East Africa, based upon elemental and isotopic analyses of sedimentary organic matter. *Journal of Paleolimnology* 23:141–164.
- Vander Zanden, M. J., S. Chandra, S.-K. Park, Y. Vadeboncoeur, and C. R. Goldman. 2006. Efficiencies of benthic and pelagic trophic pathways in a subalpine lake. *Canadian Journal of Fisheries and Aquatic Sciences* 63:2608–2620.

CHAPTER 4: Widespread burning across northern Rocky Mountain subalpine forests over the past 2500 yr: precedence and implications for contemporary fire-regime change

*This chapter is prepared as a manuscript to be submitted for publication with the following authors: Kyra D. Clark-Wolf¹, Philip E. Higuera¹, Bryan N. Shuman², Kendra K. McLauchlan³

¹ Department of Ecosystem and Conservation Sciences, University of Montana, Missoula, MT

² Department of Geology and Geophysics, University of Wyoming, Laramie, WY

³ Division of Environmental Biology, National Science Foundation, Alexandria, VA

Abstract

Increasing area burned across western North America raises questions about the precedence and magnitude of contemporary changes in fire activity, relative to the historical range of variability (HRV) that ecosystems experienced over recent centuries and millennia. Paleoecological records of past fire occurrence provide critical context for contemporary changes, particularly in ecosystems characterized by infrequent, high-severity fire regimes. Here we present a network of 12 fire-history records derived from macroscopic charcoal preserved in sediments of small (x-x ha) subalpine lakes within a c. 10,000 km² landscape in the U.S. northern Rocky Mountains (Northern Rockies). We used this network of records to characterize landscape-scale burning over the past 2500 yr and evaluate the precedence for widespread regional burning in the early 20th and 21st centuries. We compare the Northern Rockies fire history to a previously published network of paleofire records in the Southern Rockies. In Northern Rockies subalpine forests, widespread fire activity was strongly linked to seasonal climate conditions, in both contemporary, historical, and paleo records. The average estimated fire rotation period (FRP) over the past 2500 years was 164 yr, with the central 75% of FRP estimates ranging from 127 to 225 yr, providing a robust estimate of the HRV. The contemporary FRP from 1900-2021 CE was 215 yr, revealing that extensive regional fires in 1910 CE and in recent decades were not unprecedented in the context of recent millennia. Results from the Northern Rockies contrast

with the Southern Rockies, which burned with less frequency on average over the past 2500 yr, and where 21st-century burning has exceeded the HRV. Our results support expectations that fire activity in the Northern Rockies will continue to increase with climatic warming, and would surpass historical burning if more than one exceptional fire year akin to 1910 occurs within the next several decades. The ecological consequences of climatic warming in subalpine forests will depend, in large part, on the magnitude of fire-regime changes relative to the past.

Introduction

Fire activity is increasing across western North America, in part due to the impacts of anthropogenic climate change (Westerling 2016, Abatzoglou and Williams 2016, Kirchmeier-Young et al. 2017, Zhuang et al. 2021), and is expected to continue to increase under future climate (de Groot et al. 2013, Gao et al. 2021, Abatzoglou et al. 2021). Warmer and drier conditions increase fuel aridity, which makes fuels more susceptible to ignition and spread and enables extensive burning, particularly in forest ecosystems (Westerling 2016, Abatzoglou and Williams 2016, Holden et al. 2018, Juang et al. 2022). Increased fire activity in high-elevation forests across the western US has been especially pronounced, as widespread burning in these forests is typically limited by high fuel moisture and short growing seasons (Alizadeh et al. 2021). Higher fire activity in turn has wide-ranging impacts on species turnover, water resources, and human communities (Coop et al. 2020, Iglesias et al. 2022, Williams et al. 2022).

It is increasingly important to understand how changes in fire regimes are unfolding relative to the past, to assess potential implications for ecosystems and society. Efforts to evaluate the magnitude of climate-change impacts on fire regimes relative to the historical range of variability (HRV), representing the conditions ecosystems have developed with over centuries to millennia (Landres et al. 1999), are complicated by direct human impacts on fire regimes. For

example, despite clear increases in area burned across the western U.S. in recent decades, there is also evidence of a “fire deficit” over the past one to two centuries as a result of reduced Indigenous burning, land use intensification, and policies emphasizing fire suppression (Marlon et al. 2012). Additionally, in ecosystems with infrequent, high-severity fire regimes, observational and dendrochronological fire-history records only capture one to several fires at any given site.

Paleoecological archives of past fire occurrence, such as charcoal particles preserved in lake sediments, provide opportunities to quantify past variability and tease apart the influences of climate, vegetation, and human activities on fire regimes (Whitlock et al. 2010). Due to the stochastic timing of fire occurrence, individual lake-sediment records (representing a small area on the landscape) are unlikely to capture the effects of climatic variation on timescales of decades to centuries, akin to that of contemporary and future warming (Gavin et al. 2006, 2007). Combining multiple records together to form a network of site-level fire histories is therefore necessary to detect significant changes burning at landscape or regional scales (Kelly et al. 2013, Calder et al. 2015).

Densely sampled networks of lake-sediment records in North American boreal (Kelly et al. 2013) and subalpine (Calder et al. 2015) forest ecosystems highlight the sensitivity of fire activity to past centennial-scale climatic variation. Such networks have revealed increased landscape burning during a period of relative warmth c. 1000 years ago (the Medieval Climate Anomaly, MCA), and they demonstrate that fire activity in recent decades has already exceeded the HRV of recent millennia in some regions (Kelly et al. 2013, Higuera et al. 2021). These studies highlight the scale and pace of emerging shifts in fire regimes accompanying

contemporary climatic warming, and they underscore uncertainties about ecosystem responses to long-unprecedented conditions (Higuera et al. 2021).

The U.S. northern Rocky Mountains (hereafter Northern Rockies) has strongly contributed to trends in area burned in the western U.S. in recent decades (Westerling et al. 2006, Westerling 2016), and the region has experienced several extreme fire seasons and fire disasters over the past century. Fire activity in the Northern Rockies is elevated in years with early spring snowmelt and above-average spring and summer warmth and aridity (Heyerdahl et al. 2008, Morgan et al. 2008, Higuera et al. 2015, Westerling 2016), as exemplified by extensive burning across c. 12,000 km² in Idaho and Montana in 1910. The 1910 fires, called “The Big Burn”, were enabled by warm, dry summer climate conditions (Morgan et al. 2008, Higuera et al. 2015), ignited by lightning, railroad sparks, and other human activities, and driven by a high wind event in August (Egan 2009). Widespread and devastating fires in Idaho and Montana in 1910 set the stage for 20th-century U.S. policies emphasizing aggressive fire suppression (Egan 2009), and 1910 remains the record-setting year in the Northern Rockies. It has long been questioned to what degree the extensive burning in the early 20th-century, including 1910, was anomalous due to extensive Euro-American expansion in the preceding decades, or consistent with longstanding variability in fire activity. This question remains relevant for anticipating the impacts of ongoing climate warming in the Northern Rockies, and it requires understanding the sensitivity of fire activity to climatic and anthropogenic drivers over centuries to millennia.

To provide context for ongoing and expected fire-regime changes in the Northern Rockies, we developed a network of 12 lake-sediment fire-history records from within a c. 10,000 km² landscape in northern Idaho and western Montana. We reconstructed a landscape-scale fire history spanning the past 2500 yr in subalpine forests, which are characterized by high-

severity fire regimes (with fires occurring once every >100 yr on average) (Schoennagel et al. 2004). Our goals were to: 1) characterize the historical range of variability of fire activity over the past 2500 yr, including any relationships with known climate variability; and 2) explicitly evaluate the precedence of early 20th-century and 21st-century fire activity within the context of recent millennia. We further compared historical and contemporary fire activity in the Northern Rockies with that of the Southern Rockies, to evaluate broad-scale regional synchrony, assess sensitivity to climatic variation, and provide context for ongoing changes. We predicted that, in alignment with the Southern Rockies, fire activity in the Northern Rockies would increase in response to the Medieval Climate Anomaly (MCA) and 20th-21st century warming relative to the average of the past several millennia. We discuss these findings in light of ongoing and expected climatic and fire-regime changes and their impacts on ecosystems and society.

Methods

Study area and contemporary fire history

We characterized contemporary and historical fire activity in subalpine forests in the northern Bitterroot Mountains, corresponding to Bailey's M333D ecosection (Fig. 1). Subalpine forests in the region are dominated by *Picea engelmannii*, *Abies lasiocarpa*, and *Pinus contorta*; *Tsuga mertensiana* is common in the western part of the study area. Mean annual temperature and precipitation averaged $5.70\text{ }^{\circ}\text{C} \pm 0.68$ (sd) and $1156\text{ mm} \pm 161$, respectively, over 1991-2020 (PRISM Climate Group 2021). Precipitation is snow-dominated, and only 102 mm (8% of total precipitation) fall during the driest three months of July- September, on average.

The modern fire history within the ecoregion was characterized using area burned from the Northern Rockies Fire Atlas (NRFA, 1900-2008) (Gibson et al. 2014) and the Monitoring Trends in Burn Severity program (MTBS, 1984-2021) (MTBS Project (USDA Forest

Service/U.S. Geological Survey) 2022). To be consistent with MTBS data, only fires >405 ha (1000 acres) from the NRFA were used. The NRFA contains documented fire perimeters on federally managed land. Therefore, we subset MTBS fire perimeters to the same areas to ensure consistency when calculating fire-regime statistics for time periods that overlapped with the NRFA. To assess fire-climate relationships, we used two sources of annual climate data: average summer maximum VPD from PRISM for 1900-2021 (Abatzoglou 2013, PRISM Climate Group (Oregon State University) 2021) and average summer vapor pressure deficit (VPD) from gridMet for 1984-2021. Climate data were spatially averaged across the ecoregion, and relationships with annual area burned were assessed using Spearman rank correlations.

To summarize 20th- and 21st-century fire regimes, we calculated fire rotation periods (FRP), defined as the time in years it takes to burn an area equal in size to the area of interest: $\frac{t}{\sum a_i / A}$, where t is the time period evaluated, a_i is annual area burned in year i , and A is the total area of the study region. We summarized FRP for the ecoregion overall, and for subalpine forest within the ecoregion, following methods from Higuera et al. (2021). Additionally, we summarized the FRP separately for the 21st century, and for time periods previously identified from the NRFA as having distinctly different rates of burning: 1900-1942, 1943-1984, and 1985-2021 (Higuera et al. 2015).

Paleofire history and statistical analyses

To characterize historical fire regimes, we reconstructed fire histories from 12 lake-sediment records within a c. 10⁴ km² landscape (Table A.1). A total of 2-4 m of sediment was collected from each of the lakes in 2017-2019. Chronologies were constructed in *rbacon* using a combination of ²¹⁰Pb-inferred ages (n = 7-15 per site), tephra layers (n = 0-3 per site), and ¹⁴C ages of terrestrial macrofossils or charcoal (n = 3-6 per site) (Fig. B.1-B.2) (Blaauw and Christen

2011). Sediment cores were subsampled contiguously at 0.5-cm intervals for macroscopic ($>125\text{-}\mu\text{m}$) charcoal analysis (see supplementary materials for details). Concentrations of macroscopic charcoal ($\# \text{ cm}^{-3}$), interpolated to a constant timestep of 10 yr across all sites, were used to calculate charcoal accumulation rate (CHAR, $\# \text{ cm}^{-2} \text{ yr}^{-1}$). Local fire events were inferred from peaks in CHAR identified as those exceeding the 99th percentile of the “noise distribution” via standard methods using *CharAnalysis* (Fig. B.3) (Higuera 2009, The MathWorks 2021); all records were analyzed with the same parameters.

To produce a composite record of fire-event frequency across the study landscape, we calculated the percent of sites burned per century. We summed the number of fires recorded across all sites within a moving 100-yr window centered on each 10-yr timestep, and divided this sum by the average number of sites recording during the sampling window, following methods from Hoescker et al. (2020). We accounted for age uncertainty in the timing of inferred fire events by resampling the age assigned to each charcoal peak 1000 times. For each iteration, fire ages were drawn from a normal distribution with a standard deviation of 40 yr based on estimated age error (Table A.2, Fig. A.1), and we calculated the percent of sites burned per century (Hoescker et al. 2020). We present the median value from the 1000 iterations, and used the 5th and 95th percentiles to estimate 90% confidence intervals, which we smoothed over 100 yr using a loess smoother. This analysis was restricted to the past 2500 yr, when at least seven sites were recording. We used the percentage of sites burned per century to also estimate the paleo FRP in each 100-yr window, following methods from Calder et al. (2015).

To characterize changes in biomass burning, we developed a composite CHAR series, using standard methods implemented in the *paleofire* R package (Blarquez et al. 2014). To facilitate comparison with Calder et al. (2015), transformed charcoal z-scores were calculated by

rescaling individual CHAR records through mini-max, Box-Cox, and z-score transformations. The resulting transformed CHAR timeseries were pre-binned into 10-yr non-overlapping bins and smoothed to 100 yr prior to compositing (Daniau et al. 2012); results were insensitive to the selection of the bin width. Confidence intervals were generated by bootstrapping the charcoal series 1000 times.

We compared modern and historical fire activity of the Northern Rockies landscape with that of the Southern Rockies using a network of 20 lake-sediment records from northern Colorado and southern Wyoming previously summarized in Higuera et al. (2021), using original data from (Minckley et al. 2012, Higuera et al. 2014, Calder et al. 2015). We applied the analyses described above to the Southern Rockies paleofire records to calculate the percent sites burned per century and create a composite timeseries of charcoal influx (Fig. B.4). We applied these analyses to all 20 records to characterize the regional fire history, and also to a subset of 12 records from the Park Range in northwestern Colorado, within a similar-sized landscape to that represented by our Northern Rockies sites (Fig. B.4) (Calder et al. 2015).

We used several sources of paleoclimate information to compare to our fire history reconstructions. For broad-scale climate patterns over the past millennium, we drew on a multiproxy Northern Hemisphere temperature reconstruction (Mann et al. 2009) and a pollen-based North America temperature reconstruction (Trouet et al. 2013), as well as a reconstruction of ENSO variance based on North American tree-ring records (Li et al. 2011). Summer drought information in both study regions was obtained from tree-ring-based PDSI reconstructions (Cook et al. 2010). Additional paleoclimate information specific to the Northern Rockies was derived from a previously published lake-level reconstruction from one of our study sites (Parish et al. 2022), an ^{18}O -inferred snow water equivalent (SWE) reconstruction in northwest Montana

(Schoenemann et al. 2020), and a spatially-explicit summer temperature reconstruction (Anchukaitis et al. 2017). To assess the strength of correlations between paleoclimate and fire activity on a century timescale, paleoclimate data were summarized over 100-year moving windows, and time series were subset to one value every century and compared using Spearman rank correlations; p-values are thus based on a sample size reflecting the number of non-overlapping 100-yr periods represented.

Fidelity of charcoal peaks to known fire history

Comparing between fires mapped in the NRFA and charcoal peaks from 1900-2021 CE revealed a lack of fidelity at four of the sites in the Northern Rockies, which recorded charcoal peaks that were younger than the most recent known fire at the site (Table A.3). We attribute this incongruence between paleo-inferred and known fire histories to the effects of partial mixing of unconsolidated near-surface sediments while retrieving cores from > 10 m water depth, and while extruding cores immediately after collection. This interpretation is supported by the lack of stratigraphy in these surface cores, consistent with moderate sediment mixing, and by radiocarbon measurements of concentrated charcoal samples from the most recent charcoal peaks at these sites (Appendix A). Radiocarbon measurements revealed that the combusted materials pre-dated 1950 CE, and were thus older than the ^{210}Pb -inferred age of the sediment from which the charcoal derived, likely as a result of low-density charcoal fragments moving up-core following the release of pressure when sediments were brought to the surface. We attributed the four anomalous charcoal peaks to fires in 1910 recorded in the NRFA at these sites, and we manually shifted the fire dates to 1910 in the composite analysis to improve comparability between paleo-inferred and contemporary fire histories; this change had only a minor effect on the composite fire-history results. Other sites either had fidelity between paleo-inferred and

known fire histories ($n = 5$), or lacked strong evidence for shifting inferred fire dates ($n = 3$; e.g., distinct MS peaks associated with the 1980 Mt. St. Helens ash were well-preserved and consistent with the ^{210}Pb chronology). While the lack of congruence with the NRFA precludes using these records for a calibration study (e.g., Higuera et al. 2011, Kelly et al. 2013), the issues described above are limited to the upper c. 10-40 cm. Sediment compaction (as measured by bulk density, g cm^{-3}) increased below c. 10-40 cm depth in surface cores, and the presence of well-preserved tephra layers in deeper sediment layers indicates a lack of mixing. Overall, we are confident in the accuracy of our fire history, given our use of a network of sites, which reduces the influence of errors at any one site, and the 100-yr precision of our analyses.

Results

20th-21st century fire history in the Northern Rockies

Annual area burned in the Bitterroot Mountains ecoregion has increased significantly since 1984 (Sen's slope = 67.8 ha yr^{-1} , $p = 0.005$), consistent with previous studies documenting increased area burned across the northern Rocky Mountains (Westerling et al. 2006, Parks and Abatzoglou 2020). The trend of increasing area burned since 1984 also applies when subalpine forests are considered alone (Sen's slope = 8.90 ha yr^{-1} , $p = 0.003$). Fire activity in recent decades has not exceeded that of the early 20th-century; most burning in the ecoregion over the past 120 years occurred either prior to 1942 or after 2000 (Fig. 2). The vast majority of total area burned in the region occurred during years with regionally extensive fire activity, including 1910, 1919, and 2015, which alone account for 47%, 16%, and 4%, of total area burned, respectively. Within subalpine forest, the estimated fire rotation period (FRP) over 1900-2021 was 215 yr, but FRP estimates differed substantially among multidecadal periods. The FRP was 97 yr during the early 20th century (1900-1942), compared to 394 yr from 1984-2021 (Fig. 2).

Higher fire activity in the past two decades contributed to a lower 21st-century (2000-2021) FRP of 237 yr.

Ecoregion-wide annual area burned was significantly correlated with annual maximum May-September VPD ($\rho = 0.58$, $p < 0.001$), a coarse proxy for fuel aridity (e.g., Higuera and Abatzoglou 2021). Fire-climate relationships varied over multidecadal time periods (Higuera et al. 2015), with a weaker correlation during the middle of the 20th century ($\rho = 0.41$, $p = 0.007$; 1943-1983). Considering only 1984-2021, the Spearman correlation with average summer VPD was 0.55 ($p < 0.001$), lower than that in the Southern Rockies study area ($\rho = 0.75$, Fig. B.5) (Higuera et al. 2021).

Paleofire history in the Northern Rockies

Over the past 2500 yr, an average of 61% of the Northern Rockies sites burned in each 100-year period, equivalent to an estimated FRP of 164 yr (Fig. 3). The 100-yr FRP estimates varied over time, with the central 75% ranging from 133 to 220 yr. This range provides an estimate of the historical range of variability (HRV) in paleo fire activity (Higuera et al. 2021). The range of FRP estimates overlap with mean fire return interval estimates from stand origin and fire-scar analysis in four subalpine watersheds c. 100 km south of our study area, which range from 139 to 234 yr over 1527-2000 CE (Kipfmeuller 2003). Over the same time span, an average of 53% of the lakes burned per century, yielding an estimated FRP of 184 yr (central 75%: 133-300 yr).

The percentage of sites burned per century over the past 2500 yr was weakly negatively correlated with average reconstructed April 1 snow water equivalent (SWE) at Foy Lake, Montana, approximately 125 km northeast of our study area ($\rho = -0.43$, $p = 0.05$, $n = 22$ century periods after accounting for temporal autocorrelation; Fig. 4). The percentage of sites burned per

century was also weakly positively correlated with the maximum reconstructed summer temperature in each century ($\rho = 0.61$, $p = 0.05$, $n = 10$ century periods), but was not significantly correlated with the number of years per century with extreme drought from reconstructed PDSI (Fig. B.6).

The highest rate of burning in the paleorecords occurred over c. 2300-2500 yr BP, with a maximum of 99% of sites burning during the century centered on 2410 BP yielding an estimated FRP of 101 yr. The timing of maximum burning corresponds with a fluctuation in lake level at Silver Lake, MT, one of our northernmost study sites (Fig 4), although the timing of the drop in lake level is not fully constrained (Parish et al. 2022). The period with minimum burning spanned c. 100-250 BP, with an average of 25% of sites burning per century, corresponding to an estimated FRP of 400 yr. The period of minimum burning overlapped with a local maximum in SWE, which averaged 0.87 sd above the long-term mean during the century centered on 210 BP. Following this period of low fire activity, burning increased in the early 20th century, reaching a recent maximum of 75% sites burned during the century centered on 1900 CE (FRP: 133 yr).

Fire-history comparison of the Northern and Southern Rockies

Across most of the record, the Northern Rockies landscape experienced higher fire activity than in the Southern Rockies region (Fig. 5). The average paleo-inferred FRP from the Southern Rockies sites was 239 yr, with the central 75% ranging from 196 to 333 yr. Although the HRV of each of the two regions overlapped, the series-wide estimated FRP represents 45% more burning per unit time on average in the Northern Rockies study area over the past 2500 yr.

In contrast to the average of the past 2500 yr, the Southern Rockies have experienced substantially higher fire activity over the 21st century compared with the Northern Rockies, largely due to the exceptional fire year of 2020. The 2000-2020 FRP of 117 yr in subalpine

forests of the Southern Rockies exceeds the HRV of the past 2500 yr, and also exceeds both contemporary burning and the HRV of the Northern Rockies (Fig. 5).

Although both regions have strong fire-climate linkages over the contemporary record (Fig. B.5), past variability in fire activity was not synchronous across the Northern and Southern Rockies (Fig. 5). Although minima in fire activity occurred at different times in the two regions, they reflected similar FRPs of 400 years. In contrast, maximum burning in the Northern Rockies (FRP of 101 yr) represented 39% more burning per unit time than the maximum of the Southern Rockies, and it occurred at a time when burning in the Southern Rockies was low (Fig. 5). Maximum burning across sites in the Southern Rockies coincided with the early MCA.

Temporal patterns in charcoal influx were more similar between the two regions, but notably, the composite records were standardized such that overall rates of charcoal influx cannot be compared directly. In both regions, CHAR values were higher on average c. 1500-1000 BP and generally lower after c. 800 BP (Fig. 5).

Discussion

Historical, contemporary, and future fire activity in the Northern Rockies

Our network of fire history reconstructions reveals that the Northern Rockies landscape burned with an average paleo-estimated FRP of 164 yr over the past 2500 years, at rates often exceeding those experienced over the 20th and even early 21st centuries. Our study landscape also burned c. 45% more frequently on average than subalpine forests of the southern Rocky Mountains located c. 1000 km to the south, broadly consistent with previous tree-ring and lake-sediment fire-history records. In the Northern Rockies, several studies in northern Idaho and western Montana provide mFRI estimates in the range of c. 140-250 yr over recent centuries to millennia (Gabriel 1976, Brown et al. 1994, Murray et al. 1998, Kipfmeuller 2003, Brunelle et al.

2005), modestly shorter than Southern Rockies estimates of c. 180-350 yr in southern Wyoming and northern Colorado (Howe and Baker 2003, Buechling and Baker 2004, Sibold et al. 2006, Minckley et al. 2012, Higuera et al. 2014). Spatial variation in fire regimes likely stems from differences in seasonality. While the Southern Rockies receive less total annual precipitation (Fig. 1), a lack of consistent drought during summer months, in part due to monsoon-like precipitation, likely reduces fuel drying and limits fire activity (Fig. B.7). Additionally, the greater topographic relief and higher elevations of the Southern Rockies may be associated with more non-vegetated areas or natural fuel breaks as compared with the Northern Rockies (e.g., Holsinger et al. 2016).

Our findings support an overarching influence of climate on fire activity in Northern Rockies subalpine forests. Rates of burning were negatively correlated with average spring snowpack over centennial timescales, consistent with contemporary relationships between annual area burned and the timing of spring snowmelt, which directly affects fire-season length and summer fuel moisture (Abatzoglou et al. 2013, Westerling 2016) (Fig. 4). Given strong fire-climate relationships revealed from contemporary, tree-ring, and lake-sediment records spanning decades to millennia (Heyerdahl et al. 2008, Morgan et al. 2008, Higuera et al. 2015), future warming and drying will undoubtedly enable increased fire activity in these forests (Westerling et al. 2011, Gao et al. 2021, Abatzoglou et al. 2021).

Contemporary fire activity in the Northern Rockies so far remains within the historical range of variability. The widespread fire activity of the early 20th century and early 21st centuries in the Northern Rockies is consistent with the fire history prior to 300 years ago (Fig. 3). Thus, the extent of burning during the 1910 fires – which remains record-setting within the historical record – does not appear unprecedented within the longer context of recent millennia. Rather, it

is the lack of fire during the mid-20th century that differs from the past, likely due to the combination of active fire suppression and less fire-conducive climate (Fig. 2) (Morgan et al. 2008). This contrasts with the Southern Rockies, where the 21st-century rate of burning has already moved outside of the HRV of recent millennia (Higuera et al. 2021).

Our millennial-scale perspective on fire activity in Northern Rockies subalpine forests helps anticipate if and when contemporary fire activity may exceed the historical range of variability. Fire activity could increase by up to 90% above 2000-2021 levels, resulting in an FRP of 125 yr, while still keeping rates of burning below the maximum of the past 2500 yr. Such an increase is broadly consistent with fire projections for the late 21st century (Gao et al. 2021). However, exceptional fire years like 1910 in the Northern Rockies and 2020 in the Southern Rockies, in large part driven by extreme, single-day fire spread events, strongly influence fire-regime metrics. A single year with 1910-level burning over the next three decades in subalpine forests in the Northern Rockies study area would shorten the 21st-century FRP to 96 yr, surpassing the HRV (Fig. 6). Such an event will become progressively more likely as the frequency of climatic extremes increases (Stavros et al. 2014, Wang et al. 2015, Higuera and Abatzoglou 2021, Coop et al. 2022). Under a scenario of 2 °C warming, fire-season aridity like that of 2020 will be common, and the number of extreme fire-spread events in the western U.S. is expected to double (Coop et al. 2022). Thus, while a modest increase in fire activity would be consistent with historical rates of burning in the Northern Rockies, one or more extensive fire years could signal a shift in the fire regime, provided it is not followed by decades of minimal burning.

The ecological consequences of changing fire regimes depend strongly on whether future fire activity surpasses the longstanding HRV. Species composition in northern Rocky Mountain

subalpine forests have remained relatively stable over the past several millennia (Brunelle et al. 2005, Herring et al. 2018), when fire activity was similar to or greater than that of the 21st century (Fig. 3). Additionally, although the combination of warming and drying and higher fire activity can limit recruitment of subalpine species (Andrus et al. 2018, Turner et al. 2019, Hansen and Turner 2019, Rammer et al. 2021), future climate is projected to remain suitable for tree regeneration in the Northern Rockies through at least mid-century (Davis et al. In Revision). Therefore, subalpine forests in the Northern Rockies will likely remain resilient to climatic warming and modest increases in burning in the near term, but may become vulnerable to the impacts of large increases in fire activity that move the system outside of the HRV.

A key uncertainty in anticipating fire-regime changes is to what extent fire-vegetation feedbacks may limit or amplify future increases in burning in the Northern Rockies, as the climate becomes increasingly fire-conducive. Potential negative feedbacks could arise from reduced landscape fuel continuity due to extensive burning (Parks et al. 2015, Hurteau et al. 2019), although these effects will likely be small relative to the influence of climate over the next several decades (Abatzoglou et al. 2021). Additionally, climate-driven shifts in vegetation composition and structure may lead to reductions in fire severity (Parks et al. 2016). Further research to understand the ecosystem impacts of past variation in climate and fire activity in the Northern Rockies will help assess potential fire-vegetation feedbacks and clarify regional differences in ecological responses.

Asynchronous burning across regions over the past 2500 yr

Our results provide little evidence of synchronous variations in fire activity across the Southern and Northern Rockies in response to late-Holocene climatic variation. Contrary to expectation, Northern Rockies fire activity did not increase during the Medieval Climate

Anomaly (MCA, c. 1200 – 800 yr BP), when Northern Hemisphere temperatures were ~ 0.3 °C above the average of the cooler Little Ice Age (LIA, c. 750-50 yr BP) (Mann et al. 2009, Trouet et al. 2013, Anchukaitis et al. 2017), and burning was widespread in the Southern Rockies and more broadly across the West (Marlon et al. 2012, Calder et al. 2015). The lack of maximal burning during the MCA in the Northern Rockies may reflect a more subdued climate anomaly in the region. There is little evidence of anomalous MCA warmth in the Northern Rockies in terms of summer temperatures (Fig. B.6) (Anchukaitis et al. 2017), highlighting that broad-scale temperature reconstructions can obscure regional patterns. It is also possible that the effects of strong and persistent La Niña-like conditions in the tropical Pacific during the MCA (Mann et al. 2009, Trouet et al. 2013) overrode the influence of any temperature changes in the Northern Rockies. La Niña conditions are associated with above-average winter and spring precipitation in the northwestern U.S., and warm, dry climate conditions and above-average fire activity in the southwest and the Southern Rockies (Hostetler et al. 2018). Given these regional differences in the effects of ENSO variation, it is not surprising that fire activity responded differently in the two regions during the MCA.

The lack of synchrony across the records is suggestive of possible antiphase variability in fire activity between the Northern and Southern Rockies. This is most evident within the past c. 300 yr, when ENSO variability was the highest over the past millennium (Fig. 5) (Li et al. 2011). This raises the question of whether low-frequency ENSO variability on decadal to centennial timescales could drive asynchronous variations in fire activity across the western U.S., which is not possible to definitively answer given the nature of our data. Comparing between the Northern Rockies landscape and a subset of Southern Rockies sites at a similar spatial scale revealed no clear evidence of consistent antiphase variability between the regions. However, it is possible

that a true relationship over some timescale or spatial domain was obscured by stochasticity in landscape-scale fire histories, or that broader-scale trends in mean climate interact with ENSO variation in complex ways to determine centennial-scale patterns of fire activity (Anderson 2012, Hostetler et al. 2018). Asynchronous fire activity between the northwest and the Southern Rockies over decadal to centennial timescales would have important implications for ecological processes including forest demography (Littlefield et al. 2020), potentially resulting in complementary ecosystem changes in productivity and C sequestration at a regional scale. Future research combining multiple landscape-scale fire histories from across the Rockies will help resolve regional dynamics of fire-regime variability and responses to climate drivers.

Summary and conclusions

This study provides quantitative estimates of past variation in fire activity in Northern Rockies subalpine forests, and highlights strong climatic controls of fire activity across the region. Our results reveal that 21st-century burning in the Northern Rockies remains within the HRV of the past 2500 yr, implying that subalpine forests could remain resilient to climatic warming as long as fire activity remains within the HRV. As the frequency of years with high fuel aridity and associated burning increases under future climate in the Northern Rockies, fire activity will likely surpass that experienced in the past. More broadly across the West, our results imply that the emergence of fire-regime shifts will be marked by exceptional fire years in individual landscapes and regions, as seen in the Southern Rockies, which may result in a “ratchet of events” driving ecosystem changes across space and time (Jackson et al. 2009, Williams et al. 2021). Planning for community response and resource management would benefit by considering the likelihood of single-year, extreme events, which, though historically not

unprecedented, have the potential to impact vegetation dynamics, carbon storage, and water resources over wide areas.

Literature Cited

- Abatzoglou, J. T. 2013. Development of gridded surface meteorological data for ecological applications and modelling. *International Journal of Climatology* 33:121–131.
- Abatzoglou, J. T., D. S. Battisti, A. P. Williams, W. D. Hansen, B. J. Harvey, and C. A. Kolden. 2021. Projected increases in western US forest fire despite growing fuel constraints. *Communications Earth & Environment* 2:1–8.
- Abatzoglou, J. T., C. A. Kolden, J. T. Abatzoglou, and C. A. Kolden. 2013. Relationships between climate and macroscale area burned in the western United States. *International Journal of Wildland Fire* 22:1003–1020.
- Abatzoglou, J. T., and A. P. Williams. 2016. Impact of anthropogenic climate change on wildfire across western US forests. *Proceedings of the National Academy of Sciences* 113:11770–11775.
- Alizadeh, M. R., J. T. Abatzoglou, C. H. Luce, J. F. Adamowski, A. Farid, and M. Sadegh. 2021. Warming enabled upslope advance in western US forest fires. *Proceedings of the National Academy of Sciences* 118:e2009717118.
- Anchukaitis, K. J., R. Wilson, K. R. Briffa, U. Büntgen, E. R. Cook, R. D’Arrigo, N. Davi, J. Esper, D. Frank, B. E. Gunnarson, G. Hegerl, S. Helama, S. Klesse, P. J. Krusic, H. W. Linderholm, V. Myglan, T. J. Osborn, P. Zhang, M. Rydval, L. Schneider, A. Schurer, G. Wiles, and E. Zorita. 2017. Last millennium Northern Hemisphere summer temperatures

- from tree rings: Part II, spatially resolved reconstructions. *Quaternary Science Reviews* 163:1–22.
- Anderson, L. 2012. Rocky Mountain hydroclimate: Holocene variability and the role of insolation, ENSO, and the North American Monsoon. *Global and Planetary Change* 92–93:198–208.
- Andrus, R. A., B. J. Harvey, K. C. Rodman, S. J. Hart, and T. T. Veblen. 2018. Moisture availability limits subalpine tree establishment. *Ecology* 99:567–575.
- Blaauw, M., and J. A. Christen. 2011. Flexible paleoclimate age-depth models using an autoregressive gamma process. *Bayesian Analysis* 6:457–474.
- Blarquez, O., B. Vanni re, J. R. Marlon, A. L. Daniau, M. J. Power, S. Brewer, and P. J. Bartlein. 2014. Paleofire: An R package to analyse sedimentary charcoal records from the Global Charcoal Database to reconstruct past biomass burning. *Computers and Geosciences* 72:255–261.
- Brown, J. K., S. F. Arno, S. W. Barrett, and J. P. Menakis. 1994. Comparing the Prescribed Natural Fire Program With Presettlement Fires in the Selway-Bitterroot Wilderness. *International Journal of Wildland Fire* 4:157–168.
- Brunelle, A., C. Whitlock, P. Bartlein, and K. Kipfmue ller. 2005. Holocene fire and vegetation along environmental gradients in the Northern Rocky Mountains. *Quaternary Science Reviews* 24:2281–2300.
- Buechling, A., and W. L. Baker. 2004. A fire history from tree rings in a high-elevation forest of Rocky Mountain National Park. *Canadian Journal of Forest Research* 34:1259–1273.
- Calder, W. J., D. Parker, C. J. Stopka, G. Jim nez-Moreno, and B. N. Shuman. 2015. Medieval warming initiated exceptionally large wildfire outbreaks in the Rocky Mountains.

Proceedings of the National Academy of Sciences of the United States of America
112:13261–6.

Cook, E. R., R. Seager, R. R. Heim, R. S. Vose, C. Herweijer, and C. Woodhouse. 2010.

Megadroughts in North America: placing IPCC projections of hydroclimatic change in a long-term palaeoclimate context. *Journal of Quaternary Science* 25:48–61.

Coop, J. D., S. A. Parks, C. S. Stevens-Rumann, S. D. Crausbay, P. E. Higuera, M. D. Hurteau, A. Tepley, E. Whitman, T. Assal, B. M. Collins, K. T. Davis, S. Dobrowski, D. A. Falk, P. J. Fornwalt, P. Z. Fulé, B. J. Harvey, V. R. Kane, C. E. Littlefield, E. Q. Margolis, M. North, M. A. Parisien, S. Prichard, and K. C. Rodman. 2020. Wildfire-Driven Forest Conversion in Western North American Landscapes. *BioScience* 70:659–673.

Coop, J. D., S. A. Parks, C. S. Stevens-Rumann, S. M. Ritter, and C. M. Hoffman. 2022.

Extreme fire spread events and area burned under recent and future climate in the western USA. *Global Ecology and Biogeography* 31:1949–1959.

Daniau, A. -L., P. J. Bartlein, S. P. Harrison, I. C. Prentice, S. Brewer, P. Friedlingstein, T. I.

Harrison-Prentice, J. Inoue, K. Izumi, J. R. Marlon, S. Mooney, M. J. Power, J.

Stevenson, W. Tinner, M. Andrič, J. Atanassova, H. Behling, M. Black, O. Blarquez, K.

J. Brown, C. Carcaillet, E. A. Colhoun, D. Colombaroli, B. A. S. Davis, D. D’Costa, J.

Dodson, L. Dupont, Z. Eshetu, D. G. Gavin, A. Genries, S. Haberle, D. J. Hallett, G.

Hope, S. P. Horn, T. G. Kassa, F. Katamura, L. M. Kennedy, P. Kershaw, S. Krivonogov,

C. Long, D. Magri, E. Marinova, G. M. McKenzie, P. I. Moreno, P. Moss, F. H.

Neumann, E. Norström, C. Paitre, D. Rius, N. Roberts, G. S. Robinson, N. Sasaki, L.

Scott, H. Takahara, V. Terwilliger, F. Thevenon, R. Turner, V. G. Valsecchi, B.

- Vannière, M. Walsh, N. Williams, and Y. Zhang. 2012. Predictability of biomass burning in response to climate changes. *Global Biogeochemical Cycles* 26.
- Davis, K. T., and et al. In Revision. Reduced fire severity offers near-term buffer to climate-driven declines in conifer resilience across the western United States. *Proceedings of the National Academy of Sciences*.
- Egan, T. 2009. *The Big Burn: Teddy Roosevelt and the Fire That Saved America*. Mariner Books, Boston.
- Gabriel, H. 1976. *Wilderness Ecology: The Danaher Creek Drainage Bob Marshall Wilderness Montana*. Graduate Student Theses, Dissertations, & Professional Papers.
- Gao, P., A. J. Terando, J. A. Kupfer, J. Morgan Varner, M. C. Stambaugh, T. L. Lei, and J. Kevin Hiers. 2021. Robust projections of future fire probability for the conterminous United States. *Science of The Total Environment* 789:147872.
- Gavin, D. G., D. J. Hallett, F. S. Hu, K. P. Lertzman, S. J. Prichard, K. J. Brown, J. A. Lynch, P. Bartlein, and D. L. Peterson. 2007. Forest fire and climate change in western North America: insights from sediment charcoal records. *Frontiers in Ecology and the Environment* 5:499–506.
- Gavin, D. G., F. S. Hu, K. Lertzman, and P. Corbett. 2006. Weak climatic control of stand-scale fire history during the late Holocene. *Ecology* 87:1722–1732.
- Gibson, C. E., P. Morgan, and A. M. Wilson. 2014. *Atlas of digital polygon fire extents for Idaho and western Montana (2nd Edition)*. Forest Service Research Data Archive, Fort Collins, CO.
- de Groot, W. J., M. D. Flannigan, and A. S. Cantin. 2013. Climate change impacts on future boreal fire regimes. *Forest Ecology and Management* 294:35–44.

- Hansen, W. D., and M. G. Turner. 2019. Origins of abrupt change? Postfire subalpine conifer regeneration declines nonlinearly with warming and drying. *Ecological Monographs* 89:e01340.
- Herring, E. M., D. G. Gavin, S. Z. Dobrowski, M. Fernandez, and F. S. Hu. 2018. Ecological history of a long-lived conifer in a disjunct population. *Journal of Ecology* 106:319–332.
- Heyerdahl, E. K., P. Morgan, and J. P. Riser. 2008. Multi-season climate synchronized historical fires in dry forests (1650-1900) northern Rockies, USA. *Ecology* 89:705–716.
- Higuera, P. 2009. CharAnalysis 0.9: diagnostic and analytical tools for sediment charcoal analysis. User's Guide, Montana State University, Bozeman, MT.
- Higuera, P. E., and J. T. Abatzoglou. 2021. Record-setting climate enabled the extraordinary 2020 fire season in the western United States. *Global Change Biology* 27:1–2.
- Higuera, P. E., J. T. Abatzoglou, J. S. Littell, and P. Morgan. 2015. The Changing Strength and Nature of Fire-Climate Relationships in the Northern Rocky Mountains, U.S.A., 1902-2008. *PLOS ONE* 10:e0127563.
- Higuera, P. E., C. E. Briles, and C. Whitlock. 2014. Fire-regime complacency and sensitivity to centennial-through millennial-scale climate change in Rocky Mountain subalpine forests, Colorado, USA. *Journal of Ecology* 102:1429–1441.
- Higuera, P. E., B. N. Shuman, and K. D. Wolf. 2021. Rocky Mountain subalpine forests now burning more than any time in recent millennia. *Proceedings of the National Academy of Sciences* 118:e2103135118.
- Higuera, P. E., C. Whitlock, and J. A. Gage. 2011. Linking tree-ring and sediment-charcoal records to reconstruct fire occurrence and area burned in subalpine forests of Yellowstone National Park, USA. *The Holocene* 21:327–341.

- Hoecker, T. J., P. E. Higuera, R. Kelly, and F. S. Hu. 2020. Arctic and boreal paleofire records reveal drivers of fire activity and departures from Holocene variability. *Ecology* 101.
- Holden, Z. A., A. Swanson, C. H. Luce, W. M. Jolly, M. Maneta, J. W. Oyler, D. A. Warren, R. Parsons, and D. Affleck. 2018. Decreasing fire season precipitation increased recent western US forest wildfire activity. *Proceedings of the National Academy of Sciences* 115:E8349–E8357.
- Holsinger, L., S. A. Parks, and C. Miller. 2016. Weather, fuels, and topography impede wildland fire spread in western US landscapes. *Forest Ecology and Management* 380:59–69.
- Hostetler, S. W., P. J. Bartlein, and J. R. Alder. 2018. Atmospheric and Surface Climate Associated With 1986–2013 Wildfires in North America. *Journal of Geophysical Research: Biogeosciences* 123:1588–1609.
- Howe, E., and W. L. Baker. 2003. Landscape Heterogeneity and Disturbance Interactions in a Subalpine Watershed in Northern Colorado, USA. *Annals of the Association of American Geographers* 93:797–813.
- Hurteau, M. D., S. Liang, A. L. Westerling, and C. Wiedinmyer. 2019. Vegetation-fire feedback reduces projected area burned under climate change. *Scientific Reports* 9:2838.
- Iglesias, V., N. Stavros, J. K. Balch, K. Barrett, J. Cobian-Iñiguez, C. Hester, C. A. Kolden, S. Leyk, R. C. Nagy, C. E. Reid, C. Wiedinmyer, E. Woolner, and W. R. Travis. 2022. Fires that matter: reconceptualizing fire risk to include interactions between humans and the natural environment. *Environmental Research Letters* 17:045014.
- Jackson, S. T., J. L. Betancourt, R. K. Booth, and S. T. Gray. 2009. Ecology and the ratchet of events: climate variability, niche dimensions, and species distributions. *Proceedings of*

- the National Academy of Sciences of the United States of America 106 Suppl 2:19685–92.
- Juang, C. S., A. P. Williams, J. T. Abatzoglou, J. K. Balch, M. D. Hurteau, and M. A. Moritz. 2022. Rapid Growth of Large Forest Fires Drives the Exponential Response of Annual Forest-Fire Area to Aridity in the Western United States. *Geophysical Research Letters* 49:e2021GL097131.
- Kelly, R., M. L. Chipman, P. E. Higuera, I. Stefanova, L. B. Brubaker, and F. S. Hu. 2013. Recent burning of boreal forests exceeds fire regime limits of the past 10,000 years. *Proceedings of the National Academy of Sciences* 110:13055–13060.
- Kipfmeuller, K. F. 2003. Fire-climate-vegetation interactions in subalpine forests of the Selway-Bitterroot Wilderness Area, Idaho and Montana, United States. The University of Arizona.
- Kirchmeier-Young, M. C., F. W. Zwiers, N. P. Gillett, and A. J. Cannon. 2017. Attributing extreme fire risk in Western Canada to human emissions. *Climatic Change* 144:365–379.
- Landres, P. B., P. Morgan, and F. J. Swanson. 1999. Overview of the use of natural variability concepts in managing ecological systems. *Ecological Applications* 9:1179–1188.
- Li, J., S.-P. Xie, E. R. Cook, G. Huang, R. D'Arrigo, F. Liu, J. Ma, and X.-T. Zheng. 2011. Interdecadal modulation of El Niño amplitude during the past millennium. *Nature Climate Change* 1:114–118.
- Littlefield, C. E., S. Z. Dobrowski, J. T. Abatzoglou, S. A. Parks D, and K. T. Davis. 2020. A climatic dipole drives short-and long-term patterns of postfire forest recovery in the western United States. *Proceedings of the National Academy of Sciences*.

- Mann, M. E., Z. Zhang, S. Rutherford, R. S. Bradley, M. K. Hughes, D. Shindell, C. Ammann, G. Faluvegi, and F. Ni. 2009. Global Signatures and Dynamical Origins of the Little Ice Age and Medieval Climate Anomaly. *Science* 326:1256–1260.
- Marlon, J. R., P. J. Bartlein, D. G. Gavin, C. J. Long, R. S. Anderson, C. E. Briles, K. J. Brown, D. Colombaroli, D. J. Hallett, M. J. Power, E. A. Scharf, and M. K. Walsh. 2012. Long-term perspective on wildfires in the western USA. *Proceedings of the National Academy of Sciences* 109:E535–E543.
- Minckley, T. A., R. K. Shriver, and B. Shuman. 2012. Resilience and regime change in a southern Rocky Mountain ecosystem during the past 17 000 years. *Ecological Monographs* 82:49–68.
- Morgan, P., E. K. Heyerdahl, and C. E. Gibson. 2008. Multi-season climate synchronized fires throughout the 20th century, northern Rockies, USA. *Ecology* 89:717–728.
- MTBS Project (USDA Forest Service/U.S. Geological Survey). 2022. MTBS Data Access: Fire Level Geospatial Data. <http://mtbs.gov>.
- Murray, M. P., S. C. Bunting, and P. Morgan. 1998. Fire history of an isolated subalpine mountain range of the Intermountain Region, United States. *Journal of Biogeography* 25:1071–1080.
- Parish, M. C., K. D. Wolf, P. E. Higuera, and B. N. Shuman. 2022. Holocene water levels of Silver Lake, Montana, and the hydroclimate history of the Inland Northwest. *Quaternary Research*.
- Parks, S. A., and J. T. Abatzoglou. 2020. Warmer and Drier Fire Seasons Contribute to Increases in Area Burned at High Severity in Western US Forests From 1985 to 2017. *Geophysical Research Letters* 47:e2020GL089858.

- Parks, S. A., L. M. Holsinger, C. Miller, and C. R. Nelson. 2015. Wildland fire as a self-regulating mechanism: the role of previous burns and weather in limiting fire progression. *Ecological Applications* 25:1478–1492.
- Parks, S. A., C. L. Miller, J. Abatzoglou, L. M. Holsinger, M. A. Parisien, and S. Dobrowski. 2016. How will climate change affect wildland fire severity in the western US? *Environmental Research Letters* 11:35002.
- PRISM Climate Group (Oregon State University). 2021. PRISM 30-Year Normals. Oregon State University.
- Rammer, W., K. H. Braziunas, W. D. Hansen, Z. Ratajczak, A. L. Westerling, M. G. Turner, and R. Seidl. 2021. Widespread regeneration failure in forests of Greater Yellowstone under scenarios of future climate and fire. *Global Change Biology* 00:gcb.15726.
- Schoenemann, S. W., J. T. Martin, G. T. Pederson, and D. B. McWethy. 2020. 2,200-Year tree-ring and lake-sediment based snowpack reconstruction for the northern Rocky Mountains highlights the historic magnitude of recent snow drought. *Quaternary Science Advances* 2:100013.
- Schoennagel, T., T. T. Veblen, and W. H. Romme. 2004. The Interaction of Fire, Fuels, and Climate across Rocky Mountain Forests. *BioScience* 54:661–676.
- Sibold, J. S., T. T. Veblen, and M. E. González. 2006. Spatial and temporal variation in historic fire regimes in subalpine forests across the Colorado Front Range in Rocky Mountain National Park, Colorado, USA. *Journal of Biogeography* 33:631–647.
- Stavros, E. N., J. T. Abatzoglou, D. McKenzie, and N. K. Larkin. 2014. Regional projections of the likelihood of very large wildland fires under a changing climate in the contiguous Western United States. *Climatic Change* 126:455–468.

The MathWorks, Inc. 2021. MATLAB.

Trouet, V., H. F. Diaz, E. R. Wahl, A. E. Viau, R. Graham, N. Graham, and E. R. Cook. 2013. A 1500-year reconstruction of annual mean temperature for temperate North America on decadal-to-multidecadal time scales. *Environmental Research Letters* 8:024008.

Turner, M. G., K. H. Braziunas, W. D. Hansen, and B. J. Harvey. 2019. Short-interval severe fire erodes the resilience of subalpine lodgepole pine forests. *Proceedings of the National Academy of Sciences of the United States of America* 166:11319–11328.

Wang, X., D. K. Thompson, G. A. Marshall, C. Tymstra, R. Carr, and M. D. Flannigan. 2015. Increasing frequency of extreme fire weather in Canada with climate change. *Climatic Change* 130:573–586.

Westerling, A. L. 2016. Increasing western US forest wildfire activity: sensitivity to changes in the timing of spring. *Philosophical transactions of the Royal Society of London. Series B, Biological sciences* 371:20150178.

Westerling, A. L., H. G. Hidalgo, D. R. Cayan, and T. W. Swetnam. 2006. Warming and Earlier Spring Increase Western U.S. Forest Wildfire Activity. *Science* 313:940–943.

Westerling, A. L., M. G. Turner, E. A. H. Smithwick, W. H. Romme, and M. G. Ryan. 2011. Continued warming could transform Greater Yellowstone fire regimes by mid-21st century. *Proceedings of the National Academy of Sciences of the United States of America* 108:13165–70.

Whitlock, C., P. E. Higuera, D. B. McWethy, and C. E. Briles. 2010. Paleoecological Perspectives on Fire Ecology: Revisiting the Fire-Regime Concept. *The Open Ecology Journal* 3:6–23.

- Williams, A. P., B. Livneh, K. A. McKinnon, W. D. Hansen, J. S. Mankin, B. I. Cook, J. E. Smerdon, A. M. Varuolo-Clarke, N. R. Bjarke, C. S. Juang, and D. P. Lettenmaier. 2022. Growing impact of wildfire on western US water supply. *Proceedings of the National Academy of Sciences* 119:e2114069119.
- Williams, J. W., A. Ordonez, and J.-C. Svenning. 2021. A unifying framework for studying and managing climate-driven rates of ecological change. *Nature Ecology & Evolution* 5:17–26.
- Zhuang, Y., R. Fu, B. D. Santer, R. E. Dickinson, and A. Hall. 2021. Quantifying contributions of natural variability and anthropogenic forcings on increased fire weather risk over the western United States. *Proceedings of the National Academy of Sciences* 118:e2111875118.

CHAPTER 4

Figures

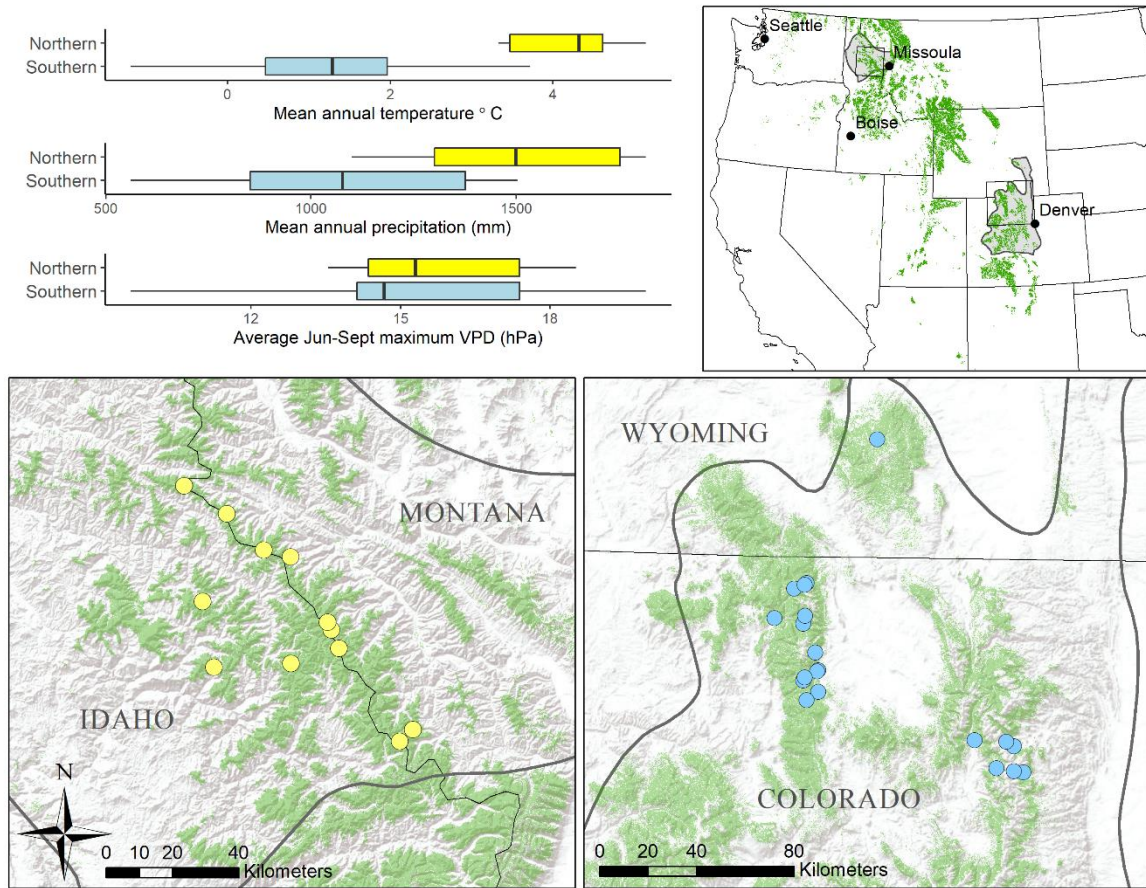


Figure 1. Map of northern and southern Rocky Mountain study regions and lake sites.

Ecoregions are outlined in grey, and boxes on the locator map show the extent of each of the two study areas. The green shaded area delineates the potential extent of Rocky Mountain subalpine forest based on LandFire Environmental Site Potential (landfire.gov). Boxplots display PRISM 30-year average climate from each lake site (1991-2020, oregonstate.edu), for $n=12$ lakes and $n=20$ lakes in the northern and southern Rocky Mountains, respectively. Climate variables include mean annual temperature, mean annual precipitation, and average daily maximum vapor pressure deficit (VPD) over June-September.

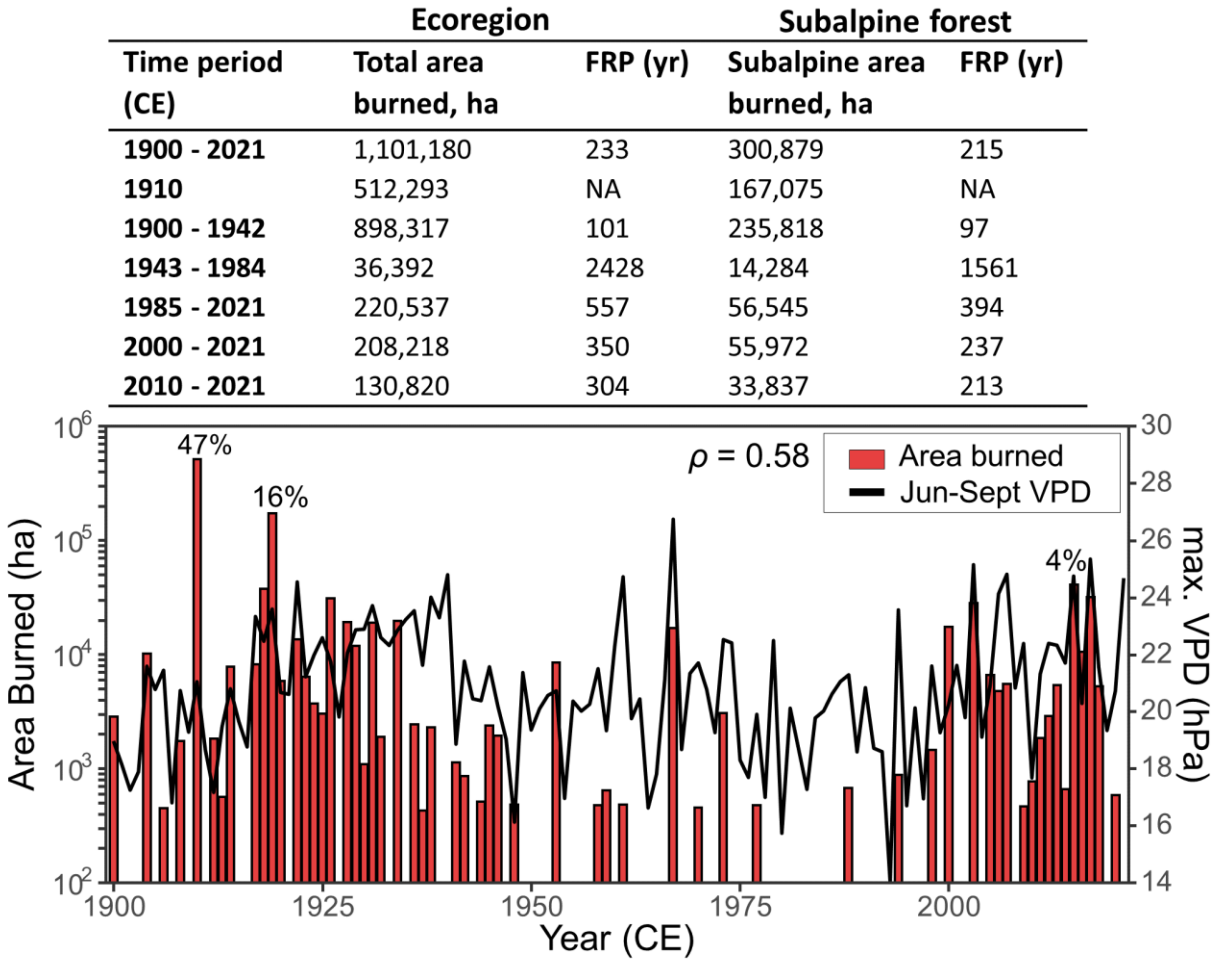


Figure 2. Modern fire history in the northern Rocky Mountain ecoregion (M333D) over 1900-2021. Ecoregion-wide annual area burned (red bars) for 1900-2008 is derived from the Northern Rockies Fire Atlas (Gibson et al. 2014), while area burned for 2009-2021 is from Monitoring Trends in Burn Severity (MTBS Project 2022). Summer average daily maximum vapor pressure deficit (VPD, black line) from PRISM data is correlated with annual area burned ($\rho = 0.58$). The table gives area burned statistics and the calculated fire rotation period for the entire ecoregion and for subalpine forest area within the ecoregion.

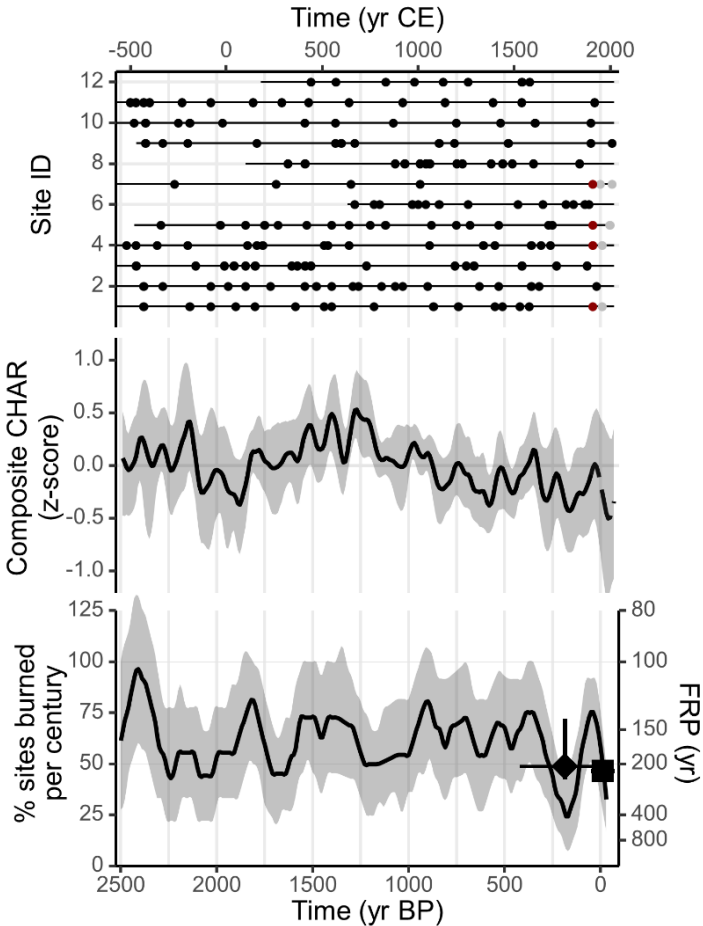


Figure 3. Fire history in the Northern Rockies study landscape over the past 2500 yr. Top panel: record length and fire timing for each individual record, organized from north to south (see supplementary for site details). Four records had recent charcoal peaks (grey dots) that were shifted to 1910 CE (red dots) in the composite analysis to match the NRFA. Center panel: transformed charcoal z-scores, smoothed over 100 yr (median \pm 90% CI). The line is dashed after 1900 CE to note uncertainty associated with unconsolidated surface sediments. Bottom panel: percentage of sites burned per century, smoothed over 100 yr (median \pm 90% CI). The range of tree-ring estimates of mean fire-return intervals (diamond) (Kipfmeuller 2003) and the 20th-21st-century fire rotation period (square) are also shown.

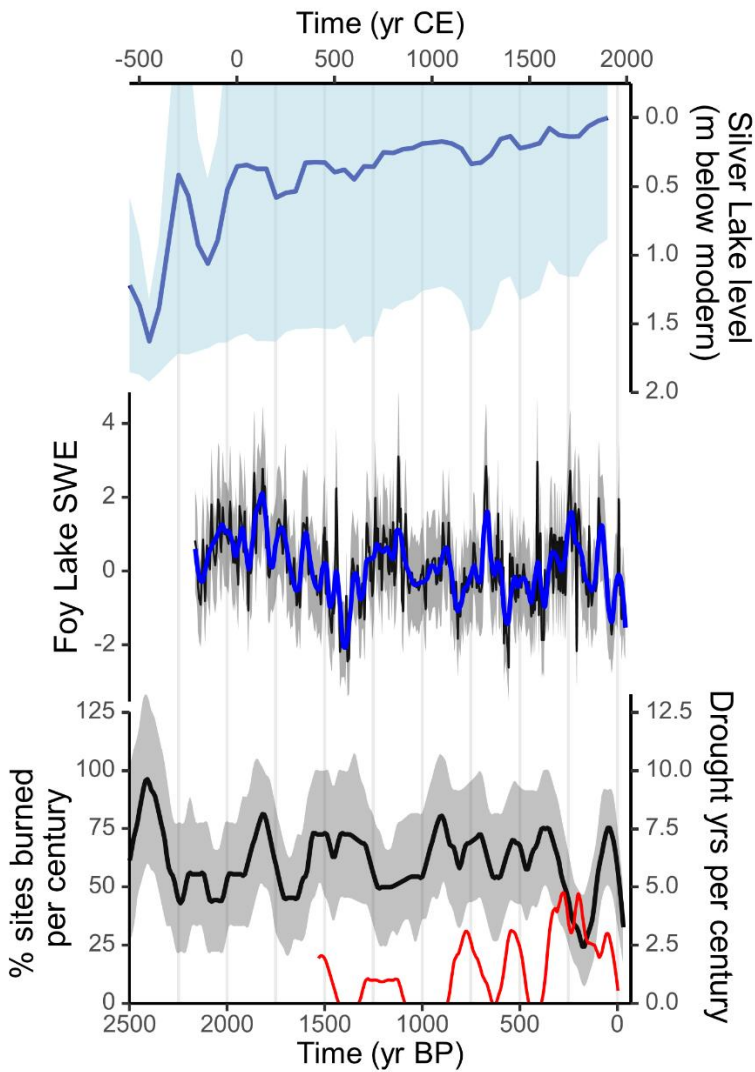


Figure 4. Paleoclimate and fire history in the Northern Rockies region. Top panel: lake-level reconstruction from Silver Lake, MT, replotted from (Parish et al. 2022). Center panel: reconstructed April 1 snow water equivalent (SWE) from Foy Lake, MT represented as z-scores (black), with 95% prediction intervals (grey bands), and smoothed over 100 yr (blue) (Schoenemann et al. 2020). Bottom panel: percentage of sites burned per century with 90% confidence bands (black/grey), and the number of years per century with extreme drought (reconstructed Jun-Aug PDSI < -4) in the study area, smoothed over 100 yr (red) (Cook et al. 2010).

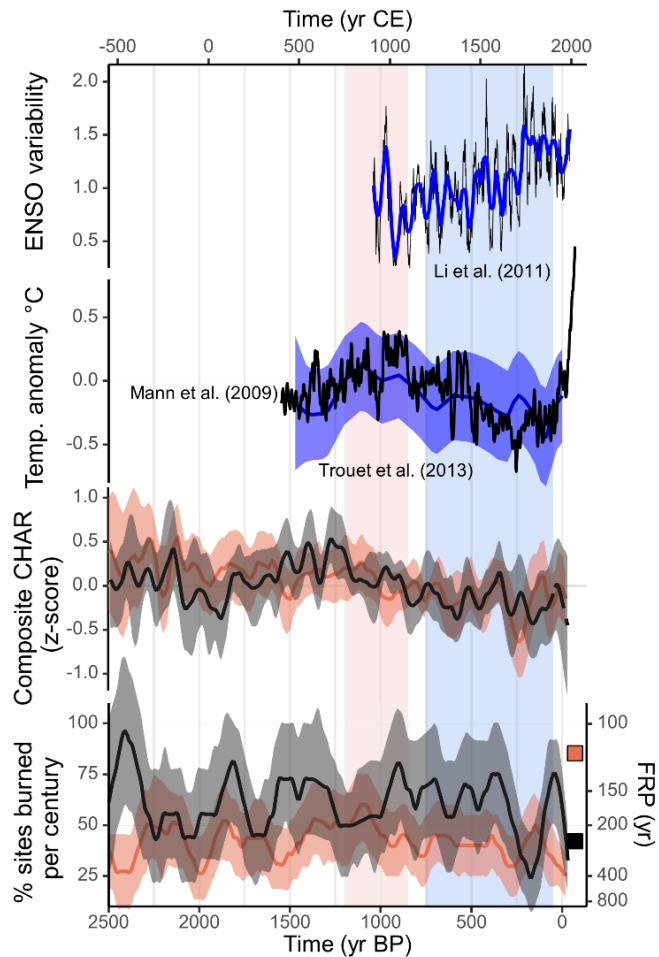


Figure 5. Fire history in the Northern and Southern Rockies study areas (black/grey and orange, respectively), with broad-scale paleoclimate information. Percent sites burned and transformed charcoal z-scores in each study region, smoothed to a 100-yr window and displaying 90% confidence bands, are shown in the bottom two panels. The 21st-century FRP estimate for each region is shown using squares (based on MTBS data). The top panel displays a decadal-scale (21-yr) reconstruction of ENSO variance, which is smoothed to 100 yr (Li et al. 2011). The center panel displays a multiproxy northern hemisphere temperature reconstruction represented as anomalies relative to the 20th-century mean (black) (Mann et al. 2009), and a pollen-based North America temperature reconstruction with 2-standard-error confidence bands (blue) (Trouet et al. 2013).

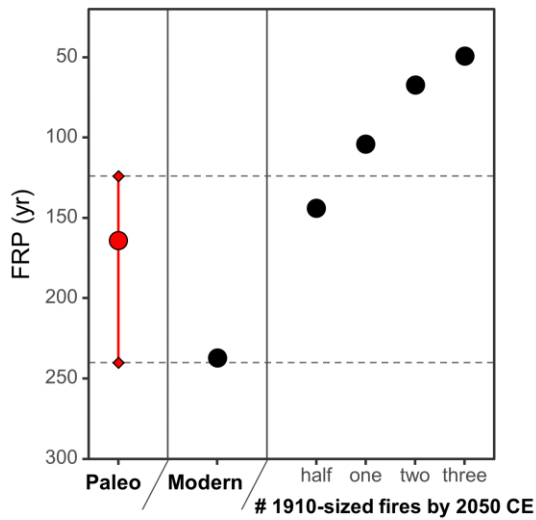


Figure 6. Paleo, modern, and future scenarios of fire rotation period in subalpine forests in the Northern Rockies study area. Paleo FRPs are the average and the central 90% of estimated FRPs over the past 2500 yr in the Northern Rockies landscape based on the % sites burned per century. Modern FRP is the 21st-century (2000-2021) estimate from MTBS data. Future scenarios are based on continued fire activity at the 21st-century average rate of burning over the next three decades, with the addition of one, two, or three years with 1910-level burning in the study area, or one year with half as much area burned as 1910.

CHAPTER 4 Supplementary Materials

Appendix A: Supplementary Methods

We cored 12 lakes, located within a 11,000-ha landscape, spanning c. 46.6 to 47.5° N and 114.6 to 116° W (Table A.1). All lakes are small (1-8 ha surface area) and deep (6-20 m), located in forested headwater catchments at 1600- 2000 m elevation, and lack significant or perennial inlet streams. Sediment cores were collected from the deepest part of each lake in 1-1.5-m sections using a 7.6-cm diameter polycarbonate tube fitted with a piston (for surface sediments), or a 5-cm-diameter modified Livingstone corer for deeper sediments (Wright et al. 1984). Sediment cores were split lengthwise, and magnetic susceptibility was measured on core surfaces at 0.5-cm intervals using a Bartington MS3 Meter and MS2E Core Logging Sensor (Bartington Instruments, Oxford, UK). Individual sections were correlated based on visual stratigraphy, magnetic susceptibility measurements, and macroscopic charcoal counts to produce a continuous record for each site.

Sediments in the uppermost 20-40 cm were dated by measuring ^{210}Pb activity (Flett Research Ltd., Manitoba, CA), and ages were estimated using the constant rate of supply model (Binford 1990). One to two ^{226}Ra measurements were taken in each core to verify background ^{210}Pb activity. Tephra layers were identified in several lakes based on visual stratigraphy and peaks in magnetic susceptibility, which were inferred as originating from Mount St. Helens in 1980 and c. 1480 CE, and Mt. Mazama c. 7600 BP (Egan et al. 2015). Chronologies were also based on ^{14}C dates of terrestrial macrofossils or charcoal (Table A.2). Chronologies were constructed using *rbacon*, with flexible priors to allow a range of sediment accumulation rates (Fig. A.2) (Blaauw and Christen 2011).

Sediment cores were sliced at 0.5-cm intervals and subsampled contiguously for charcoal analysis. Samples of 1-3 cm³ were disaggregated in 5% sodium metaphosphate solution for 72 hours, sieved through a 125- μ m wire mesh sieve, treated with 2% bleach for 24 hours, and sieved a second time to isolate macroscopic charcoal pieces. Charcoal particles were counted at 10-40x magnification under a stereomicroscope.

Interpolated charcoal accumulation rates (CHAR) were fitted with a 500-yr loess smoother robust to outliers to estimate background charcoal accumulation (Cleveland 1979), which was subtracted from the interpolated CHAR series to yield residuals reflecting high-frequency variation in charcoal accumulation. Residual CHAR was decomposed using a locally-fit Gaussian mixture model to separate out distinct peaks in CHAR from noise (e.g., resulting from sediment mixing and redeposition, long-distance charcoal transport, and sampling variability). The 99th percentile of the noise distribution was used to define a local threshold for identifying charcoal peaks (Higuera et al. 2010), representing fire events within c. 1 km of the lake (Higuera et al. 2007, Kelly et al. 2013). Finally, a minimum count test was applied to screen out peaks that represent small changes in charcoal abundance (Gavin et al. 2006, Higuera et al. 2010). All records had a median signal to noise index >3 over the past 2500 yr (Table A.1), indicating suitability for charcoal peak detection analysis (Kelly et al. 2011).

To validate the comparison between paleo-inferred and known fire histories over 1900-2021 CE, we compared the timing of charcoal peaks at each site and fires mapped in the Northern Rockies Fire Atlas (NRFA). The congruence between inferred ages of charcoal peaks and known fires varied among our sites depending on mixing in the surface cores. Silver and Missoula Lakes – the two records with the best-preserved surface cores, as indicated by visible laminations and clear tephra layers from MSH 1980 – both had charcoal peaks that broadly

corresponded with known fire events in the NRFA, in 1918 and 1910 CE, respectively. In contrast, four lakes which last burned in 1910 (Lower Bonanza, Kid, Saint Joe, and Bacon) recorded charcoal peaks in shallower sediments, which corresponded to dates after 1950 CE based on robust ^{210}Pb chronologies (Table A.2). We suggest that in these cases, the release of pressure when cores were brought to the surface may have allowed low-density charcoal particles to move up-core through waterlogged sediments, resulting in charcoal peaks from fires that are older than the surrounding sediment. We make this interpretation based on the depth of these lakes (>12 m), as well as field observations noting flocculent near-surface sediments that with little visible stratigraphy, suggesting some degree of mixing. This is further supported by the lack of a distinct tephra layer from MSH 1980 in these cores, despite high MS measurements implying the presence of volcanic ash in near-surface sediments. Lastly, radiocarbon dating of concentrated charcoal samples from the four charcoal peaks indicated that the combusted materials predated 1950, and thus were older than the sediment at the depth from which the charcoal was derived. The resulting ^{14}C ages preclude precise calibration, and were not used to inform the chronologies. Based on these several lines of evidence, we attribute these four anomalous charcoal peaks to fires in 1910 recorded in the NRFA, and we manually shifted the four fire dates to 1910 in the composite analysis.

While the lack of fidelity between paleo-inferred and modern fire histories at several of our sites precludes using these records for a calibration analysis, we are confident that the issues described above are limited to surface sediments. Deeper, more compacted sediments are resistant to mixing, and remain well-preserved during collection. This is supported by the presence of visible stratigraphy in deeper sediment sections, as well as a well-defined tephra layer from an earlier MSH eruption (c. 1480 CE) in cores from at least five of our sites.

Additionally, robust chronologies indicating consistent sediment accumulation over time, and a high charcoal peak signal-to-noise index, provide additional evidence that the sediments at our study sites are not mixed (Table A.1). Therefore, the challenges associated with interpreting fire histories in unconsolidated near-surface cores do not extend to deeper sediment sections.

Table A.1. Metadata for the twelve lakes, including their coordinates in decimal degrees, elevation, surface area, maximum depth, the number of ^{210}Pb and radiocarbon dates used in the chronology, the median sample resolution over the past 2500 years, the median signal to noise index (SNI) of the charcoal record, and the inferred number of fires and estimated mean fire return interval (mFRI) within the past 2500 yrs. Sites are organized from north to south.

<i>Lake Name</i>	<i>Site ID</i>	<i>Lat. (°N)</i> <i>Lon. (°W)</i>	<i>Elev. (m)</i>	<i>Surf. Area (ha)</i>	<i>Max. Depth (m)</i>	<i>Number of ^{210}Pb, ^{14}C ages</i>	<i>Median Res. (yr)</i>	<i>SNI</i>	<i># fires</i>	<i>mFRI (yr)</i>
<i>St. Regis</i>	SR19	47.427 115.744	1707	3.2	12.3	11, 4	7	4.5	8	163
<i>Silver</i>	SI17	47.360 115.566	1623	5.26	18.8	12, 13	6	4.3	15	155
<i>Clear</i>	CL18	47.269 115.408	1789	3.6	13.2	12, 6	16	4.8	12	194
<i>Lenore</i>	LE18	47.256 115.299	1671	0.78	7	15, 5	5	4.7	12	221
<i>Dismal</i>	DI19	47.117 115.635	1631	2.9	20.3	7, 4	5	5.4	14	117
<i>Lower Bonanza</i>	LB18	47.087 115.133	1922	6.52	17	8, 4	25	12	6	421
<i>Missoula</i>	ML18	47.067 115.116	1807	4.61	15.5	9, 6	5	4.4	14	94
<i>St Joe</i>	SJ19	47.018 115.080	1978	7.53	13.4	9, 3	8	4.2	17	146
<i>Bacon</i>	BA19	46.968 115.265	1830	2.23	17	12, 4	7	4.6	19	142
<i>North-bound</i>	NB19	46.943 115.569	1670	4.9	15.5	9, 3	10	3.4	17	131
<i>Little Montana</i>	LM18	46.813 114.765	2011	0.77	5.6	14, 4	5	5.8	22	131
<i>Kid</i>	KI18	46.778 114.815	1909	4.9	14.5	13, 3	12	3.8	16	152

Table A.2. Radiocarbon dates used to construct age models for each of the twelve lakes.

<i>Material Dated</i>	<i>Depth (cm)</i>	<i>Laboratory ID¹</i>	<i>¹⁴C age (yr BP)²</i>	<i>±</i>
Bacon Lake				
needle macrofossil	43.75	CAMS.185615	465	35
needle macrofossil	105.25	CAMS.185616	1445	30
needle macrofossil	133.75	CAMS.187962	1900	35
needle macrofossil	165.25	CAMS.185617	2485	35
Clear Lake				
needle macrofossil	49.45	CAMS.183267	1285	30
needle macrofossil	68.31	CAMS.183268	1910	30
concentrated charcoal	78.25	CAMS.185618	2160	45
concentrated charcoal	86.5	CAMS.185619	2210	40
needle macrofossil	100.25	CAMS.183269	2515	30
macrofossil, unidentified	122.75	CAMS.183270	3115	30
Dismal Lake				
needle macrofossil	79.5	CAMS.185620	1040	30
needle macrofossil	128	CAMS.185621	1600	30
needle macrofossil	154.5	CAMS.187963	1540	35
needle macrofossil	188.5	CAMS.185622	1770	30
Kid Lake				
concentrated charcoal	69.25	CAMS.185623	1280	40
macrofossil, unidentified	99.75	CAMS.183287	1885	30
macrofossil, unidentified	192.25	CAMS.183288	4190	30
Lower Bonanza Lake				
concentrated charcoal	51	CAMS.187966	2340	35
wood macrofossil	74	CAMS.183271	145	30
macrofossil, unidentified	120.5	CAMS.183272	3910	30
macrofossil, unidentified	127	CAMS.183273	4130	30
Lenore Lake				
wood macrofossil	78.75	CAMS.185624	950	30
needle macrofossil	94.75	CAMS.183285	1005	30
needle macrofossil	125.25	CAMS.183286	1405	30
wood macrofossil	169.75	CAMS.185625	1695	35
needle macrofossil	214.25	CAMS.185626	2160	35
Little Montana Lake				
needle macrofossil	71	CAMS.185631	545	45
needle macrofossil	99.5	CAMS.183278	1055	30
needle macrofossil	152.5	CAMS.183279	1675	30
needle macrofossil	206.5	CAMS.183280	2120	30
Missoula Lake				
needle macrofossil	36.77	CAMS.183274	270	30
needle macrofossil	47.75	CAMS.183275	260	30
wood macrofossil	89.25	CAMS.183276	875	30
wood macrofossil	116	CAMS.183277	975	30

Chapter 4 Supplementary Material

needle macrofossil	148.25	CAMS.185632	1350	40
needle macrofossil	191.5	CAMS.185633	2010	35
Northbound Lake				
needle macrofossil	64	CAMS.185634	1260	30
wood macrofossil	88	CAMS.185635	1795	30
wood macrofossil	161.5	CAMS.185636	3340	30
Silver Lake				
needle macrofossil	62.5	CAMS.179896	660	30
concentrated charcoal	94	CAMS.185640	1095	40
needle macrofossil	121	CAMS.179897	1915	40
needle macrofossil	163.5	CAMS.179898	2245	35
wood macrofossil	204	CAMS.179899	5920	30
needle macrofossil	248	CAMS.179900	3005	35
needle macrofossil	331	CAMS.179901	3390	35
needle macrofossil	394.5	CAMS.179902	3700	30
needle macrofossil	424	CAMS.179903	4165	30
needle macrofossil	456	CAMS.179904	4495	40
cone macrofossil	500	CAMS.185641	4680	30
needle macrofossil	519.5	CAMS.179905	5615	35
wood macrofossil	571.5	CAMS.179906	4800	80
wood macrofossil	632	CAMS.179925	5875	30
needle macrofossil	674.5	CAMS.179907	6310	45
Saint Joe Lake				
cone macrofossil	62	CAMS.185637	930	30
cone macrofossil	104.5	CAMS.185638	1575	35
needle macrofossil	147.5	CAMS.185639	2165	40
Saint Regis Lake				
needle macrofossil	64.3	CAMS.187967	855	30
needle macrofossil	100.8	CAMS.187968	1495	35
needle macrofossil	133.3	CAMS.187969	1920	45
needle macrofossil	170.3	CAMS.187970	2155	35

¹CAMS: Center for Accelerator Mass Spectrometry, Lawrence Livermore National Laboratory, Livermore, CA. ²Conventional radiocarbon years before present (CE 1950).

Table A.3. Radiocarbon measurements of four concentrated charcoal samples from charcoal peaks that did not match the most recent known fire recorded by the Northern Rockies Fire Atlas. The fraction modern carbon indicates that the age of the combusted material is from pre-1950 CE, older than the ^{210}Pb -inferred age of the sediment at the depth from which the charcoal was derived. The resulting ^{14}C ages of these samples preclude precise calibration, and therefore are not used to inform the chronologies of these records. The ages associated with these charcoal peaks were adjusted in the composite analysis to correspond to the known fires in 1910 CE.

<i>Lake Name</i>	<i>Lab ID</i> ¹	<i>Fraction modern C</i>	\pm	<i>Core Depth (cm)</i>	<i>^{210}Pb-inferred age</i> ²	<i>Adjusted age</i> ²
<i>Lower Bonanza</i>	CAMS. 190220	0.9692	0.0034	1	-58	-40
<i>St Joe</i>	CAMS. 190222	0.9804	0.0040	3	-48	-40
<i>Bacon</i>	CAMS. 190219	0.9805	0.0036	9	-8	-40
<i>Kid</i>	CAMS. 190221	0.9786	0.0037	10.5	-8	-40

¹CAMS: Center for Accelerator Mass Spectrometry, Lawrence Livermore National Laboratory, Livermore, CA. ²Calibrated years before present (CE 1950).

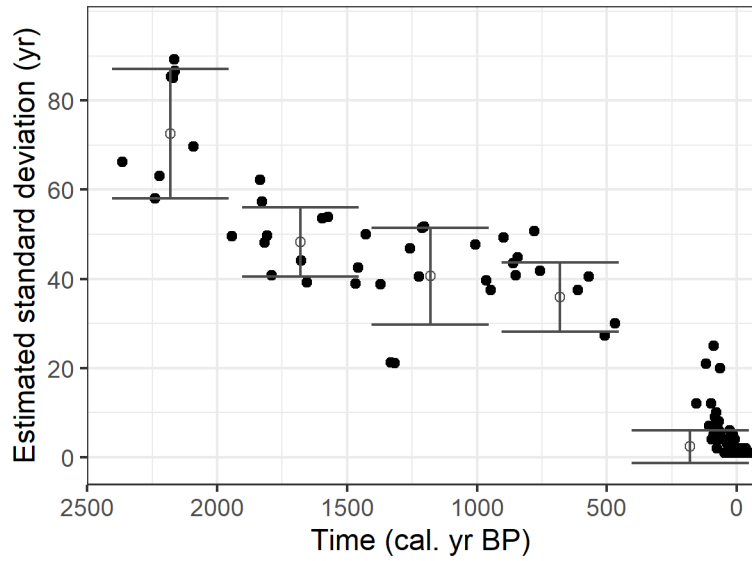


Fig. A.1. Estimated age uncertainties from Northern Rockies paleofire records used in this study. Dots represent the standard deviation of calibrated ages associated with each ^{14}C , tephra, or ^{210}Pb -inferred date used to inform the chronologies. Open circles and error bars give the mean \pm one standard deviation of age uncertainties within non-overlapping 500-year windows spanning the past 2500 yr.

Appendix B: Supplementary Results

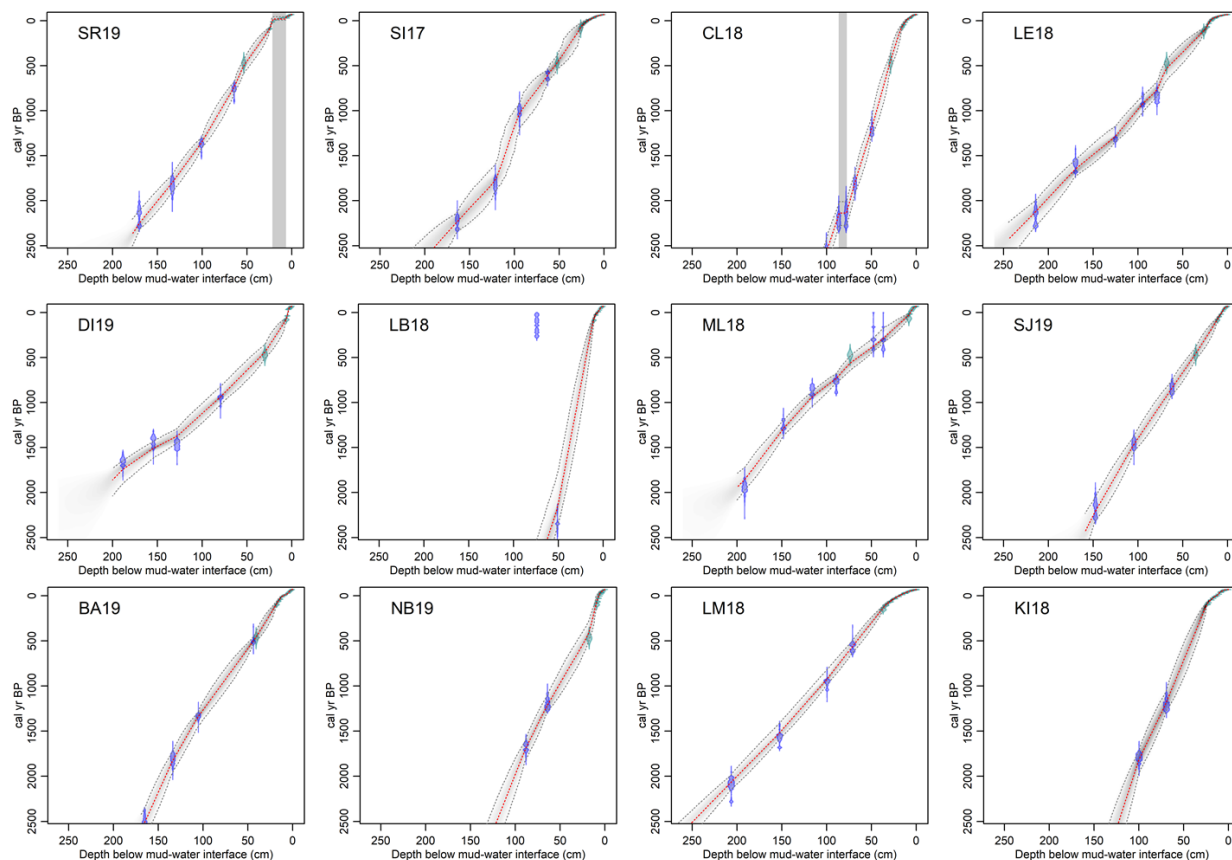


Fig. B.1. Age-depth relationship for each of the twelve lakes on the same scale spanning the past 2500 years to show relative differences in sediment accumulation rates among sites. Shaded bars show inferred instantaneous sedimentation events excluded from chronologies. Purple ranges show the distribution of ages for calibrated radiocarbon dates, while green shows additional dates (tephra layers and Pb²¹⁰-inferred ages), and the curve shows median and 95% confidence intervals for the estimated age at each core depth. Prior and posterior distributions for parameters are shown at the top. See Table A.1 for site IDs.

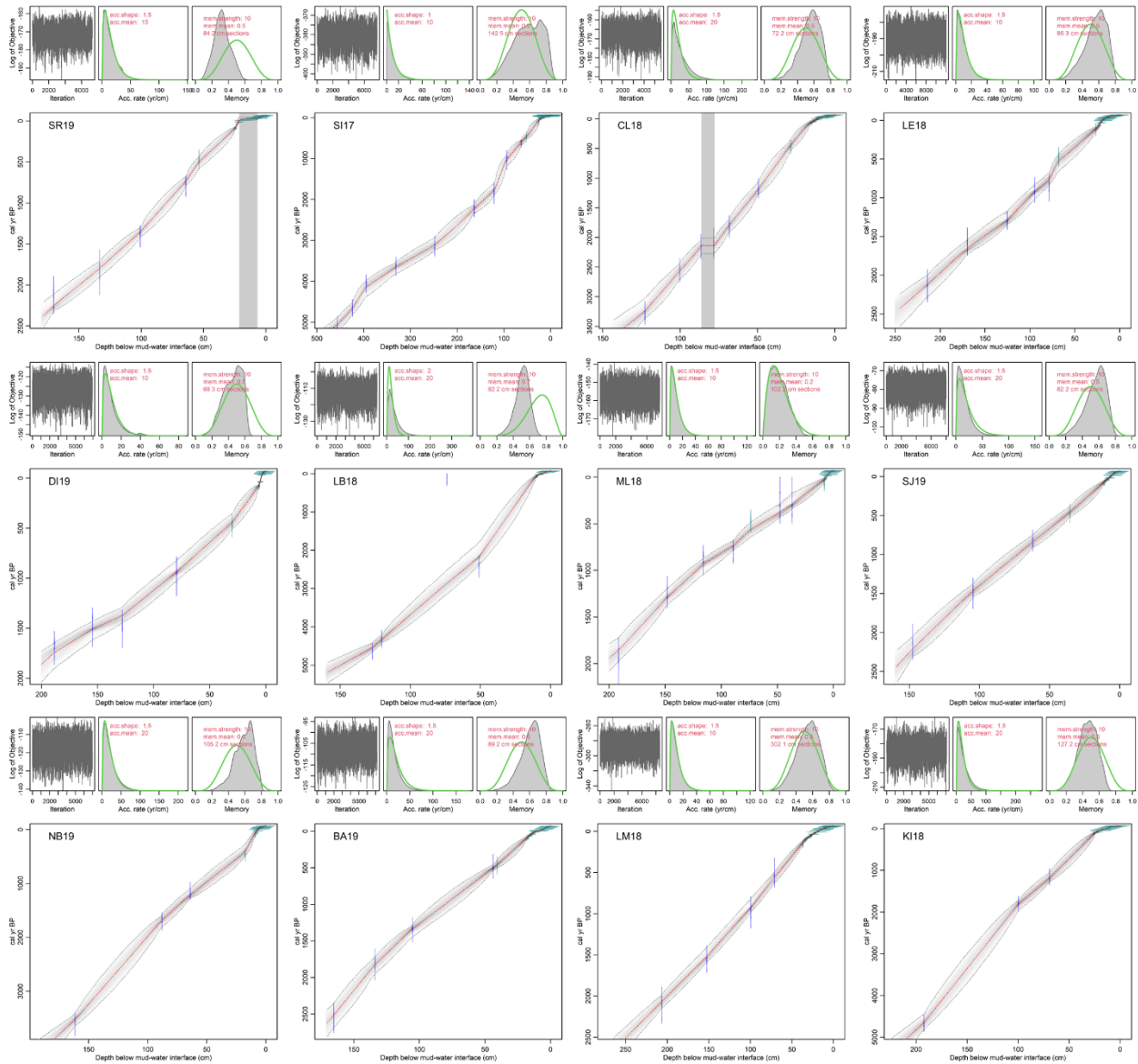


Fig. B.2. Age-depth relationships for each of the twelve lake records, modeled using *rbacon*.

Axis ranges are scaled to show all dates included in the chronology for each site. Shaded bars show inferred instantaneous sedimentation events excluded from chronologies. Purple ranges show the distribution of ages for calibrated radiocarbon dates, while green shows additional dates (tephra layers and Pb²¹⁰-inferred ages), and the curve shows median and 95% confidence intervals for the estimated age at each core depth. Prior and posterior distributions for parameters are shown at the top. See Table A.1 for site IDs.

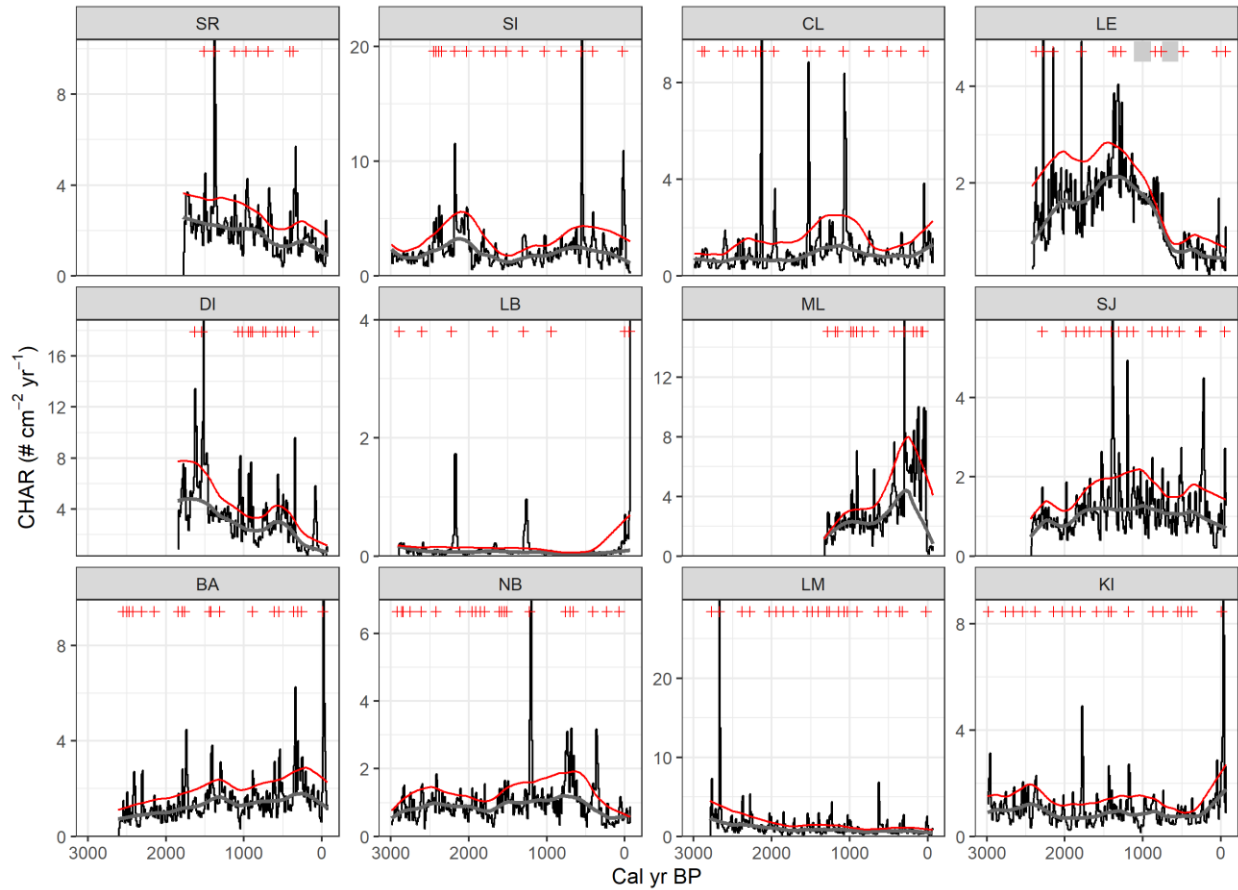


Fig. B.3. Timeseries of charcoal accumulation rate (CHAR) for each of the twelve lakes.

Background CHAR smoothed over 500 yr is shown in grey, with the threshold for identifying peaks in red. The timing of inferred charcoal peaks is shown at the top of each plot; the grey bands for Lenore Lake (LE) are sections of the record with accumulation of moss in the sediment, which were excluded from the analysis. See Table A.1 for site IDs.

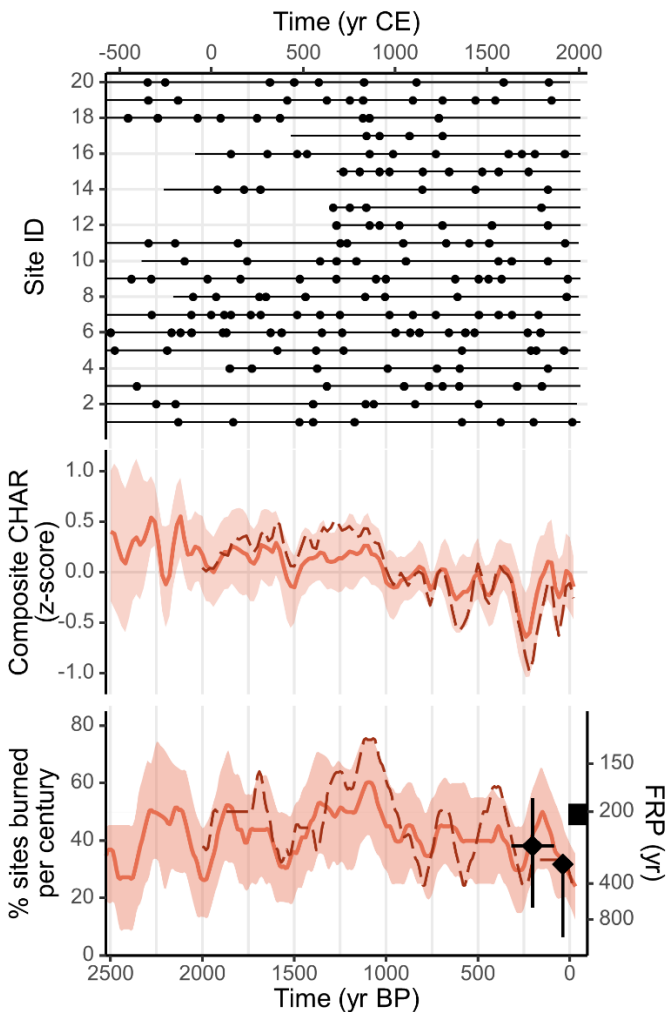


Fig. B.4. Fire history in the Northern Rockies study region over the past 2500 yr. Top panel: record length and fire timing for each individual record, organized from north to south (see (Higuera et al. 2021) for site details). Center and bottom panels: transformed charcoal z-scores and percentage of sites burned per century, smoothed over 100 yr (median \pm 90% CI). The dashed line shows the median transformed charcoal influx and % sites burned per century for a subset of 12 lakes (#2-13) from a similar-sized landscape to that represented by the Northern Rockies sites (Calder et al. 2015). The ranges of tree-ring FRP estimates in subalpine forests in the region (diamonds) (Kipfmüller and Baker 2000, Howe and Baker 2003, Buechling and Baker 2004, Sibold et al. 2006) and the 1984-2020 fire rotation period (square) are also shown.

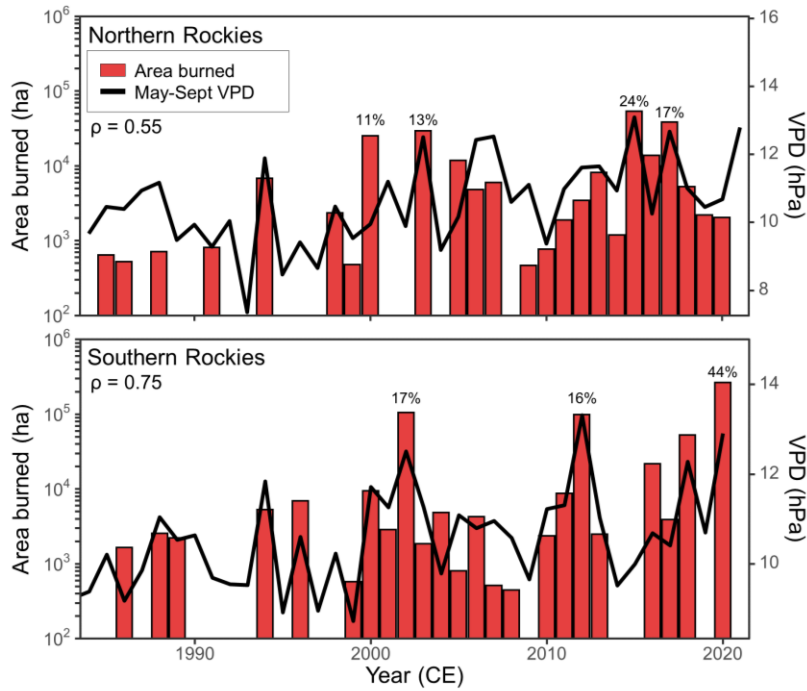


Fig. B.5. Ecoregion-wide annual area burned and May-September average VPD in the Northern Rockies and Southern Rockies. Percentages above the bars are the proportion of the total area burned over 1984-2020 contributed by each year. The lower panel is replotted from Fig. 1B in Higuera et al. (2021).

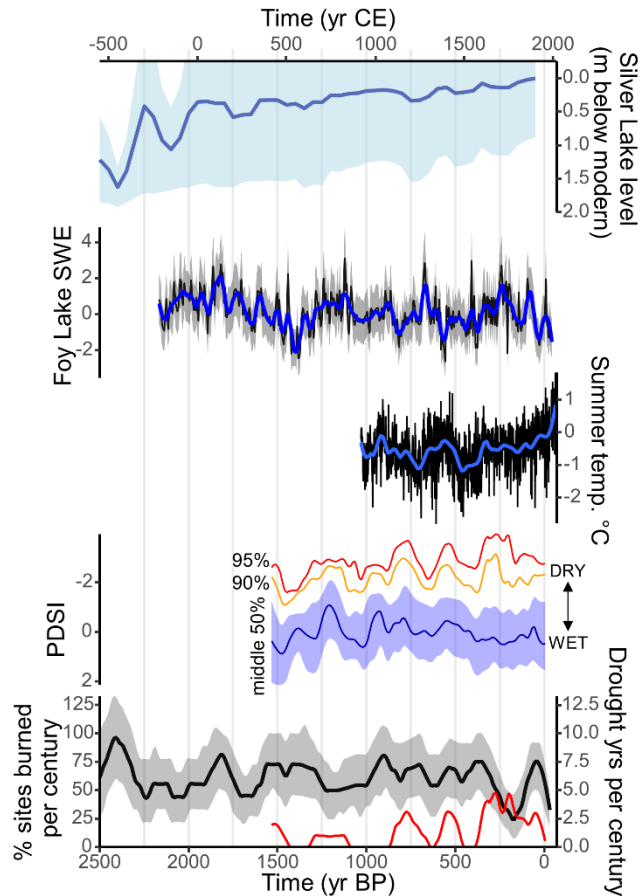


Fig. B.6. Paleoclimate and fire history in the Northern Rockies region. Top panel: lake-level reconstruction from Silver Lake, MT, replotted from (Parish et al. 2022). Top middle panel: reconstructed April 1 snow water equivalent (SWE) from Foy Lake, MT represented as z-scores (black), with 95% prediction intervals (grey bands), and smoothed over 100 yr (blue) (Schoenemann et al. 2020). Middle panel: spatially explicit multiproxy summer (May-August) temperature reconstruction for the study region at annual resolution (black), and smoothed over 100 yr (blue) (Anchukaitis et al. 2017). Bottom middle panel: spatially explicit PDSI reconstruction averaged over the study area and summarized as quantiles within a moving 100-yr window, smoothed over 100 yr (Cook et al. 2010). Bottom panel: percentage of sites burned per century with 90% confidence bands (black/grey), and the number of years per century with extreme drought (reconstructed PDSI < -4), smoothed over 100 yr (red) (Cook et al. 2010).

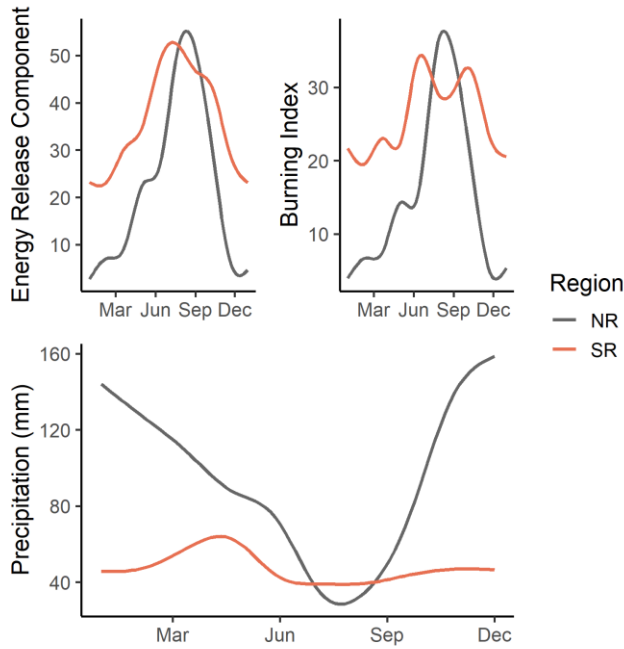


Fig. B.7. Average seasonal progression in fire danger metrics (from GridMet) and precipitation (from PRISM) in the Northern and Southern Rockies ecoregions, summarized over 1979-2022 using a gam smoother. Spatially averaged timeseries data across each study area were accessed from climatologylab.org. Energy Release Component is related to the potential fire intensity at the flaming front, and reflects fuel moisture, while Burning Index provides a metric of the potential effort needed to contain a fire, and is influenced by both fuel moisture and fire weather.

Literature Cited

- Anchukaitis, K. J., R. Wilson, K. R. Briffa, U. Büntgen, E. R. Cook, R. D'Arrigo, N. Davi, J. Esper, D. Frank, B. E. Gunnarson, G. Hegerl, S. Helama, S. Klesse, P. J. Krusic, H. W. Linderholm, V. Myglan, T. J. Osborn, P. Zhang, M. Rydval, L. Schneider, A. Schurer, G. Wiles, and E. Zorita. 2017. Last millennium Northern Hemisphere summer temperatures from tree rings: Part II, spatially resolved reconstructions. *Quaternary Science Reviews* 163:1–22.
- Binford, M. W. 1990. Calculation and uncertainty analysis of ^{210}Pb dates for PIRLA project lake sediment cores. *Journal of Paleolimnology* 3:253–267.
- Blaauw, M., and J. A. Christen. 2011. Flexible paleoclimate age-depth models using an autoregressive gamma process. *Bayesian Analysis* 6:457–474.
- Buechling, A., and W. L. Baker. 2004. A fire history from tree rings in a high-elevation forest of Rocky Mountain National Park. *Canadian Journal of Forest Research* 34:1259–1273.
- Calder, W. J., D. Parker, C. J. Stopka, G. Jiménez-Moreno, and B. N. Shuman. 2015. Medieval warming initiated exceptionally large wildfire outbreaks in the Rocky Mountains. *Proceedings of the National Academy of Sciences of the United States of America* 112:13261–6.
- Cleveland, W. S. 1979. Robust Locally Weighted Regression and Smoothing Scatterplots. *Journal of the American Statistical Association* 74:829–836.
- Cook, E. R., R. Seager, R. R. Heim, R. S. Vose, C. Herweijer, and C. Woodhouse. 2010. Megadroughts in North America: placing IPCC projections of hydroclimatic change in a long-term palaeoclimate context. *Journal of Quaternary Science* 25:48–61.

- Egan, J., R. Staff, and J. Blackford. 2015. A high-precision age estimate of the Holocene Plinian eruption of Mount Mazama, Oregon, USA. *The Holocene* 25:1054–1067.
- Gavin, D. G., F. S. Hu, K. Lertzman, and P. Corbett. 2006. Weak climatic control of stand-scale fire history during the late Holocene. *Ecology* 87:1722–1732.
- Higuera, P. E., D. G. Gavin, P. J. Bartlein, and D. J. Hallett. 2010. Peak detection in sediment–charcoal records: impacts of alternative data analysis methods on fire-history interpretations. *International Journal of Wildland Fire* 19:996–1014.
- Higuera, P. E., M. E. Peters, L. B. Brubaker, and D. G. Gavin. 2007. Understanding the origin and analysis of sediment-charcoal records with a simulation model. *Quaternary Science Reviews* 26:1790–1809.
- Higuera, P. E., B. N. Shuman, and K. D. Wolf. 2021. Rocky Mountain subalpine forests now burning more than any time in recent millennia. *Proceedings of the National Academy of Sciences* 118:e2103135118.
- Howe, E., and W. L. Baker. 2003. Landscape Heterogeneity and Disturbance Interactions in a Subalpine Watershed in Northern Colorado, USA. *Annals of the Association of American Geographers* 93:797–813.
- Kelly, R., M. L. Chipman, P. E. Higuera, I. Stefanova, L. B. Brubaker, and F. S. Hu. 2013. Recent burning of boreal forests exceeds fire regime limits of the past 10,000 years. *Proceedings of the National Academy of Sciences* 110:13055–13060.
- Kelly, R. F., P. E. Higuera, C. M. Barrett, and F. S. Hu. 2011. A signal-to-noise index to quantify the potential for peak detection in sediment–charcoal records. *Quaternary Research* 75:11–17.

- Kipfmüller, K. F., and W. L. Baker. 2000. A fire history of a subalpine forest in south-eastern Wyoming, USA. *Journal of Biogeography* 27:71–85.
- Parish, M. C., K. D. Wolf, P. E. Higuera, and B. N. Shuman. 2022. Holocene water levels of Silver Lake, Montana, and the hydroclimate history of the Inland Northwest. *Quaternary Research*.
- Schoenemann, S. W., J. T. Martin, G. T. Pederson, and D. B. McWethy. 2020. 2,200-Year tree-ring and lake-sediment based snowpack reconstruction for the northern Rocky Mountains highlights the historic magnitude of recent snow drought. *Quaternary Science Advances* 2:100013.
- Sibold, J. S., T. T. Veblen, and M. E. González. 2006. Spatial and temporal variation in historic fire regimes in subalpine forests across the Colorado Front Range in Rocky Mountain National Park, Colorado, USA. *Journal of Biogeography* 33:631–647.
- Wright, H. E., D. H. Mann, and P. H. Glaser. 1984. Piston corers for peat and lake sediments. *Ecology* 65:657–659.